DEVELOPING AN ARTIFICIAL INTELLIGENCE MODEL FOR ESTIMATING THE COMPRESSIVE STRENGTH OF CONCRETE BASED ON COMBINED NON-DESTRUCTIVE TEST RESULTS

by
Seyed Alireza Alavi

Under Supervision of
Dr. Martin Noël

Thesis submitted to the University of Ottawa
in partial Fulfillment of the requirements for the
Doctor of Philosophy
in Civil Engineering

Department of Civil Engineering
Faculty of Engineering
University of Ottawa

Abstract

The most important mechanical property of concrete for design and evaluation is its compressive strength, which, for new structures, is typically determined by breaking cylindrical or cubic concrete specimens under uniaxial load in controlled laboratory conditions. The accurate and quick evaluation of the compressive strength of concrete in existing structures has been of primary concern to engineers and researchers for decades.

The evaluation of concrete compressive strength for existing reinforced concrete (RC) structures is currently done mainly by destructive testing (DT) of extracted core samples which can be both costly and time consuming. To be representative of the in-situ concrete, a relatively large number of samples are needed which is often impractical or unfeasible. Non-destructive test (NDT) methods have been developed to provide indirect measurements that can be correlated to concrete strength. Among them, the SonReb method, which combines ultrasonic pulse velocity (UPV) readings with rebound hammer (RN) measurements, has shown promising results. This approach can reduce the number of concrete cylinders or cores that are needed, saving time and money for building owners. However, despite its advantages, the need to develop calibration curves for each project presents a notable limitation of all NDT methods. This study is the first comprehensive investigation in which a Machine Learning (ML)-based model is developed using the SonReb method for evaluating the actual in-place compressive strength of concrete in existing RC structures using only NDT measurements, without the need for new calibration curves.

In this study, ML techniques are applied to improve the SonReb method for practical use in four phases: 1) developing a preliminary ML-based model and graphical user interface (GUI) that converts UPV and RN values to estimates of concrete compressive strength; 2) evaluating the initial ML model performance against three case studies to assess the opportunities and limitations

of the proposed approach in practice; 3) comparing the performance of alternative ML algorithms and adding input parameters to account for specimen geometry to improve prediction accuracy; and 4) assessing the uncertainty and prediction intervals of the new ML-based model versus conventional regression models.

The ML-based SonReb approach presented in this thesis was, in general, able to provide reasonable approximations of concrete compressive strengths for various concrete mix designs, with mean absolute percent errors (MAPEs) within 10-15%, without calibration. Some discrepancies were also noted, which highlight the role of engineering judgment in proper interpretation of results and use of modern and conventional tools. The results of this study suggest that although artificial intelligence (AI) has the potential to improve predictions of the in-place compressive strength of RC structures using simple and fast NDT methods in certain cases, challenges related to data collection can affect model performance. A road map for improved data collection is proposed that can be used for future development of a reliable and robust ML prediction model for concrete compressive strength of existing structures.

Acknowledgements

This study would not have been possible without the support and contributions of many individuals throughout my Ph.D. journey.

First and foremost, it is with great pleasure that I express my deepest gratitude to my supervisor, Dr. Martin Noël, for his unwavering guidance and support throughout these years. His insightful advice and encouragement have been invaluable, helping me overcome numerous challenges and navigate the research process with greater efficiency and clarity.

I would also like to extend my sincere thanks to FPrimeC Solutions Inc. and Mitacs for their financial support. This research, driven by industrial needs, was made possible through the financial and technical support of FPrimeC Solutions Inc, the industrial partner of the research.

My sincere appreciation is extended to the technical officers in the structural lab at the University of Ottawa, Dr. Muslim Majeed and Dr. Gamal Elnabelsya, for their assistance and advice. Also, I would like to thank everyone who helped me in the lab works. My sincere thanks to Aws Hasak, Issa Fowai, Hamidreza Asghari, Pablo Aguilera Clouet, Mohammed Skalli, and all my friends.

Finally, I wish to express my profound appreciation to my father and my mother for their constant support and encouragement. Last but certainly not least, my deepest thanks go to my beloved wife, Minoo, for her unwavering support and patience during the most challenging times of my studies. I dedicate this thesis to you, Minoo.

Table of Contents

List of Figures

List of Tables

Chapter 1- Introduction

1.1 Introduction

Today, in every part of the world, structures such as buildings, bridges, dams, tunnels, canals, reservoirs, and tanks are made of reinforced concrete (RC). The widespread use of RC in construction is due to its advantages that include availability and low cost of materials, long-life operation compared to other building materials, high rigidity, and less costly maintenance (McCormac & Brown, 2015).

The compressive strength of concrete is typically determined by uniaxial tests on standard cylindrical and cubic specimens. There is a relatively high degree of variability in compressive strength results due to the heterogeneity of concrete as well as factors such as differences in the curing procedure or environmental conditions. In addition, the representativeness of test specimens with respect to the overall performance of the associated structure is not always clear (Mehta & Monteiro, 2005; Monteiro, 2006).

Many existing RC structures, after a period of time from their construction, also need to be evaluated for various reasons that can include mistakes during the design and construction process, exposure to harsh environmental conditions, evaluation of damage after an earthquake, upgrading of existing structures due to development, and structure health monitoring (Ganesh & Murthy, 2019; Haji et al., 2018; Soh et al., 2000). The accurate prediction of behaviour requires a good estimation of the in-place mechanical properties of concrete, one of the main concerns of engineers and researchers.

For this purpose, there are various tests that can be divided into three main categories: destructive tests (DT), semi-destructive tests, and non-destructive tests (NDT). Based on the cost of the test, the speed of the test, and the conditions of the structure, one can choose the appropriate method to estimate the compressive strength of concrete on-site (Asteris & Mokos, 2020; Breysse, 2012; Kayed, 2021; Poorarbabi et al., 2020). NDT can usually be done faster, cheaper, and with a higher number of repetitions than DT methods. The rebound hammer (Schmidt hammer) and Ultrasonic Pulse Velocity (UPV) are two popular NDTs often used by engineers to evaluate the compressive strength of concrete on-site.

It should be noted, however, that the accuracy of concrete strength estimates can vary greatly depending on the method used. Naturally, NDTs provide only indirect estimates of the compressive strength of concrete. For this reason, their accuracy cannot be confirmed without also performing DT. The fundamental limitation of NDT approaches in the evaluation of compressive strength is that the characteristic of concrete being measured can be influenced by several parameters and, on the other hand, there is no significant physical relationship between the measured parameter and the expected characteristic of concrete. For example, in the UPV test, the velocity of the pulse in concrete is measured, which is then correlated to concrete mechanical properties such as compressive strength. Therefore, the use of these methods in evaluating the target properties of concrete (especially compressive strength) is faced with errors and requires the preparation of calibration curves for each concrete mix, which is expensive and time-consuming.

Diversity and heterogeneity of concrete materials lead to an inaccurate prediction of material properties as well as the performance and behaviour of concrete members. Accordingly, the use of any single NDT is not enough to evaluate the compressive strength of concrete; more accurate and reliable results could be obtained by combining the results of two or more NDT methods. Many studies have been conducted on so-called combined methods, of which the most promising has been the SonReb method based on the combination of UPV and rebound hammer (RN). Although several empirical equations have been proposed, their accuracy has generally been poor when applied to concrete from other sources. Hence, calibration curves must be generated for each specific project and concrete type.

In recent years, Artificial Intelligence (AI) and its key subfield, Machine Learning (ML), have been increasingly applied to address complex problems across various domains. Advances in ML algorithms and computing power have led to a substantial rise in the use of AI and ML in the industry. In this context, this thesis was developed in response to a stated industry need to explore the practical application of ML on a combined NDT method—UPV and Rebound Number (RN)—and to provide a comprehensive investigation into this approach.

1.2 Motivation

Due to the challenges associated with performing core tests on existing reinforced concrete structures—such as the owner's dissatisfaction and reluctance to conduct destructive testing, the inability to repeat these tests, limitations on conducting a large number of tests due to structural safety considerations, the high cost, and the time-consuming nature of core extraction—the core test has become a challenging option for engineers. It is also worth noting that even with the performance of the core test, there is no guarantee of obtaining valid results, as core samples sometimes have poor quality due to issues such as cutting through reinforcement, cracks in the cores, the presence of voids, and variability in core size.

According to current codes and guidelines, even if non-destructive tests like UPV and RN are used, it is still necessary to perform core tests for the calibration process in order to rely on the results of NDT measurements (Breysse, 2012, Alavi et al., 2024). It is also important to note that several mathematical regression equations have been proposed over the past decades to convert NDT results to concrete compressive strength, and the calibration process must be performed to use these equations.

Therefore, the main goal of this research is to develop an ML-based model that can predict concrete compressive strength with good accuracy and without the need for calibration based solely on two inputs that are accessible and common among industry practitioners, namely UPV and RN. This approach assumes that computer-based models, such as ML models, have fewer limitations than mathematical regression models to identify complex relationships between multiple parameters (an assumption which is tested in this thesis). If such an ML-based model can be developed to reduce or even eliminate the need for core tests, it would certainly enhance structural safety, as these two NDT methods—relatively inexpensive and quick—would become more widely used.

1.3 Objectives and Structure of Thesis

This research is a comprehensive investigation involving the development of a ML model and its application to an existing methodology that combines NDT results from UPV and RN tests (known as the SONREB method) to determine whether it is possible to accurately and reliably predict the compressive strength of concrete using AI. Accordingly, the goals of this project are:

- To develop an ML model that can estimate the compressive strength of concrete based solely on the results of two NDT measurements;
- To apply the new ML model in real case studies and identify challenges for practical use in the field;

- To investigate the role of ML model architecture on its predictive performance as well as other modifications to improve the results; and
- To assess the uncertainty and prediction intervals of this new ML approach compared to the conventional regression approach.

The remainder of the thesis is structured in a paper-based format as follows:

Chapter 2 presents a detailed review of the two NDT methods used in this study and the related prediction models reported in the literature. A review of relevant literature associated with ML models and their application is also presented. This chapter is an expanded version of a conference paper presented at the Canadian Society for Civil Engineers Annual Conference in 2022.

Chapter 3 discusses the details associated with the development of the preliminary ML model. This includes the process of building the database, followed by building, training, and testing the model and comparing its performance against a regression-based analysis using the same data. This chapter has been published in the Journal of Building Engineering in 2023.

Chapter 4 takes a practical look at the model performance by applying the proposed ML model to three case studies. Opportunities and limitations of AI for concrete strength evaluation are discussed. The content of this chapter was published in Concrete International in 2024.

Chapter 5 investigates the role of architecture on the predictive performance of the ML model. A total of six 2- and 3-parameter models are built using artificial neural networks, deep learning, and adaptive neuro-fuzzy inference systems to compare their advantages and disadvantages. The updated models also explore the role of specimen geometry (cylinder or cube) using an expanded dataset. This chapter has been published in the Journal of Engineering Structures in 2025.

Chapter 6 presents an analysis on the uncertainty and prediction intervals of the ML-based approach and compares its performance with proposed equations from reported literature. Taking a closer look at the error distribution for each model, owners and engineers can make better informed decisions about the need for additional testing based on different comfort or error threshold levels. A roadmap for improved data collection practices is also proposed. Chapter 6 has been submitted for review to an international journal.

Finally, Chapter 7 presents the conclusions of this work and provides recommendations for future work. Supplementary information, including data and code, is provided in the Appendix.

1.4 References

Asteris, P. G., & Mokos, V. G. (2020). Concrete compressive strength using artificial neural networks. Neural Computing and Applications, 32(15), 11807–11826.

Alavi, S. A., Noël, M., Layssi, H., & Moradi, F. (2024). Can Artificial Intelligence Improve Nondestructive Evaluation of Concrete Strength?. Concrete International, 46(5).

Breysse, D. (2012). Nondestructive evaluation of concrete strength: An historical review and a new perspective by combining NDT methods. Construction and Building Materials, 33, 139–163.

Ganesh, P., & Murthy, A. R. (2019). Repair, retrofitting and rehabilitation techniques for strengthening of reinforced concrete beams-A review. Advances in Concrete Construction, 8(2), 101–117.

Haji, M., Naderpour, H., & Kheyroddin, A. (2018). Strengthening of Reinforced Concrete Bridge Columns with FRP, Using Wrapping, Near-surface Mounted and Combined Methods. Journal of Transportation Infrastructure Engineering, 3(4), 33–48. https://doi.org/10.22075/JTIE.2018.13650.1275

Kayed, A. R. (2021). The Strength of Concrete in Existing RC Structures. Politecnico di Torino.

McCormac, J. C., & Brown, R. H. (2015). Design of reinforced concrete. John Wiley & Sons.

Mehta, P. K., & Monteiro, P. J. (2005). Concrete: microstructure, properties, and materials. 452 McGraw-Hill. New York, 453.

Monteiro, P. (2006). Concrete: microstructure, properties, and materials. McGraw-Hill Publishing.

Poorarbabi, A., Ghasemi, M., & Moghaddam, M. A. (2020). Concrete Compressive Strength Prediction Using Neural Networks Based on Non-destructive Tests and a Self-calibrated Response Surface Methodology. Journal of Nondestructive Evaluation, 39(4), 1–11.

Soh, C. K., Tseng, K. K. H., Bhalla, S., & Gupta, A. (2000). Performance of smart piezoceramic patches in health monitoring of a RC bridge. Smart Materials and Structures, 9(4), 533.

Chapter 2– Literature Review[1]

2.1 Destructive and semi-destructive test methods

Engineers conduct various types of tests to evaluate compressive strength of concrete (f_c'): completely non-destructive testing (NDT), semi-destructive testing, and completely destructive testing (DT). These methods can be used for both new concrete and also for concretes that have been cast for a long time. In Table 2.1, the tests that are used to evaluate the compressive strength of concrete are listed and some characteristics of these tests are presented for comparison (Breysse et al., 2009; Kayed, 2021).

Table 2.1: Summary of principal strength tests for concrete (Breysse et al., 2009; Kayed, 2021)

Test	Cost	Speed of test	Damage	Representativeness	Reliability for strength prediction
Drilled Core	High	Slow	High (Destructive)	Moderate	Good
Pull-out	Moderate	Moderate	Moderate/Minor (Semi-Destructive)	Near surface only	Moderate/Good
Penetration Resistance	Moderate	Moderate	Minor (Semi-Destructive)	Near surface only	Moderate
Pull-off	Moderate	Moderate	Minor (Semi-Destructive)	Near surface only	Moderate/Good
UPV	Low	Fast	No (Nondestructive)	Good	Poor
Rebound Hammer	Very low	Fast	No (Nondestructive)	Surface only	Poor

According to Table 2.1, the most reliable method to obtain the compressive strength of concrete in an existing structure (hardened concrete) is to perform the core test which causes damage to the structure and is time-consuming (known as a destructive test). As shown in Fig. 2.1, to

[1] An abridged version of this chapter has been published as: Alavi, S. A., Noel, M. (2021). Challenges for the development of artificial intelligence models to predict the compressive strength of concrete using non-destructive tests: a review. Canadian Society for Civil Engineers Annual Conference, May 25-28, Whistler, British Columbia.

perform the core test a specific drill with diamond bits is used to cut the concrete and extract concrete core samples for compressive tests (ASTM, 1999; Ergun & Kurklu, 2012).

Figure 2.1: Extracting concrete cores

An alternative method is the pull-out test. In this method, the peak force that is needed to pull out a metal rod installed in concrete is measured and then this value correlates to the concrete compressive strength (Fig. 2.2 and Fig. 2.3). The pull-out test is known as a semi-destructive test as it causes damage to the concrete surface (Crawford, 1997; Moczko & Moczko, 2018).

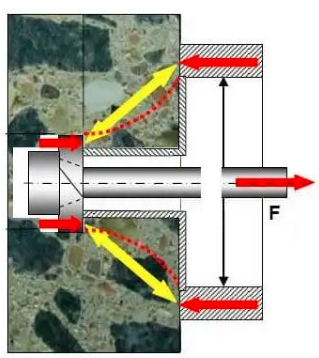

Figure 2.2: Concept of pull-out test on concrete (Nasrin et al., 2024)

Figure 2.3: Pull-out test on concrete (Brencich et al., 2021)

The penetration resistance test, also known as a Windsor Probe, is another semi-destructive test of concrete. In this test method, a steel rod (probe) rapidly penetrates the concrete by a sudden explosion (Fig. 2.4(a)). Then the penetration value of the rod is measured, and this value is correlated to the compressive strength of the concrete (Fig. 2.4(b)) (Pucinotti, 2009).

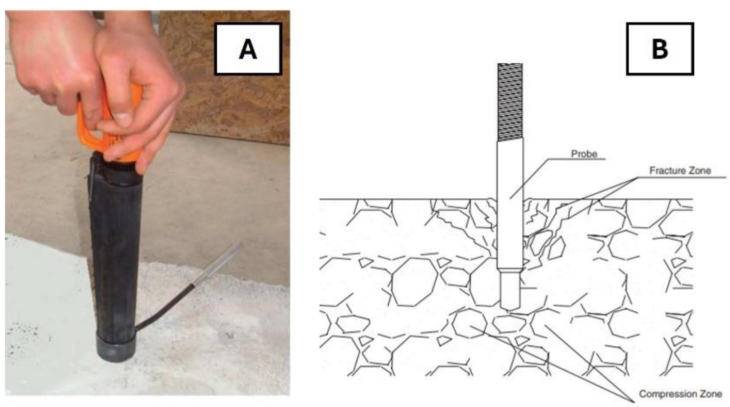

Figure 2.4 : (a): Windsor Probe test machine, (b): penetration resistance test on concrete (Pucinotti, 2009)

The last test method in the list of semi-destructive tests of concrete is the pull-off testing method. In this method, the compressive strength is estimated by measuring the near-surface tensile strength of the concrete (Fig. 2.5 and Fig. 2.6) (Pereira & de Medeiros, 2012; Yang et al., 2020).

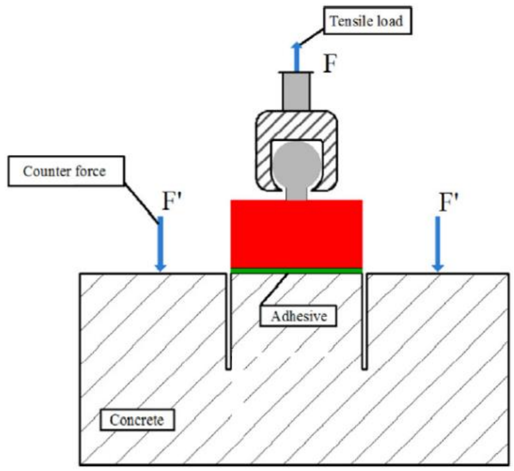

Figure 2.5: Concept of pull-off test on concrete (Yang et al., 2020)

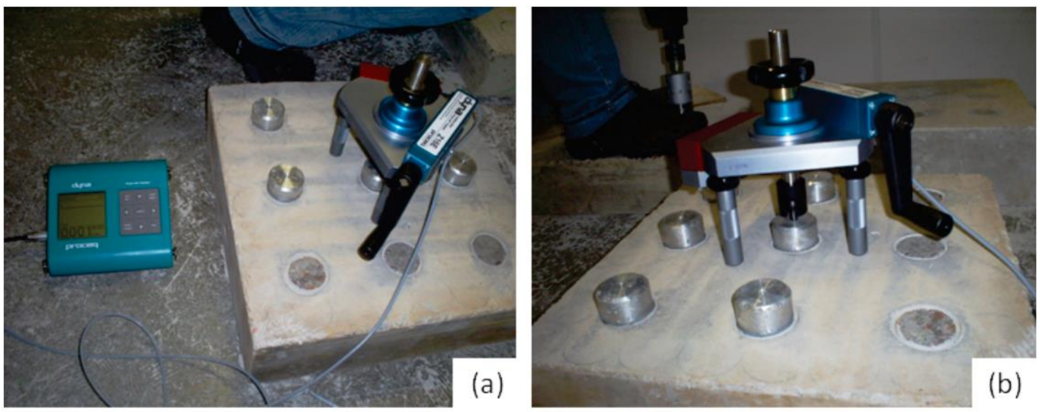

Figure 2.6: Pull-off test on concrete block (Pereira & de Medeiros, 2012)

The two remaining test methods listed in Table 2.1 are both NDT: the UPV and RN are considered the easiest, cheapest, and fastest methods for evaluating the compressive strength of concrete both on-site and in the laboratory. These methods are highlighted in the next section and related previous research studies are reviewed.

2.2 Non-Destructive Tests

2.2.1 Rebound Number (RN) Test

A rebound hammer, also known as a Schmidt hammer (or Swiss hammer) designed by Ernst Schmidt in 1945, measures the rebound of a spring-loaded mass impacting the surface of concrete or rock. The test hammer hits the concrete at a defined energy (Fig. 2.7). Its rebound is dependent on the hardness of the concrete surface and is measured by the device. In other words, the compressive strength of concrete is estimated indirectly based on surface hardness. For this device, correlation curves were developed between the compressive strength of standard cube samples and the rebound number (Fig. 2.8). However, the correlation is not unique, and it should be checked and calibrated for different devices and different test conditions (Breysse, 2012; Pedreros et al., 2020; Willetts, 1958).

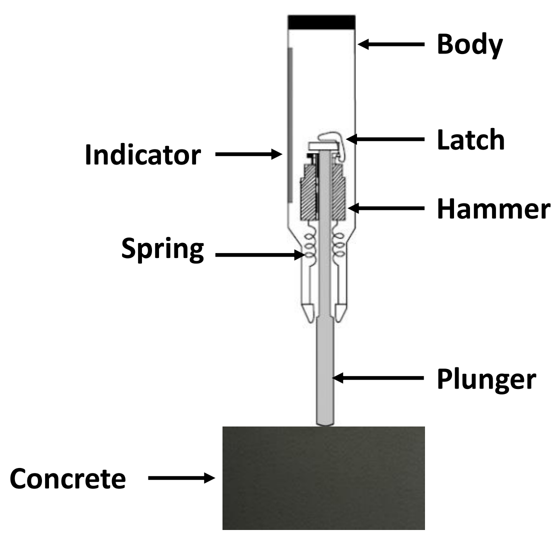

Figure 2.7: The rebound number (RN) test on concrete

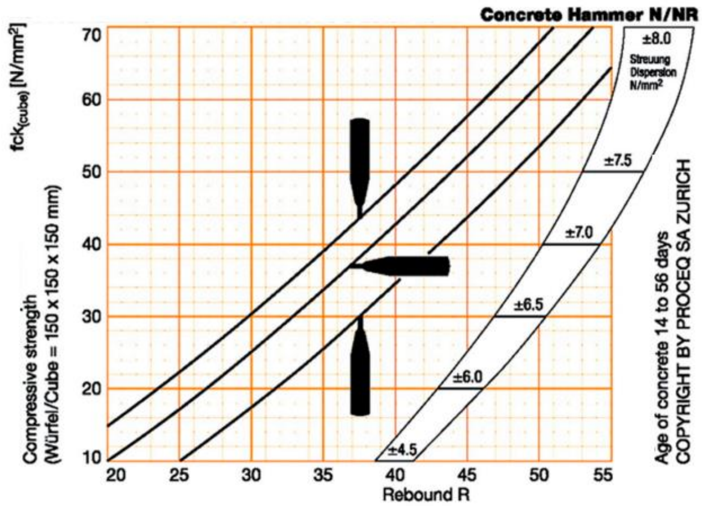

Figure 2.8: Correlation curve provided by the device manufacturer (Proceq, 2017)

The RN test is standardized in ASTM C805 and BS 1881: Part 202. It is important to mention that only the test procedure is given, and no correlation curve or equation is provided to use. In Table 2.2, the most important codes and guidelines related to the rebound test on concrete are listed, of which the most comprehensive guideline in this field was proposed by the International Atomic Energy Agency (IAEA).

Table 2.2: List of important codes and guidelines for rebound hammer test

Name	Proposed By
- ASTM C805 / C805M – 18: Standard test method for rebound number of hardened concrete	American Society for Testing and Materials, 2018
- Training course series no. 17: Guidebook on non-destructive testing of concrete structures	International Atomic Energy Agency (IAEA), 2002
- JGJ/T 23: Technical specification for inspection of concrete compressive strength by rebound method (In Chinese)	Chinese Standard, 2001
- FHWA-SA-97-105: Guide to Nondestructive Testing of Concrete	U.S Federal Highway Administration, 1997
- IS 13311: Part 2: Nondestructive testing of concrete methods of test - rebound hammer	Indian Standards, 1992
- BS 1881: Part 202: Recommendations for surface hardness testing by rebound hammer	British Standard, 1986

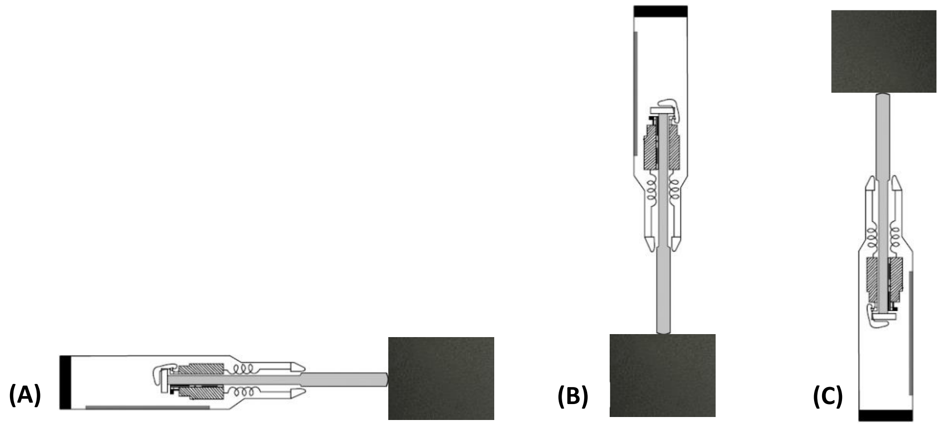

Figure 2.9: RN test direction: (A) horizontal, (B) vertical downward, and (C) vertical upward

The RN test can be conducted in three different directions as shown in Fig. 2.9, enabling its use for various types of structural elements such as beams, columns, and foundations. Therefore, due to the simplicity of the test and the low cost of the machine, the RN test has become one of the most common methods of assessing the compressive strength of concrete. Over the past few decades, research has shown that this test is not accurate on its own and therefore cannot be used solely to determine the compressive strength of concrete. The RN test only provides information of the concrete surface with depth between 30 to 50 mm (as shown in Fig. 2.10) and is not representative of all of the concrete (Asteris & Mokos, 2020; Brencich et al., 2013; Breysse, 2012; Kim et al., 2009; Kolek, 1969; Kumavat et al., 2021; Szilágyi et al., 2011). In other words, considering that concrete is a heterogeneous material, and approximately 5 cm thick concrete cover in reinforced concrete members, it can be concluded that the test indirectly estimates the compressive strength of concrete based on the surface hardness of the cover of RC members.

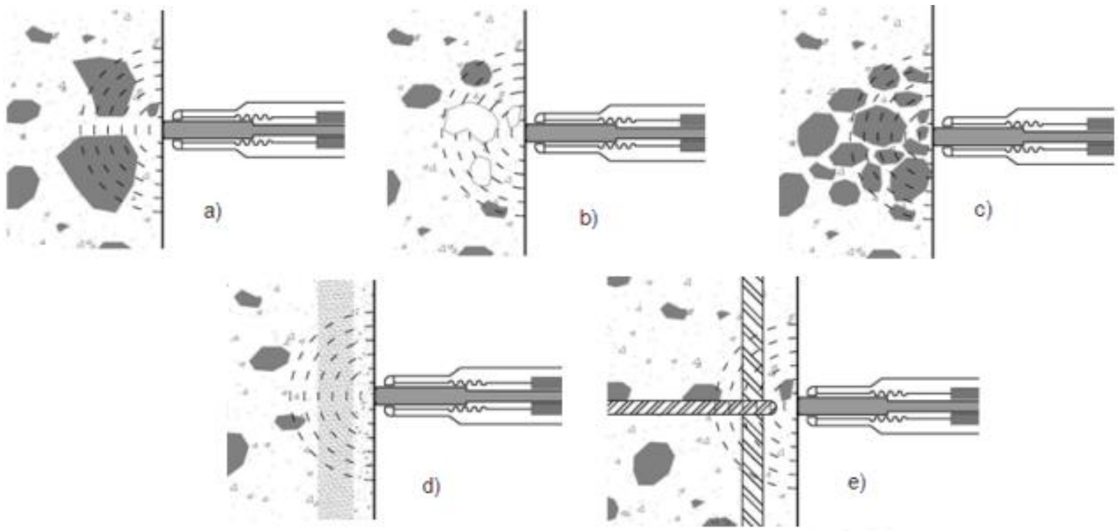

Figure 2.10: Local factors that affect the rebound test; a) large gravel; b) voids; c) gravel aggregate; d) bleeding; e) rebars close to the surface (Brencich et al., 2013)

Several factors such as surface finishing, aggregate percentage, the maximum size of aggregate, humidity, concrete maturity, dimension and location of the reinforcement, concrete mixture properties, age of concrete, and distance from the free edges can all have an influence on the results (Fig. 2.10) (Brencich et al., 2013; Kim et al., 2009; Kolek, 1969; Szilágyi et al., 2011). Table 2.3 gives the most important factors affecting rebound test results. However, it is not possible to give an exact relationship or correction curve for each of these factors.

Table 2.3: List of influencing factors on rebound number

Factor	Level	Note	Ref.
Voids and crack	High	- Voids have a direct impact on rebound number based on the location and distance from the device.	Breysse et al., 2019
Age (carbonation)	High	- "The rebound value is affected by the rise in carbonated concrete surface hardness" - "Rebound numbers can be up to 50% higher than those obtained on an uncarbonated concrete surface" (Agency, 2002)	Agency, 2002
Hardness and density of aggregate	High	- Increase in rebound number	Breysse, 2012
Maximum size of aggregate	Average	- Increase in rebound number	Breysse, 2012
Humidity	Average	- "Concrete in a moist condition gives a lower reading than concrete in a dry condition" - "Hammer readings are influenced more by surface moisture than by hammer position"	Grieb, 1958; Mehta & Monteiro, 2005; Monteiro & Gonçalves, 2009; Willetts, 1958
Surface condition (Curing condition and framework)	Average	- Research has shown that troweled surfaces or surfaces formed by metal forms yield rebound numbers 5 to 25 percent higher than surfaces cast against wooden forms. - "Readings are taken on a polished surface are high, whereas readings were taken on a rough surface (such as a broomed surface) are low"(Grieb, 1958)	Crawford, 1997; Grieb, 1958
Thickness, shape and size of specimen	Average	- The rebound number for the cylindrical sample is lower than cubic sample (~75%). - A decrease in the specimen size leads to increasing the rebound number.	Poorarbabi et al., 2021; Yang et al., 2018
Temperature	Moderate	- High temperature may be increased in rebound number.	Bodnarova et al., 2013; Brozovsky & Bodnarova, 2016
Others: Percentage of cement Type of cement Type of aggregate Self-compacting or regular vibrated concrete Hammer direction	Moderate to Average		Kazemi et al., 2019; Kovler et al., 2018; Nepomuceno & Bernardo, 2019

Since the introduction of the Schmidt hammer, researchers have been trying to present a model, mathematical relation, or correction curve to accurately predict the compressive strength of concrete using only the Schmidt hammer. These studies have resulted in various models for different boundary conditions, which are given in Table 2.4. However, none of these models and mathematical relations can be applied in general practice because each of them considers only one or two influence factors in the rebound test and cannot account for all of the factors listed in Table 2.3. Research has indicated that the compressive strength of concrete cannot be directly correlated by a single function. Therefore, a model with multiple functions is needed. Thus, the empirical equations and curves proposed could only be used within the boundary condition (influence factors) of a particular study.

Table 2.4: Information about relationships between compressive strength of concrete and rebound number

Type of Model	Form of Equation	Ref.
Power	$f_c = a \times R^b$	Balakrishna et al., 2017; Brencich et al., 2013; Brozovsky, 2014; Brozovsky & Bodnarova, 2016; Di Leo et al., 1984; El Mir & Nehme, 2017; Greene, 1954; Kheder, 1999; Lima & Silva, 2000; Nash't et al., 2005; Pascale et al., 2003; Szilágyi et al., 2015; Yang et al., 2018
Linear	$f_c = (a \times R) + b$	Abdulkadir et al., 2017; Agunwamba & Adagba, 2012; Aydin & Saribiyik, 2010; Brozovsky & Bodnarova, 2016; "EN 13791, 2007; Hajjeh, 2012; Hobbs & Kebir, 2007; Kim et al., 2009; Monteiro & Gonçalves, 2009; Qasrawi, 2000; Shariati et al., 2011; Soshiroda et al., 2006; Zabihi, 2012
Polynomial	$f_c = (a \times R^2) + (b \times R) + C$	Brencich et al., 2013; Brozovsky, 2014; Brozovsky & Bodnarova, 2016; Di Leo et al., 1984; Lima & Silva, 2000; Mikulić et al., 1992; Nash't et al., 2005; Pascale et al., 2003; Proceq, 2003; Szymanowski & Sadowski, 2020
Exponential	$f_c = a\ exp\ (b \times R)$	Malhotra & Carino, 2003
Note: f_c: compressive strength of concrete R: rebound number a , b , c: constant value (based on boundary condition of experimental research e.g.; age, aggregate type, …)		

In recent years, the Proceq Company has introduced a new type of Schmidt hammer to the industry to evaluate the strength of stone and concrete called "Silver Schmidt" (Fig. 2.11(b)). It works with optical measurement technology to measure the impact and rebound velocity immediately before and after (real-time). This device can measure concretes of lower as well as higher strength and is also used to test very young concrete. The measurement accuracy has increased in comparison with the original Schmidt hammer but does not overcome all of the challenges associated with evaluating the strength of concrete discussed above.

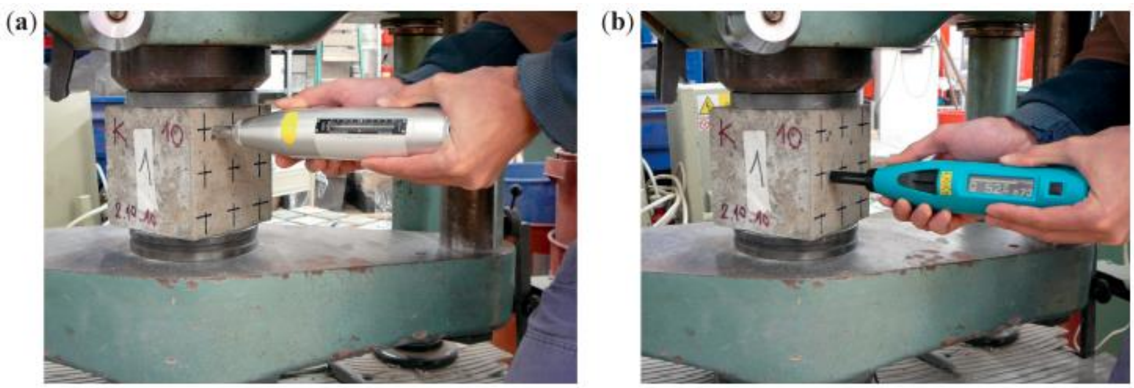

Figure 2.11: (a) Original Schmidt; and (b) Silver Schmidt (Kocáb et al., 2019)

2.2.2 UPV Test

Unlike the Schmidt hammer, which determines the strength based on the hardness of the concrete surface, the UPV test evaluates the internal properties of the concrete. It is worth mentioning that the UPV has traditionally been used for the quality control of materials such as concrete.

UPV testing is utilized to evaluate the integrity of structural concrete by measuring the velocity of compressive stress waves passing through a member to evaluate the density and elastic properties of the material (Malek & Kaouther, 2014; Poorarbabi et al., 2021). Fig. 2.12 shows the function of the UPV test. As shown in Fig. 2.13, three configurations are used for the UPV test on RC members; direct, semi-direct, and indirect.

The pulse velocity technique is an efficient method to evaluate the quality of the concrete because it depends only on the elastic properties of the material and is independent of the geometry of the specimen. According to previous studies, there are several reasons that UPV test readings are correlated to concrete strength. Firstly, in the first days after casting the concrete when hardening occurs, it is observed that the velocity of ultrasonic waves in concrete increases significantly. Moreover, theoretical considerations support the existence of a direct relationship between Young's modulus and wave velocity in an elastic condition. Finally, between Young's modulus and strength, empirical relationships have long been established (Agunwamba & Adagba, 2012; Breysse, 2012; Rajabi et al., 2020).

The UPV test is standardized in ASTM C597, which is the main reference for this test, although the guidelines provided by the International Atomic Energy Agency are much more comprehensive (ASTM C597 – 16, and IAEA, 2002).

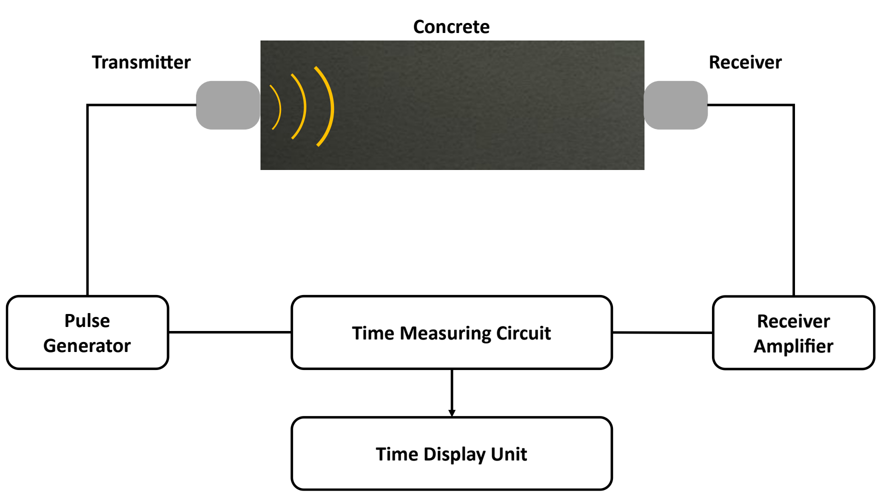

Figure 2.12: Schematic of Ultrasonic Pulse Velocity (UPV)

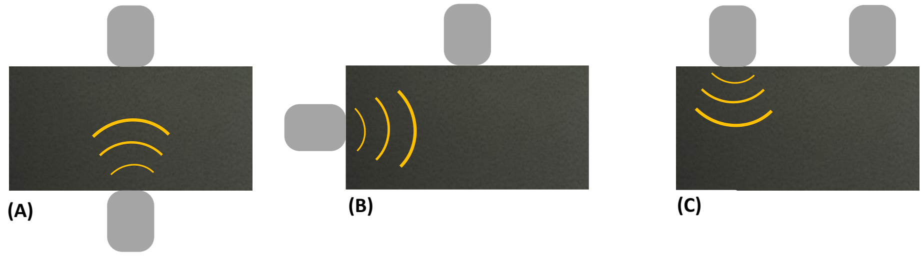

Figure 2.13: (A) direct, (B) semi-direct, and (C) indirect UPV test

As shown in Fig. 2.12, the equipment includes a transmitter, a receiver, and a device to show the transformation time where the pulse velocity is defined as following:

$V = \frac{L}{t}$ (Eq. 1)

Where; V: pulse velocity (km/s), L: path length (mm), and t: transmit time (μs).

Table 2.5 proposed by Whitehurst shows how the values of the obtained UPV can be used to classify the quality of concrete (Whitehurst, 1951).

Table 2.5: Quality of concrete with respect to UPV (Whitehurst, 1951)

Ultrasonic pulse velocity (m/s)	Quality of concrete
Above 4500	Excellent
3500–4500	Generally good
3000–3500	Questionable
2000–3000	Generally poor
Below 2000	Very poor

Two forms of electronic timing apparatus and displays are available, one of which uses a cathode ray tube on which the received pulse is displayed in relation to a suitable time scale, the other uses an interval timer with a direct reading digital display (IAEA, 2002; Poorarbabi et al., 2021). The IEAE guideline for NDT suggests using high-frequency transducers for short path lengths and low-frequency transducers for long path lengths. Also, IAEA recommends using the range of transmitter frequency as mentioned in Table 2.6 (IAEA, 2002).

Table 2.6: Suitable frequency for different UPV test condition based on IAEA's guideline

Frequency	Used for
10 kHz	- long concrete path
50 ~ 60 kHz	- normal condition
1 MHz	- short concrete path - mortar - grout

According to previous studies on evaluation of concrete strength using the UPV test, it has been determined that several factors affect this test that have made it difficult to obtain the compressive strength of concrete accurately. Table 2.7 lists the most important influencing factors on the UPV test. In 1981, Samarin and Meynink conducted a comprehensive study on UPV and reported that "the range of variation of velocity with time is much lower when concrete is older than 28 days: sensitivity of UPV to the rate of concrete strength is extremely high in the first few days but considerably lower after about 5–7 days, depending on curing conditions" (Breysse, 2012; Samarin & Meynink, 1981).

Moreover, another important problem is that reinforcing bars in the concrete cause errors in the test. Rebars provide an easier path for wave propagation at a higher velocity in comparison with concrete. It is recommended to detect the location of rebars first, then measure UPV at regions where the influence of rebar can be neglected (Fig. 2.14(a)). This problem also applies to cracks (Fig. 2.14(b)) (Breysse, 2012; Fodil et al., 2019; Kalyan & Kishen, 2013; Lencis et al., 2011).

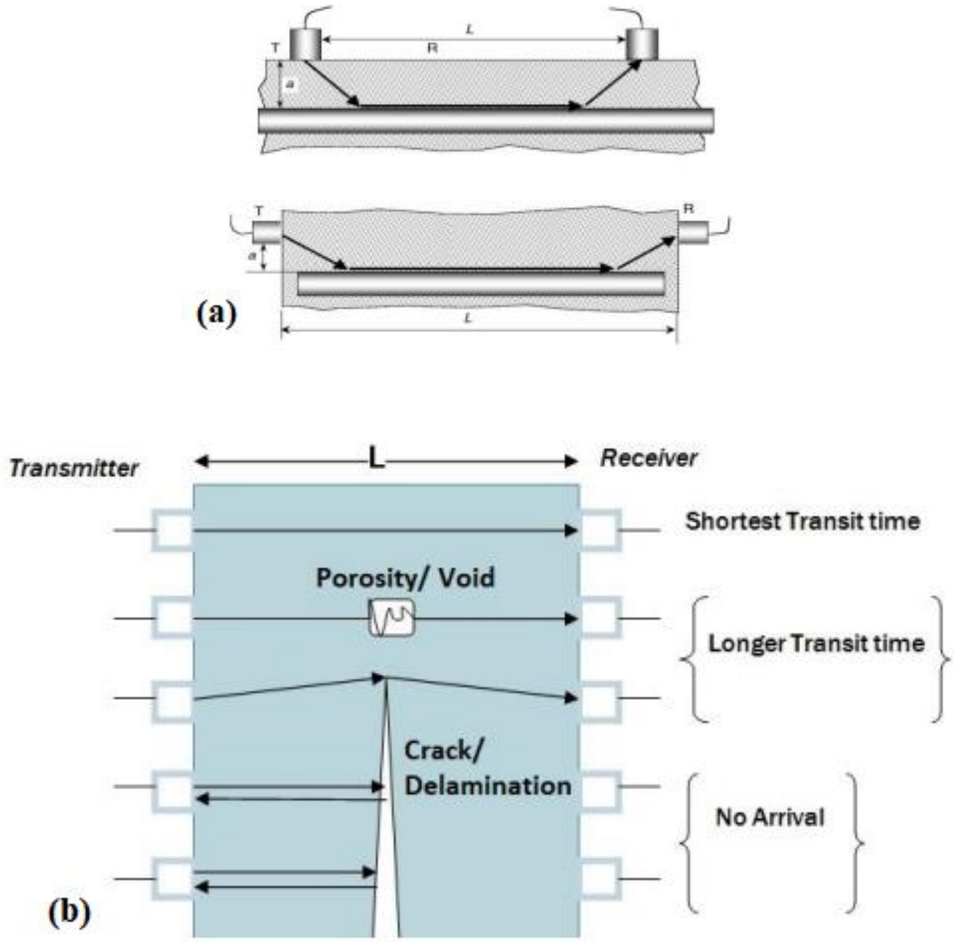

Figure 2.14*:* (a) the effect of rebar's location on UPV (Naik et al., 2003), (b) the effect of cracks and voids on UPV (Jain et al., 2021)

Table 2.7: List of influencing factors on UPV test

Factor	Level	Note	Ref.
Cracks and voids	High	- Its effect is based on the position of the crack in the concrete and configurations of UPV test. - The cracks changed the direction of the path of pulse travelling between transmitter and receiver. - "The UPV value decreases when the oxygen permeability and porosity of the sample material are increased."(Ngo et al., 2021)	Breysse, 2012; Ikpong, 1993; Kalyan & Kishen, 2013; Ngo et al., 2021
Aggregate; • percentage of aggregate • type of aggregate • density of aggregate • aggregate textural properties • maximum size of aggregate	High to Average	- "larger aggregate results in a higher pulse velocity" (Ngo et al., 2021) - "As the surface roughness value of the aggregates increases, the UPV is increased" (Güçlüer, 2020)	Güçlüer, 2020; Ngo et al., 2021; Selçuk & Nar, 2016
Sand to aggregate (s/a) volume ratio	High	- "With the increase of s/a ratio, UPV of concrete is reduced" (Mohammed & Rahman, 2016)	Mohammed & Rahman, 2016; Molero et al., 2009
Rebars	High		Breysse, 2012; Fodil et al., 2019; Lencis et al., 2011
Water to cement (w/c) ratio	High		Breysse, 2012
Temperature	Moderate	- The effect of temperature can be neglected in the range of 0 C to 30 C. - Few studies reported that there is an influence for hot or cold weather, for example: "A further increase in temperature of 10°C increases UPV of average 34 m/s" (Güneyli et al., 2017).	Breysse, 2012; Güneyli et al., 2017
Fly ash content	Average		Breysse, 2012
Humidity (water content)	Average to Moderate	- May increased in pulse velocity to 5% (Between the air-dry and saturated condition)	Breysse, 2012; Bungey & Grantham, 2006; Güneyli et al., 2017
Percentage of cement	Moderate		Breysse, 2012
Type of cement	Moderate		Breysse, 2012
Curing condition	Moderate to Average	- "Longer curing period increases the UPV because the ratio of gel/space changes during a longer curing period"(Ngo et al., 2021)	Mohammed et al., 2011; Ngo et al., 2021; Ulucan et al., 2008
Age	Moderate		Kou et al., 2012; Ngo et al., 2021

According to the boundary conditions, many equation forms are proposed to evaluate the strength of concrete with the UPV test that are given in Table 2.8 (Breysse, 2012), which can be calibrated with experimental results.

Table 2.8: information about relationships between compressive strength of concrete and UPV, (Breysse, 2012)

Type of Model	Form of Equation	Ref
Power	$f_c = a \times V^b$	Breysse, 2012
Linear	$f_c = (a \times V) + b$	MacLeod, 1971
Polynomial	$f_c = (a \times V^2) + (b \times V) + C$	Knaze & Beno, 1984
Exponential	$f_c = a\, exp\, (b \times V)$	Facaoaru, 1961; Klieger, 1957
Note: f_c: compressive strength of concrete V: UPV value a , b , c: constant value (based on boundary condition of experimental research e.g.; age, aggregate type, …)		

2.3 Combination of NDT Methods (SonReb)

Due to the fact that the relationships and models presented to evaluate the compressive strength of concrete based on the results of the RN or UPV are not reliable and each proposed model has only considered specific boundary conditions in the NDT-strength relationship, researchers have attempted to combine NDT methods to improve the accuracy of compressive strength predictions and reduce their sensitivity to the influencing parameters discussed earlier. Based on this, many different models and equations have been proposed (Breysse, 2012; Kayed, 2021; Liu et al., 2009).

The combination between the RN test and UPV, known as the “SonReb method”, is one of the most famous combined approaches developed by RILEM Technical Committees (RILEM, 1993). The main advantage of SonReb is that the compressive strength of concrete can be evaluated at both the surface and in-depth levels of concrete. A few other methods have also combined NDT tests with semi-destructive tests like penetration and pull-out test. The ‘‘SonRebWin’’ is a method that comes from the combination of the SonReb with a third technique like penetration test (Breysse & Martínez-Fernández, 2014; Cabral-Fonseca et al., 2018; Erdal, 2009; Liang & Wu, 2002; Moczko, 2009; Pucinotti, 2015; Yoo & Ryu, 2008).

The SonReb method is the most widespread NDT combination method. Based on this method, many models and equations have been proposed to predict the concrete strength. These models can be divided into three general categories as shown in Fig 2.15. The following is a brief overview of traditional regression models, while artificial intelligence models are reviewed in more detail.

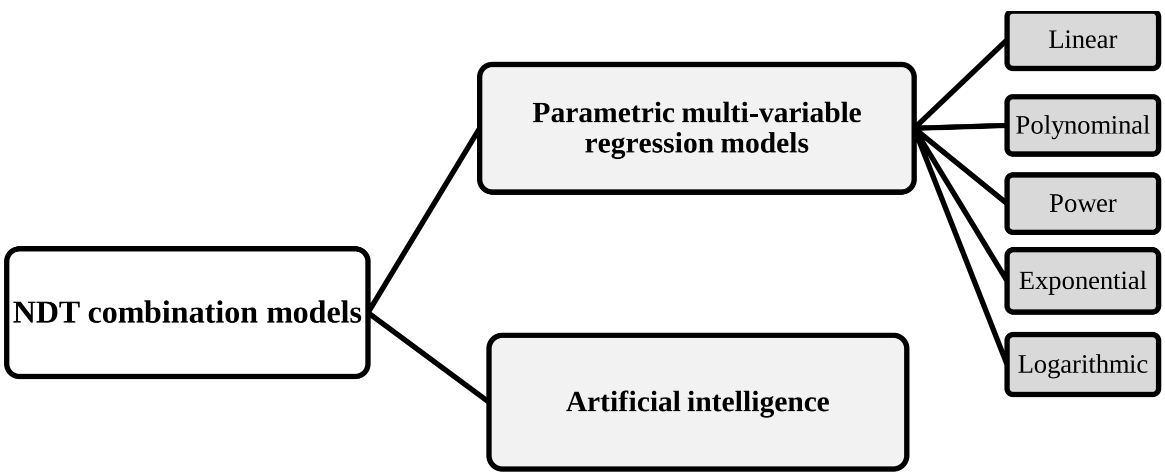

Figure 2.15: Flowchart of NDT combination models

Some studies have used parametric multi-variable regression models to propose correlation formulas for the prediction of compressive strength using destructive test results on cores drilled in adjacent locations (Alwash et al., 2015; Bonagura & Nobile, 2021; Nobile, 2015; Nobile & Bonagura, 2014). In 2020, Cristofaro and Tanganelli checked the reliability of seventeen commonly used models with experimental data. They reported that “some formulations should not be always considered trustworthy, since they can largely overestimate the mechanic features of the construction material" (Cristofaro et al., 2020).

Cristofaro at al. checked the accuracy of the equations with experimental results; Fig. 2.16 shows the mean square error (MSE) for each equation. Regression methods have shown less accuracy in concrete strength predictions when applied to diverse datasets. This result has been confirmed by other researchers; for example, in 2021, Ngo et al. reported that: "traditional concrete compressive strength estimations have a mean absolute percentage error (MAPE) of over 20% when compared to the actual compressive strength obtained by destructive tests" (Ngo et al., 2021).

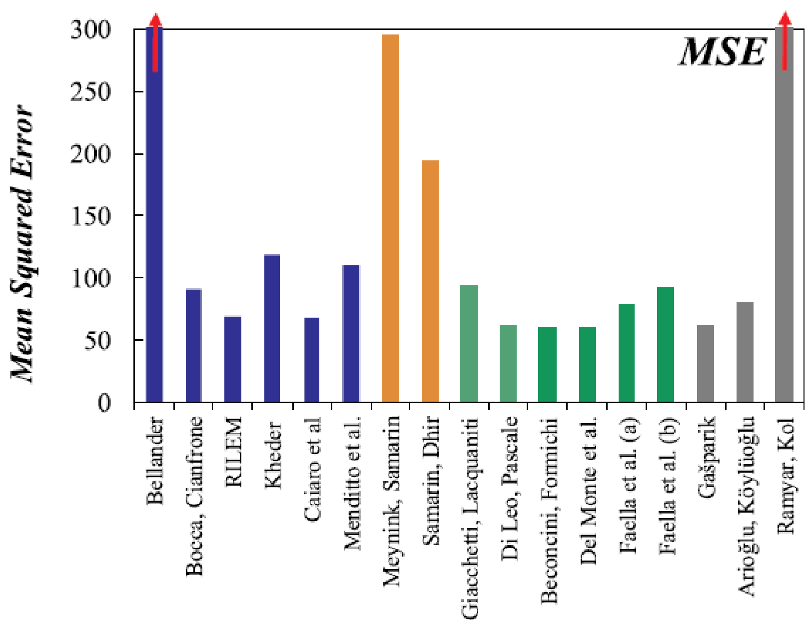

Figure 2.16: Concrete strength provided by the considered models in Cristofaro et al.'s study., 2020

According to Cristofaro et al.'s study, the average percentage difference between the experimental value and the predicted value of compressive strength was 136% based on Bellender's equation. However, Chingalata et al. evaluated the accuracy of equations based on their experimental data and they reported the average percentage difference between the experimental value and the predicted value of compressive strength was 66.19% based on Bellender's equation (Chingălată et al., 2017; Cristofaro et al., 2020). In other words, the equations' accuracy varied according to the datasets, which highlights the main problem that makes current models unreliable to be used without calibration in the construction industry; hence, it is still necessary to extract cores to confirm model validity. New codes have attempted to reduce the number of core tests that are needed and reduce the size of the cores (EN 13791: 2019; Sefrin & Glock, 2022), but these key challenges remain.

An alternative approach is computational modeling which is based on the modeling of complex physical phenomena and thus is usually not practical (Bonagura & Nobile, 2021; Kayed, 2021). For this reason, these models have not been reviewed in this study.

2.4 Artificial Intelligence (AI)

In the 1950s, John McCarthy defined the term "Artificial Intelligence" as "the science and engineering of making intelligent machines" (Andresen, 2002). During past decades, AI has made significant progress to enable computer systems (machines) to perform tasks that used to require human intelligence such as: making decisions, solving complex problems, increasing the accuracy of systems, and object detection. Various categories have been defined for subsets of AI, but the most famous and well-known ones are given in Fig. 2.17 (Namatherdhala et al., 2022; Thai, 2022; Valarmathi et al., 2021).

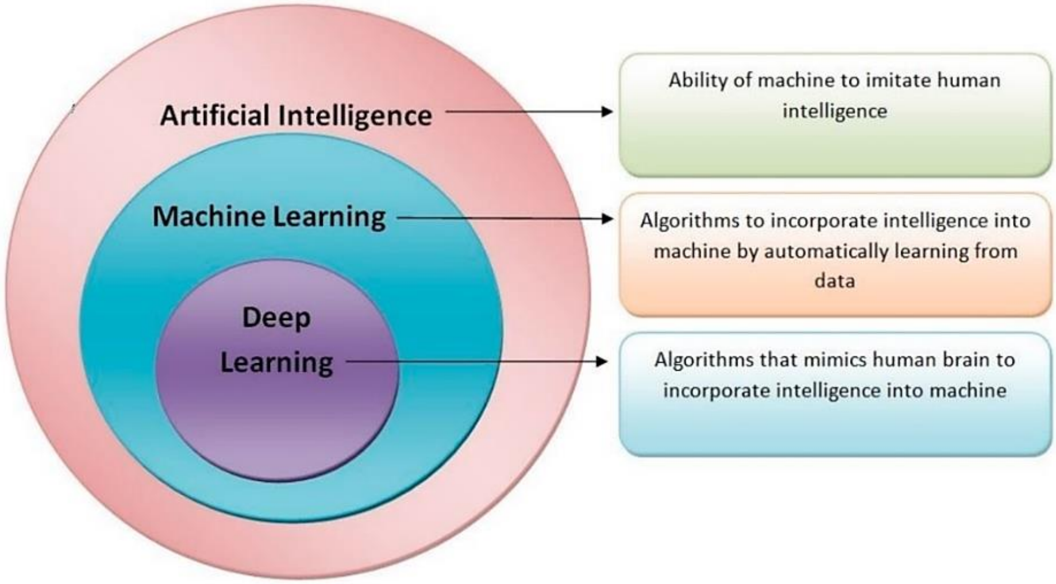

Figure 2.17: The subsets of AI and their brief definition (Namatherdhala et al., 2022)

2.4.1 Machine Learning

Machine Learning (ML) is arguably the most important subfield of AI. It is a process that teaches machines (computers) how to learn new things from data. Using ML algorithms, computers find relationships between input and output parameters of a dataset. After an initial learning process, the machine can make decisions for new input data without human intervention. Fig. 2.18 shows a typical ML flowchart used for prediction and forecasting modelling. According to Fig. 2.18, two sets of data usually are used in the modelling procedure: training data and testing data. Applying a learning algorithm to the training data, the computer "learns" potential relationships between input and output data. Typically, ML models are improved by increasing the size of the training dataset until the target performance is achieved. The testing data are then used to evaluate the performance of the model (Thai, 2022).

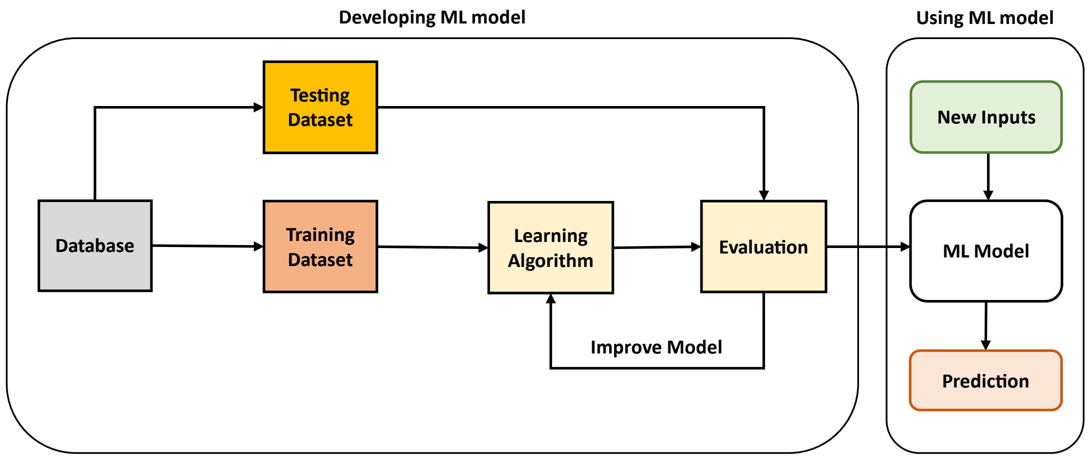

Figure 2.18: The flowchart of building Machine Learning (ML) models

Using ML techniques can approach more accurate and more rational solutions to complex problems, with fewer cost calculations and errors (Naderpour & Alavi, 2017). In recent years, for the prediction of compressive strength of concrete with NDT, basic research is in the process of being conducted and no practical model has been presented yet. However, the studies in this field show encouraging results (Asteris & Mokos, 2020; Bilgehan & Turgut, 2010; Bonagura, 2012a; Bonagura & Nobile, 2021; Chopra et al., 2016, 2018; Khashman & Akpinar, 2017; Mishra et al., 2020; Poorarbabi et al., 2020; Subaşı et al., 2013; Thapa et al., 2021; Wang et al., 2018).

2.4.2 Current ML models

In order to investigate the challenges and progress in this field, all AI models for concrete strength predictions that were developed using UPV and RN are presented below in chronological order.

In 2009, Na et al. investigated the application of Neuro-Fuzzy (also known as Adaptive Neuro-Fuzzy Inference System (ANFIS)) concrete strength prediction using combined UPV and RN tests (Na et al., 2009). Na et al. developed four ANFIS models with different inputs as shown in Table 2.9. They wanted to consider the main parameters that affect the strength and reflect the in-situ conditions of the concrete through NDT results. For the training of models, they used 1551 collected data from previous studies. Then, the trained models were tested with experimental datasets; 20 cube specimens and 210 cylinders were prepared, and compressive tests and NDTs were conducted on them to test the models. Cubic specimens were considered for NDT and cylindrical specimens for compressive tests (5 mix proportions × 7 ages × 2 curing conditions). They prepared concrete specimens with a w/c ratio of 30, 40, 50, 60, and 70% and at the ages of 3, 7, 14, 28, 90, 180, and 365 days in two curing conditions (in water or air). In Table 2.9, the MAPE is the mean absolute percentage error, and the R^2 is the correlation coefficient between the actual compressive strength and the predicted value of strength. They showed that by considering both UPV and RN, the accuracy of the model increased. Also, they reported that neuro-fuzzy models could be a reliable tool to predict compressive strength of concrete in comparison with costly experimental tests. Finally, they suggested involving other input parameters such as cement grade, maximum aggregate size, curing temperature, and air entrainment to improve the accuracy of future models (Na et al., 2009).

Table 2.9: Input specifications of different models and accuracy of their results, from Na et al., 2009

Model	ANFIS-B	ANFIS-U	ANFIS-R	ANFIS-UR
Inputs	1) w/c ratio 2) sand/aggregate ratio 3) unit weight of cement 4) unit weight of sand 5) unit weight of gravel 6) unit weight of water 7) superplasticiser (%) 8) unit weight of fly ash 9) unit weight of silica fume 10) unit weight of slag 11) age 12) curing condition	1) w/c ratio 2) sand/aggregate ratio 3) unit weight of cement 4) unit weight of sand 5) unit weight of gravel 6) unit weight of water 7) superplasticiser (%) 8) unit weight of fly ash 9) unit weight of silica fume 10) unit weight of slag 11) age 12) curing condition 13)UPV	1) w/c ratio 2) sand/aggregate ratio 3) unit weight of cement 4) unit weight of sand 5) unit weight of gravel 6) unit weight of water 7) superplasticiser (%) 8) unit weight of fly ash 9) unit weight of silica fume 10) unit weight of slag 11) age 12) curing condition 13) rebound number	1) w/c ratio 2) sand/aggregate ratio 3) unit weight of cement 4) unit weight of sand 5) unit weight of gravel 6) unit weight of water 7) superplasticiser (%) 8) unit weight of fly ash 9) unit weight of silica fume 10) unit weight of slag 11) age 12) curing condition 13)UPV 14) rebound number
Output	Compressive strength	Compressive strength	Compressive strength	Compressive strength
Model prediction accuracy (for testing data)				
R^2	0.95	0.97	0.981	0.983
MAPE (%)	27.42	18.24	16.01	10.99

In 2012, Bonagura applied artificial neural networks (ANNs) to non-destructive testing (NDT) methods. Bonagura compared two cases of ANN models: the first using a single input, which was the UPV value, and the second using two inputs, the UPV and RN (SonREB), to predict concrete strength. The data used in this study is unclear and appears to be based on only 16 data points. Additionally, the research seems to focus on the ANN's hidden layer parameters (Bonagura, 2012b).

In 2015, Shih et al. proposed an AI model using the Support Vector Machines (SVMs) method to estimate the compressive strength of concrete. They developed three SVM models with different input variables using MATLAB: RN only (Model.1), UPV only (Model.2), and RN + UPV (Model.3), then compared the results. For this purpose, they collected 95 data (12*24 cm cylinder samples) from other researchers to develop and validate their models. Of these, 85 samples (~89%) were randomly selected for training and the remaining 10 data were used for testing for each of the three different models. In Table 2.10, the output results of each model are compared to experimental results (compressive test results of samples). They considered mean absolute percentage error (MAPE) to evaluate the accuracy of their models. According to Table 2.10, the combined NDT (i.e., SonReb) gives better results in comparison with single input models. Also, they reported that the SVM model improves the NDT estimation for concrete compressive strength. However, they did not compare their results with the available SonReb models (empirical equations).

Table 2.10: SVMs model prediction accuracy by Shih et al., 2015

No.	Input(s)	Mean Absolute Percentage Error (MAPE) (%)
Model.1	RN	8.92%
Model.2	UPV	9.25%
Model.3	RN+UPV	6.77%

In 2015, Demir used the ANN method to predict the strength of fiber-reinforced concrete. In addition to the compressive strength, their model also predicted the bending strength of concrete with the NDT tests. As shown in Fig. 2.19, the model had five inputs and two outputs. For the datasets, 105 cylindrical specimens (150 × 300 mm) and 105 specimens with dimensions of 100 x 100 x 400 mm (for bending tests) were fabricated and then used for NDT and DT. 70% of the data were selected randomly for the training dataset and the remaining 30% were selected for the testing dataset. The R^2 value between the measured and predicted compressive strengths for the testing dataset was 0.995, and for the next output parameter, bending strength, this value was equal to 0.975 (Demir, 2015).

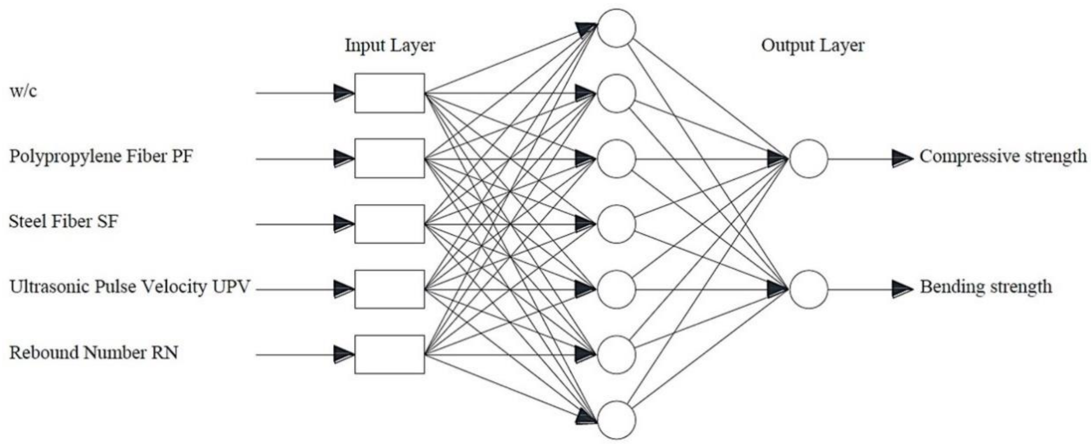

Figure 2.19: The architecture of Demir's ANN model (Demir, 2015)

In 2015, Kumar and Kumar predicted the compressive strength using Genetic Programming (GP) and NDT results. For this purpose, 100 cubes (150 mm) with different grades of concrete were casted and then tested to build the datasets. 70% of the data were selected for training and 30% for testing. Two different GP models were developed: the first model had two inputs; the weight of specimens and RN, the second model had three inputs; weight, RN, and UPV value. They reported that the models predicted the strength value with 6.74 % and 7.44% error respectively (Kumar & Kumar, 2015).

In 2016, Nobile and Bonagura compared three methods that are used to predict compressive strength based on the SonReb measurements: computational modeling, AI, and parametric multi-variable regression models. The ANN method was selected for the AI approach, and 16 data from in-situ compressive strength tests were used for their study. They reported that the ANN approach provided the best performance in their study; however, no additional details were given (Nobile & Bonagura, 2016).

In 2018, Wang et al. proposed an adaptive ANN model to estimate the concrete compressive strength using UPV and RN test data. For this purpose, they tested 315 cylinder samples (15*30 cm) to develop and validate the prediction model. They reported that "with the proposed model, the estimation error of SonReb test can be reduced to 5.98% (measured by MAPE)" (Wang et al., 2018). However, it should be noted that no information was provided about the data or their modeling procedure.

In 2019, Sai and Singh developed seven ML models with different inputs based on three NDT methods (RN, UPV, and Windsor Penetration). The SVM method and the data from the tests on 350 cubic (150 mm) specimens were used to create the models. The input variables and coefficient of determination (R^2) value of each model are given in Table 2.11. They did not share detailed information about their database, simply reporting that 70% of the data was used for training and 30% for testing. It was reported that for the single NDT technique, strength prediction using RN was the most reliable method with a coefficient of determination of 0.902, and for the combination NDT models, a higher value of the coefficient of determination of 0.925 could be achieved with the combination of the RN and Windsor Penetration (Sai & Singh, 2019). It is important to mention that Windsor Penetration is considered to be a semi-destructive test, and to judge the results of this study detailed information of the data is needed, which unfortunately has not been provided.

Table 2.11: The coefficient of determination (R2) for seven ML models, by Sai and Singh, 2019

No.	Number of inputs	Test Method	R^2
1	1	RN	0.902
2	1	Windsor' Penetration	0.821
3	1	UPV	0.745
4	2	RN + Windsor' Penetration	0.925
5	2	Windsor' Penetration + UPV	0.702
6	2	UPV + RN	0.8612
7	3	RN + Windsor' Penetration + UPV	0.8647

In 2020, Asteris and Mokos investigated the application of ANNs for predicting the compressive strength of concrete in existing structures. They developed six ANN models in MATLAB with different neural network architectures; two models with one input of UPV, two models with one input of RN, and two models with two inputs of both UPV and RN. The database is an important part of any AI model; accordingly, they reported that the experimental database should include the features presented in Table 2.12 (Asteris & Mokos, 2020).

Table 2.12: The features of experimental data for the development of AI models by Asteris and Mokos, 2020

No.	Features
1	Sufficient experimental data that cover all cases. (Note: A higher amount of data can be harmful if the data is not correct.)
2	All data are obtained under the same environmental conditions. • All samples must be made to the same standards at the same time, • Tests should be done by the same devices, • Experimental samples should be created and tested by only one researcher (or the same researchers).
3	Tests should be done by accurate and reliable devices.

For this purpose, they used a database consisting of 209 datasets based on experimental results from a PhD thesis that was done in 1978 at the National Technical University of Athens; 36 batches of cubic concrete specimens where each batch consisted of 6 specimens (Asteris & Mokos, 2020; Logothetis, 1978). The optimum model was the model that considered both UPV and RN. Moreover, they compared the results of the ANN model with the results of 14 empirical equations from other researchers. In Table 2.13, they ranked the models based on the accuracy of the results for the estimation of concrete compressive strength. In Table 2.13, RMSE is the root mean square error and R^2 is the correlation coefficient, that the lower RMSE represents the more accurate prediction results and the higher R^2 values represent a greater fit between the analytical and predicted values (Asteris & Mokos, 2020).

Table 2.13: Ranking of models for the estimation of concrete strength by Asteris and Mokos, 2020

No.	Model	Input parameters	R^2	RMSE
1	ANN	UPV + RN	0.9891	1.47
2	Equation of Logothetis	RN	0.9521	2.18
3	Equation of Logothetis	UPV + RN	0.9342	4.19
4	Equation of Logothetis	UPV	0.8198	4.23
5	Equation of Kheder	UPV + RN	0.9759	5.15
6	Equation of Kheder	RN	0.9745	5.90
7	Equation of Qasrawi	RN	0.9732	5.56
8	Equation of Trtnik et al.	UPV	0.8119	7.71
9	Equation of Nash't et al.	UPV	0.9032	6.59
10	Equation of Erdal	UPV + RN	0.9421	7.09
11	Equation of Amini et al.	UPV + RN	0.8961	8.27
12	Equation of Kheder	UPV	0.8942	7.46
13	Equation of Arioglu et al.	UPV + RN	0.9535	8.13
14	Equation of Qasrawi	UPV	0.8893	12.24
15	Equation of Turgut	UPV	0.9035	12.84

In 2020, Poorarbabi et al. investigated two different methods using ANN and Response Surface Methodology (RSM) to estimate the strength of concrete by using the combination of three non-destructive tests: UPV, RN, and a third NDT parameter which is surface electrical resistivity (SR) were considered in this research (Poorarbabi et al., 2020). The SR test is used to estimate concrete permeability. According to their research, a connection exists between the electrical resistivity of concrete and the deterioration processes such as an increase in permeability and corrosion of embedded steel (Azarsa & Gupta, 2017). The response surface methodology (RSM) is a statistical and mathematical method that explores the relationships between several explanatory variables and one or more response variables. This method is useful for analyzing experiments in which one or more independent variables (as responses) are affected by many variables and the goal is to optimize the response (Box, 1951).

Poorarbabi et al. conducted tests on 180 concrete specimens with 20 different concrete mix designs at three different ages (7, 28, and 90 days of age). They considered the age of concrete as a boundary condition in their study. First, they developed RSM and ANN models with two inputs (UPV and RN), then developed RSM and ANN models with three inputs (UPV, RN, and SR). According to their results that are given in Table 2.14, they reported that "the accuracy of RSM and ANN are increased by adding SR to the combination of UPV and RN in all of the ages". The results show that both RSM and ANN are in good agreement with experimental data for estimating the strength of concrete (Poorarbabi et al., 2020).

Table 2.14: Determination coefficient of different approaches by Poorarabi et al., 2020

Method	Inputs Parameters	R^2			
		7 days	28 days	90 days	All data
RSM	UPV+RN	0.863	0.8708	0.9341	0.8676
ANN	UPV+RN	0.8892	0.9262	0.9592	0.9194
RSM	UPV+RN+SR	0.8717	0.9168	0.9370	0.8780
ANN	UPV+RN+SR	0.9094	0.9606	0.9803	0.9449

In 2021, Du et al., predicted the compressive strength of high-performance self-compacting concrete by using a genetic algorithm (GA)-optimized backpropagation neural network (BPNN) method based on RN and UPV. They casted six sets of 100 cubes (150 mm) with concrete grades of C50, C60, C70, C80, C90, and C100 MPa (total 600 cubes) to develop their model. The 600 data were split randomly into three categories: 420 data for training (70%), 90 data for testing (15%), and 90 data points (15%) for verification. Finally, they compare the results of the best BPNN models which is the model with two inputs (RN and UPV) with 14 empirical equations (Table 2.15). They reported that the results of their proposed GA-BPNN model were closest to the experimental results with 0.976 for the correlation coefficient value and 3.36 MPa for the RMSE values (Du et al., 2021).

Table 2.15*:* Concrete compressive strength prediction models ranked by RMSEs, by Du et al., 2021

Rank	Model	Input Parameters	R2	RMSE
1	BPNN	UPV, RN	0.9761	3.360
2	Equation of Qasrawi	RN	0.9490	9.1322
3	Equation of Arioglu et al.	UPV, RN	0.9157	10.6093
4	Equation of Kheder	RN	0.9491	15.5343
5	Equation of Kheder	UPV, RN	0.9485	16.9512
6	Equation of Logothetis	UPV, RN	0.9139	25.5159
7	Equation of Erdal	UPV, RN	0.9063	28.4509
8	Equation of Logothetis	RN	0.9489	29.3858
9	Equation of Turgut	UPV	0.7874	34.9199
10	Equation of Amini et al.	UPV, RN	0.2628	38.1740
11	Equation of Trtnik et al.	UPV	0.7819	41.7633
12	Equation of I.H.Nash’t	UPV	0.7877	42.4471
13	Equation of G.F.Kheder	UPV	0.7879	45.2446
14	Equation of Logothetis	UPV	0.7870	46.4956
15	Equation of G.F.Kheder	UPV	0.7885	48.2633

In 2021, Thapa et al. created an ANN model and two multiple regression analysis models to predict the compressive strength of concrete with different percentages of recycled brick aggregate. They created 189 cubic samples with normal concrete (strength range 20 to 30 MPa). After 7, 28, and 84 days of curing, the samples were tested with RN and UPV then samples were taken for destructive testing to determine their compressive strength (Thapa et al., 2021).

For the ANN model, they considered RN and UPV as the inputs and used randomly 70%, 15%, and 15% of the total data sets (189 data) for training, testing, and validating of the ANN model, respectively. It is worth mentioning that sometimes all data is split into three datasets to develop ANN models. The main difference between testing and validation (or verification) datasets is that the validation dataset is used to optimize the model parameters during the training process (at each training epoch) while the testing dataset is just used to check the accuracy of the final model and does not change training parameters. Allocating validation datasets is an optional procedure.

MATLAB was used to develop the ANN model. Their results showed that the ANN model had the highest correlation (R^2) value between the predicted output and experimental results from testing and had the minimum mean square error (MSE) in comparison with the multiple regression analysis models (bilinear and double powered) (Table 2.16). It is indicated that the ANN model is a reliable tool to predict compressive strength in comparison to the multiple regression models considering physical change effects in concrete. Also, they investigated the influence of inputs on the results; the results show that the RN was given more importance to predict compressive strength in comparison to UPV (Thapa et al., 2021).

Table 2.16: Comparison between different models to predict compressive strength by Thapa et al. (Thapa et al., 2021)

Model Type	R^2	MSE
ANN	0.825	4.943
Bilinear	0.772	9.96
Double powered	0.768	10.5

In 2021, Bonagura and Noble evaluated the performance of the ANN method for predicting concrete compressive strength by SonReb. They developed 9 ANN models with different training parameters. Then the best one was selected and compared with four different correlation formulations (parametric multi-variable regression models). They reported the best performance of the ANN approach in comparison with regression models. However, their process of data collection and comparison of the results is not clear since no information was provided about the experimental dataset, as well as how to compare the results of the neural network model with the results of regression models.

In 2021, Ngo et al. investigated applying different methods of AI to improve on-site NDT for estimating concrete compressive strength. They created several models based on three AI methods (ANN, SVM, and ANFIS) then selected the best model from each method (Table 2.17). For this purpose, they conducted NDT and DT to collect 98 data sets. First, RN and UPV tests were conducted on 98 non-structural beams in the basement of a large residential complex. For each beam, 10 RN measurements were taken with the Silver Schmidt electronic RN. Four UPV measurements were taken at each test location. After the RN and UPV tests, core samples were taken at the same location as shown in Fig. 2.20(c). Fig. 2.20 (a) and (b) show the in-situ NDT test on beams, and Fig. 2.20 (c) shows the location details of core, RN, and UPV measurements. In Fig. 2.20(c), the red dots are for the RN and the four yellow dots are for UPV measurements (Ngo et al., 2021). They considered the average of 10 RN measurements and the average of 4 UPV measurements as inputs of models to predict concrete compressive strength. Of the total number of 98 datasets, 71% of the total data was used for training and 28% for testing the models (randomly selected).

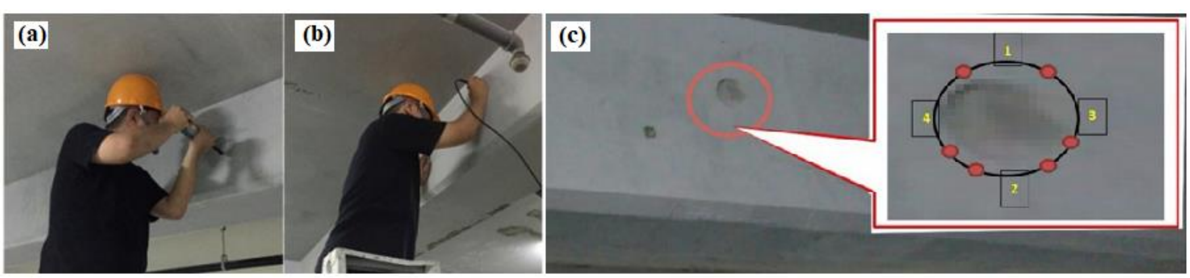

Figure 2.20*:* In-situ experimental test of Ngo et al. (Ngo et al., 2021)

The models' prediction accuracy is given in Table 2.18, where RMSE is the root mean square error and MAPE is the mean absolute percentage error. According to the results in Table 2.18, ANNs, SVMs, and ANFIS models predict the concrete strength prediction with MAPE's of 14.69%, 10.00%, and 10.01%, respectively. The performance of both SVMs and ANFIS models is better than ANNs, and the performance of both SVMs and ANFIS are similar.

Table 2.17*:* Models' information of Ngo et al, (Ngo et al., 2021)

AI method	Software	Note
Artificial Neural Networks (ANNs)	Neuro Solutions 7	• ANN functions: linear regression, a radial basic function network (RBFN) • ANN training type: Bayesian regularization, a generalized regression network, and multilayer perceptron
Support vector machines (SVMs)	MATLAB	• Two SVM parameters of sigma and gamma were determined by trial and error.
Adaptive Neural Fuzzy Inference System (ANFIS)	MATLAB	• The number of ANFIS membership functions: two, three, four, and five. • Types of ANFIS membership functions; trimf, trapmf, gbellmf, gaussmf, gauss2mf, pimf, dsigmf, and psigmf.

Table 2.18: Best model prediction accuracy summary, by Ngo et al., (Ngo et al., 2021)

Model	Parameter Setting	RMSE	MAPE (%)
ANNs	linear regression	95.65	14.69
SVMs	gamma = 1000, sigma = 32	70.76	10.00
ANFIS	Two triangular membership function	64.49	10.01

In 2021, Shishegaran et al. developed six different models based on six different algorithms (three single and three hybrid models) to predict the compressive strength of concrete with only two inputs; UPV and RN. For this purpose, step-by-step regression (SBSR), gene expression programming (GEP), ANFIS models, and three hybrid models of HCVCM-SBSR, HCVCM-GEP, and HCVCM-ANFIS were used to predict the compressive strength of concrete. For the dataset, 516 data were collected based on 8 previous studies, then 70% of the whole dataset was randomly selected to train all models, and the remaining 30% was used to test the models. They did not provide any details about their dataset, just mentioning that they collected 516 data of the concrete which the compressive strength tests were done on them at ages 3, 7, 14, 28, 56, and 90 days. Information such as the type of concrete specimens that were tested (concrete cores, cylindrical or cubic specimens, etc.) was not provided. In Table 2.19, three different error terms including the maximum positive error, maximum negative error, and mean absolute percentage error (MAPE) was used to compare the accuracy and performance of models. Accordingly, they reported that the best single model is ANFIS, and also using hybrid method with all single models could improve the accuracy of the results.

Table 2.19: The comparison of results of error for all six models, by Shishegaran et al. (Shishegaran et al., 2021)

Error terms	SBSR	HCVCM-SBSR	GEP	HCVCM-GEP	ANFIS	HCVCM-ANFIS
The max positive error	102.3	31.7	35.8	39.1	28.8	31.7
The max negative error	-89.7	-81.8	-86.2	-86.3	-85.3	-79.3
MAPE (%)	15.7	13.9	13.6	12.8	12.1	10.1

In 2021, Asteris et al. evaluated six soft computing models for predicting the compressive strength (CS) of concrete using two non-destructive testing (NDT) methods: ultrasonic pulse velocity (UPV) and rebound number (RN), based on 629 collected data points from NDT and destructive testing (DT) on cubic specimens. The models tested include back-propagation neural networks (BPNN), relevance vector machine, minimax probability machine regression, genetic programming, Gaussian process regression, and multivariate adaptive regression splines (MARS). They considered combinations of inputs: (1) UPV, (2) RN, and (3) both UPV and RN (SonREB) for predicting concrete strength. They reported an increase in accuracy when both UPV and RN values were used for predicting concrete compressive strength (CS). The most accurate model for predicting concrete strength was the BPNN with UPV and RN as inputs, showing a MAPE of 6.577% and an R-squared value of 0.959, according to their report (Asteris et al., 2021).

In 2022, Almasaeid et al. investigated the evaluation of high-temperature damaged concrete using NDT and ANN modeling. This study was novel research in this field, according to the fact that DT (i.e. taking cores from damaged structures) can exacerbate integrity issues for damaged RC structures. For the experimental program, six different mix designs were used; for each mix, 20 samples were prepared to be tested at five different temperature levels (150 mm cubic specimens were used). Then DT and NDT (UPV+RN) were conducted on each specimen. According to their results, high-temperature levels up to 200◦C did not affect the RN significantly, but the RN started to decrease when the concrete was exposed to temperatures exceeding 400◦C. Also, high temperature affected UPV at temperature levels of 200◦C and above. To build the datasets, 360 data from the experimental program and 694 collected data from previous studies were used. From the total of 994 data, 694 data were selected for the training dataset, 200 data for the testing dataset, and 100 data for validation. Six input and three output parameters were considered for the model (Table 2.20). Finally, they reported that ANN was able to model the relationship between NDT and concrete compressive strength for the concrete that was damaged by high temperature with R^2 of 0.94 (Almasaeid et al., 2022).

Almasaeid et al. conducted another study in 2022 using an ANN model to predict the compressive strength of geopolymer concrete using NDT. ANN model with two inputs (UPV+RN) and single output (compressive strength) were developed based on 66 collected data, 50 selected for training and 16 selected for the testing datasets. They predicted the compressive strength of geopolymer concrete with R^2 of 0.9286 using the ANN method (Almasaeid et al., 2022).

Table 2.20: Input and output parameters of the ANN model, by Almasaeid et al. (Almasaeid et al., 2022)

Type	Parameter	Definition
Input	RN	Rebound number
	UPV	ultrasonic pulse velocity
	I_1	1 if UPV direct test, 0 otherwise
	I_2	1 if UPV semi-direct test, 0 otherwise
	I_3	1 if UPV indirect test, 0 otherwise
	D_1	1 if the concrete is damaged, 0 otherwise
Output	CS	concrete compressive strength
	DL	concrete damage level
	T	exposure temperature

In 2024, Arora et al. conducted a comprehensive comparison study of machine learning approaches for predicting the compressive strength (CS) of concrete using two NDT methods of the RN and UPV tests. They developed prediction models using six ML algorithms (AdaBoost, CatBoost, gradient boosting tree (GBT), random forest (RF), stacking, and extreme gradient boosting (XGB)) based on a dataset of 721 samples from laboratory tests, in-situ tests, and collected data, with an 80% training and 20% testing split. The models were categorized into three groups based on their inputs: (1) RN, (2) UPV, and (3) combined RN and UPV. They found that the model with combined inputs (UPV and RN) delivered the highest accuracy. Among the algorithms, XGB outperformed the others with significantly lower MAPE values of 1.69%, demonstrating it to be the best model compared to both the other machine learning techniques and traditional equations (Arora et al., 2024).

2.5 Summary and research needs

Based on past studies from 1979 until today, at least 69 mathematical equations and models have been presented to convert the values obtained from the SonReb method to the compressive strength of concrete. But as mentioned in the previous section, each of these equations is based on the results of tests on a specific type of concrete, and studies have shown that the use of these equations without calibration is not valid. Accordingly, the codes still recommend coring to correlate NDT results with proposed equations and models.

In recent years, research on the use of ML as one of the powerful tools of AI has increased significantly in all sciences, due to its ability to solve difficult problems and predict complex phenomena (Khan et al., 2022; Thai, 2022). In the previous section, a summary of ML models that predict the compressive strength of concrete using SonReb results was presented. Despite these studies, a practical, universally-applicable model has yet to be proposed. Furthermore, no comprehensive study has been conducted to identify the challenges in the field. Additionally, some issues with the current ML models will be discussed in the following section.

For a more detailed review, the proposed models in which only RN and UPV values (SonReb) were considered as input parameters to predict the concrete strength are summarized in Table 2.21. Some models also include additional parameters, such as Na et al.'s model which requires 12 other input parameters in addition to UPV and RN, such as W/C ratio, curing condition, sand/aggregate ratio, etc. Models with multiple input parameters are not necessarily practical for widespread use given that detailed information about mix design and curing condition of concrete of existing buildings is not always available after many years from construction. Therefore, this study considers only input parameters that can be obtained through NDT.

Regardless of the accuracy of the ML models that are given in Table 2.21 and their potential to improve estimates of concrete strength when compared to the basic SonReb method, their general applicability and usefulness in practice is questionable for at least three reasons. First, most of these models was developed using datasets collected from only a few sources and are likely not representative of the wide range of concrete types used in the industry. Second, in all these models the training and testing datasets were selected randomly from the same database and therefore have not been validated using independent data from third parties. Third, in most of these studies, the main database was split into two training and testing datasets having different proportions (i.e., 70%-30%, 71%-29%, 85%-15%, and 93%-7%), and past studies show that the data splitting ratio has a significant effect in the percentage error of the model; in other words, it is not possible to say how accurate these ML models would be for predicting the compressive strength of concrete when applied to general practice. Fourth, the models apply to either cubes or cylinders based on the data gathered from each type of specimen, and no model can work for both standards.

Accordingly, it is necessary to investigate the ability of ML models to predict the compressive strength of concrete using a large dataset representing a wide range of concrete mixtures. This study aims to fill this gap by 1) creating a large database from of SonReb measurements from a variety of sources and representing a wide range of concrete types for model development; 2) using completely separate datasets for training and testing the model to avoid bias and ensure robust performance; 3) verifying the model accuracy using field data from a third party to identify potential influencing factors for its application to real structures; 4) creating a user-friendly interface to simplify adoption; 5) finding a novel way to improve the accuracy of the model based on just UPV and RN accounting for specimen geometry; and 6) presenting a roadmap for the practical implementation of AI for non-destructive evaluation of existing structures and its associated challenges.

Table 2.21: Current ML models to evaluate strength of concrete with SonReb method

Work	Data	Method	Input variables	Type
Na et al., 2009	1551	ANFIS	(1) UPV, (2) RN, (3) w/c ratio, (4) sand/aggregate ratio, (5) unit weight of cement, (6) unit weight of sand, (7) unit weight of gravel, (8) unit weight of water, (9) % superplasticiser, (10) unit weight of fly ash, (11) unit weight of silica fume, (12) unit weight of slag, (13) age, and (14) curing condition	(Mix)
Bonagura, 2012c	(N/A)	ANN	(1) UPV and (2) RN	(N/A)
Kumar & Kumar, 2015	100	GP	(1) UPV, (2) RN, and (3) Weight of sample	Cubic
Shih et al., 2015	95	SVM	(1) UPV and (2) RN	Cylindrical
Wang et al., 2018	315	ANN	(1) UPV and (2) RN	Cylindrical
Sai & Singh, 2019	350	SVR	(1) UPV and (2) RN	Cubic
Asteris & Mokos, 2020	209	ANN	(1) UPV and (2) RN	Cubic
Poorarbabi et al., 2020	180	ANN	(1) UPV and (2) RN	Cubic
Ngo et al., 2021	98	ANFIS ANN SVM	(1) UPV and (2) RN	Core
Shishegaran et al., 2021	516	SBSR HCVCM-SBSR GEP HCVCM-GEP ANFIS HCVCM-ANFIS	(1) UPV and (2) RN	(N/A)
Asteris et al., 2021	629	ANN RVM MPMR GP GPR MARS	(1) UPV and (2) RN	(N/A)
Arora et al., 2024	721	AdaBoost CatBoost GBT RF XGB	(1) UPV and (2) RN	Cubic

2.6 References

Abdulkadir, M. R., Karim, A. A., & Abdullah, A. H. (2017). Destructive and Non Destructive Strength Evaluation of Concrete Exposed to Fire. Journal of Zankoy Sulaimani, Part-A-(Pure and Applied Sciences), 19, 43–55.

Agency, I. A. E. (2002). Guidebook on non-destructive testing of concrete structures. In Training Course Series.

Agunwamba, J. C., & Adagba, T. (2012). A comparative analysis of the rebound hammer and ultrasonic pulse velocity in testing concrete. Nigerian Journal of Technology, 31(1), 31–39.

Almasaeid, H., Alkasassbeh, A., & Yasin, B. (2022). Prediction of Geopolymer Concrete Compressive Strength Utilizing Artificial Neural Network and Nondestructive Testing. Civil and Environmental Engineering.

Almasaeid, H. H., Suleiman, A., & Alawneh, R. (2022). Assessment of high-temperature damaged concrete using non-destructive tests and artificial neural network modelling. Case Studies in Construction Materials, 16, e01080.

Alwash, M., Breysse, D., & Sbartaï, Z. M. (2015). Non-destructive strength evaluation of concrete: Analysis of some key factors using synthetic simulations. Construction and Building Materials, 99, 235–245.

Andresen, S. L. (2002). John McCarthy: father of AI. IEEE Intelligent Systems, 17(5), 84–85.

Arora, H. C., Bhushan, B., Kumar, A., Kumar, P., Hadzima-Nyarko, M., Radu, D., Cazacu, C. E., & Kapoor, N. R. (2024). Ensemble learning based compressive strength prediction of concrete structures through real-time non-destructive testing. Scientific Reports, 14(1), 1824.

Asteris, P. G., & Mokos, V. G. (2020). Concrete compressive strength using artificial neural networks. Neural Computing and Applications, 32(15), 11807–11826.

Asteris, P. G., Skentou, A. D., Bardhan, A., Samui, P., & Lourenço, P. B. (2021). Soft computing techniques for the prediction of concrete compressive strength using Non-Destructive tests. Construction and Building Materials, 303, 124450.

ASTM, C. (1999). 42/C 42M,“Standard test method for obtaining and testing drilled cores and sawed beams of concrete.” Annual Book of ASTM Standards, 4.

ASTM C597 - 16 Standard Test Method for Pulse Velocity Through Concrete. (2016). American Society for Testing and Materials.

Aydin, F., & Saribiyik, M. (2010). Correlation between Schmidt Hammer and destructive compressions testing for concretes in existing buildings. Scientific Research and Essays, 5(13), 1644–1648.

Azarsa, P., & Gupta, R. (2017). Electrical Resistivity of Concrete for Durability Evaluation: A Review. Advances in Materials Science and Engineering, 2017. https://doi.org/10.1155/2017/8453095

Balakrishna, M. N., Mohammad, F., Evans, R., & Rahman, M. M. (2017). Interpretation of concrete mix designs by surface hardness method. Malaysian Journal of Civil Engineering, 29(2).

Bilgehan, M., & Turgut, P. (2010). Artificial neural network approach to predict compressive strength of concrete through ultrasonic pulse velocity. Research in Nondestructive Evaluation, 21(1), 1–17.

Bodnarova, L., Valek, J., Sitek, L., & Foldyna, J. (2013). Effect of high temperatures on cement composite materials in concrete structures. Acta Geodynamica et Geomaterialia, 10(2), 173–180.

Bonagura, M. (2012a). Nondestructive evaluation of concrete compression strength by means of Artificial Neural Network (ANN). alma.

Bonagura, M. (2012b). Nondestructive evaluation of concrete compression strength by means of Artificial Neural Network (ANN).

Bonagura, M. (2012c). Nondestructive evaluation of concrete compression strength by means of Artificial Neural Network (ANN).

Bonagura, M., & Nobile, L. (2021). Artificial Neural Network (ANN) Approach for Predicting Concrete Compressive Strength by SonReb. Structural Durability & Health Monitoring, 15(2), 125.

Box, G. E. P. (1951). Wilson. KB [1951] On the Experimental Attainment of Optimum Conditions. Journal of the Royal Statistical Society, Series B (Methodological), 13(1), 1–45.

Brencich, A., Cassini, G., Pera, D., & Riotto, G. (2013). Calibration and reliability of the rebound (Schmidt) hammer test. Civil Engineering and Architecture, 1(3), 66–78.

Brencich, A., Hasweh, F., & Pera, D. (2021). Calibration of Pull-Out tests on Historical-like Concrete. Materials and Structures, 54, 1-15.

Breysse, D. (2012). Nondestructive evaluation of concrete strength: An historical review and a new perspective by combining NDT methods. Construction and Building Materials, 33, 139–163.

Breysse, D., Balayssac, J.-P., Biondi, S., Corbett, D., Goncalves, A., Grantham, M., Luprano, V. A. M., Masi, A., Monteiro, A. V., & Sbartai, Z. M. (2019). Recommendation of RILEM TC249-ISC on non destructive in situ strength assessment of concrete. Materials and Structures, 52(4), 1–21.

Breysse, D., & Martínez-Fernández, J. L. (2014). Assessing concrete strength with rebound hammer: review of key issues and ideas for more reliable conclusions. Materials and Structures, 47(9), 1589–1604.

Breysse, D., Soutsos, M., Felicetti, R., KRAUSE, M., Lataste, J., & MOCZKO, A. (2009). How to improve the quality of concrete assessment by combining several NDT measurements. Proceedings of International Symposium on Non-Destructive Testing in Civil Engineering.

Brozovsky, J. (2014). High-strength concrete–NDT with rebound hammer: influence of aggregate on test results. Nondestructive Testing and Evaluation, 29(3), 255–268.

Brozovsky, J., & Bodnarova, L. (2016). Contribution to the issue of evaluating the compressive strength of concrete exposed to high temperatures using the Schmidt rebound hammer. Russian Journal of Nondestructive Testing, 52(1), 44–52.

Bungey, J. H., & Grantham, M. G. (2006). Testing of concrete in structures. Crc Press.

Cabral-Fonseca, S., Correia, J. R., Custódio, J., Silva, H. M., Machado, A. M., & Sousa, J. (2018). Durability of FRP-concrete bonded joints in structural rehabilitation: a review. International Journal of Adhesion and Adhesives.

Chingălată, C., Budescu, M., & Lupăşteanu, R. (2017). Accuracy in predicting the compressive strength of concrete using SonReb method. Buletinul Institutului Politehnic Din Lasi. Sectia Constructii, Arhitectura, 63(3), 97–106.

Chopra, P., Sharma, R. K., & Kumar, M. (2016). Prediction of compressive strength of concrete using artificial neural network and genetic programming. Advances in Materials Science and Engineering, 2016.

Chopra, P., Sharma, R. K., Kumar, M., & Chopra, T. (2018). Comparison of machine learning techniques for the prediction of compressive strength of concrete. Advances in Civil Engineering, 2018.

Crawford, G. I. (1997). Guide to nondestructive testing of concrete. United States. Federal Highway Administration.

Cristofaro, M. T., Viti, S., & Tanganelli, M. (2020). New predictive models to evaluate concrete compressive strength using the SonReb method. Journal of Building Engineering, 27, 100962.

Demir, A. (2015). Prediction of hybrid fibre-added concrete strength using artificial neural networks. Computers and Concrete, 15(4), 503–514.

Di Leo, A., Pascale, G., & Viola, E. (1984). Core Sampling Size in Nondestructive Testing of Concrete Structures. Special Publication, 82, 459–478.

Du, G., Bu, L., Hou, Q., Zhou, J., & Lu, B. (2021). Prediction of the compressive strength of high-performance self-compacting concrete by an ultrasonic-rebound method based on a GA-BP neural network. Plos One, 16(5), e0250795.

El Mir, A., & Nehme, S. G. (2017). Repeatability of the rebound surface hardness of concrete with alteration of concrete parameters. Construction and Building Materials, 131, 317–326.

EN 13791: Assessment of in-situ compressive strength in structures and precast concrete componentes. (2007). Brussels: CEN-CENELEC Management Centre, 2015, 744–748.

EN 13791:2019: Assessment of in-situ compressive strength in structures and precast concrete components. (2019). CEN-CENELEC Management Centre.

Erdal, M. (2009). Prediction of the compressive strength of vacuum processed concretes using artificial neural network and regression techniques. Scientific Research and Essay, 4(10), 1057–1065.

Ergun, A., & Kurklu, G. (2012). Assessing the relationship between the compressive strength of concrete cores and molded specimens. Gazi University Journal of Science, 25(3), 737–750.

Facaoaru, I. (1961). Contribution à i'étude de la relation entre la résistance du béton à la compression et de la vitesse de propagation longitudinale des ultrasons. Rilem, 22, 125–154.

Fodil, N., Chemrouk, M., & Ammar, A. (2019). The influence of steel reinforcement on ultrasonic pulse velocity measurements in concrete of different strength ranges. IOP Conference Series: Materials Science and Engineering, 603(2), 22049.

Greene, G. W. (1954). Test hammer provides new method of evaluating hardened concrete. Journal Proceedings, 51(11), 249–256.

Grieb, W. E. (1958). Use of Swiss hammer for estimating compressive strength of hardened concrete. Highway Research Board Bulletin, 201.

Güçlüer, K. (2020). Investigation of the effects of aggregate textural properties on compressive strength (CS) and ultrasonic pulse velocity (UPV) of concrete. Journal of Building Engineering, 27, 100949.

Güneyli, H., Karahan, S., Güneyli, A., & Yapıcı, N. (2017). Water content and temperature effect on ultrasonic pulse velocity of concrete. Russian Journal of Nondestructive Testing 2017 53:2, 53(2), 159–166. https://doi.org/10.1134/S1061830917020024

Hajjeh, H. R. (2012). Correlation between destructive and non-destructive strengths of concrete cubes using regression analysis. Contemp. Eng. Sci, 5(10), 493–509.

Hobbs, B., & Kebir, M. T. (2007). Non-destructive testing techniques for the forensic engineering investigation of reinforced concrete buildings. Forensic Science International, 167(2–3), 167–172.

IAEA. (2002). Guidebook on non-destructive testing of concrete structures. Training Course Series.

Ikpong, A. A. (1993). The relationship between the strength and non-destructive parameters of rice husk ash concrete. Cement and Concrete Research, 23(2), 387–398.

In-Situ Concrete Pull Out Test for Compressive Strength. (n.d.). https://gharpedia.com/blog/in-situ-concrete-pull-out-test-for-compressive-strength/

Jain, H., Patankar, V. H., & Kulkarni, M. S. (2021). Ultrasonic testing of concrete structures: a review.

Kalyan, T., & Kishen, J. C. (2013). Experimental Evaluation of Cracks in Concrete by Ultrasonic Pulse Velocity. Proceedings of the APCNDT.

Kayed, A. R. (2021). The Strength of Concrete in Existing RC Structures. Politecnico di Torino.

Kazemi, M., Madandoust, R., & de Brito, J. (2019). Compressive strength assessment of recycled aggregate concrete using Schmidt rebound hammer and core testing. Construction and Building Materials, 224, 630–638.

Khan, K., Ahmad, W., Amin, M. N., & Ahmad, A. (2022). A Systematic Review of the Research Development on the Application of Machine Learning for Concrete. Materials, 15(13), 4512.

Khashman, A., & Akpinar, P. (2017). Non-destructive prediction of concrete compressive strength using neural networks. Procedia Computer Science, 108, 2358–2362.

Kheder, G. F. (1999). A two stage procedure for assessment of in situ concrete strength using combined non-destructive testing. Materials and Structures, 32(6), 410–417.

Kim, J.-K., Kim, C.-Y., Yi, S.-T., & Lee, Y. (2009). Effect of carbonation on the rebound number and compressive strength of concrete. Cement and Concrete Composites, 31(2), 139–144.

Klieger, P. (1957). Long-Time Study of Cement Performance in Concrete Chapter 10-Progress Report on Strength and Elastic Properties of Concrete. Journal Proceedings, 54(12), 481–504.

Knaze, P., & Beno, P. (1984). The use of combined non-destructive testing methods to determine the compressive strength of concrete. Matériaux et Construction, 17(3), 207–210.

Kocáb, D., Misák, P., & Cikrle, P. (2019). Characteristic Curve and Its Use in Determining the Compressive Strength of Concrete by the Rebound Hammer Test. In Materials (Vol. 12, Issue 17). https://doi.org/10.3390/ma12172705

Kolek, J. (1969). Analysis of answers to Rilem questionnaire on the Schmidt Rebound Hammer. Materiaux et Constructions, 2(10), 285–291.

Kou, S.-C., Poon, C.-S., & Wan, H.-W. (2012). Properties of concrete prepared with low-grade recycled aggregates. Construction and Building Materials, 36, 881–889.

Kovler, K., Wang, F., & Muravin, B. (2018). Testing of concrete by rebound method: Leeb versus Schmidt hammers. Materials and Structures, 51(5), 1–14.

Kumar, P., & Kumar, A. (2015). Prediction of compressive strength using genetic programming involving NDT results. NATIONAL INSTITUTE OF TECHNOLOGY ROURKELA.

Kumavat, H. R., Chandak, N. R., & Patil, I. T. (2021). Factors Influencing the Performance of Rebound Hammer Used for Non-Destructive Testing of Concrete Members: A Review. Case Studies in Construction Materials, e00491.

Lencis, U., Udris, A., & Korjakins, A. (2011). Decrease of the ultrasonic pulse velocity in concrete caused by reinforcement. Journal of Materials Science and Engineering. A, 1(7A), 1016.

Liang, M. T., & Wu, J. (2002). Theoretical elucidation on the empirical formulae for the ultrasonic testing method for concrete structures. Cement and Concrete Research, 32(11), 1763–1769.

Lima, F. B., & Silva, M. F. B. (2000). „Correlation between the compressive strength and surface hardness of concrete (Correlação entre a resistência à compressão do concreto ea sua dureza superficial)". Proc. IV. Congresso de Engenharia Civil, 429–440.

Liu, J.-C., Sue, M.-L., & Kou, C.-H. (2009). Estimating the strength of concrete using surface rebound value and design parameters of concrete material. Journal of Applied Science and Engineering, 12(1), 1–7.

Logothetis, L. (1978). Combination of three non destructive methods for the determination of the strength of concrete. National Technical University of Athens.

MacLeod, G. (1971). An assessment of two non-destructive techniques as a means of examining the quality and variability of concrete in structures.

Malek, J., & Kaouther, M. (2014). Destructive and non-destructive testing of concrete structures. Jordan Journal of Civil Engineering, 159(3269), 1–10.

Malhotra, V. M., & Carino, N. J. (2003). Handbook on nondestructive testing of concrete. CRC press.

Mehta, P. K., & Monteiro, P. J. (2005). Concrete: microstructure, properties, and materials. 452 McGraw-Hill. New York, 453.

Mikulić, D., Pauše, Ž., & Ukrainčik, V. (1992). Determination of concrete quality in a structure by combination of destructive and non-destructive methods. Materials and Structures, 25(2), 65–69.

Mishra, M., Bhatia, A. S., & Maity, D. (2020). Predicting the compressive strength of unreinforced brick masonry using machine learning techniques validated on a case study of a museum through nondestructive testing. Journal of Civil Structural Health Monitoring, 1–15.

Moczko, A. (2009). Determination of actual in-situ compressive strength in concrete bridges, 10 th ACI Int. Conf. on Recent Advances in Concrete Technology, 14–16.

Moczko, A., & Moczko, M. (2018). In-situ examination of the concrete quality European standard approach. MATEC Web of Conferences, 196, 2045.

Mohammed, B. S., Azmi, N. J., & Abdullahi, M. (2011). Evaluation of rubbercrete based on ultrasonic pulse velocity and rebound hammer tests. Construction and Building Materials, 25(3), 1388–1397.

Mohammed, T. U., & Rahman, M. N. (2016). Effect of types of aggregate and sand-to-aggregate volume ratio on UPV in concrete. Construction and Building Materials, 125, 832–841.

Molero, M., Segura, I., Izquierdo, M. A. G., Fuente, J. V, & Anaya, J. J. (2009). Sand/cement ratio evaluation on mortar using neural networks and ultrasonic transmission inspection. Ultrasonics, 49(2), 231–237.

Monteiro, A., & Gonçalves, A. (2009). Assessment of characteristic compressive strength in structures by the rebound hammer test according to EN 13791: 2007. Actes Des Journées Scientifiques Du LCPC, 249–254.

Na, U. J., Park, T. W., Feng, M. Q., & Chung, L. (2009). Neuro-fuzzy application for concrete strength prediction using combined non-destructive tests. Magazine of Concrete Research, 61(4), 245–256.

Naderpour, H., & Alavi, S. A. (2017). A proposed model to estimate shear contribution of FRP in strengthened RC beams in terms of Adaptive Neuro-Fuzzy Inference System. Composite Structures, 170, 215–227. https://doi.org/10.1016/J.COMPSTRUCT.2017.03.028

Naik, T. R., Malhotra, V. M., & Popovics, J. S. (2003). The ultrasonic pulse velocity method. In Handbook on Nondestructive Testing of Concrete, Second Edition (pp. 1–8). CRC Press.

Namatherdhala, B., Mazher, N., & Sriram, G. K. (2022). Artificial Intelligence in Product Management: Systematic review. International Research Journal of Modernization in Engineering Technology and Science, 4(7).

Nash't, I. H., A'bour, S. H., & Sadoon, A. A. (2005). Finding an unified relationship between crushing strength of concrete and non-destructive tests. Middle East Nondestructive Testing Conference & Exhibition, 27–30.

Nasrin, U. S., Khair, A., & Ahsan, R. (2024). Compressive strength assessment of concrete with brick chips using the CAPO-test. Scientific Reports, 14(1), 12881.

Nepomuceno, M., & Bernardo, L. F. A. (2019). Evaluation of self-compacting concrete strength with non-destructive tests for concrete structures. Applied Sciences, 9(23), 5109.

Ngo, T. Q. L., Wang, Y.-R., & Chiang, D.-L. (2021). Applying Artificial Intelligence to Improve On-Site Non-Destructive Concrete Compressive Strength Tests. Crystals, 11(10), 1157.

Nobile, L. (2015). Prediction of concrete compressive strength by combined non-destructive methods. Meccanica, 50(2), 411–417.

Nobile, L., & Bonagura, M. (2014). Recent advances on non–destructive evaluation of concrete compression strength. International Journal of Microstructure and Materials Properties, 9(3–5), 413–421.

Nobile, L., & Bonagura, M. (2016). Parametric Regression Model and ANN (Artificial Neural Network) Approach in Predicting Concrete Compressive Strength by SonReb Method. Int. J. Struct. Civ. Eng. Res, 5, 183–186.

Pascale, G., Di Leo, A., & Bonora, V. (2003). Nondestructive assessment of the actual compressive strength of high-strength concrete. Journal of Materials in Civil Engineering, 15(5), 452–459.

Pedreros, L., Cárdenas, F., Ramírez, N., & Forero, E. (2020). NDT non-destructive test for quality evaluation of concrete specimens by ultrasonic pulse velocity measurement. IOP Conference Series: Materials Science and Engineering, 844(1), 12041.

Penetration Resistance Test on Hardened Concrete - Purpose and Application. (n.d.). https://theconstructor.org/concrete/penetration-resistance-test-concrete/2853/

Pereira, E., & de Medeiros, M. H. F. (2012). Pull Off test to evaluate the compressive strength of concrete: an alternative to Brazilian standard techniques. Revista IBRACON de Estruturas e Materiais, 5, 757–780.

Poorarbabi, A., Ghasemi, M., & Moghaddam, M. A. (2020). Concrete Compressive Strength Prediction Using Neural Networks Based on Non-destructive Tests and a Self-calibrated Response Surface Methodology. Journal of Nondestructive Evaluation, 39(4), 1–11.

Poorarbabi, A., Ghasemi, M. R., & Azhdari Moghaddam, M. (2021). Conversion factors between non-destructive tests of cubic and cylindrical concrete specimens. AUT Journal of Civil Engineering, 5(1), 1.

Proceq, S. A. (2003). Concrete Test Hammer N/NR, L/LR and DIGI SCHMIDT ND/LD–Rebound Measurement and Carbonation. Info Sheet.

Proceq, S. A. (2017). Original Schmidt operating instructions.

Pucinotti, R. (2015). Reinforced concrete structure: Non destructive in situ strength assessment of concrete. Construction and Building Materials, 75, 331–341.

Pullout Tests On Hardened Concrete. (n.d.). https://theconstructor.org/concrete/pullout-lok-capo-test-hardened-concrete/2861/

Qasrawi, H. Y. (2000). Concrete strength by combined nondestructive methods simply and reliably predicted. Cement and Concrete Research, 30(5), 739–746.

Rajabi, A. M., Omidi Moaf, F., & Abdelgader, H. S. (2020). Evaluation of mechanical properties of two-stage concrete and conventional concrete using nondestructive tests. Journal of Materials in Civil Engineering, 32(7), 4020185.

RILEM. (1993). Draft recommendation for in situ concrete strength determination by combined non-destructive methods. In Mater. Struct (Vol. 26). Springer.

Sai, G. J., & Singh, V. P. (2019). Prediction of compressive strength using support vector regression. MENDEL, 25(1), 51–56.

Samarin, A., & Meynink, P. (1981). Use of combined ultrasonic and rebound hammer method for determining strength of concrete structural members. Concrete International, 3(3), 25–29.

Sefrin, R., & Glock, C. (2022). Characteristic concrete compressive strength of existing structures—Evaluation of EN 13791: 2019 for small sample sizes. Structural Concrete, 23(2), 822–835.

Selçuk, L., & Nar, A. (2016). Prediction of uniaxial compressive strength of intact rocks using ultrasonic pulse velocity and rebound-hammer number. Quarterly Journal of Engineering Geology and Hydrogeology, 49(1), 67–75.

Shariati, M., Ramli-Sulong, N. H., Arabnejad, M. M., Shafigh, P., & Sinaei, H. (2011). Assessing the strength of reinforced concrete structures through Ultrasonic Pulse Velocity and Schmidt Rebound Hammer tests. Scientific Research and Essays, 6(1), 213–220.

Shih, Y.-F., Wang, Y.-R., Lin, K.-L., & Chen, C.-W. (2015). Improving non-destructive concrete strength tests using support vector machines. Materials, 8(10), 7169–7178.

Shishegaran, A., Varaee, H., Rabczuk, T., & Shishegaran, G. (2021). High correlated variables creator machine: Prediction of the compressive strength of concrete. Computers & Structures, 247, 106479.

Soshiroda, T., Voraputhaporn, K., & Nozaki, Y. (2006). Early-stage inspection of concrete quality in structures by combined nondestructive method. Materials and Structures, 39(2), 149–160.

Subaşı, S., Beycioğlu, A., Sancak, E., & Şahin, İ. (2013). Rule-based Mamdani type fuzzy logic model for the prediction of compressive strength of silica fume included concrete using non-destructive test results. Neural Computing and Applications, 22(6), 1133–1139.

Szilágyi, K., Borosnyói, A., & Zsigovics, I. (2011). Rebound surface hardness of concrete: Introduction of an empirical constitutive model. Construction and Building Materials, 25(5), 2480–2487.

Szilágyi, K., Borosnyói, A., & Zsigovics, I. (2015). Understanding the rebound surface hardness of concrete. Journal of Civil Engineering and Management, 21(2), 185–192.

Szymanowski, J., & Sadowski, Ł. (2020). Functional and adhesive properties of cement-based overlays modified with amorphous silica nanospheres. The Journal of Adhesion, 96(1–4), 207–228.

Thai, H.-T. (2022). Machine learning for structural engineering: A state-of-the-art review. Structures, 38, 448–491.

Thapa, S., Sharma, R. P., & Halder, L. (2021). Developing SonReb models to predict the compressive strength of concrete using different percentage of recycled brick aggregate. Canadian Journal of Civil Engineering, ja.

Ulucan, Z. Ç., Türk, K., & Karataş, M. (2008). Effect of mineral admixtures on the correlation between ultrasonic velocity and compressive strength for self-compacting concrete. Russian Journal of Nondestructive Testing, 44(5), 367–374.

Valarmathi, G., Suganthi, S. U., Subashini, V., Janaki, R., Sivasankari, R., & Dhanasekar, S. (2021). CNN algorithm for plant classification in deep learning. Materials Today: Proceedings, 46, 3684–3689.

Wang, Y. R., Ngo, L. T. Q., Shih, Y. F., Lu, Y. L., & Chen, Y. M. (2018). Adapting ANNs in SONREB Test to Estimate Concrete Compressive Strength. Key Engineering Materials, 792, 166–169.

Whitehurst, E. A. (1951). Soniscope tests concrete structures. 47(2), 433–444.

Willetts, C. (1958). Investigation of Schmidt Concrete Test Hammer, Miscellaneous Paper No. 6-267. US Army Engineer Waterways Experiment Station, Vicksburg, MS.

Yang, S., Xu, Z., & Bian, Z. (2020). Prediction on compressive strength concrete using modified pull-off testing method (MPTM). Construction and Building Materials, 250, 118834.

Yang, Y., Zhang, Y., & She, W. (2018). Characterization of surface hardness and microstructure of high performance concrete. Journal of Wuhan University of Technology. Materials Science Edition, 33(1), 124–132.

Yoo, J. K., & Ryu, D. W. (2008). A study of the evaluation of strength development property of concrete at early ages. 3rd ACF International Conference-ACF/VCA.

Zabihi, N. (2012). Effect of specimen size and shape on strength of concrete. Eastern Mediterranean University (EMU).

Chapter 3– Development of Machine Learning and Regression Models [1]

3.1 Introduction

Regardless of the type of structure (buildings, bridges, dams, etc.), accurate and reliable evaluation of the compressive strength of concrete is an essential requirement for engineers during construction for quality assessment and also after construction for structural evaluation. The primary and most reliable method to evaluate concrete compressive strength is performing tests on cylinder specimens or cores that are extracted from the structure. However, this approach often presents several drawbacks, not least of which is the need for relatively large sample sizes in some cases and uncertainty with respect to the representativeness of the samples obtained. In existing structural elements, it is not always possible to extract cores since they induce damage to the structure. Moreover, cores from sound portions of a structure are not representative of regions containing defects, while coring of defective concrete is generally not accepted. In new reinforced concrete (RC) construction, owners are generally reluctant to create holes in a brand-new structure, especially with minimum sample numbers that are set by codes and guidelines (ACI 228, 2019; EN 13791, 2007).

Some guidelines have attempted to reduce the number of core tests that are needed and reduce the size of the cores (EN 13791, 2019; Sefrin & Glock, 2022), but these key challenges remain. Accordingly, two simple, fast, and economical non-destructive test (NDT) methods

[1] This chapter has been published as: Alavi, S. A., Noel, M., Moradi, F., & Layssi, H. (2024). Development of a machine learning model for on-site evaluation of concrete compressive strength by SonReb. Journal of Building Engineering, 82, 108328.

have gained traction in recent years, namely ultrasonic pulse velocity (UPV) and rebound number (RN) measurements. NDT methods provide a relatively low-cost and repeatable assessment tool which enables strength estimates to be obtained while significantly reducing the number of cores required. Nevertheless, it is still necessary to perform compressive tests on core samples for each project to correlate the results to NDT measurements to use the results of the NDT evaluation (ACI 228, 2019; EN 13791, 2007).

Previous studies show that many influencing factors affect the results of both UPV and RN tests, which makes it difficult to evaluate the compressive strength of concrete using either method on their own (Breysse, 2012; Chandak & Kumavat, 2020). For this reason, single NDT measurements (UPV or RN) cannot be reliably used to accurately estimate concrete compressive strength. This challenge motivated the research efforts that eventually led to the development of the SonReb method which combines results from both test methods to reduce sensitivity to certain influencing parameters leading to more consistent outcomes (Breysse et al., 2020; Kouddane et al., 2022; RILEM, 1993; Sbartaï et al., 2021). In the SonReb method, UPV and RN tests are performed at the same location on the concrete structure. The results of both NDT methods are simultaneously used to evaluate the concrete strength using one of various proposed equations developed through regression analysis of experimental data (Facaoaru, 1961).

Several research efforts have attempted to apply the SonReb method using mathematical approaches and regression equations derived by curve-fitting a particular set of data. However, the accuracy and reliability of these models is still low (Breysse, 2012; Cristofaro et al., 2020; Poorarbabi et al., 2020a). In past years, in addition to regression models, different types of performance evaluation methods such as response surface methodology (RSM), optimization techniques, and other mathematical approaches have been applied in attempts to evaluate concrete properties with improved accuracy (Breysse, 2012; Hamada et al., 2023; B. Liu et al., 2020; Poorarbabi et al., 2020b, 2021).

These days, there has been a growing trend in the application of artificial intelligence (AI) methods in various engineering fields to find new solutions for problems that are still unsolved, or that conventional mathematics cannot adequately address. Among the AI methods, machine learning (ML) has become a popular method with a notable surge in the use of ML methods in structural engineering in this decade (Naderpour & Alavi, 2017; Thai, 2022). Several studies have previously been conducted on the use of ML techniques to predict the compressive strength of concrete. The results of these studies are very valuable, but there are still some notable gaps preventing their widespread application.

Na et al. conducted the first research on applying ML to predict concrete strength by using combined NDT (Na et al., 2009). They investigated the effects of in situ conditions and the results of two NDTs (UPV and RN) as input parameters on the predicted results; the best performing model had fourteen inputs that included UPV and RN measurements along with twelve additional parameters such as water/cement ratio, curing condition, and sand/aggregate ratio. Although the accuracy of their model was reasonably high (10.99% mean absolute percent error, or MAPE), in practice many details of the concrete mix design of existing structures are unknown which limits the applicability of their model.

Following Na et al's study, several other researchers developed ML models using fewer input parameters to predict concrete compressive strength. Shih et al. developed a two-parameter model (UPV and RN) (Shih et al., 2015), while Kumar and Kumar considered the weight of cubic specimens as a third input to predict the concrete strength (Kumar & Kumar, 2015). Sai and Singh applied ML technique to predict concrete strength based on results of three test methods: RN, UPV, and Windsor Penetration (Sai & Singh, 2019) (which is considered to be a semi-destructive test). Asteris and Mokos investigated the application of artificial neural networks (ANNs) for predicting the compressive strength of concrete in existing structures and showed that including both UPV and RN as inputs gave better predictions than single input models (UPV or RN) (Asteris & Mokos, 2020). Poorarbabi et al. compared the use of ANNs and RSM to predict the strength of concrete using UPV, RN, and surface electrical resistivity (SR) (Poorarbabi et al., 2020a). Du et al. used ML to estimate the strength of high-performance self-compacting concrete (SCC) based on the results of RN and UPV tests (Du et al., 2021). Bonagura and Noble evaluated the performance and accuracy of the ANN method for predicting concrete compressive strength by SonReb and reported a considerable improvement over regression models (Bonagura & Nobile, 2021). Ngo et al. applied different methods of ML to improve on-site NDT for estimating concrete compressive strength by creating several models based on three different algorithms using 98 datapoints (Ngo et al., 2021). Shishegaran et al. used the High Correlated Variables Creator Machine (HCVCM) technique to create hybrid ML models for concrete strength prediction using UPV and RN (Shishegaran et al., 2021). Asteris et al. employed soft computing techniques to predict the concrete strength using NDT results (UPV and RN) (Asteris et al., 2021). Almasaeid et al. utilized ML to predict the compressive strength of geopolymer concrete using two NDT inputs (UPV and RN) (Almasaeid et al., 2022).

Previous literature has shown promising results in the use of ML to improve the accuracy of NDT-based concrete strength predictions. Nevertheless, to use ML models in practice, several limitations and research gaps remain to be addressed. First, almost all of the previous models were trained and tested based on the same datasets; in other words, they built a single database and then 70% to 93% of the data was randomly used as the training dataset and the remaining data from the same database was selected as the testing dataset. None of these models have been evaluated with independent data in order to objectively evaluate the model's performance. Second, most of their datasets include a relatively small number of data. Third, regardless of the number of training data, the range of the data is also consequential; the mechanical characteristics of concrete vary uniquely within each RC structure. The factors affecting the mechanical properties of concrete (type of cement, type of aggregate, age, etc.) also influence the relationship between concrete compressive strength and both UPV and RN (Brencich et al., 2013; Breysse, 2012; Chandak & Kumavat, 2020; Günaydın et al., 2023; Kumavat et al., 2021). Finally, in almost all previous studies, the ML models were trained and tested using data obtained from small plain concrete specimens (cubic or cylindrical), and they did not validate their models with independent data from real RC structures. In summary, based on a limited number of data obtained from limited types of concrete, it has not yet been demonstrated whether a general-purpose ML model can be developed to produce satisfactory outcomes for independent data that is different from training and testing data.

Therefore, the main objective of this study is to develop a practical ML model based on a wide variety of data sources, and then evaluate the ML model performance with independent data from NDT measurements from a larger RC element and compare with other approaches. To the authors' knowledge, this study presents the first time an ML model has been applied to large scale RC components to independently evaluate concrete strength, rather than assessing model performance using only plain concrete specimens extracted from the same database used for training. A large database was created by collecting data from previous literature (794 data from 13 resources) in addition to an independent experimental program (96 data from sixteen different mixtures). Then three adaptive neuro-fuzzy inference system (ANFIS) models were developed using two distinct approaches: two models were developed based on the conventional approach (i.e., the random selection of training and testing data from a single database with ratios of 75% and 80% of data used for training) and a third model which employed a novel approach in which the training and testing data were obtained from different sources to evaluate the model performance more objectively while maximizing the number of the training data. The ANFIS algorithm was selected for this purpose as this method combines two robust methodologies of fuzzy logic (FL) and artificial neural networks (ANN) (Jang, 1993; Naderpour & Alavi, 2015; Thai, 2022). A graphical user interface (GUI) application was also developed based on the best ANFIS model to facilitate its use on-site. In addition to the ML model, linear and nonlinear regression models were also extracted. By comparing all models as well as other regression models from literature, the improvements afforded by ML can be directly evaluated. In the final step, the proposed ML model and regression equations were validated with new independent data using a RC slab as a case study.

In summary, this study addresses the previously unanswered question: "can concrete strength be accurately predicted in practice using ML considering only the two parameters proposed by the SonReb method?" In the process of answering this question, the present study makes the following contributions to advancing the state-of-the-art:

- A new approach is proposed and evaluated for the selection of training and testing data for ML development to eliminate bias and maximize the number of data available for training.

- For the first time, an ML model was developed based on completely distinct sources of data used for training and testing, and subsequently validated using a large RC member rather than plain concrete specimens.
- An easy-to-use GUI application was developed to facilitate use of the ML model without the need for an advanced skillset or knowledge base.
- A novel method was introduced to improve the consistency of results obtained from UPV tests on concrete specimens using 3D printing technology.
- A detailed discussion of the main challenges associated with concrete strength predictions using NDT and suggestions for future improvements in ML predictions with SonReb are presented.
- In addition to the ML model developed, two new regression equations (linear and non-linear) are proposed based on the wide range of data collected for this study, and the results of each method are compared.

3.2 Methodology

3.2.1 Ultrasonic Pulse Velocity (UPV) Test

In this method, the speed of an ultrasonic pulse that passes through concrete is measured. It is worth mentioning that the primary purpose of the UPV test is to evaluate the quality and uniformity of concrete. In Fig. 3.1, the function of the UPV device is illustrated. Accordingly, the UPV device records the time of an ultrasonic pulse that traverses from the transmitter to the receiver. Then, the ultrasonic pulse velocity is determined by Eq. 5.1.

$UPV = {}^{L}/_{t}$ (Eq. 5.1)

Where; UPV: ultrasonic pulse velocity (Km/s), L: path length in concrete (mm), and t: transmit time (μs).

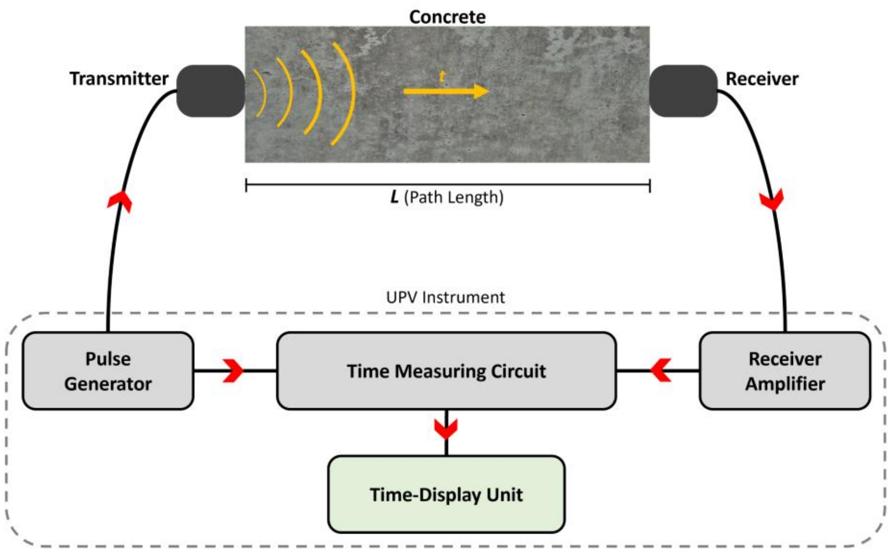

Figure 3.1: Schematic of UPV on a concrete block

Although UPV measurements can be helpful to identify locations for coring (i.e., lower quality concrete), there is no precise universal relationship between the compressive strength of concrete and the UPV value (Breysse, 2012; Cristofaro et al., 2020). In fact, the correlation between concrete' compressive strength and pulse velocity is not uniform across all concrete varieties and is subject to the influence of various factors such as type of cement, aggregate size and type, humidity, etc.) (Alavi et al., 2022; Breysse, 2012; Günaydın et al., 2023; Ndagi et al., 2019).

3.2.2 Rebound Number Test

In this method, a mechanical device known as rebound hammer or Schmidt hammer is used to estimate concrete strength based on the surface hardness of concrete. The rebound number

(RN) is the output of this method (Fig. 3.2). This device provides a measure of how much energy is reflected when a spring-loaded mass dynamically strikes the surface of concrete block by using some equations or correlation curves to convert the RN to the compressive strength of concrete. However, the proposed equations are unreliable due to the same problem as the UPV method. For example, one of the main issues is that the RN results highly depend on the concrete surface condition (Asteris & Mokos, 2020; Brencich et al., 2013; Breysse, 2012; Kim et al., 2009; Kolek, 1969; Kumavat et al., 2021; Szilágyi et al., 2011).

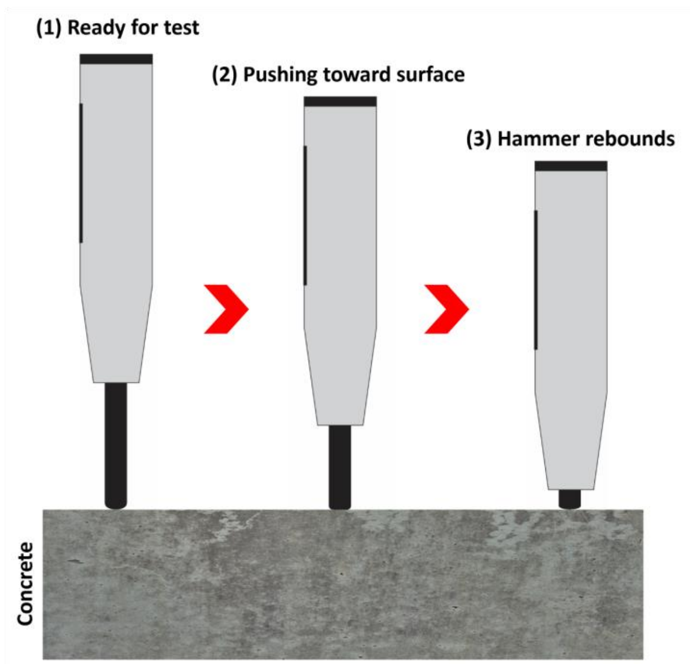

Figure 3.2: Schematic of RN test on a concrete surface

3.2.3 Combined SonReb Method

SonReb is the combination of UPV and RN that was introduced to engineers by RILEM technical committees (Facaoaru, 1961; RILEM, 1993). By combining two disparate methods, the results are less sensitive than either method individually to the influencing effects of secondary parameters. This has attracted the attention of engineers and researchers in the past years and several equations have been presented to convert the SonReb results to concrete compressive strength (Bolborea et al., 2022; Breccolotti & Bonfigli, 2015; Breysse, 2012; Chingălată et al., 2017; Kayed, 2021; Kouddane et al., 2023; J.-C. Liu et al., 2009). However, the accuracy of these equations varies between different datasets, which makes them impossible to use without first calibrating their performance with core tests.

3.3 Machine Learning

Machine learning (ML) is recognized as the most important subfield of artificial intelligence (AI). ML is a field of computer science that concentrates on instructing machines (computers) in the way of learning from data. In other words, ML algorithms empower computers to learn from data to make decisions and predictions. In the learning phase, the machine recognizes patterns in data autonomously without requiring explicit human programming (Abioye et al., 2021; Alavi et al., 2022; Moein et al., 2023; Thai, 2022). ML provides valuable tools to solve complex problems that are difficult to solve with conventional mathematical approaches (Alavi & Noël, 2022; Salehi & Burgueño, 2018). ML includes three main categories which are supervised learning, unsupervised learning, and reinforcement learning (Thai, 2022). For this study, supervised learning was employed in which the ML algorithm learns from a dataset with labels (inputs and output). As illustrated in Fig. 3.3, two datasets are required to develop such a ML model which are the testing dataset and the training dataset. The former is used to train the model while the latter serves to evaluate its performance.

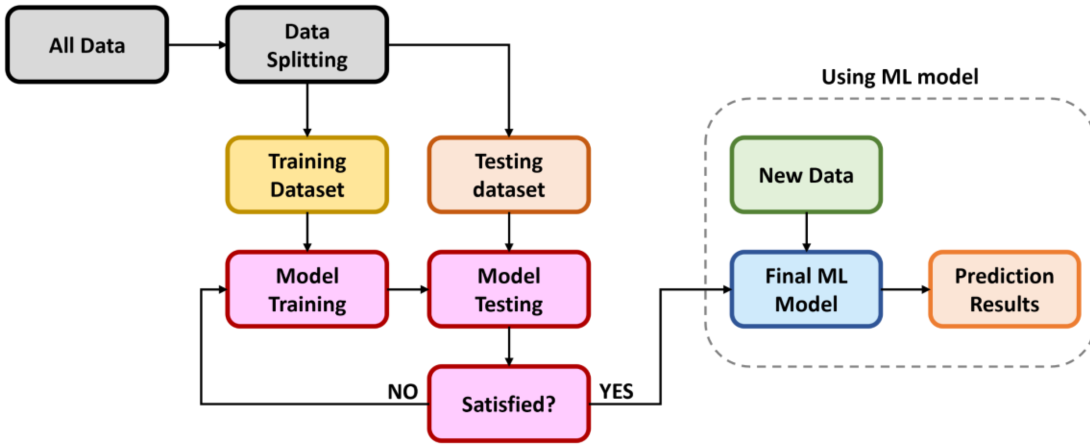

Figure 3.3 Flowchart of developing Machine Learning (ML) models and their application

One of the well-known ML techniques is Adaptive Neuro-Fuzzy Inference System (ANFIS) also known as Neuro-fuzzy (Jang, 1993). ANFIS is the combination of Artificial Neural Networks (ANN) and Fuzzy Systems (FS).

ANNs process information in a similar way as an animal's brain by establishing links between different nodes to detect patterns. ANNs are highly nonlinear allowing them to capture complicated interactions between input and output variables without any prior knowledge about their nature (Naderpour et al., 2011; Ngo et al., 2021). Fuzzy Systems (FS) are models that are based on Fuzzy Logic (FL). Fuzzy systems are widely used for problems that include uncertainty and can identify empirical relationships between different parameters. FS models place each input variable into specific categories known as a fuzzy "Membership Function" (MF). Then the fuzzy system uses "fuzzy roles" to give outputs. In other words, FL is based on approximation, and it is a type of many-valued logic that deals with uncertain, rather than fixed-valued parameters. Variables can be any real number between 0 and 1 instead of binary functions of 0 or 1 (true or false). Complexity of selecting the best and optimum type and the number of MF, and also defining the fuzzy roles are the main challenges to create an accurate FS. The learning ability of ANNs are used in the Neuro-Fuzzy systems to solve the above issue.

Integrating these two powerful methods simultaneously provides the parallel computation and learning abilities of ANNs with the human-like knowledge processing capabilities of FL (Jang, 1993; Naderpour & Alavi, 2015, 2017). The ANFIS technique has been widely used in many fields of engineering, including structural engineering, and it has provided acceptable and encouraging results for developing predictive models (Thai, 2022). Based on this, the ANFIS method was selected in this study, and as shown in Fig. 3.4, UPV (from direct UPV test) and RN (from horizontal RN test) are considered as input variables for the ML model—accordingly, the compressive strength of concrete was the target value (output) for the model. Also, the architecture of ANFIS model with two inputs and one output can be seen in Fig. 3.5.

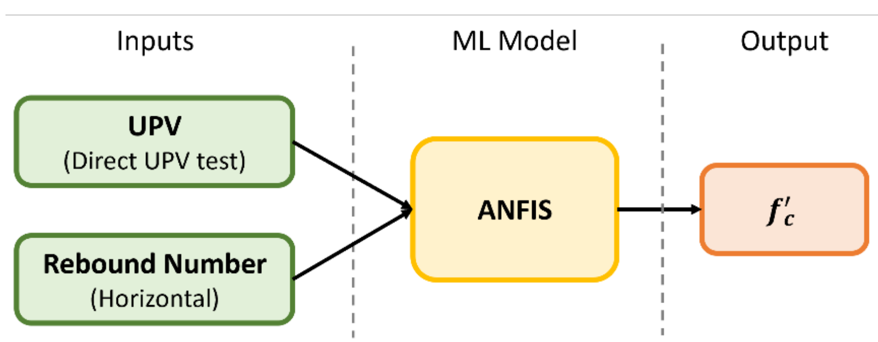

Figure 3.4: The flowchart of proposed ML model to evaluate compressive strength of concrete

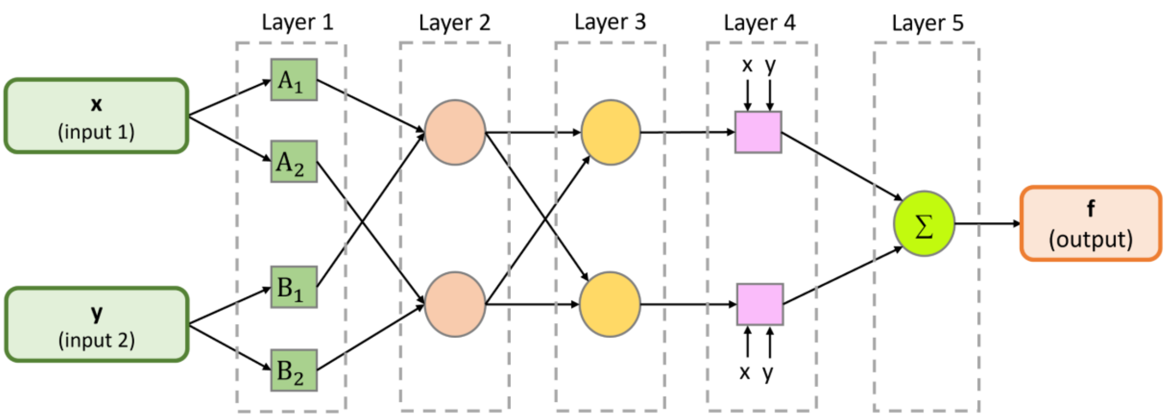

Figure 3.5: The ANFIS structure for the proposed ML model

Fig. 3.5 shows the structure of ANFIS based on the Jang's proposed model with two input variables and one output variable with two fuzzy rules (Takagi-Sugeno rule type) as follows (Jang, 1993);

- Rule No.1: If x is A_1 and y is B_1, then $\mathrm{f}_1 = (p_1 x + q_1 y + r_1)$
- Rule No.2: If x is A_2 and y is B_2, then $\mathrm{f}_2 = (p_2 x + q_2 y + r_2)$

where x and y are the normalized inputs of the ANFIS model, A_1 and A_2 are the MF for the first input (x), and B_1 and B_2 are MF for the second input (y).

The first layer (fuzzification): Each node generates the fuzzy membership grades, and the inputs (x and y) are transformed into linguistic variables by using the fuzzy membership function (MF):

$O_i^1 = \mu_{Ai}\,(x),\ \text{for } i = 1{,}2$ (Eq. 3.2)

where x is the input for node i, A_i is the linguistic label, and O_i^1 is the membership function of A_i.

Second layer (rule): the membership values obtained from the fuzzification layer are used to generate firing strengths (w_i) according to Equation 3.3:

$O_i^2 = w_i = \mu_{Ai}\,(x) \times \mu_{Bi}\,(y),\ \text{for } i = 1{,}2$ (Eq. 3.3)

Third layer (normalization): each node in this layer estimates the average firing strength for each rule according to Equation 3.4:

$O_i^3 = \overline{w}_i = \frac{w_i}{w_1 + w_1}$, for $i = 1{,}2$ (Eq. 3.4)

Fourth layer (defuzzification): this layer is comprised of adaptive nodes described by Equation 3.5:

$O_i^4 = \overline{w}_i \mathrm{f}_i = \overline{w}_i(p_i x + q_i y + r_i)$, for $i = 1{,}2$ (Eq. 3.5)

where $\overline{w}_i$ is the output of the normalization layer, and (p_i, q_i, r_i) are the consequent parameters (CPs) of each node updated in the training phase.

The fifth layer (summation): the single node in this layer is a fixed node that computes the output by adding up all incoming values from the fourth layer as follows:

$O_i^5 = \sum_{i=1}^{2} \overline{w}_i f_i = \sum_{i=1}^{2} \overline{w}_i (p_i x + q_i y + r_i)$ (Eq. 3.6)

3.4 Experimental Program and Dataset Development

To develop an accurate and practical ML model, a dataset that encompasses a wide range of input and output parameters is needed. To create this database (Appendix B.1), three different sources were used in this study: (1) collected data from literature, (2) data from tests on concrete specimens provided by two ready-mix concrete companies, and (3) data from laboratory-fabricated concrete specimens.

According to Table 3.1, 794 data were collected from literature which included the UPV, RN, and compressive strength of concrete. Additional information including mix design details, age of concrete, and specimen geometry were also recorded when these values were reported.

Sources No.1 and No.2 in Table 3.1 each contained 180 individual data points obtained from tests conducted on 60 batches of concrete with three replicate specimens tested for each batch, while other studies presented either average results for each set or did not include replicate samples. Therefore, for this study, the average results from each set of three tests reported in source No.1 and No.2 were considered as one unique data point, reducing the size of the overall dataset. Plotting the data also revealed a number of outliers that seemed to be outside the normal range or data cloud, which could be indicative of poor-quality readings and were removed (known as visual screening method (Breysse et al., 2021)). After averaging results from replicated tests and removing suspected low-quality results, the final dataset contained 454 unique data points.

Table 3.1 Information of collected data

No.	Number of data	Type of specimens	Available information	Ref.
1	180	Cubic	UPV, RN, f_c', mix design, age	Poorarbabi et al., 2020a
2	180	Cylindrical	UPV, RN, f_c', mix design, age	Poorarbabi, 2020
3	18	Cubic	UPV, RN, f_c', mix design, age	Chandak & Kumavat, 2020
4	27	Cubic	UPV, RN, f_c', mix design, age, slump	Rashid & Waqas, 2017
5	7	Coring	UPV, RN, f_c'	Masi et al., 2016
6	16	Unknown	UPV, RN, f_c'	Nobile, 2015
7	10	Coring	UPV, RN, f_c'	Alwash et al., 2015
8	20	Cubic	UPV, RN, f_c', mix design, age	Nikhil et al., 2015
9	40	Cubic	UPV, RN, f_c', mix design, age	Jain et al., 2013
10	35	Cubic	UPV, RN, f_c', mix design, age, slump	Na et al., 2009
11	12	Unknown	UPV, RN, f_c', mix design, age, slump	Domingo & Hirose, 2009
12	40	Cubic	UPV, RN, f_c', mix design, age	Cianfrone & Facaoaru, 1979
13	209	Cubic	UPV, RN, f_c'	Logothetis, 1978

It is important to note that the collected data in Table 3.1 were obtained from studies carrying out different experimental programs. In most cases, all NDT and DT were performed on one type of specimen (cubic or cylindrical), while in certain studies the NDT were performed first on the existing structures followed by DT of cored samples (i.e., source No.5 and No.7 in Table 3.1). In addition, the cubic and cylindrical specimens do not all have the same dimensions; for example, in source No. 10, the size of the cubic specimens is equal to 200 mm, and in source No.1 it is equal to 150 mm. Based on this variety of collected data, it was decided not to consider the geometry of the concrete sample as an independent input parameter for the AI model in this study. Although geometry is known to influence both NDT measurements (particularly RN) and compressive strength, doing so would have effectively divided the overall dataset into smaller subsets—some of which would contain relatively few data points—which would reduce the overall robustness of the model. Development of a three-parameter model accounting for specimen geometry is part of an ongoing investigation that will be made available at a later date once sufficient data from each category is collected. As a result, the ML models were developed with only two input variables (UPV, RN), and other influencing factors such as mix design, geometry, and age of concrete (which are usually hard to find in the case of older existing structures) were not considered as additional input parameters.

Most of the collected data presented in Table 3.1 were obtained using cubic specimens with different mix designs that were tested at different ages. To address this gap, the experimental test program intentionally included a higher proportion of cylindrical specimens to improve the robustness of the databank.

Accordingly, two experimental programs were conducted:

(1) Concrete specimens were obtained from two local ready-mix concrete companies; total of 48 cylindrical specimens from twelve different batches (Fig. 3.6).

(2) Casting a total of 48 specimens including 150 mm cubic specimens and 100*200 mm cylindrical specimens (Fig. 3.7) with four different mix designs given in Table 3.2. Six cubic and six cylindrical specimens were fabricated for each mix design.

For both experimental programs, each batch of specimens were cured at high humidity for 28 days. The non-destructive tests (UPV and RN) and compression strength tests were conducted on concrete specimens at the age of 28 days and 90 days. As shown schematically in Fig. 3.8, each set of three replicate samples were first tested using the direct UPV test, followed by the rebound hammer test (horizontal configuration), and finally the compression test.

Figure 3.6: The concrete specimens provided by local companies

Figure 3.7: The casting of cubic and cylindrical specimens in the laboratory; (A) materials, (B) mixing and vibrating, (C) molds, and (D) specimens

Table 3.2: Concrete mix designs

Mix ID	Cement (kg/m^3)	Slag (kg/m^3)	Coarse aggregate (kg/m^3)	Sand (kg/m^3)	Water (L/m^3)	Retarder (ml/100kg)	High range water reducer (ml/100kg)	Air entrainment (%)	W/C
MD1	265	-	1055	940	162	-	-	-	0.60
MD2	375	-	1070	755	150	-	-	-	0.40
MD5	353	77	1085	675	155	200	-	6.0	0.36
MD6	290	185	1070	815	171	200	150	-	0.36

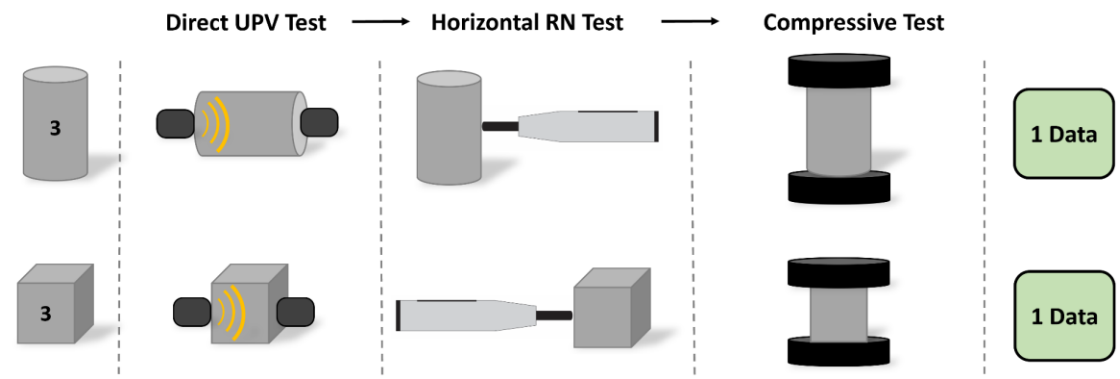

Figure 3.8: The process of conducting NDT and DT on specimens

There are many influencing factors that affect results of UPV and RN tests. Among the two NDT methods, UPV is more sensitive, and human factors also affect its results. To mitigate human factors and to improve the quality of data, 3D printer technology was used to increase accuracy in the UPV test to ensure the quality of readings extracted from this test. To prevent sliding of the UPV transmitters during the test, plastic stands were fabricated with 3D printers to hold the system in place and ensure consistent readings. Therefore, one stand for cylindrical (Fig. 3.9(A)) and one for cubic specimens (Fig. 3.9(B)) were designed and fabricated and used to perform UPV tests on the specimens (Fig. 3.9(C) and Fig. 3.9(D)). To ensure the results, the UPV test was performed twice on each specimen, and the average value of the two UPV tests was considered.

RN tests were performed according to ASTM C805, which requires that the test be conducted on a rigid base to obtain reliable readings. Accordingly, as shown in Fig. 3.10, specimens were placed in the compressive strength testing machine under a pressure equal to 10% of the design strength of the concrete (ASTM C805, 2018; Ju et al., 2017). Ten RN measurements were taken for each specimen. The average readings for each set of three replicate samples was considered as one unique data point for the model (12 data points from the ready-mix concrete and 16 for the laboratory mixes).

After performing both UPV and RN tests on each specimen, the compressive strength test was done on the specimens, as shown in Fig. 3.11. The compressive tests on cylindrical specimens followed the Canadian standard (CSA A23.2, 2019). For the DT on cubic specimens, one rigid plate was used in the test setup (Fig. 3.10(B)), and the plate was placed on top of the cubic specimens.

After compiling 28 unique data from the experiments and 454 collected data from literature, the final database contained 482 unique data points to develop the ANFIS model. Table 3.3 presents statistical information while Fig. 3.12 gives the histogram information for the three main parameters: UPV, RN, and compressive strength of concrete (f_c'). As shown in Table 3.3, the data covers a wide range of concrete compressive strengths from 11 to 76 MPa. However, the histogram shows that most of the data are for concrete with normal strength, from 18 to 44 MPa, and the data are not equally distributed from the minimum to maximum range of compressive strength of the concrete. The same is also true for the two input parameters (UPV and RN).

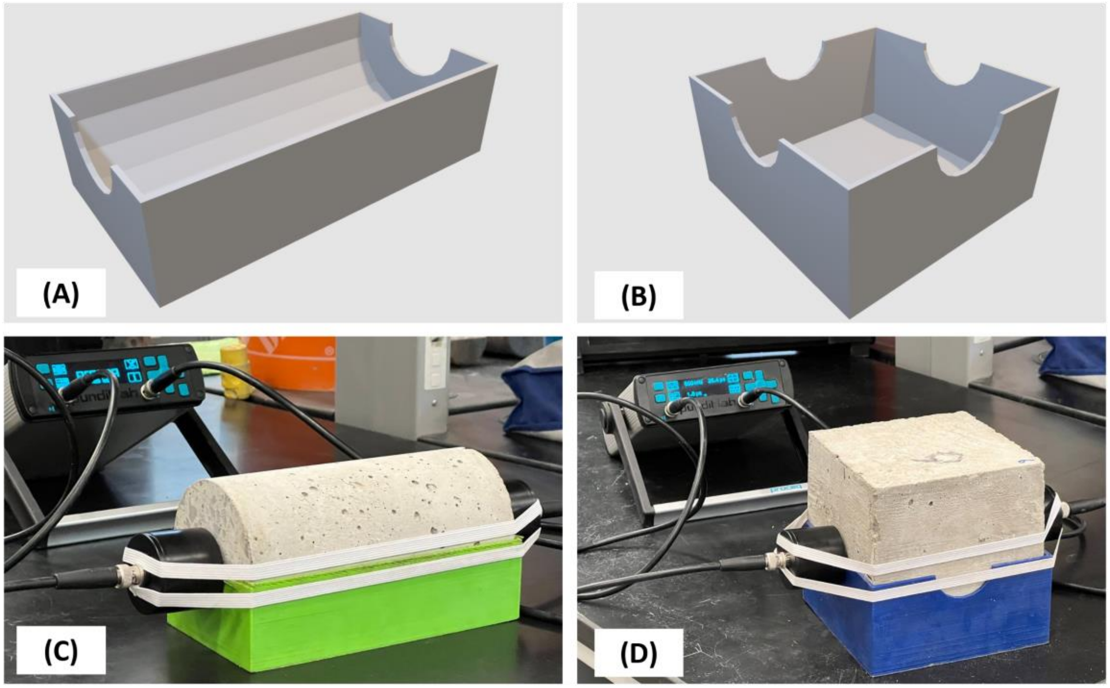

Figure 3.9: Drawings of 3D stands and direct UPV tests to extract accurate and reliable results, (A & C) for cylindrical specimens, and (B & D) for cubic specimens

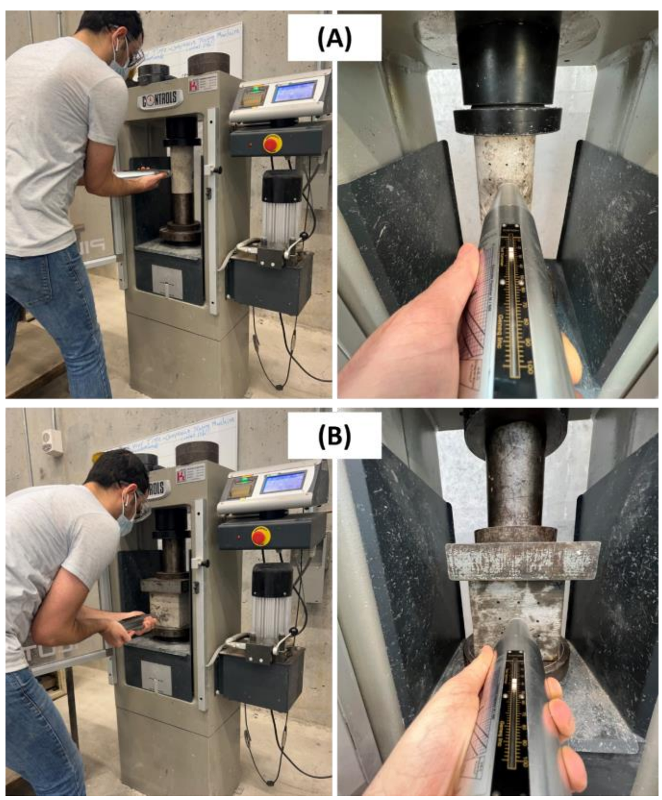

Figure 3.10: RN tests, (A) on cylindrical specimens and (B) on cubic specimens

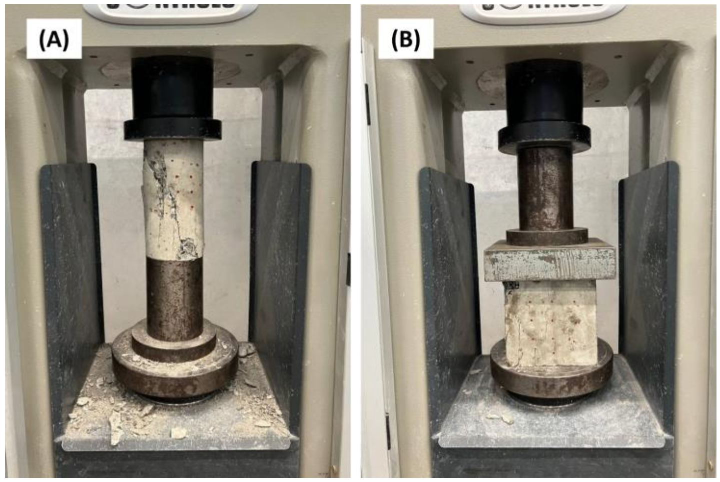

Figure 3.11: Compressive tests, (A) on cylindrical specimens and (B) on cubic specimens

Table 3.3 Statistical information of inputs and output variables

Variable	Unit	Type	Min	Max	Average
f_c'	MPa	Output	11.08	76.32	31.31
UPV	km/s	Input	3.243	5.39	4.56
RN	-	Input	10.33	55.5	30.6

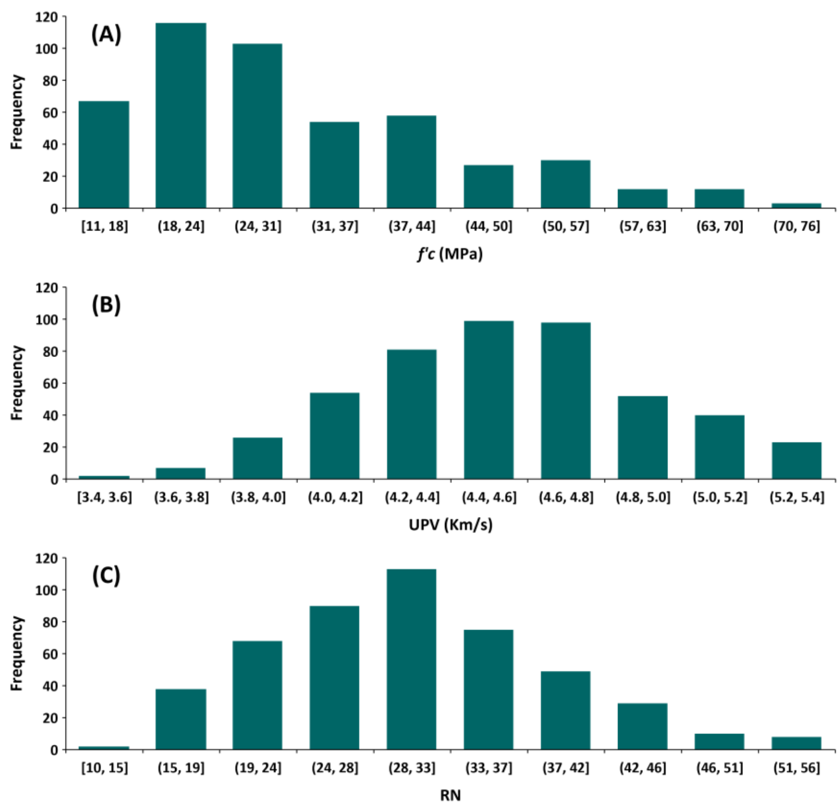

Figure 3.12: The histogram of inputs and output variables; (A) compressive strength, (B) UPV, and (C) RN

3.5 Machine Learning Model Development

3.5.1 Developing ANFIS Models

Most ML models are tested using randomly selected data obtained from the same database as the training set (Tapeh & Naser, 2022). This process does not capture the model's ability to successfully predict outcomes when data is introduced from new sources (Alavi et al., 2022). To achieve a more robust and reliable ANFIS model, a different approach is used. For this purpose, as shown in Fig. 3.13, three ANFIS models based on different training and testing datasets were developed:

- ANFIS-A: 75% of the combined database was randomly selected for the training dataset and the remaining 25% was selected as the testing dataset.
- ANFIS-B: 80% of the combined database was randomly selected for the training dataset and the remaining 20% was selected as the testing dataset.
- ANFIS-C: The collected data from previous literature, as well as the data from testing on specimens prepared by one of the two concrete ready-mix companies, were selected for the training dataset (462 unique data points). For the testing dataset, data from tests on cubic and cylindrical laboratory-fabricated specimens, and the data from tests on specimens provided by one of the companies were selected (20 unique data). In this way, the data used for the training and testing datasets are completely independent of each other.

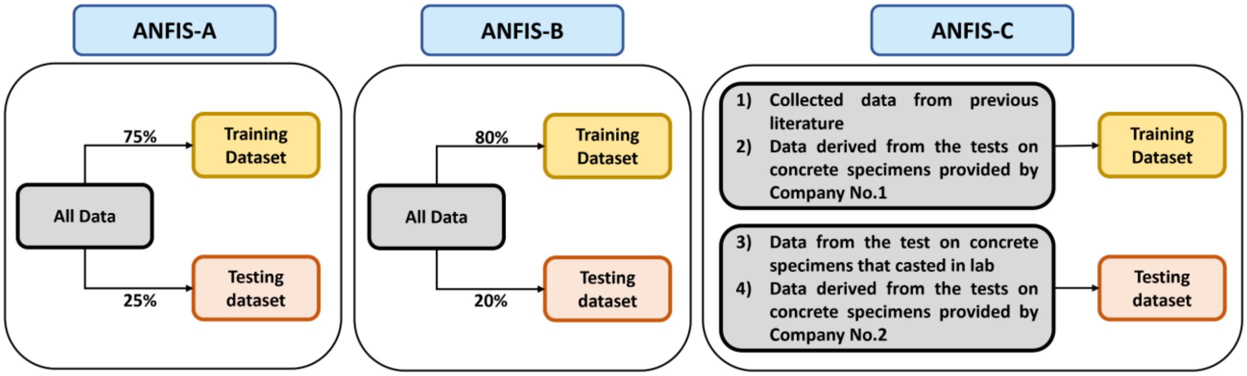

Figure 3.13: Comparison of selecting training and testing data in three different ANFIS models

The performance of these three models is compared in detail in Table 3.4. Two statistical parameters of Mean Absolute Percentage Error (MAPE) and R-squared are considered for this purpose (Eq. 3.7 and Eq. 3.8). The R-squared value indicates how the model-predicted value of the compressive strength is close to the measured value of the compressive strength of concrete from the experimental test. Additionally, the MAPE indicates the compressive strength prediction error in forecasting models. The optimal values for the R-squared and MAPE are 1 and 0%, respectively.

$$R^2 = 1 - \frac{\sum_{i=1}^{n}\left(f_{c(predict)} - f_{c(experimental)}\right)^2}{\sum_{i=1}^{n}\left(f_{c(predict)}\right)^2} \qquad \text{(Eq. 3.7)}$$

$$MAPE = \frac{1}{n}\sum_{i=1}^{n}\left(\frac{\left|f_{c(predict)} - f_{c(experimental)}\right|}{f_{c(experimental)}}\right) \times 100 \qquad \text{(Eq. 3.8)}$$

Table 3.4: Comparison of performance measured for generated ANFIS models

	Number of data		MAPE (%)			R^2		
Model	Training data	Testing data	Training data	Testing data	Combined data	Training data	Testing data	Combined data
ANFIS-A	362	120	12.10	14.46	12.69	0.9815	0.9805	0.9813
ANFIS-B	386	96	11.98	12.81	12.14	0.9819	0.9813	0.9818
ANFIS-C	462	20	11.64	14.95	11.78	0.9826	0.9688	0.9815

By comparing ANFIS-A and ANFIS-B, both developed using the conventional approach of splitting the data randomly into training and testing datasets, the results clearly show how increasing the proportion of data used for training (from 75% to 80% of the combined database) has a significant effect of reducing the MAPE value of the testing dataset (from 14.46% to 12.81%). The R-squared values for the testing datasets for both ANFIS-A and ANFIS-B are in the same range (0.9805 and 0.9813) that shows that both models have good overall performance.

However, the ANFIS-C model was developed with a new approach using two separate datasets (i.e., training and testing datasets were obtained from different sources). The number of training data for the ANFIS-C model (462 data) is more than the other two models (ANFIS-A and ANFIS-B), but the MAPE for the testing data is also higher (14.95%). Moreover, the R-squared value for the testing data was the lowest of the three models (0.97).

The ANFIS-C model is considered to be more representative of the true predictive ability of concrete compressive strength in general because it was developed using the largest dataset and was evaluated using independent data. It can be seen that the R-squared value for the training and testing datasets for both ANFIS-A and ANFIS-B is in the same range (i.e., 0.98). But, in the ANFIS-C model the R-squared for the training dataset (0.98) is higher than the testing dataset (0.97). In other words, the testing data were not seen by the ANFIS-C in the training procedure, and the outputs of the model are without any bias. Although the R-squared value for the testing data is slightly lower than the training dataset in the ANFIS-C model, it still indicates a strong predictive ability. Finally, the ANFIS-C model was selected as the best model for use in the next step in this study.

Fig. 3.14 gives the scatter graph of data information for the three main parameters: UPV, RN, and compressive strength of concrete (f_c') for the ANFIS-C model. Fig. 3.14 clearly shows that the testing datasets contain a relatively wide range of all three parameters (UPV, RN, and f_c'). The details of all 482 data points used for the proposed ANFIS-C model are presented in Table 3.1.

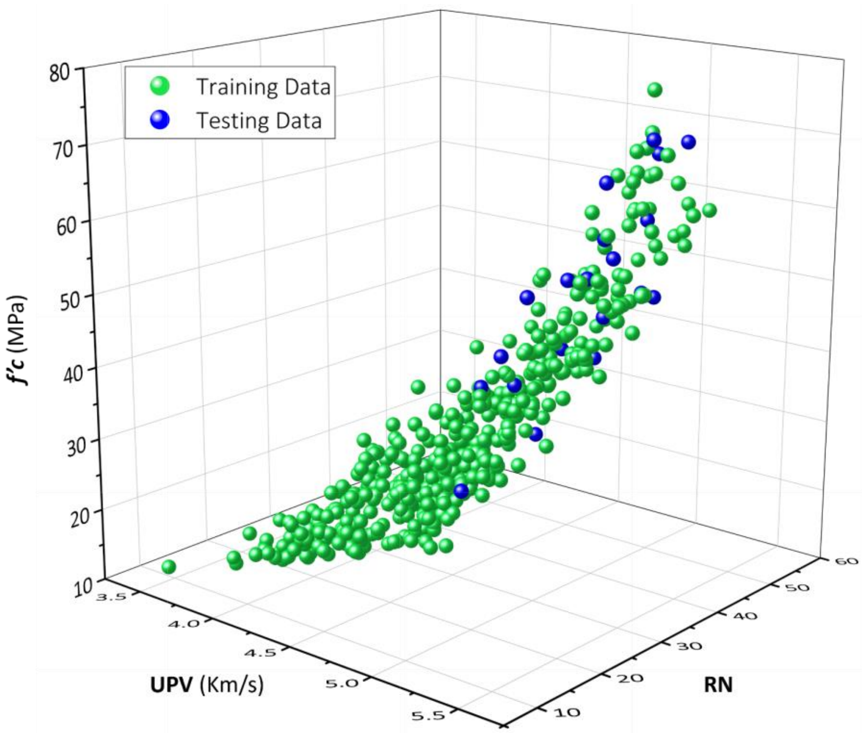

Figure 3.14: The three-dimensional scatter graph for the training data and the testing data of the ANFIS-C model

3.5.2 Graphical User Interface (GUI) for the ML Model

The main goal of this study is to present a practical model based on ML that is robust and easy to use. However, the proposed model ML model (ANFIS-C) requires MATLAB software to be able to run the model and obtain outputs. Moreover, it is necessary to normalize the crisp inputs (Eq. 3.9) and de-normalize the model's output (Eq. 3.10) (all data were normalized within the range of 0.1 to 0.9 using Eq. 3.9 to expedite the training process of the model).

$$x_{ni} = \left(\frac{8}{10} \times \frac{x_i - x_{min}}{x_{max} - x_{min}}\right) + \frac{1}{10} \qquad \text{(Eq. 3.9)}$$

$$x_i = ((x_{ni} - \frac{1}{10}) \times (x_{max} - x_{min})/\frac{8}{10}) + x_{min} \qquad \text{(Eq. 3.10)}$$

where x_{ni} is the normalized value of each parameter, x_i is the actual value (crisp value) of that parameter, x_{max} and x_{min} are the maximum and minimum values in the database for each parameter (Table 3.3). The selection of the range [0.1, 0.9] avoids the possibility of models collapsing due to parameters being assigned a value of zero (Naderpour & Alavi, 2017).

The procedure to obtain crisp output from the proposed ML model is a time-consuming process and requires basic knowledge of MATLAB and programming. Accordingly, a simple Graphical User Interface (GUI) application was designed (Fig. 3.15). By using the proposed app, the user can easily run the proposed ML model to predict the compressive strength of concrete on-site. For example, for a UPV reading of 4 Km/s and RN reading of 40, the proposed app gives a value of 26.27 MPa for compressive strength as shown in Fig. 3.15.

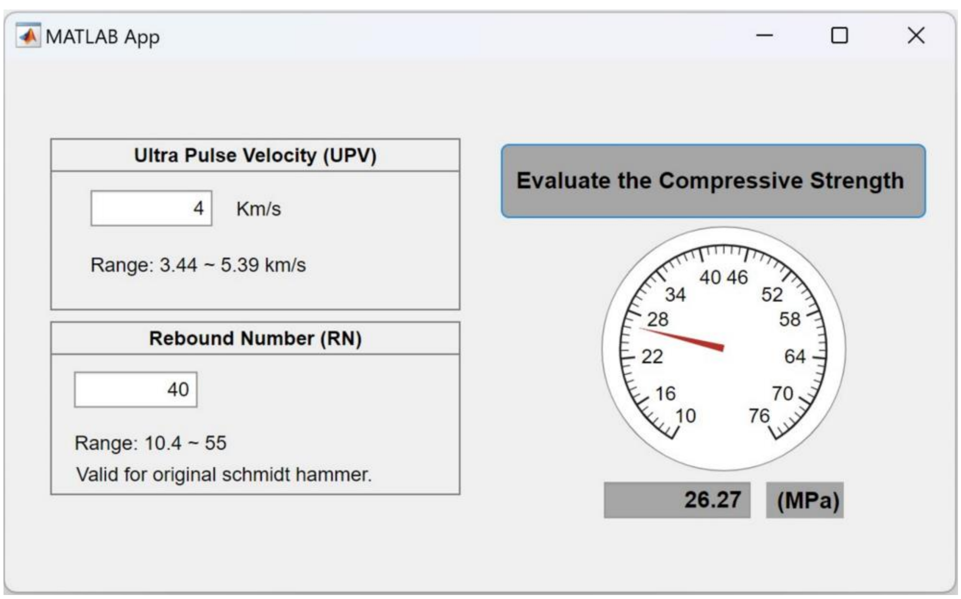

Figure 3.15: Screenshot of the GUI of the app that run the proposed ML model (ANFIS-C)

3.6 Multi-Variable Regression Model

3.6.1 Linear Equation

In addition to the proposed ML model that represents a powerful tool to capture complex relationships within the databank, a multi-variable linear regression model also was extracted from the databank. The linear regression model assumes a linear relationship between the three variables of UPV, RN, and compressive strength of concrete. In comparison to ML technique, the linear regression method is a simpler method used to establish a relationship between a dependent variable and independent variables (Lewis-Beck & Lewis-Beck, 2015; Montgomery et al., 2012). The linear regression formulation is presented in the form of Eq. 3.11, where 'Y' is the dependent variable (compressive strength), 'X_i' are the independent variables (UPV and RN), 'β_i' are regression coefficients which represent the slope of the line, and 'b' is the intercept.

$$Y = b + \beta_1 X_1 + \beta_2 X_2 \qquad \text{(Eq. 3.11)}$$

By fitting this line to our data points, an equation was obtained to make a prediction for compressive strength of concrete. For this purpose, the data analysis kit tool in Microsoft Excel was used to extract the linear equation (Najim, 2017). Accordingly, all 482 data points were used as the observation data for correlation of UPV and RN variables with the compressive strength of concrete. Finally, the following equation was extracted:

$$f_c' = -74.04 + (17.767 \times UPV) + (0.794 \times RN) \quad \text{(Eq. 3.12)}$$

where 'f_c'' is the concrete compressive strength (MPa), 'UPV' is ultrasonic pulse velocity (Km/s) from UPV test, and 'RN' is rebound number. The mean absolute percentage error (MAPE) of the extracted linear regression equation based on the complete dataset is 17.16%, and the R-squared value is 0.971. It is worth mentioning that the proposed equation only applies to combined NDT results with values greater than 3.37 km/s for UPV and 18 for RN.

3.7 Nonlinear Equation

Various forms of nonlinear equations for converting SonReb results to the concrete compressive strength have been proposed (Breysse, 2012). Among these, exponential equations in the form of Eq. 3.13 have been commonly used by previous researchers (Meynink & Samarin, 1979; Samarin & Dhir, 1984).

$f_c' = \beta_1 \times (UPV^4) + \beta_2 \times (RN) + b$ (Eq. 3.13)

where 'f_c'' is the concrete compressive strength, 'UPV' is ultrasonic pulse velocity, 'RN' is rebound number, β_i' is coefficient of two dependent variable of UPV and RN, and 'b' is the intercept. Accordingly, in this study, this form of equation was calibrated with all 482 data to find the coefficients values for β_1 and β_2, and the intercept value of b. Finally, the following equation was extracted;

$f_c' = -14.003 + 0.052 \times (UPV^4) + 0.711 \times (RN)$ (Eq. 3.14)

where 'f_c'' is the concrete compressive strength (MPa), 'UPV' is ultrasonic pulse velocity (Km/s), and 'RN' is rebound number. For this equation, the average error (MAPE) based on the complete dataset is 15.53% and the R-squared value is 0.975.

3.8 Comparison and Analysis

To have a better understanding of the performance of the proposed ML model and two regression equations (Eq. 3.12 and Eq. 3.14), the results of these three models were compared with four equations from literature which are listed in Table 3.5. Accordingly, the performance comparison is based on the information in Table 3.6, Fig. 3.16, Fig. 3.17, Fig. 3.18, and Fig. 3.19.

The equations presented in Table 3.5 were selected for this study because they provide compressive strength of cylinders (rather than cubes) and therefore are more appropriate for the subsequent validation using core samples (Cristofaro et al., 2020). According to Table 3.5, the Ramyar & Kol equation (Eq. 3.17) is in the linear (LN) form, and three remaining equations (Eq. 3.15, 3.16, and 3.18) are in polynomial (PL) form similar to Equation 3.14.

Table 3.5: Selected Equations to evaluate the strength with the SonReb method

No.	Author	Formulation	Units	Type
1	Meynink & Samarin,	$f_c' = -24.668 + 1.427 \times RN + 0.0294 \times UPV^4$ (Eq. 3.15)	MPa, km/s	PL
2	Samarin & Dhir	$f_c' = -12 + 0.1 \times UPV^4 + 0.76 \times RN$ (Eq. 3.16)	MPa, km/s	PL
3	Ramyar & Kol	$f_c' = -39.57 + 1.532 \times RN + 5.0614 \times UPV$ (Eq. 3.17)	MPa, km/s	LN
4	Beconcini & Formichi,	$f_c' = 5.9 + 2.712 \times 10^{-15} \times RN \times UPV^4$ (Eq. 3.18)	MPa, m/s	PL

Table 3.6: Comparison of performance in prediction of compressive strength for all models

No.	Model	MAPE (%)	R^2
1	ML model	11.78	0.981
2	Nonlinear equation	15.53	0.975
3	Linear equation	17.16	0.971
4	Ramyar, Kol	19.65	0.959
5	Meynink, Samarin	32.96	0.933
6	Beconcini, Formichi	45.73	0.879
7	Samarin, Dhir	87.06	0.803

According to Table 3.6, Fig. 3.16, and Fig. 3.17, the proposed ML model demonstrated the most optimized outcomes when assessed in terms of the MAPE and R-squared metrics in comparison to all the other equations. Fig. 3.16 and Fig. 3.17 shows the prediction accuracy of each model for all 482 data points. An ideal model is a model where all the points are located on the X=Y line (0% error); in other words, the predicted values of compressive strength are exactly equal to the experimental value. Accordingly, the proposed ML model gives the best prediction in comparison to the other five plots. In Fig. 3.16(A), which belongs to the ML model, the points are distributed on both sides of the line X=Y (predicted value equal to experimental value), which means that the model is not highly overestimated (points located in the positive error region) or highly underestimated (points located in negative error region). Also, most of the points in the graph are located between the two lines that show +20% and -20% differences between predicted and experimental values. Regarding the proposed linear and nonlinear equations, although they give a better prediction in comparison to the other four equations (based on the information in Table 3.6), it can be seen in both Fig. 3.16(B) and Fig. 3.16(C) that these model's results are highly underestimated, and many points exceeded the line of -20% error.

It is important to examine how the input parameters (UPV, RN) relate to and impact the target parameter, which is the compressive strength. For this purpose, the 3-dimensional interaction plots (surface) were extracted from the ML model, proposed equations, and other four equations, and are presented in Fig. 3.18 and Fig. 3.19. As can be seen, the proposed ML model's 3D graph (Fig. 3.18(A)) has discontinuities which make it difficult to explicitly define the relationship between inputs and outputs by a mathematical formula. This is contrasted by the other 3D plots for the proposed equation and the four equations from literature. The complex and discontinuous nature of the relationship between these parameters is evidence that supports the development of ML as a valuable alternative to common mathematical approaches in conjunction with the SonReb method.

Moreover, by comparing the 3D plots of Fig. 3.19(A) to Fig. 3.19(D), it can be seen that Ramyar and Kol's plot (Fig. 3.19(C)) is closer in shape to the proposed ML model (Fig. 3.18(A)), which is in agreement with its improved performance relative to the other equations proposed in literature.

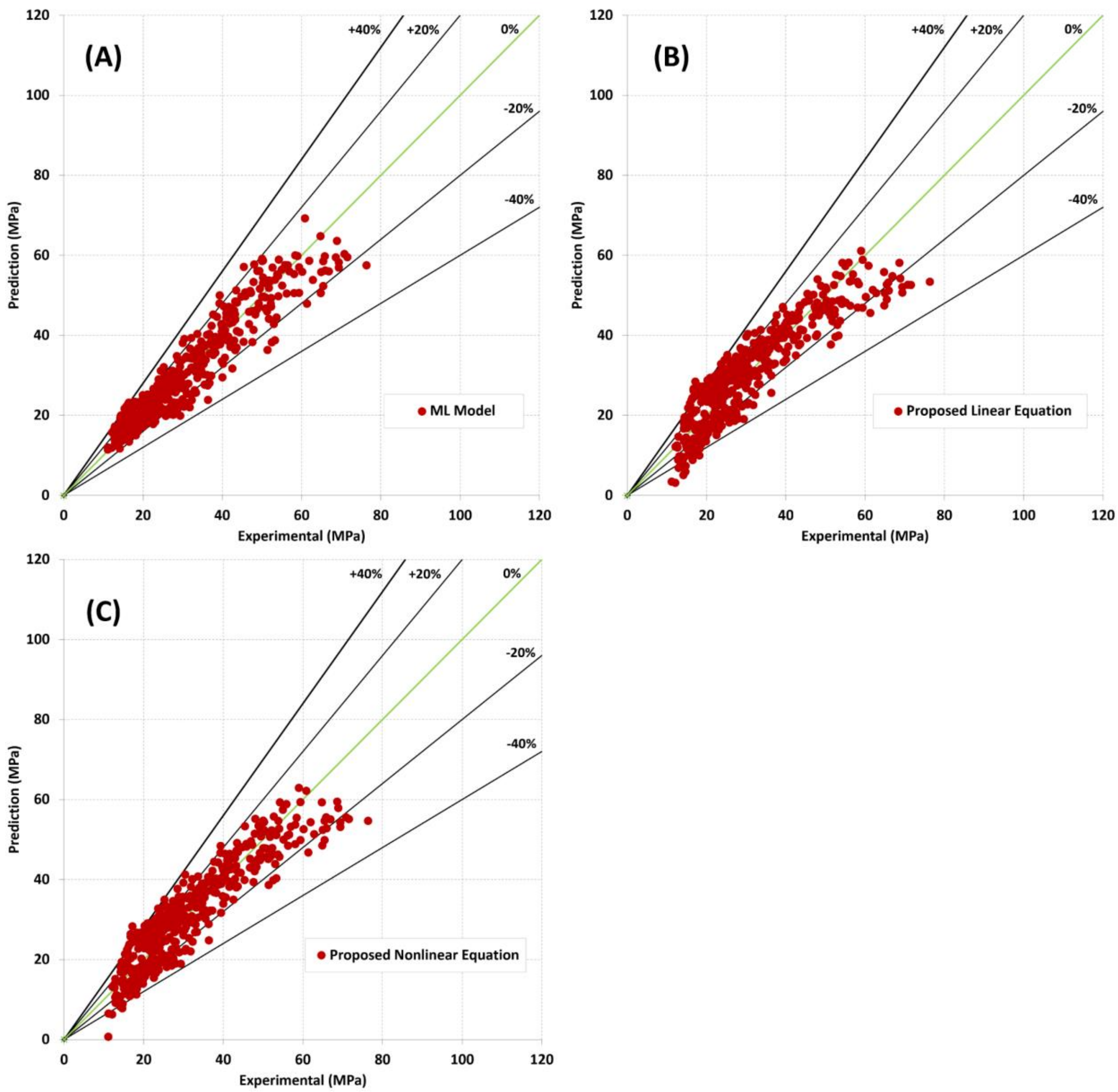

Figure 3.16: Scatterplot of the predicted value of concrete strength vs. the experimental value of concrete strength for: (A) proposed ML model, (B) proposed linear equation, (C) proposed nonlinear equation

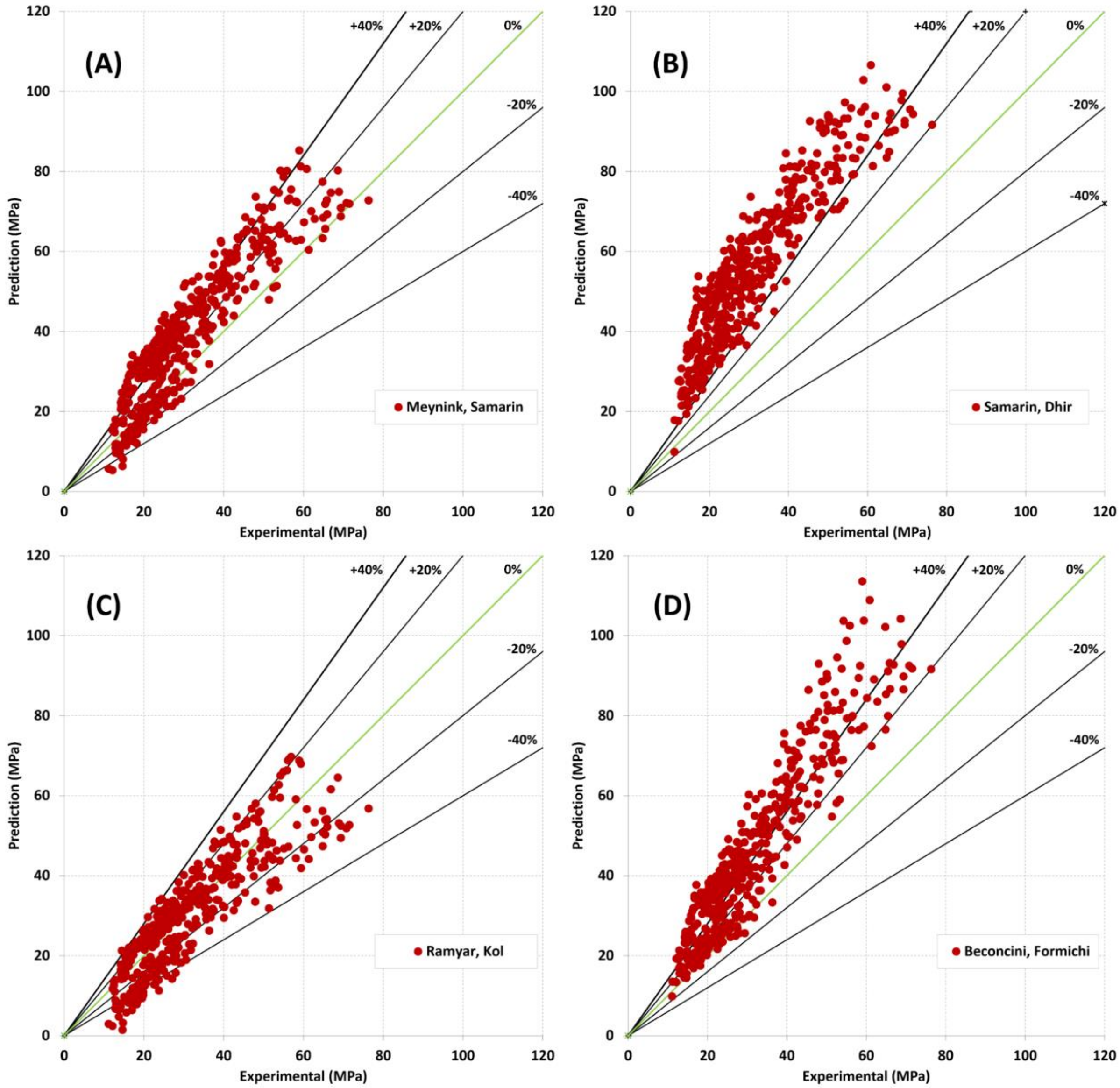

Figure 3.17: Scatterplot of the predicted value of concrete strength vs. the experimental value of concrete strength for: (A) Meynink and Samarin's equation, (B) Samarin and Dhir's equation, (C) Ramyar and Kol's equation, and (D) Beconcini and Formichi's equation

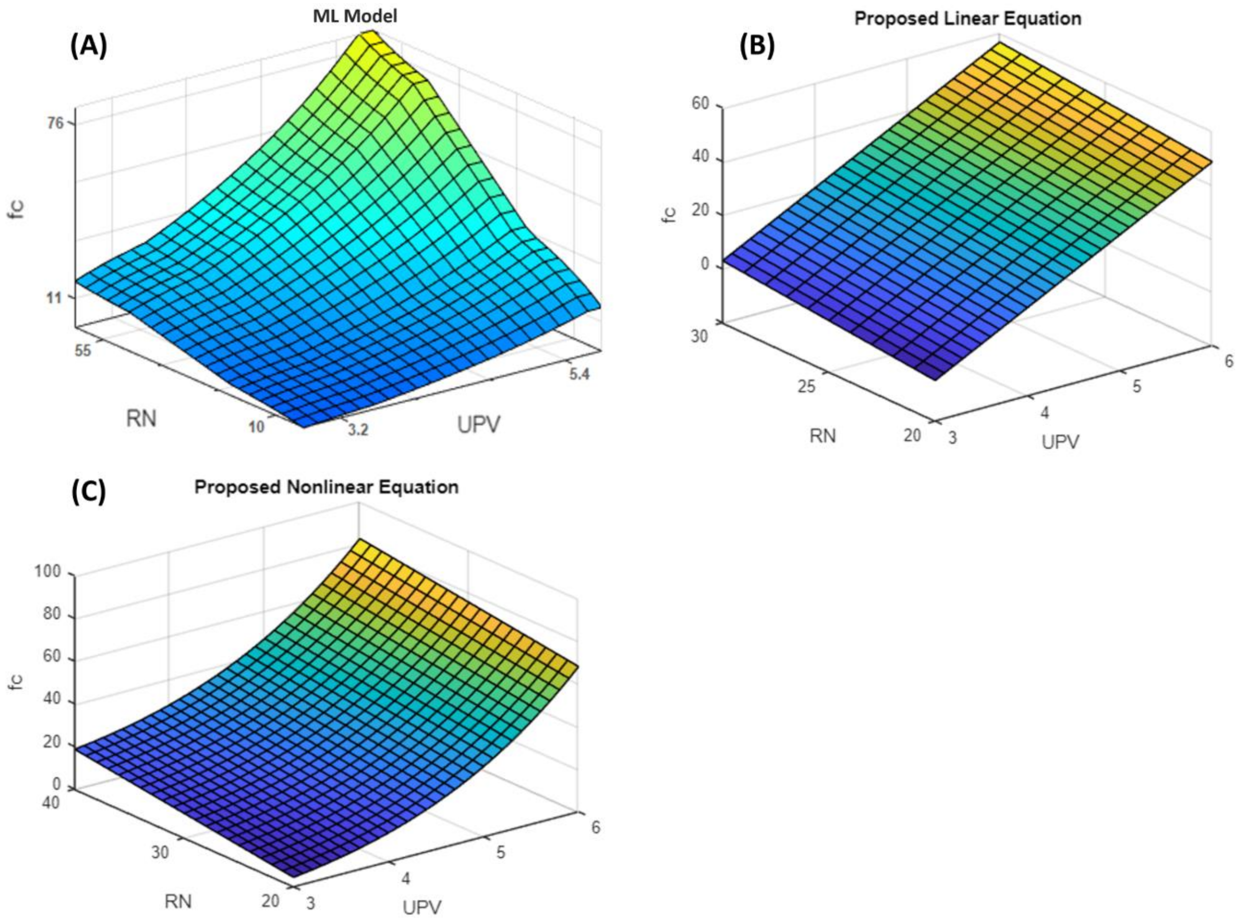

Figure 3.18: The surface graph between the three parameters of UPV, RN, and compressive strength for: (A) Proposed ML model, (B) proposed linear equation, and (C) proposed nonlinear equation

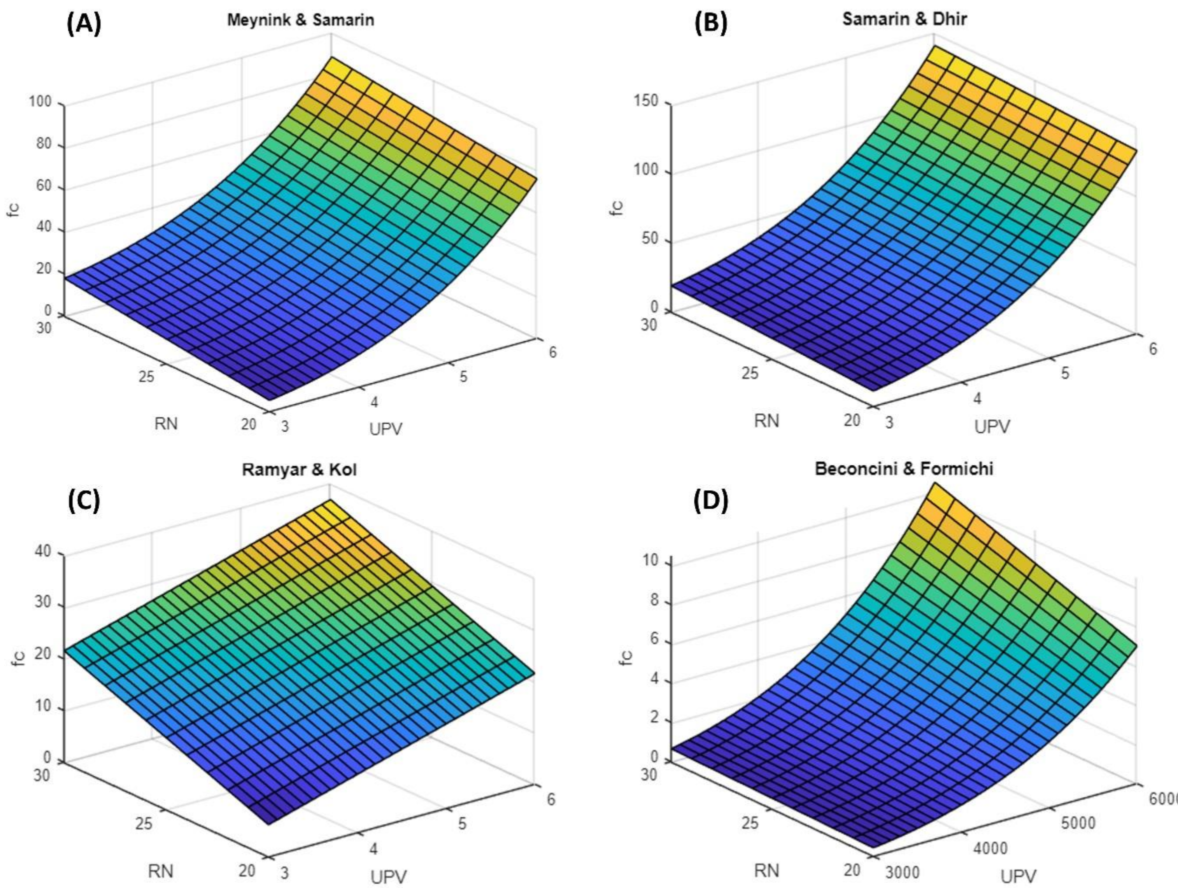

Figure 3.19: The surface graph between the three parameters of UPV, RN, and compressive strength for: (A) Meynink and Samarin's equation, (B) Samarin and Dhir's equation, (C) Ramyar and Kol's equation, and (D) Beconcini and Formichi's equation

3.9 Validation

The ML model and proposed equations were developed based on data from plain concrete samples. To further validate the models' performance, a reinforced concrete slab having dimensions of 2×2 m by 0.3 m depth that was cast with typical ready-mix concrete with a target 28-day design strength of 25 MPa was used. The concrete used to pour the slab had a maximum aggregate size of 20 mm, a water-cement ratio of 0.63, and a slump of 80 mm. The average compressive strength of concrete cylinders tested at an age of 28 days was 29.6 MPa. The slab contained a geometric discontinuity in the form of a step-change in thickness of the slab, from

200 mm to 300 mm. Half of the slab contained reinforcing steel while the other half was unreinforced (Fig. 3.20 and Fig. 3.21) (Lacroix et al., 2021).

The NDT testing points were determined on the slab as shown in Fig. 3.21. At each testing point, first one direct UPV test was performed (Fig. 3.22(A)), followed by a rebound hammer test (Fig. 3.22(B)), and finally one core sample was extracted (Fig. 22(C)).

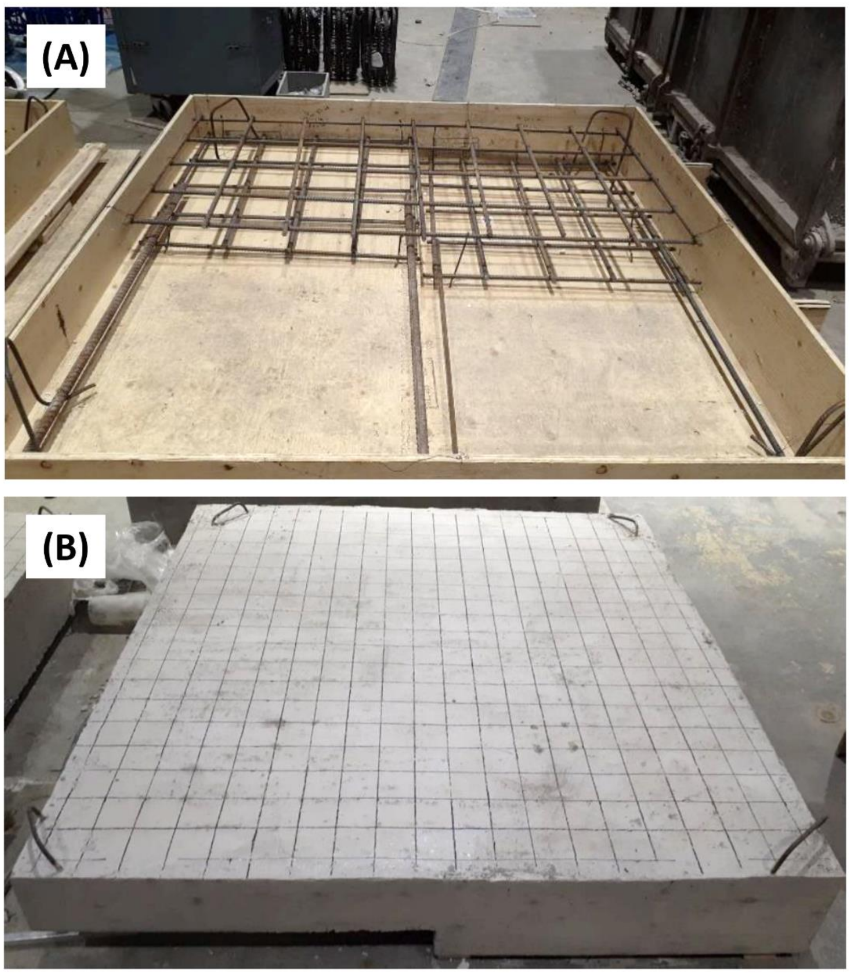

Figure 3.20: (A) The reinforcement of the RC slab (Lacroix et al., 2021) and (B) after two years from concrete casting

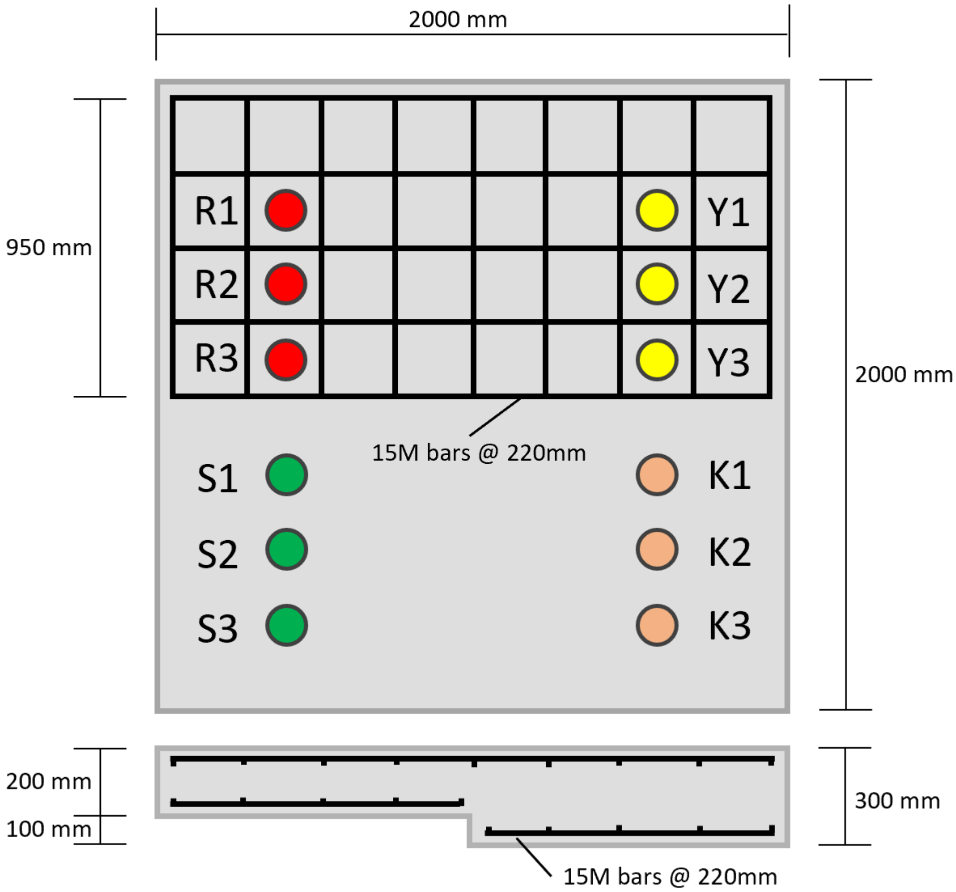

Figure 3.21: Drawing of the slab with the locations of NDT testing and coring points

Figure 3.22: (A) Direct UPV tests, (B) downward rebound hammer test, and (C) getting cores

Because of the dimensions of the slab, it was not possible to do both direct UPV and horizontal RN tests at the same point. On the other hand, direct UPV and downward RN tests were done at the same testing points on the slab (Fig. 3.22). To solve this issue, the downward RN were converted to horizontal RN using the graph provided by the rebound hammer manufacturer.

The results of the NDT, core tests, the proposed ML model, proposed linear and nonlinear equations, and the other four equations from literature are presented in Table 3.7 and Fig. 3.23 shows a head-to-head comparison of compressive strength for measured values from core tests and predicted values from the models. Table 3.8 summarizes the error terms for each model, and in Fig. 3.24 the scatter plot is presented to show the distribution of the measured values from core tests versus the predicted values from the models. Fig. 3.25 presents a detailed comparison between the proposed ML model, linear equation, and nonlinear equation in different regions of the slab.

Table 3.7: Results of NDT, core tests, and predicted strength from ML model and equations

Point	UPV	RN	Core Test	ML Model	Linear Equation	Nonlinear Equation	Meynink, Samarin	Samarin, Dhir	Ramayar, Kol	Beconcini, Formichi
	(Km/s)	--	(MPa)	(MPa)	(MPa)	(MPa)	(MPa)	(MPa)	(MPa)	(MPa)
R1	4.501	41.6	34.93	31.16	38.76	37.07	51.29	60.66	46.94	52.2
R2	4.291	41.2	33.4	30.78	34.72	33.04	46.65	53.21	45.27	43.78
R3	4.331	42	36.39	30.82	36.06	34.28	48.39	55.1	46.69	45.98
Y1	4.314	40.5	34.44	31.67	34.57	32.93	46.21	53.42	44.31	43.94
Y2	4.344	40.8	34.19	31.71	35.34	33.65	47.15	54.62	44.92	45.3
Y3	4.328	41.6	35.27	34.15	35.69	33.95	47.83	54.7	46.07	45.49
S1	4.529	40.7	34.63	33.79	38.55	36.97	50.77	61.01	45.71	52.34
S2	4.582	40.9	30.36	36.65	39.65	38.16	52.18	63.16	46.28	54.79
S3	4.496	41	32.86	34.17	38.2	36.55	50.44	60.02	46	51.33
K1	4.531	40.8	34.02	36.12	38.66	37.08	50.94	61.16	45.87	52.54
K2	4.598	41.6	37.94	34.91	40.48	38.98	53.41	64.31	47.43	56.33
K3	4.2	39.8	26.6	32.61	31.99	30.59	43.3	49.36	42.66	39.49

Table 3.8: Performance statistics of all models based on the error terms

Term	ML Model	Linear Equation	Nonlinear Equation	Meynink, Samarin	Samarin, Dhir	Ramayar, Kol	Beconcini, Formichi
MAPE (%)	9.7	9.9	7.7	46.0	71.3	36.1	44.6
The maximum absolute error (%)	22.6	30.6	25.7	71.9	108.0	60.4	80.5
The minimum absolute error (%)	2.4	0.4	1.1	33.0	51.4	25.0	26.3

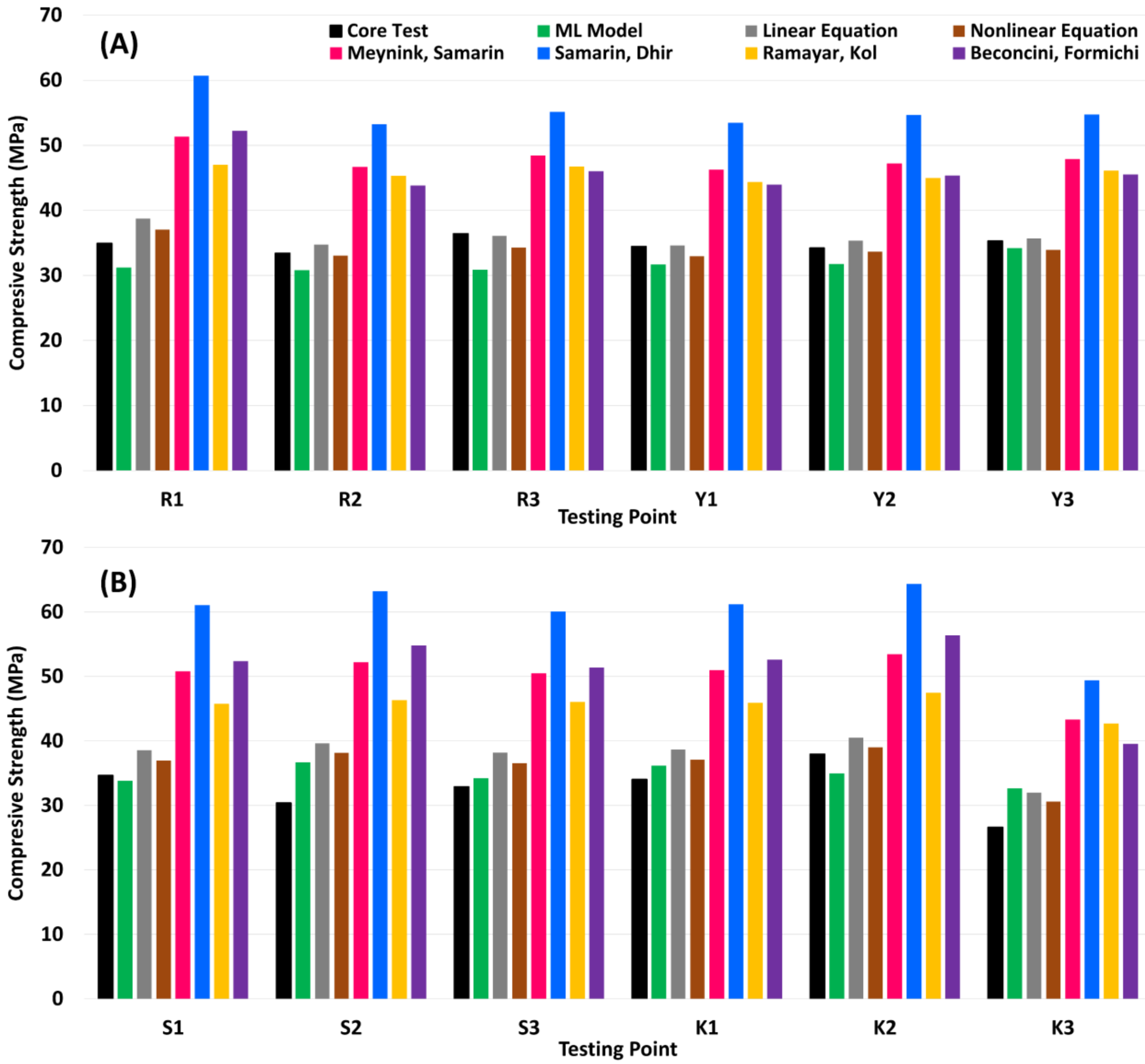

Figure 3.23: Concrete strength from the results of core tests and the models' prediction for: (A) testing points on reinforced region and (B) unreinforced region of the slab

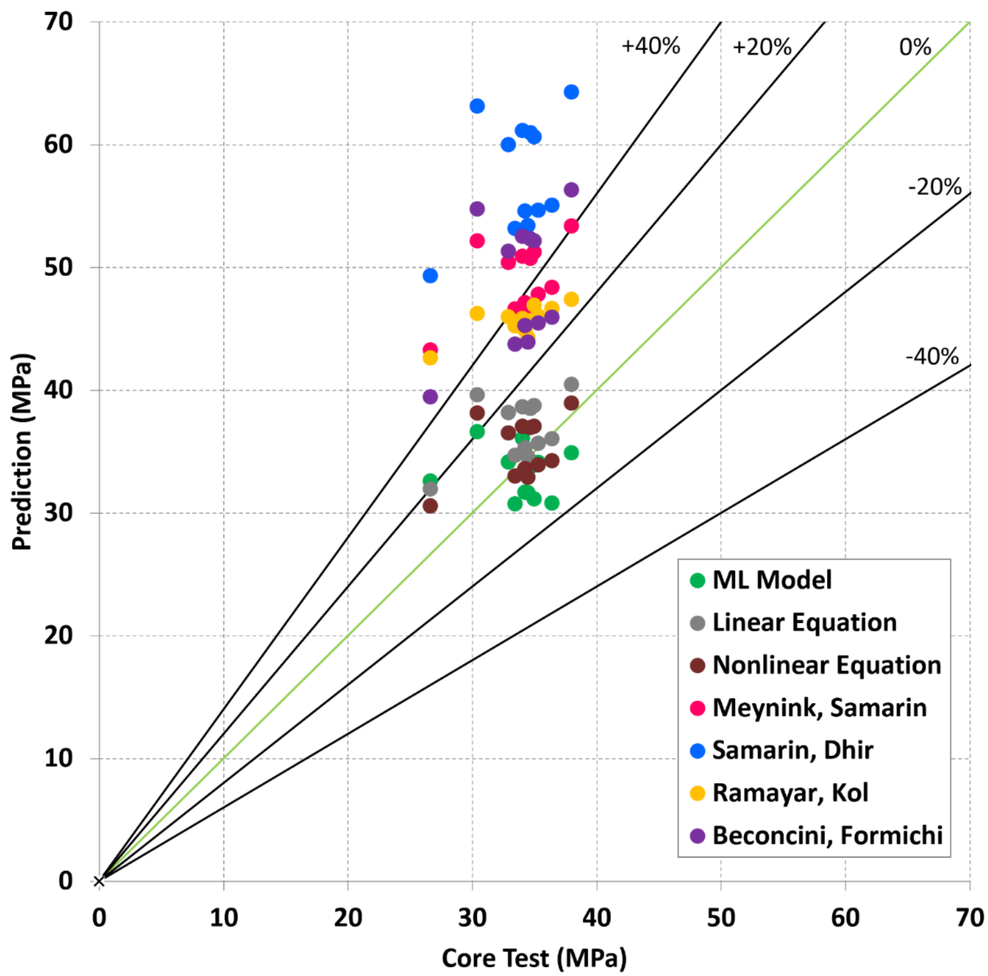

Figure 3.24: Predicted values vs. core tests value of compressive strength from the proposed ML model, proposed equations, and other four equations

According to Table 3.8, when considering the MAPE parameter, the proposed nonlinear equation demonstrates the lowest average error for the slab. However, upon conducting a thorough examination of the maximum absolute error and analyzing the scatter plot for the proposed nonlinear equation, it becomes evident that the nonlinear equation gives a higher maximum error compared to the proposed ML model. In other words, although the MAPE value for the proposed ML model is 9.7%, it can be observed in Table 3.8 that the lowest value for the maximum absolute error parameter belongs to the ML model.

Also, according to Table 3.7 and Fig. 3.23, almost all equations except the ML model tended to overestimate the concrete's compressive strength in all twelve testing points. However, the ML model slightly underestimated the concrete's strength in the reinforced region of the slab (Fig. 3.23(A)) and overestimated in the unreinforced region of the slab (Fig. 3.23(B)). On the other hand, according to Fig. 3.24, only for the ML model, the points were distributed on both sides of the line X=Y with the lowest error. Regarding the four selected equations from previous literature, it was expected that Ramayar and Kol's formulation would give a better estimation in comparison with the other three formulations (Meynink & Samarin, Samarin, Dhir, Beconcini, Formichi). Based on the 3D plots shown in Fig. 3.19, Ramayar and Kol's plot is the most similar plot to the ML model among the other three formulations (Meynink & Samarin, Samarin, Dhir, Beconcini, Formichi). The results presented in Table 3.8 and Fig. 3.24 confirmed this fact.

A detailed comparison between the ML model, linear equation, and nonlinear equation is presented in Fig. 3.25. The proposed linear equation was the most accurate model for three locations (R3, Y1 and Y3) out of twelve, which were all located in the reinforced region of the slab. The proposed nonlinear equation provided the most accurate strength estimates at five locations (R1, R2, Y2, K2, and K3) while the ML model had the best performance at four locations (S1, S2, S3, and K1), which were all located in the non-reinforced region. Overall, the nonlinear equation performed significantly better than the linear equation (MAPE of 7.7% vs 9.9%), while the ML model consistently outperformed the other methods in unreinforced regions.

It can also be observed from Fig. 3.25 that the prediction lines belonging to the linear and nonlinear equations are parallel with the linear equation overestimating the concrete strength in comparison to the nonlinear equation in all four regions of the slab. On the other hand, it can be seen that the green line that represents the ML model shows a different pattern in comparison with both equations with smaller fluctuations; comparing the difference between the maximum absolute error and the minimum absolute error values in Table 3.8, this value is equal to 20.2% for the ML model, 30.2% for the linear equation, and 24.6% for the nonlinear equation. On this basis, it can be concluded that the ML model generated the most consistent predictions for concrete strength for this case study.

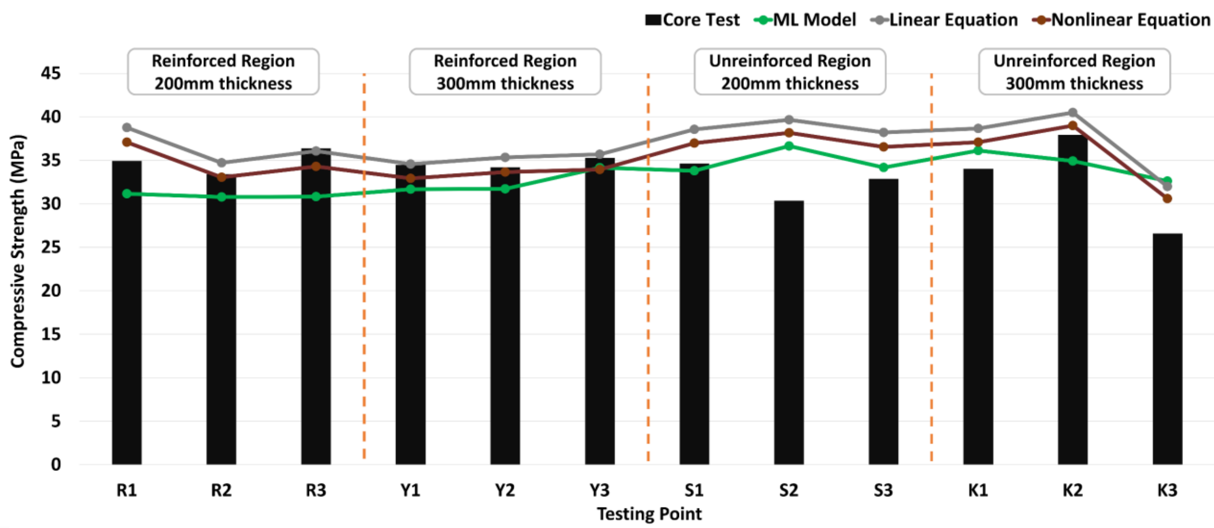

Figure 3.25: Comparison between proposed ML model, LN equation, and NLN equation with core tests

In this case study, the proposed ML model was able to predict the compressive strength of concrete with an average error of less than 10% and the presence of steel reinforcement did not make a significant difference in the accuracy of the model. It should be noted that the NDT and cores were intentionally not performed directly over reinforcing bars. Although the model performed well in this particular case study, it is needed to evaluate the proposed model with data obtained from field studies in the future to confirm its performance in real structures. It should be mentioned that different sets of concrete experiments can exhibit significant variations in characteristics. While the testing and training databases did include a wide range of concrete types and properties to be representative of common applications, concrete placed in the field can vary and the effectiveness and accuracy of this model have not been assessed for all possible cases. The effects of concrete composition and exposure conditions—among other factors which are known to affect RN and UPV results—on model performance in field structures is of considerable interest and importance in the development of a practical general-use method for concrete strength predictions.

3.10 Discussion on ML Model: Limitations and Future Study

In this study, the ML model was developed using only two input parameters (UPV and RN) that can be obtained using common NDT methods, with the main goal of developing a practical ML model and easy to use approach for estimating the in-place strength of concrete. The application of ML models to improve the accuracy of the SonReb method could potentially reduce the number of DT required for the evaluation of RC structures. Moreover, a reliable and accurate ML model could help engineers to obtain concrete strength information for all parts of an existing RC structure to make informed management decisions.

It is also worth pointing out that developing a perfect model with MAPE = 0% and/or R-squared = 1 is not a realistic possibility. Concrete is a heterogeneous material and compressive strength tests from a single batch of concrete can vary considerably. In most cases, it is not reasonable or necessary to know the precise in-place strength of concrete with a high degree of certainty, and an average error of 15% is likely to be acceptable in many applications. In cases where a higher degree of certainty is required, core testing is the only solution to obtain exact values of compressive strength. Nevertheless, the proposed methodology (combining NDT with

AI) has the potential to reduce the number of cores needed. Using a small number of core tests to validate the model for a particular structure may still lead to significant benefits compared to an extensive testing campaign that would be necessary to characterize the variation in strength for a large structure.

Limitations of the ML models presented in this paper should also be acknowledged. For instance, it was previously mentioned that specimen geometry was ignored (as a third input for the model) even though it is known to influence NDT and compressive strength results. It is likely that as the database is expanded to include more results from different geometries, a three-parameter model could be developed with increased accuracy by accounting for this effect. The effects of other parameters, such as concrete age or coarse aggregate type, could also be considered for future versions of the model provided sufficient data.

Morever, there are limitations on the model inputs which are (1) the RN from the horizontal rebound hammer test, and (2) pulse velocity from the direct UPV test. It is possible to convert the vertical RN value (for both upward and downward tests) to a horizontal value; however, for the UPV test, it is not possible to convert the results of indirect and semi-direct UPV tests into direct UPV test results. In many field applications, indirect UPV tests may be the only option; a database of field studies with both direct and indirect UPV measurements is needed to investigate this further.

These limitations present opportunities for future work that considers the effects of additional parameters to improve the model's performance. For example, developing the model for fresh concrete (less than 14 days) and accounting for the presence of steel reinforcement (particularly for congested reinforcement configurations) would be valuable contributions. Despite remaining challenges and limitations, the results of this study have highlighted the potential for AI to augment structural evaluation practices using simple NDT methods to estimate the mechanical properties of in-place concrete.

3.11 Conclusions

In this study, an ML model was developed to investigate whether AI models could be used to predict the on-site compressive strength of concrete in practice using only two NDT measurements. Also, besides the ML model, two linear and nonlinear equations were proposed. To develop the ML model and extract the equations, an experimental program was carried out along with extensive data collection from available literature to create a large databank with 482 unique data points (after cleaning). Then, to validate the ML model and the equation with the individual data, the NDT and DT tests were performed on twelve points on the RC slab with an age of two years to use as a validation dataset. According to the results, the following conclusions have been drawn:

1) It is clearly shown that the number of training data is a significant influencing factor for ML models if the training and testing data are selected randomly from one databank (conventional approach). In this study, a new approach was presented to reduce bias in model results using distinct datasets for training and testing, and also able to maximize the number of training data. The resulting model (ANFIS-C) achieved an average error of 11.78% (MAPE) based on all data in comparison to the model that was trained with 75% of all data (ANFIS-A) which achieved an average error of 14.46%, the model that was trained with 80% of all data (ANFIS-B) with an average error of 12.81%.
2) The proposed ML model (ANFIS-C model) was trained with the highest number of training data (462) and evaluated using concrete obtained from different sources. The primary results showed that the model was slightly conservative and had a MAPE value

of 14.95% based on the testing dataset. The proposed model performed well in the validation phase for a RC slab with a MAPE value of 9.7%. Further investigation with additional case studies is recommended to confirm the model performance in a wide range of real-life scenarios.

3) A GUI application was designed to enable engineers to use the ML model without needing a programing background to facilitate knowledge transfer to general practice. By increasing the number of users, the advantages and disadvantages of the presented ML model can be better identified.

4) The proposed nonlinear regression equation shows good results in comparison with the proposed linear equation as well as equations from literature. The MAPE value of the proposed nonlinear equation for 482 observation data is 15.53% and for the validation dataset is 7.7%. The proposed equation shows good prediction results, but with further investigation, it was shown that it is not as reliable as the proposed ML model due to higher variability.

5) It was demonstrated that a two-parameter ML-based model could give reasonable estimations of concrete compressive strength using only UPV and RN measurements and without any further information (e.g., mix design, age, geometry, etc) of concrete. However, many factors affect concrete performance that can also affect UPV and RN, which can be considered as additional parameters to increase the accuracy of the model in the future. Future model improvements may be achievable by considering additional parameters, although this likely requires an expanded database with sufficient data points corresponding to each category. This is the subject of ongoing study.

6) Based on the results of this study, ML models have the potential to significantly reduce or eliminate the need for core testing of sound concrete in the future for common applications through effective use of NDT data. However, it is important to note that the current model is not applicable to all concrete types. For a comprehensive, practical, and accurate model, additional training data is needed to cover the full range of possible input and output variables.
7) The main challenge to the development of a reliable ML model is building a comprehensive databank that includes all influencing factors on concrete. This is a complex problem, since concrete is a heterogeneous material that is made from a combination of different constituent materials with different proportions, and it is also affected over time by physical and environmental elements. Any model, simple or sophisticated, should only be considered as a tool and its results should always be interpreted using good engineering judgment.

3.12 References

Abioye, S. O., Oyedele, L. O., Akanbi, L., Ajayi, A., Delgado, J. M. D., Bilal, M., Akinade, O. O., & Ahmed, A. (2021). Artificial intelligence in the construction industry: A review of present status, opportunities and future challenges. Journal of Building Engineering, 44, 103299.

ACI Committee 228. (2019). 228.1R: In-Place Methods to Estimate Concrete Strength. American Concrete Institute.

Alavi, S. A., & Noël, M. (2022). Challenges for the development of artificial intelligence models to predict the compressive strength of concrete using non-destructive tests: a review. Canadian Society of Civil Engineering Annual Conference 2022.

Alavi, S.A., Hasak, A., Noel, M., Moradi, F., Layssi, H. (2022). Non-Destructive Evaluation of Concrete Compressive Strength Using Neuro-Fuzzy Modelling Approach. The International Symposium on Nondestructive Testing in Civil Engineering. https://www.ndt.net/search/docs.php3?id=27244

Ali Poorarbabi. (2020). Assessment of concrete compressive strength and electrical resistivity using NDT techniques and artificial neural networks. The University of Sistan & Baluchestan.

Almasaeid, H., Alkasassbeh, A., & Yasin, B. (2022). Prediction of Geopolymer Concrete Compressive Strength Utilizing Artificial Neural Network and Nondestructive Testing. Civil and Environmental Engineering.

Alwash, M., Breysse, D., & Sbartaï, Z. M. (2015). Non-destructive strength evaluation of concrete: Analysis of some key factors using synthetic simulations. Construction and Building Materials, 99, 235–245.

Asteris, P. G., & Mokos, V. G. (2020). Concrete compressive strength using artificial neural networks. Neural Computing and Applications, 32(15), 11807–11826.

Asteris, P. G., Skentou, A. D., Bardhan, A., Samui, P., & Lourenço, P. B. (2021). Soft computing techniques for the prediction of concrete compressive strength using Non-Destructive tests. Construction and Building Materials, 303, 124450.

ASTM C805-08: Test for Rebound Number of Hardened Concrete. (2018). American Society for Testing and Materials, USA.

Beconcini, M. L., & Formichi, P. (2003). Resistenza del calcestruzzo, misure sclerometriche e di velocità di propagazione degli ultrasuoni in strutture esistenti: risultati di una campagna di indagini. 10th Congresso Nazionale Dell’AIPnD, Ravenna, Italy, 372–380.

Bolborea, B., Dan, S., Baeră, C., Gruin, A., Enache, F., & Perianu, I. A. (2022). Study Regarding the Evaluation of Prediction Models for Determining the Concrete Compressive Strength Using Non-Destructive Testing (NDT) Data: Validation Stage. Solid State Phenomena, 332, 173–181.

Bonagura, M., & Nobile, L. (2021). Artificial Neural Network (ANN) Approach for Predicting Concrete Compressive Strength by SonReb. Structural Durability & Health Monitoring, 15(2), 125.

Breccolotti, M., & Bonfigli, M. F. (2015). I-SonReb: an improved NDT method to evaluate the in situ strength of carbonated concrete. Nondestructive Testing and Evaluation, 30(4), 327–346.

Brencich, A., Cassini, G., Pera, D., & Riotto, G. (2013). Calibration and reliability of the rebound (Schmidt) hammer test. Civil Engineering and Architecture, 1(3), 66–78.

Breysse, D. (2012). Nondestructive evaluation of concrete strength: An historical review and a new perspective by combining NDT methods. Construction and Building Materials, 33, 139–163.

Breysse, D., Balayssac, J.-P., Alwash, M., Biondi, S., Chiauzzi, L., Corbett, D., Garnier, V., Gonçalves, A., Grantham, M., & Gunes, O. (2021). In-Situ Strength Assessment of Concrete: Detailed Guidelines. In Non-Destructive In Situ Strength Assessment of Concrete: Practical Application of the RILEM TC 249-ISC Recommendations (pp. 3–56). Springer.

Breysse, D., Romao, X., Alwash, M., Sbartai, Z. M., & Luprano, V. A. M. (2020). Risk evaluation on concrete strength assessment with NDT technique and conditional coring approach. Journal of Building Engineering, 32, 101541.

Canadian Standards Association. (2019). CSA-A23. 3-19: Design of concrete structures for buildings. In Mississauga, ON.

Chandak, N. R., & Kumavat, H. R. (2020). SonReb Method for Evaluation of Compressive Strength of Concrete. InIOP Conference Series: Materials Science and Engineering, 810(1), 12071.

Chingălată, C., Budescu, M., & Lupăşteanu, R. (2017). Accuracy in predicting the compressive strength of concrete using SonReb method. Buletinul Institutului Politehnic Din Lasi. Sectia Constructii, Arhitectura, 63(3), 97–106.

Cianfrone, F., & Facaoaru, I. (1979). Study on the introduction into Italy on the combined non-destructive method, for the determination ofin situ concrete strength. Matériaux et Construction 1979 12:5, 12(5), 413–424. https://doi.org/10.1007/BF02478819

Cristofaro, M. T., Viti, S., & Tanganelli, M. (2020). New predictive models to evaluate concrete compressive strength using the SonReb method. Journal of Building Engineering, 27, 100962.

Domingo, R., & Hirose, S. (2009). Correlation between concrete strength and combined nondestructive tests for concrete using high-early strength cement. The Sixth Regional Symposium on Infrastructure Development, 12–13.

Du, G., Bu, L., Hou, Q., Zhou, J., & Lu, B. (2021). Prediction of the compressive strength of high-performance self-compacting concrete by an ultrasonic-rebound method based on a GA-BP neural network. Plos One, 16(5), e0250795.

EN 13791: Assessment of in-situ compressive strength in structures and precast concrete componentes. (2007). Brussels: CEN-CENELEC Management Centre, 2015, 744–748.

EN 13791:2019: Assessment of in-situ compressive strength in structures and precast concrete components. (2019). CEN-CENELEC Management Centre.

Facaoaru, I. (1961). Contribution à i'étude de la relation entre la résistance du béton à la compression et de la vitesse de propagation longitudinale des ultrasons. Rilem, 22, 125–154.

Günaydın, O., Akbaş, E., Özbeyaz, A., & Güçlüer, K. (2023). Machine learning based evaluation of concrete strength from saturated to dry by non-destructive methods. Journal of Building Engineering, 107174.

Hamada, H. M., Al-Attar, A., Shi, J., Yahaya, F., Al Jawahery, M. S., & Yousif, S. T. (2023). Optimization of sustainable concrete characteristics incorporating palm oil clinker and nano-palm oil fuel ash using response surface methodology. Powder Technology, 413, 118054.

Jain, A., Kathuria, A., Kumar, A., Verma, Y., & Murari, K. (2013). Combined use of non-destructive tests for assessment of strength of concrete in structure. Procedia Engineering, 54, 241–251.

Jang, J.-S. R. (1993). ANFIS: adaptive-network-based fuzzy inference system. IEEE Transactions on Systems, Man, and Cybernetics, 23(3), 665–685. https://doi.org/10.1109/21.256541

Ju, M., Park, K., & Oh, H. (2017). Estimation of compressive strength of high strength concrete using non-destructive technique and concrete core strength. Applied Sciences, 7(12), 1249.

Kayed, A. R. (2021). The Strength of Concrete in Existing RC Structures. Politecnico di Torino.

Kim, J.-K., Kim, C.-Y., Yi, S.-T., & Lee, Y. (2009). Effect of carbonation on the rebound number and compressive strength of concrete. Cement and Concrete Composites, 31(2), 139–144.

Kolek, J. (1969). Analysis of answers to Rilem questionnaire on the Schmidt Rebound Hammer. Materiaux et Constructions, 2(10), 285–291.

Kouddane, B., Sbartaï, Z. M., Alwash, M., Ali-Benyahia, K., Elachachi, S. M., Lamdouar, N., & Kenai, S. (2022). Assessment of Concrete Strength Using the Combination of NDT—Review and Performance Analysis. Applied Sciences, 12(23), 12190.

Kouddane, B., Sbartaï, Z. M., Elachachi, S. M., & Lamdouar, N. (2023). New multi-objective optimization to evaluate the compressive strength and variability of concrete by combining non-destructive techniques. Journal of Building Engineering, 107526.

Kumar, P., & Kumar, A. (2015). Prediction of compressive strength using genetic programming involving NDT results. NATIONAL INSTITUTE OF TECHNOLOGY ROURKELA.

Kumavat, H. R., Chandak, N. R., & Patil, I. T. (2021). Factors Influencing the Performance of Rebound Hammer Used for Non-Destructive Testing of Concrete Members: A Review. Case Studies in Construction Materials, e00491.

Lacroix, F., Noël, M., Moradi, F., Layssi, H., & Tingson, T. (2021). Nondestructive condition assessment of concrete slabs with artificial defects using wireless impact echo. Journal of Performance of Constructed Facilities, 35(6), 04021072.

Lewis-Beck, C., & Lewis-Beck, M. (2015). Applied regression: An introduction (Vol. 22). Sage publications.

Liu, B., Shi, J., Zhou, F., Shen, S., Ding, Y., & Qin, J. (2020). Effects of steam curing regimes on the capillary water absorption of concrete: Prediction using multivariable regression models. Construction and Building Materials, 256, 119426.

Liu, J.-C., Sue, M.-L., & Kou, C.-H. (2009). Estimating the strength of concrete using surface rebound value and design parameters of concrete material. Journal of Applied Science and Engineering, 12(1), 1–7.

Logothetis, L. (1978). Combination of three non destructive methods for the determination of the strength of concrete. National Technical University of Athens.

Masi, A., Chiauzzi, L., & Manfredi, V. (2016). Criteria for identifying concrete homogeneous areas for the estimation of in-situ strength in RC buildings. Construction and Building Materials, 121, 576–587. https://doi.org/10.1016/J.CONBUILDMAT.2016.06.017

Meynink, P., & Samarin, A. (1979). Assessment of compressive strength of concrete by cylinders, cores, and non destructive tests. Quality Control of Concrete Structures, Rilem Symposium, 1979, Stockholm, Sweden, 1.

Moein, M. M., Saradar, A., Rahmati, K., Mousavinejad, S. H. G., Bristow, J., Aramali, V., & Karakouzian, M. (2023). Predictive models for concrete properties using machine learning and deep learning approaches: A review. Journal of Building Engineering, 63, 105444.

Montgomery, D. C., Peck, E. A., & Vining, G. G. (2012). Introduction to linear regression analysis. John Wiley & Sons.

Na, U. J., Park, T. W., Feng, M. Q., & Chung, L. (2009). Neuro-fuzzy application for concrete strength prediction using combined non-destructive tests. Magazine of Concrete Research, 61(4), 245–256.

Naderpour, H., & Alavi, S. A. (2015). Application of Fuzzy Logic in Reinforced Concrete Structures. In J. K. Y. Tsompanakis & B. H. V. Topping (Eds.), Proceedings of the Fourth International Conference on Soft Computing Technology in Civil, Structural and Environmental Engineering. Civil-Comp Press. https://doi.org/10.4203/ccp.109.10

Naderpour, H., & Alavi, S. A. (2017). A proposed model to estimate shear contribution of FRP in strengthened RC beams in terms of Adaptive Neuro-Fuzzy Inference System. Composite Structures, 170, 215–227. https://doi.org/10.1016/J.COMPSTRUCT.2017.03.028

Naderpour, H., Kheyroddin, A., Amiri, G. G., & Vaez, S. R. H. (2011). Estimating the Behavior of FRP-Strengthened RC Structural Members Using Artificial Neural Networks. Procedia Engineering, 14, 3183–3190. https://doi.org/10.1016/j.proeng.2011.07.402

Najim, K. B. (2017). Strength evaluation of concrete structures using ISonReb linear regression models: Laboratory and site (case studies) validation. Construction and Building Materials, 149, 639–647.

Ndagi, A., Umar, A. A., Hejazi, F., & Jaafar, M. S. (2019). Non-destructive assessment of concrete deterioration by ultrasonic pulse velocity: A review. InIOP Conference Series: Earth and Environmental Science, 357(1), 12015.

Ngo, T. Q. L., Wang, Y.-R., & Chiang, D.-L. (2021). Applying Artificial Intelligence to Improve On-Site Non-Destructive Concrete Compressive Strength Tests. Crystals, 11(10), 1157.

Nikhil, M. V, Minal, B. R., Deep, C. S., Vijay, G. D., Vishal, T. S., & Shweta, P. (2015). The Use of Combined Non Destructive Testing in the Concrete Strength Assessment from Laboratory Specimens and Existing Buildings. Int. J. Curr. Eng. Scientific Res., 2(5), 55–59.

Nobile, L. (2015). Prediction of concrete compressive strength by combined non-destructive methods. Meccanica, 50(2), 411–417.

Poorarbabi, A., Ghasemi, M., & Moghaddam, M. A. (2020a). Concrete Compressive Strength Prediction Using Neural Networks Based on Non-destructive Tests and a Self-calibrated Response Surface Methodology. Journal of Nondestructive Evaluation, 39(4), 1–11.

Poorarbabi, A., Ghasemi, M., & Moghaddam, M. A. (2020b). Concrete compressive strength prediction using non-destructive tests through response surface methodology. Ain Shams Engineering Journal, 11(4), 939–949.

Poorarbabi, A., Ghasemi, M. R., & Azhdari Moghaddam, M. (2021). Conversion factors between non-destructive tests of cubic and cylindrical concrete specimens. AUT Journal of Civil Engineering, 5(1), 1.

Ramyar, K., & Kol, P. (1996). Destructive and non-destructive test methods for estimating the strength of concrete. Cement and Concrete World, 2, 46–54.

Rashid, K., & Waqas, R. (2017). Compressive strength evaluation by non-destructive techniques: An automated approach in construction industry. Journal of Building Engineering, 12, 147–154.

RILEM. (1993). Draft recommendation for in situ concrete strength determination by combined non-destructive methods. In Mater. Struct (Vol. 26). Springer.

Sai, G. J., & Singh, V. P. (2019). Prediction of compressive strength using support vector regression. MENDEL, 25(1), 51–56.

Salehi, H., & Burgueño, R. (2018). Emerging artificial intelligence methods in structural engineering. Engineering Structures, 171, 170–189.

Samarin, A., & Dhir, R. K. (1984). Determination of in situ concrete strength: rapidly and confidently by nondestructive testing. Special Publication, 82, 77–94.

Sbartaï, Z. M., Luprano, V. A. M., & Vasanelli, E. (2021). Evaluation of Concrete Strength by Combined NDT Techniques: Practice, Possibilities and Recommendations. In Non-

Destructive In Situ Strength Assessment of Concrete: Practical Application of the RILEM TC 249-ISC Recommendations (pp. 101–116). Springer.

Sefrin, R., & Glock, C. (2022). Characteristic concrete compressive strength of existing structures—Evaluation of EN 13791: 2019 for small sample sizes. Structural Concrete, 23(2), 822–835.

Shih, Y.-F., Wang, Y.-R., Lin, K.-L., & Chen, C.-W. (2015). Improving non-destructive concrete strength tests using support vector machines. Materials, 8(10), 7169–7178.

Shishegaran, A., Varaee, H., Rabczuk, T., & Shishegaran, G. (2021). High correlated variables creator machine: Prediction of the compressive strength of concrete. Computers & Structures, 247, 106479.

Szilágyi, K., Borosnyói, A., & Zsigovics, I. (2011). Rebound surface hardness of concrete: Introduction of an empirical constitutive model. Construction and Building Materials, 25(5), 2480–2487.

Tapeh, A. T. G., & Naser, M. Z. (2022). Artificial Intelligence, Machine Learning, and Deep Learning in Structural Engineering: A Scientometrics Review of Trends and Best Practices. Archives of Computational Methods in Engineering, 1–45.

Thai, H.-T. (2022). Machine learning for structural engineering: A state-of-the-art review. Structures, 38, 448–491.

Chapter 4– Practical Application[1]

4.1 Introduction

Compressive strength is commonly adopted as a representative indicator of many hardened properties of concrete. For existing structures, knowledge of in-place concrete properties is vital to any evaluation and rehabilitation project. Nevertheless, there exist several challenges associated with conventional methods for evaluating concrete strength once a structure has been built (Breysse et al., 2009; Breysse & Balayssac, 2021; Na et al., 2009; Pucinotti, 2015). Core sampling is not always a viable option for many concrete structures (for example, concrete tanks, sewer trunks, and tunnel linings) and representativeness of samples in large structures is difficult to obtain.

In-place nondestructive test (NDT) methods can be correlated to concrete compressive strength to reduce the number of required cores (ACI Committee 228, 2019). The SonReb method (RILEM, 1993) estimates concrete compressive strength based on combined ultrasonic pulse velocity (UPV) and rebound number (RN) measurements. Like all NDT methods, project-specific calibration curves are required due to the heterogeneous nature and diversity of concrete mixtures (Bolborea et al., 2022; Cristofaro et al., 2020; Kouddane et al., 2022), hence, it is not currently possible to accurately estimate concrete strength of existing structures without extraction of cores.

Artificial intelligence (AI) is a tool used to interpret complex information and increase productivity. Adoption of AI for civil engineering applications has been relatively slow but is beginning to garner increasing attention through demonstration of practical use cases. This

[1] This chapter has been published as: Alavi, S. A., Noël, M., Layssi, H., & Moradi, F. (2024). Can Artificial Intelligence Improve Nondestructive Evaluation of Concrete Strength? Concrete International, 46(5), 51-56.

article explores the extent to which AI can be integrated with the SonReb method for nondestructive evaluation of concrete compressive strength in reinforced concrete structures.

4.2 NDT Methods

ACI 228.2R-13 provides a comprehensive overview of NDT methods for concrete strength evaluation, including the rebound hammer test (ASTM C805/C805M-08) and UPV measurements (ASTM C597-16). The rebound hammer test is an easy and cost-effective means of evaluating the in-place uniformity of concrete (primarily near the surface), while UPV measurements are generally used to evaluate the internal quality and integrity of concrete materials by measuring the velocity of compressive stress waves passing through a member (Malek & Kaouther, 2014; Poorarbabi et al., 2021). Theoretical formulations support the existence of a direct relationship between Young's modulus and wave velocity, while empirical relationships have long been established to link Young's modulus with compressive strength (Agunwamba & Adagba, 2012; Breysse, 2012; Rajabi et al., 2020). Because of the challenges in predicting concrete strength by means of NDT resulting from inherent variabilities in concrete material properties, NDT methods, and physical/scientific connections and relevance between any NDT method and concrete strength, ACI Committee 228, Nondestructive Testing of Concrete, recommends the development of site/material specific calibration curves and a statistical approach to analyze the data. For existing structures, ACI 228.1R-19 recommends that six to nine different locations should be selected for coring, and a minimum of two cores should be obtained to establish the in-plane compressive strength (that is, a minimum of 12 cores is needed to establish a strength relationship). EN13791:2019 outlines a procedure that allows the use of RN measurements without any core tests under certain conditions, though this approach provides only conservative estimates of the strength class of concrete rather than accurate predictions of compressive strength (EN13791, 2019).

NDT methods can be combined to improve their general reliability and reduce sensitivity to factors such as moisture content, aggregate size, cement type, and reinforcement ratio (Alavi & Noël, 2022a; Breysse, 2012; Kayed, 2021). The SonReb method has been proposed as a simple approach that nevertheless presents a notable improvement over single-input test methods. Some authors have suggested that UPV and RN are distinctly affected by potential influencing factors (Alavi et al., 2024; Breysse, 2012; Gasparik & diagnostica, 1992; RILEM, 1993), though the extent to which this may be the case is still up for debate.

4.3 Artificial Intelligence

AI excels at predicting outcomes based on implicit relationships identified through various algorithms used to interpret large amounts of data. Machine learning (ML) is a subset of AI focusing on algorithms that enable computers to learn and make predictions or decisions without being programmed (Tapeh & Naser, 2022; Thai, 2022). Fig. 4.1 presents a flowchart for a typical supervised ML model. Two datasets are used in the modeling procedure: the training dataset and the testing dataset. Applying a learning algorithm to the training data, the computer “learns” potential relationships between input and output data. The testing dataset is then used to evaluate the performance of the model, and the procedure is repeated until the ML model satisfies the evaluation criteria.

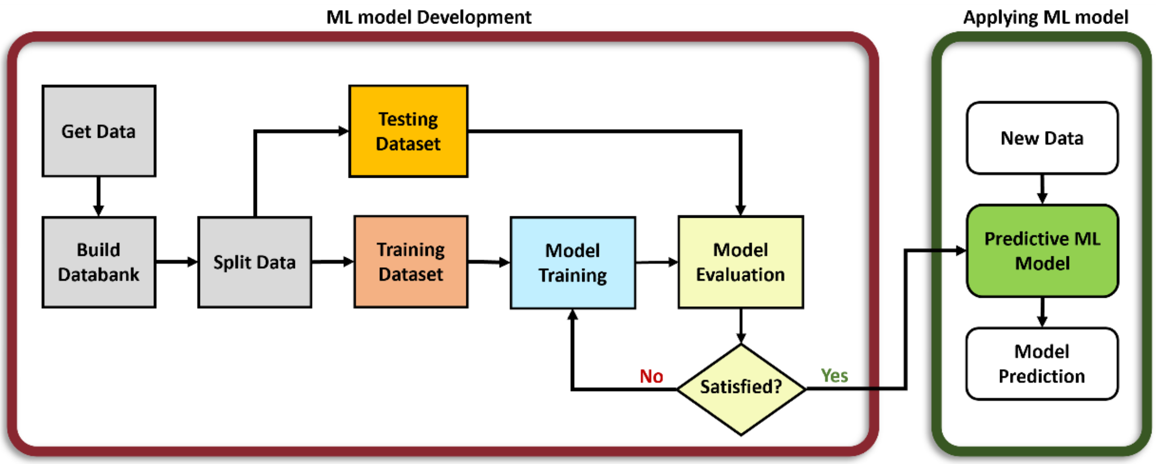

Figure 4.1: Flowchart for supervised ML model

AI has recently been proposed as a tool to estimate the compressive strength of concrete based on the SonReb method (Asteris & Mokos, 2020; Ngo et al., 2021; Poorarbabi et al., 2020; Sai & Singh, 2019; Shih et al., 2015; Shishegaran et al., 2021; Wang et al., 2018). Although the results of previous studies are promising, there is still no practical model for use in industry (Alavi & Noël, 2022b). In a separate paper, the development of an ML model based on the SonReb method is described and compared to existing approaches (Alavi et al., 2024). To emphasize simplicity and compatibility with current practice, and considering the lack of concrete mixture information available for many existing structures, the ML model was developed with only two inputs: (1) pulse velocity from the direct UPV test; and (2) RN from the horizontal rebound hammer test as shown in Fig. 4.2. For the development of the ML model, a database was created using results from published literature as well as an experimental testing program with concrete cylinders and cubes between 7 to 365 days in age and representing a wide range of mixture designs and compressive strengths. (Additional details on the training and testing databases are presented elsewhere (Alavi et al., 2024).)

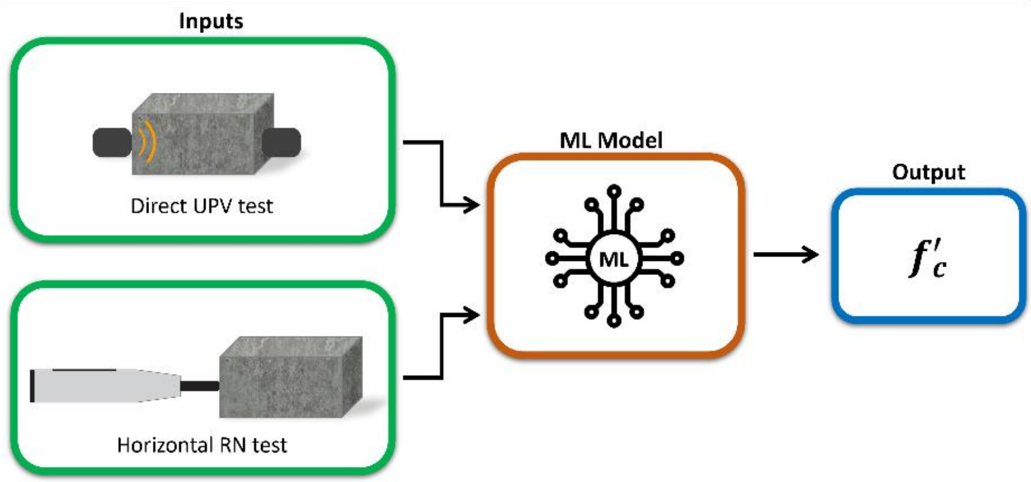

Figure 4.2: ML model parameters

The experimental procedure for each specimen tested in the laboratory included direct UPV tests, followed by the horizontal rebound hammer test, and finally the compressive strength test on the same specimens as shown in Fig. 4.3.

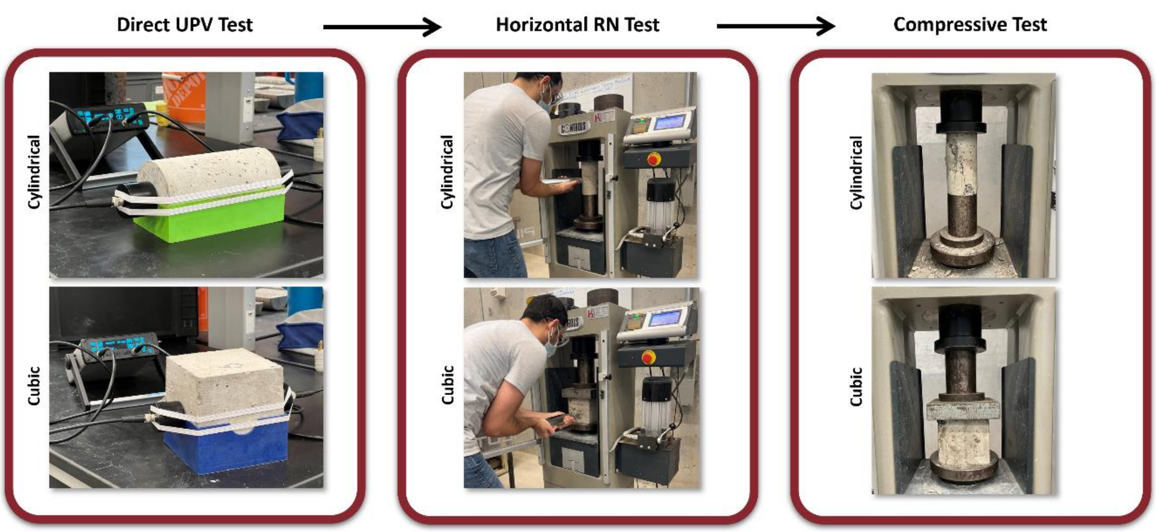

Figure 4.3: Experimental test procedure

The model was developed using the adaptive neuro fuzzy inference system (ANFIS) algorithm in MATLAB. To ensure a robust model performance and avoid a biased outcome, the training

(462 data points) and testing datasets (20 data points) were obtained from distinct sources. The model performance was compared against linear and nonlinear regression analyses, as well as existing equations in the literature, and was found to provide the most reliable predictions of concrete strength among the considered models, with a mean absolute error of less than 10% (Alavi et al., 2024). After developing the ML model, a graphical user interface (GUI) app was produced and used for three case studies that are presented in the following section. Each case study provided unique data that had not been seen by the model during its training phase. This approach was adopted to thoroughly evaluate the real-world performance of the ML model.

4.4 Case Studies

The accuracy of the model for real world applications was evaluated using three case studies. In each case study, a systematic methodology was followed, including: 1) performing NDT (UPV and RN) on the concrete structures at select test areas; 2) extracting concrete core samples from the same test areas for compressive strength tests; 3) estimating compressive strength using the proposed ML model and traditional mathematical models, commonly known as the Breysse equation and the Gasparik equation; and 4) comparing the test results from each method.

4.4.1 Case Study 1: RC slab

A partially reinforced concrete slab was fabricated in the laboratory for an independent research project (Lacroix et al., 2021) with overall dimensions of 2 x 2 m (6.5 x 6.5 ft) and 300 mm (12 in.) thick. The concrete for the slab was supplied from a local ready mixed concrete company. Twelve testing points (as shown in Fig. 4.4) were selected for this case study.

Fig. 4.5 presents the test results. The best prediction was obtained from the proposed ML model with a mean absolute percent error (MAPE) of 9.69% and coefficient of variation (COV) of 6.1%. Breysse and Gasparik's equations produced average errors of 28.96% (COV 8.4%) and 36.35% (COV 6.2%), respectively, and both consistently over-predicted the compressive strength of the core samples.

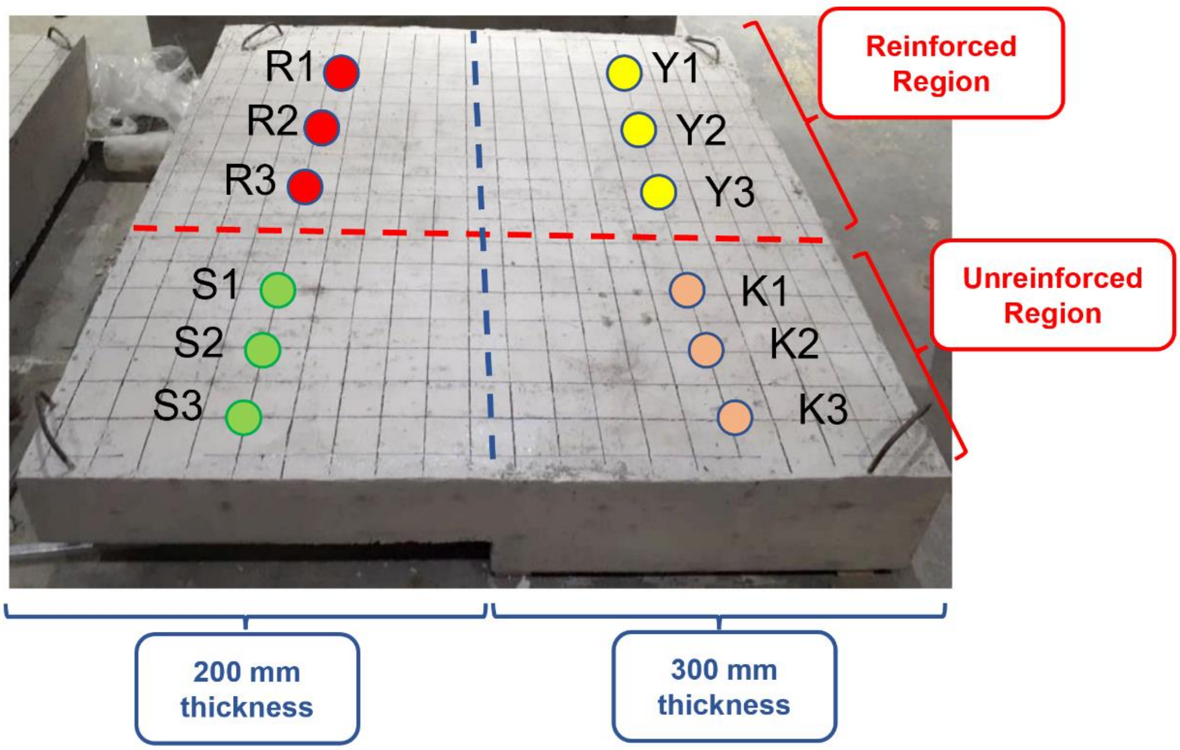

Figure 4.4: RC slab with marked testing points (Note: 1 mm = 0.04 in.)

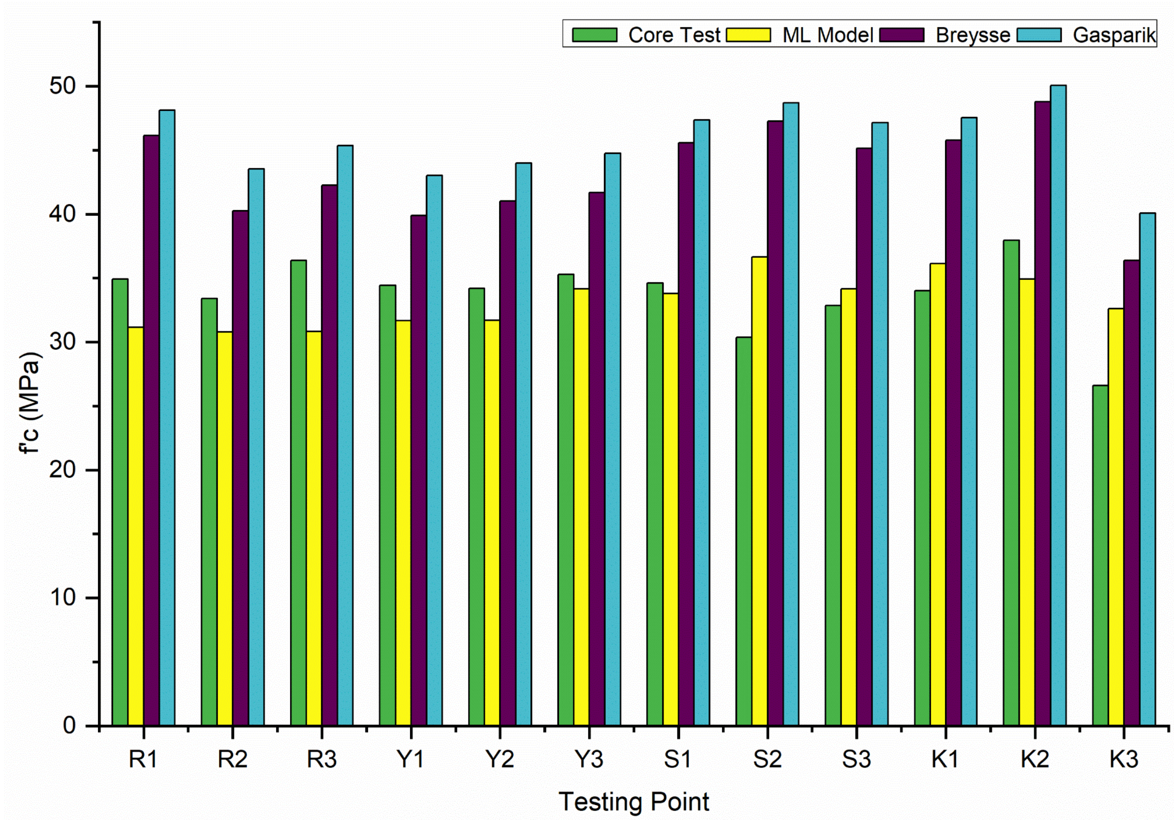

Figure 4.5: Strength predictions for Case Study 1 (Note: 1 MPa = 145 psi)

4.4.2 Case Study 2: Existing concrete building

A two-story building in a university campus in Canada required in-place assessment of concrete members as part of its rehabilitation program. The predicted strength results are presented in Fig. 4.6. The MAPE of the ML model was 12.85% (COV 11.4%), while the errors of the Breysse and Gasparik equations were 19.79% (COV 18.9%) and 33.73% (COV 16.4%), respectively. The MAPE for the ML model reduces to 10.2% if the two column measurements (Col G4Z and Col G4) are excluded. The results suggest that the model performed generally better for flat slab and wall sections than for columns, although the reason for this discrepancy is still under investigation.

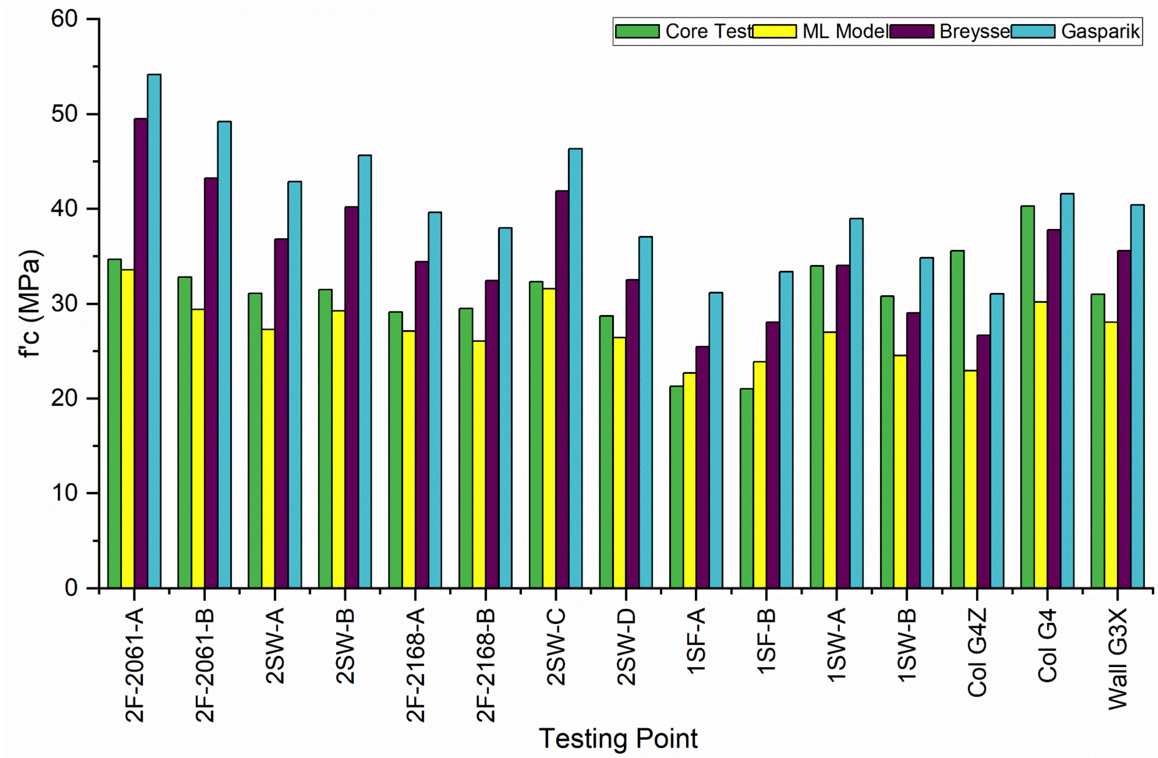

Figure 4.6: Strength predictions for Case Study 2 (Note: 1 MPa = 145 psi)

4.4.3 Case Study 3: Elevated foundation

A construction error in the elevated foundation of a storage silo in a mining facility resulted in poor consolidation of concrete and moderate to severe honeycombing on or around the lower layer of steel reinforcement, as well as the area close to the embedded plates near the opening. A detailed test plan was designed to evaluate the damaged area (Fig. 4.7).

The results of the ML model and the Breysse and Gasparik equations are compared in Fig. 4.8. All of the predictive models tended to underpredict the concrete strength; Gasparik's equation had the lowest MAPE of 21.75% and COV of 17.02%, while both the ML model and Breysse's equation gave similar performance (with average errors of 33.33% and 32.9%, and COV values of 11% and 20%, respectively).

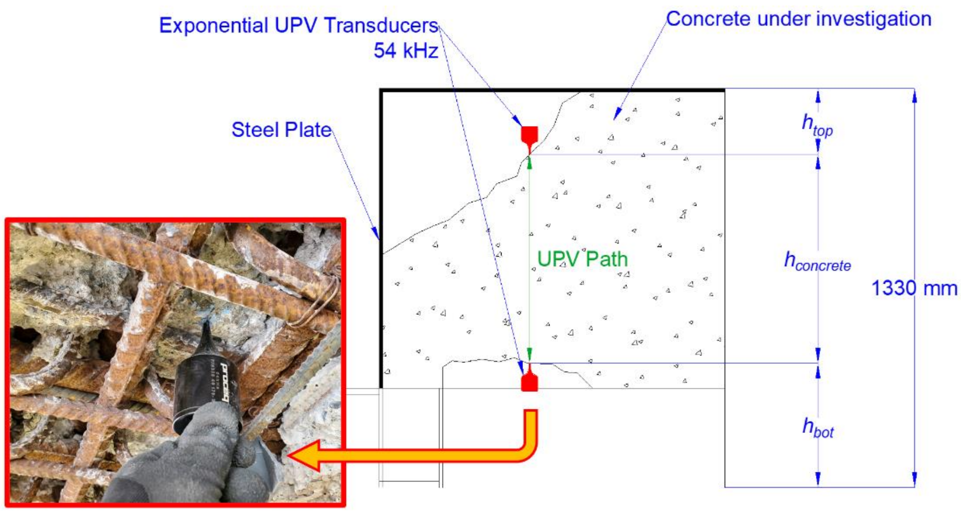

Figure 4.7: UPV tests for Case Study 3 (Note: 1 mm = 0.04 in.)

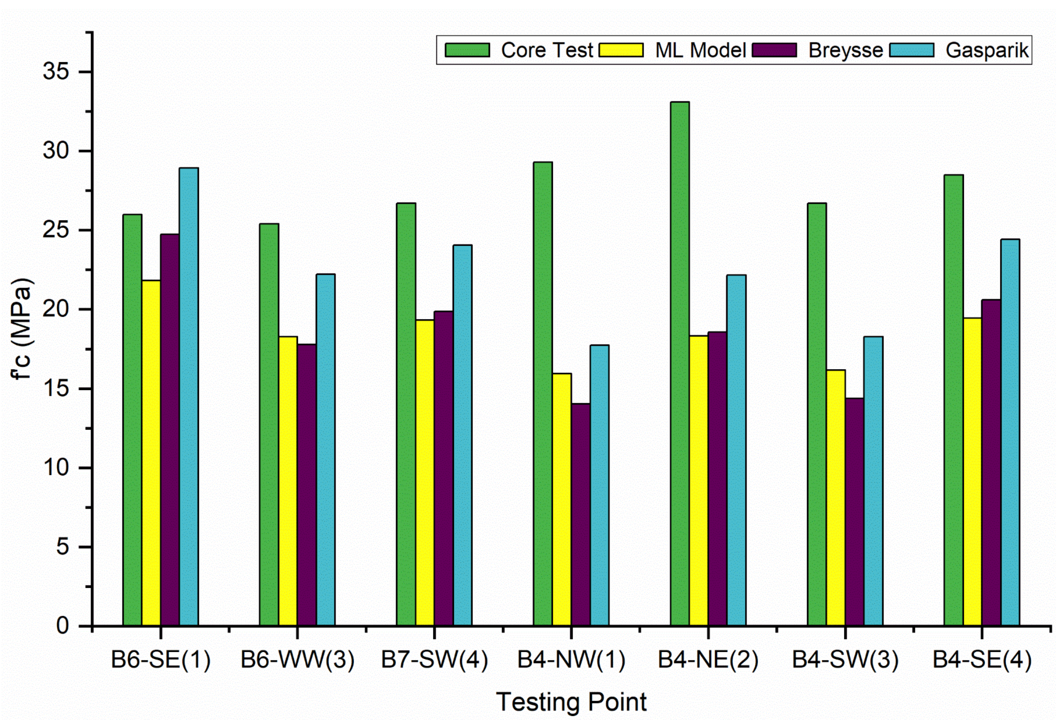

Figure 4.8: Strength predictions for Case Study 3 (Note: 1 MPa = 145 psi)

4.5 Discussion

Concrete is a heterogeneous and diverse material. Compressive strength values obtained by crushing cylinders from a single batch of concrete can easily vary by 10% or more (Rahal, 2007; Vu et al., 2020). In this context, achieving 100% accuracy from any model is unrealistic; ensuring consistency and reliability of predictions, as well as identifying potential model limitations, is a more important and achievable goal. This study has presented evidence that AI is a tool that can contribute toward this effort. And in the same way that all tools are used, engineering judgement is required to interpret the outcomes.

The AI model presented in this article maintains the simplicity of the SonReb method by keeping only two input parameters (UPV and RN) (Alavi et al., 2024). The benefits of this approach include more available data for model training, as well as wide applicability because no information on concrete mixture design, curing conditions, or age are required. As demonstrated through the presented case studies, reasonably good predictions were obtained for sound reinforced concrete and flat surfaces with low to moderate amounts of reinforcement. Notable exceptions were obtained for columns in Case Study 2 (possibly attributed to higher reinforcement ratios or geometric effects) and for defective/damaged concrete in Case Study 3. In both cases, the model under-predicted the actual concrete strength by approximately 30% on average (that is, estimates were conservative). As further investigation on the effects of reinforcement congestion and member geometry on NDT measurements and associated model outputs are warranted, it is unsurprising that the poor-quality concrete with visible honeycombing corresponded to a higher average error in the compressive strength predictions because all the training data was obtained from sound concrete specimens. This serves to highlight the engineer’s role in interpreting results from tools such as AI. As AI models become more robust and larger training databases are available, their capabilities will also increase; while AI can increase our productivity, engineers will continue to play a vital role in the condition assessment of structures for the foreseeable future.

Ongoing work is currently being conducted to investigate whether model accuracy can be further improved by considering additional input parameters, such as geometry (which was initially ignored despite its known effect on concrete strength and NDT measurements), age, and basic mixture design parameters. The obvious challenge is that in order to consider more parameters, the size of the database must be correspondingly increased. Compiling sufficient good quality data and filtering outliers/poor quality results is a complex task; however, as seen in the proliferation of AI in other disciplines, the result can be quite powerful. Overall, the results obtained to date are encouraging and suggest that AI can be adapted to solve key challenges in the construction industry when sufficient data is available.

Finally, the importance of statistical/confidence level concepts to interpret ML predictions, as ACI 228.1R-19 recommends for all cases, should not be overlooked. This is the subject of ongoing work by the authors and is an essential step for evaluating and applying model outcomes.

4.6 References

ACI Committee 228. (2019). ACI PRC-228.1-19: Report on Methods for Estimating In-Place Concrete Strength. American Concrete Institute.

ACI Committee 228. (2013). ACI PRC-228.2-13 Report on Nondestructive Test Methods for Evaluation of Concrete in Structures. American Concrete Institute.

Agunwamba, J. C., & Adagba, T. (2012). A comparative analysis of the rebound hammer and ultrasonic pulse velocity in testing concrete. Nigerian Journal of Technology, 31(1), 31–39.

Alavi, S. A., & Noël, M. (2022a). Challenges for the development of artificial intelligence models to predict the compressive strength of concrete using non-destructive tests: a review. Canadian Society of Civil Engineering Annual Conference 2022.

Alavi, S. A., & Noël, M. (2022b). Challenges for the Development of Artificial Intelligence Models to Predict the Compressive Strength of Concrete Using Non-destructive Tests: A Review. Canadian Society of Civil Engineering Annual Conference, 839–857.

Alavi, S. A., Noel, M., Moradi, F., & Layssi, H. (2024). Development of a machine learning model for on-site evaluation of concrete compressive strength by SonReb. Journal of Building Engineering, 82, 108328.

American Society for Testing and Materials. (n.d.). ASTM C805-08: Standard Test Method for Rebound Number of Hardened Concrete (2008th ed.).

Asteris, P. G., & Mokos, V. G. (2020). Concrete compressive strength using artificial neural networks. Neural Computing and Applications, 32(15), 11807–11826.

ASTM C-597-16: Standard Test Method for Pulse Velocity Through Concrete (2023). https://doi.org/10.1520/C0597-16

Bolborea, B., Dan, S., Baeră, C., Gruin, A., Enache, F., & Perianu, I. A. (2022). Study Regarding the Evaluation of Prediction Models for Determining the Concrete Compressive Strength Using Non-Destructive Testing (NDT) Data: Validation Stage. Solid State Phenomena, 332, 173–181.

Breysse, D. (2012). Nondestructive evaluation of concrete strength: An historical review and a new perspective by combining NDT methods. Construction and Building Materials, 33, 139–163.

Breysse, D., & Balayssac, J.-P. (2021). Non-destructive in situ strength assessment of concrete. Springer.

Breysse, D., Soutsos, M., Felicetti, R., KRAUSE, M., Lataste, J., & MOCZKO, A. (2009). How to improve the quality of concrete assessment by combining several NDT measurements. Proceedings of International Symposium on Non-Destructive Testing in Civil Engineering.

Cristofaro, M. T., Viti, S., & Tanganelli, M. (2020). New predictive models to evaluate concrete compressive strength using the SonReb method. Journal of Building Engineering, 27, 100962.

EN 13791:2019: Assessment of in-situ compressive strength in structures and precast concrete components. (2019). CEN-CENELEC Management Centre.

Gasparik, J., & diagnostica, A. italiana prove non distruttive monitoraggio. (1992). Prove non distruttive nell'edilizia. Associazione italiana prove non distruttive.

Kayed, A. R. (2021). The Strength of Concrete in Existing RC Structures. Politecnico di Torino.

Kouddane, B., Sbartaï, Z. M., Alwash, M., Ali-Benyahia, K., Elachachi, S. M., Lamdouar, N., & Kenai, S. (2022). Assessment of Concrete Strength Using the Combination of NDT—Review and Performance Analysis. Applied Sciences, 12(23), 12190.

Lacroix, F., Noël, M., Moradi, F., Layssi, H., & Tingson, T. (2021). Nondestructive condition assessment of concrete slabs with artificial defects using wireless impact echo. Journal of Performance of Constructed Facilities, 35(6), 04021072.

Malek, J., & Kaouther, M. (2014). Destructive and non-destructive testing of concrete structures. Jordan Journal of Civil Engineering, 159(3269), 1–10.

Na, U. J., Park, T. W., Feng, M. Q., & Chung, L. (2009). Neuro-fuzzy application for concrete strength prediction using combined non-destructive tests. Magazine of Concrete Research, 61(4), 245–256.

Ngo, T. Q. L., Wang, Y.-R., & Chiang, D.-L. (2021). Applying Artificial Intelligence to Improve On-Site Non-Destructive Concrete Compressive Strength Tests. Crystals, 11(10), 1157.

Poorarbabi, A., Ghasemi, M., & Moghaddam, M. A. (2020). Concrete Compressive Strength Prediction Using Neural Networks Based on Non-destructive Tests and a Self-calibrated Response Surface Methodology. Journal of Nondestructive Evaluation, 39(4), 1–11.

Poorarbabi, A., Ghasemi, M. R., & Azhdari Moghaddam, M. (2021). Conversion factors between non-destructive tests of cubic and cylindrical concrete specimens. AUT Journal of Civil Engineering, 5(1), 1.

Pucinotti, R. (2015). Reinforced concrete structure: Non destructive in situ strength assessment of concrete. Construction and Building Materials, 75, 331–341.

Pucinotti, R. (2009). In situ concrete strength assessment: Influence of the aggregate hardness on the Windsor probe test results. Journal of Building Appraisal, 5, 75-85.

Rahal, K. (2007). Mechanical properties of concrete with recycled coarse aggregate. Building and Environment, 42(1), 407–415.

Rajabi, A. M., Omidi Moaf, F., & Abdelgader, H. S. (2020). Evaluation of mechanical properties of two-stage concrete and conventional concrete using nondestructive tests. Journal of Materials in Civil Engineering, 32(7), 4020185.

RILEM. (1993). Draft recommendation for in situ concrete strength determination by combined non-destructive methods. In Mater. Struct (Vol. 26). Springer.

Sai, G. J., & Singh, V. P. (2019). Prediction of compressive strength using support vector regression. MENDEL, 25(1), 51–56.

Shih, Y.-F., Wang, Y.-R., Lin, K.-L., & Chen, C.-W. (2015). Improving non-destructive concrete strength tests using support vector machines. Materials, 8(10), 7169–7178.

Shishegaran, A., Varaee, H., Rabczuk, T., & Shishegaran, G. (2021). High correlated variables creator machine: Prediction of the compressive strength of concrete. Computers & Structures, 247, 106479.

Tapeh, A. T. G., & Naser, M. Z. (2022). Artificial Intelligence, Machine Learning, and Deep Learning in Structural Engineering: A Scientometrics Review of Trends and Best Practices. Archives of Computational Methods in Engineering, 1–45.

Thai, H.-T. (2022). Machine learning for structural engineering: A state-of-the-art review. Structures, 38, 448–491.

Vu, C.-C., Plé, O., Weiss, J., & Amitrano, D. (2020). Revisiting the concept of characteristic compressive strength of concrete. Construction and Building Materials, 263, 120126.

Wang, Y. R., Ngo, L. T. Q., Shih, Y. F., Lu, Y. L., & Chen, Y. M. (2018). Adapting ANNs in SONREB Test to Estimate Concrete Compressive Strength. Key Engineering Materials, 792, 166–169.

Chapter 5 – Model Architecture and Input Parameters [1]

5.1 Introduction

A significant proportion of infrastructure and buildings around the world is made of reinforced concrete (RC) (Aïtcin, 2000; Amin et al., 2024; Forty, 2013). For a variety of reasons, such as aging, environmental conditions, earthquakes, unexpected events, routine maintenance, or any other consideration, these structures will require a condition assessment and/or evaluation before potentially proceeding with a plan for repairs, rehabilitation, or even demolition. To enable owners to make informed decisions, it is crucial to have reliable information about the concrete properties in-situ. Accordingly, the most important information needed for evaluating concrete structures or individual members is typically the compressive strength (CS) of the existing concrete, which affects structural performance but is also indirectly linked to quality and durability characteristics that can be more difficult to assess.

To reliably estimate the CS of in-situ concrete, it is common to extract core samples and perform compression tests on them. This process is intrusive (i.e., creates holes in the structure) and is a destructive test (DT) because it relies on breaking a representative number of concrete samples (Ali-Benyahia et al., 2023; Breysse, 2012; Frappa et al., 2022). Due to the damage introduced to the structure, as well as limitations associated with the number of samples and lack of repeatability of tests from a specific point of the structure, engineers have faced various types of challenges. For example, the core from one location of a RC structure does not necessarily represent the concrete used throughout the whole structure, and it is also impractical or

[1] This chapter has been published as: Alavi, S. A., & Noel, M. (2025). Effect of model architecture and input parameters to improve performance of artificial intelligence models for estimating concrete strength using SonReb. Journal of Engineering Structures, 323, 119285.

impossible to extract cores from all members of the structure. Accordingly, there are other indirect methods that have been developed for estimating the CS of concrete, which can be categorized into two main groups: (1) semi-destructive tests and (2) non-destructive tests (NDT).

Among all the existing indirect methods for evaluating the CS of concrete, two NDT methods have become popular: the Ultrasonic Pulse Velocity (UPV) test and the Rebound Number (RN) test (Amini et al., 2016; Breysse, 2012). Both test methods are straightforward, fast, and economical, and like all NDT methods they are repeatable and non-intrusive. However, despite their popularity, UPV and RN generally do not have good accuracy for predicting CS when compared with core tests (Alavi et al., 2024b; Breysse, 2012).

To exploit the advantages of these two methods while reducing the degree of prediction errors, a combined method called "SonReb" has been presented in which the results of UPV and RN are merged to evaluate the CS of concrete. Based on this principle, a series of models based on regression analysis have been proposed to convert the values obtained from combined UPV and RN results to CS estimates for concrete (f_c') (Bolborea et al., 2022; Breysse, 2012). However, the SonReb method cannot be used on its own and still requires core tests to verify results (EN 13791, 2019).

The rapid growth of Artificial Intelligence (AI) in the construction industry in the past years has attracted the attention of researchers and engineers in this field (Alavi et al., 2024b; Alavi & Noël, 2022). CS prediction by AI and machine learning (ML) has become a big trend in the past few years and several studies have investigated the potential of this approach (Li et al., 2023; Tapeh & Naser, 2022; Thai, 2022). Whereas AI models can be developed with a high degree of complexity and many input parameters, it is important to note that even basic information about existing structures is often difficult to obtain. Therefore, CS prediction based on the SonReb method is attractive mainly due to its practicality, since no prior information is needed and the two input parameters (UPV and RN) are easily obtainable. It should also be mentioned that alternative methods to AI are also being investigated by various researchers. For example, Miano et al. used a Bayesian framework to estimate the reliability of concrete CS using data from NDT on RC structures (Miano et al., 2023).

Table 5.1 summarizes the previous studies using AI and SonReb to predict the CS of normal concrete types (i.e., those with mix designs and characteristics typical of the construction industry and widely used in RC structures). Accordingly, the first study to apply AI to improve the results of the SonReb method was conducted in 2009 (Na et al., 2009). Table 5.1 also indicates the increased recent interest in AI-based solutions, with almost half of the relevant studies conducted in the past four years.

According to Table 5.1, although Na et al.'s model obtained good results with fourteen inputs (Na et al., 2009), it required detailed information about the concrete mix design and curing. Since these details are seldom known for existing structures, most of the subsequent studies were based on only two inputs, UPV and RN, which are commonly obtained and hence more practical and realistic.

Two of the models listed in Table 5.1 were developed for cylindrical specimens (f'_{c-cyl}), four were developed for cubic specimens (f'_{c-cub}), and two used data from both specimen types and ignored the effect of geometry. While specimen geometry has a negligible effect on UPV measurements, previous studies have shown that it does affect both the CS and the RN of test specimens (Alavi et al., 2024b; Ali Poorarbabi, 2020; Poorarbabi et al., 2021).

In Table 5.1, it can be seen that various AI models have been developed based on different types of algorithms, different number of data, and different types and sources of data (cylindrical or cubic). Additionally, these models have been evaluated using different parameters, making it impossible to directly compare their performance, especially against new datasets that were not used for model training. Models by Na et al. and Kumar & Kumar include multiple parameters that are not generally available for existing structures, making them impractical for widespread use. In the remaining models, most are either developed from data obtained from cubic specimens (e.g. Asteris & Mokos's model), where the output is cubic strength, or on data from cylindrical specimens, where the output is cylindrical strength (e.g. Wang et al.'s model). In a few models, specimen data from both geometries were combined and the effect of specimen geometry was ignored during model development. Therefore, the main objective of this research is to develop an AI-based model that can work for both cubic and cylindrical standards by considering the geometric effects of the samples without using conversion factors. This approach enables the use of more data and increases its potential for practical and widespread use.

The present authors previously developed an AI model and applied it to three case studies to investigate the potential of AI to assist in making accurate SonReb-based predictions of CS. The results showed that the AI model produced more accurate predictions of concrete CS compared to traditional regression mathematical methods (Alavi et al., 2024a; Alavi et al., 2024b). However, the previous study neglected the effect of specimen geometry and only considered one type of model architecture. While combining cubic and cylindrical data permits the use of a larger database for training and testing AI models, it also a potential source of error that could limit model accuracy. It is worth noting that for the development of a universal model, the variety of data sources is at least as important as the total number of data points used for training.

Table 5.1 Summary information of existing AI models (chronologically sorted)

Work	Data	Method	Input variables	Type
Na et al., 2009	1551	ANFIS	(1) UPV, (2) RN, (3) w/c ratio, (4) sand/aggregate ratio, (5) unit weight of cement, (6) unit weight of sand, (7) unit weight of gravel, (8) unit weight of water, (9) % superplasticiser, (10) unit weight of fly ash, (11) unit weight of silica fume, (12) unit weight of slag, (13) age, and (14) curing condition	(Mix)
Bonagura, 2012	(N/A)	ANN	(1) UPV and (2) RN	(N/A)
Kumar & Kumar, 2015	100	GP	(1) UPV, (2) RN, and (3) Weight of sample	Cubic
Shih et al., 2015	95	SVM	(1) UPV and (2) RN	Cylindrical
Wang et al., 2018	315	ANN	(1) UPV and (2) RN	Cylindrical
Sai & Singh, 2019	350	SVR	(1) UPV and (2) RN	Cubic
Asteris & Mokos (2020)	209	ANN	(1) UPV and (2) RN	Cubic
Poorarbabi et al. (2020)	180	ANN	(1) UPV and (2) RN	Cubic
Ngo et al. (2021)	98	ANFIS ANN SVM	(1) UPV and (2) RN	Core
Shishegaran et al.	516	SBSR HCVCM-SBSR GEP HCVCM-GEP ANFIS HCVCM-ANFIS	(1) UPV and (2) RN	(N/A)
Asteris et al., (2021)	629	ANN RVM MPMR GP GPR MARS	(1) UPV and (2) RN	(N/A)
Arora et al., (2024)	721	AdaBoost CatBoost GBT RF XGB	(1) UPV and (2) RN	Cubic
Alavi et. al., (2024b)	482	ANFIS	(1) UPV and (2) RN	(Mix)

- (N/A): No information available, (Mix): the combined data from cylindrical, cubic, and core. ANFIS: adaptive neuro-fuzzy inference system, ANN: artificial neural networks, GEP: gene expression programming, GP: genetic programming, GPR: gaussian process regression, HCVCM: high correlated variables creator machine, MARS: multivariate adaptive regression spline, MPMR: minimax probability machine regression, RVM: relevance vector machine, SBSR: step-by-step regression, SVM: support vector machine, SVR: support vector regression, RF: random forests, and XGB: extreme gradient boosting.

This study aims to improve on our previous work by including the effect of specimen geometry and comparing the performance of different machine learning algorithms for predicting the CS of concrete using SonReb data. As illustrated in Fig. 5.1, six new AI-based models were developed using two distinct approaches. The first approach (approach A) involved the development of three AI models (ANN-2i, DNN-2i, and ANFIS-2i) having different architectures: an artificial neural network (ANN), deep neural network (DNN), and adaptive neuro-fuzzy inference system (ANFIS), respectively, utilizing only two input parameters (UPV and RN). Subsequently, three additional models (ANN-3i, DNN-3i, and ANFIS-3i) were developed, also based on ANN, DNN, and ANFIS, but incorporating a third input parameter to consider the type of geometry alongside UPV and RN (approach B). Notably, this study marks the first instance where a DNN was employed and investigated as a deep learning method for CS prediction by SonReb.

To develop any robust AI model a good databank is needed. The databank used for this study was developed in three stages (Fig. 5.1). In Part (1), an initial experimental program was conducted in which a broad range of concrete types were cast into cylindrical and cubic specimens in the laboratory and collected from local ready-mix suppliers. In Part (2), data was collected from literature to increase the amount and range of data available for training. The data collected in Parts (1) and (2) are discussed in more detail elsewhere [8]. Upon further review of the database, it was found that data corresponding to cylindrical samples with medium to high values of CS were relatively sparse. Therefore, a targeted experimental program was conducted (Part 3) in which an additional 72 cylinders were fabricated and tested to fill this gap. In the development of the models, the splitting approach previously proposed by Alavi et al. (Alavi et al., 2024b; Alavi et al., 2022) was employed instead of random splitting to remove bias between training and testing datasets and increase the volume of the training dataset. In brief, the proposed splitting approach ensures that training and testing data are obtained from distinct sources to better gauge the model's performance when exposed to new data. The performance of each model was analyzed and compared based on six statistical parameters: mean absolute percentage error (MAPE), root mean square error (RMSE), mean absolute error (MAE), correlation coefficient (R), coefficient of determination (R^2), and performance index (PI).

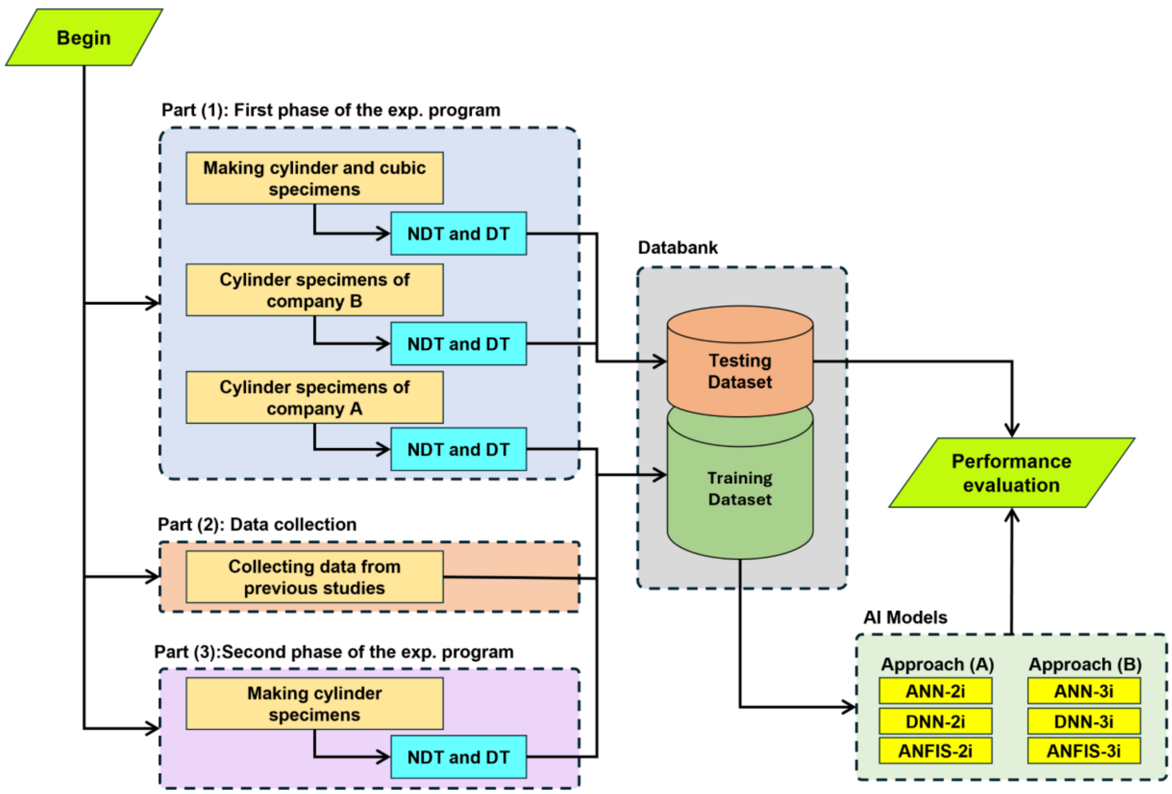

Figure 5.1: The workflow framework of the current study

5.2 Methods

5.2.1 SonReb

The SonReb method combines the results of two NDT techniques, UPV and RN, for evaluating CS (f_c') in existing RC structures (Breysse, 2012; Facaoaru, 1961; RILEM, 1993). The UPV test measures the velocity of a transmitting pulse in the concrete. As shown in Fig. 5.2 (A), by using two probes (transmitter and receiver), the UPV device continuously shows the transit time of the pulse in the concrete. By dividing the distance between the two probes (millimetre: mm) by the transmitting time (microsecond: μs), the velocity of the pulse is obtained (kilometres per second: km/s) (ASTM C-597-16, 2023; Hannachi & Guetteche, 2014; Naik et al., 2003). Generally, higher velocity represents a higher value of CS of tested concrete.

The RN test (Fig. 5.2 (B)) uses a mechanical tool named "Schmidt Hammer" or "Rebound Hammer" which contains an internal spring connected to a plunger that strikes the concrete surface. The "rebound" measured by the device is related to the concrete surface hardness, which is indicated by a unitless number called the rebound number (RN) (El-Mir et al., 2023; Shariati et al., 2011; Xu & Li, 2018). Generally, concrete with higher CS shows higher RN in comparison with concrete with lower CS.

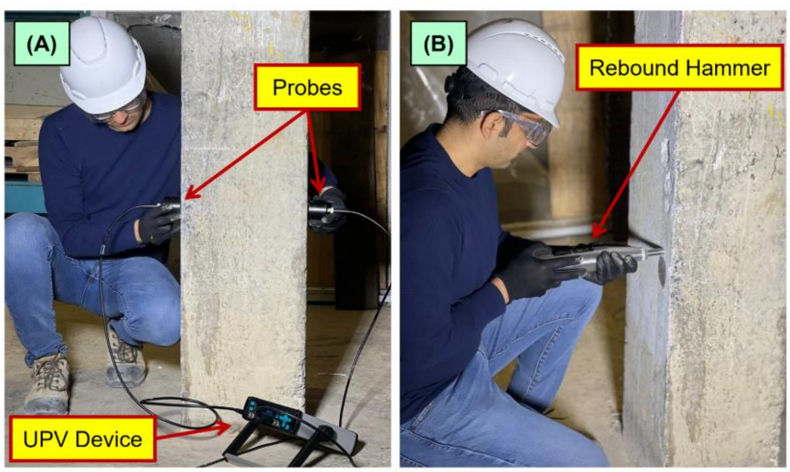

Figure 5.2: Using the SonReb method by performing two NDT: (A) UPV and (B) RN tests

5.2.2 Artificial Intelligence

AI can be briefly defined as methods that enable machines to mimic human brain behaviour or function. As shown in Fig. 5.3, Machine Learning (ML) is a subcategory of AI and subsequently Deep Learning (DL) is a subcategory of ML (Janiesch et al., 2021; Moein et al., 2023). ML uses algorithms to learn patterns from data and make predictions or decision-making models without being explicitly programmed. In this study, three methods—ANN, ANFIS, and DNN—were utilised for concrete CS predictions. ANN and ANFIS are subcategories of ML and DNN is a subcategory of DL.

An ANN, also known as a neural network (NN), is a tool inspired by an animal's brain (or human brain) for data processing (Chen et al., 2023). ANN is a nonlinear method that enables a computer to capture complicated interactions between input and output parameters without any prior knowledge about the nature of the relationship between them (May et al., 2011). Fig. 5.4(A) shows the simplified architecture of the ANN method. According to Fig. 5.4(A), a starting point of the ANN architecture is the input layer where information is introduced into the system, followed by a hidden layer where computations are performed on the input data by interconnected neurons using weighted sums and activation functions, and finally an output layer where the output value is produced based on the processed data. Each neuron in the hidden layer receives inputs from the neurons in the input layer, processes them, and passes the result to the neurons in the output layer. In the training phase of ANN models, the adjustment of the weights of these connections to minimize the difference between predicted outputs and actual outputs takes place (in this case, the difference between predicted CS from the model and actual CS from an experimental test). Usually, the training phase is performed by a technique called backpropagation. As shown in Fig. 5.4(B), DNN is similar to ANN except with more than one hidden layer (Hu et al., 2016). The multiple hidden layers help to improve the training phase for more complex problems or complex data in the DNN method. In this study, a DNN with two hidden layers was used.

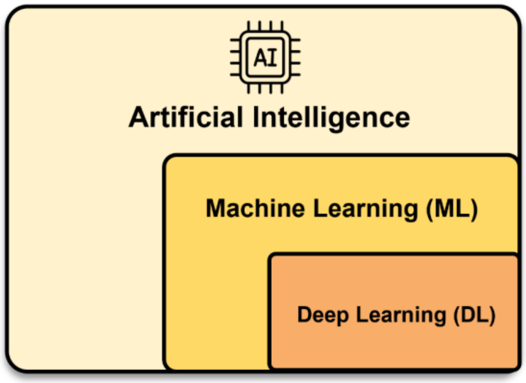

Figure 5.3: AI and its subcategories

The third method used in this study is the adaptive neuro-fuzzy inference system (ANFIS) that is also known as neuro-fuzzy (Fig. 5.5). The ANFIS method is hybrid technique achieved by the combination of ANN and fuzzy logic (FL) (Jang, 1993). Combining these two powerful tools simultaneously provides the parallel learning abilities from the ANN and decision-making abilities from FL. It works through multiple layers as shown in Fig. 5.5. The input layer receives crisp input data, which is then fuzzified into linguistic terms in the fuzzification layer by applying fuzzy membership functions (MF). Then fuzzy rules (IF-THEN) are applied in the rule layer to combine inputs into fuzzy outputs, which are subsequently defuzzified in the defuzzification layer to generate crisp outputs (Jang, 1993; Naderpour & Alavi, 2017).

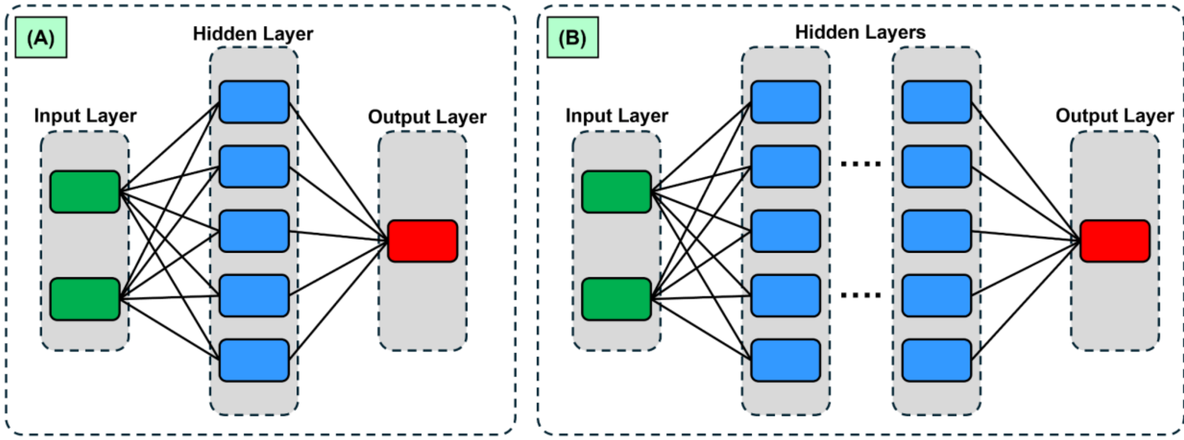

Figure 5.4: Schematic architecture of (A) ANN and (B) DNN methods

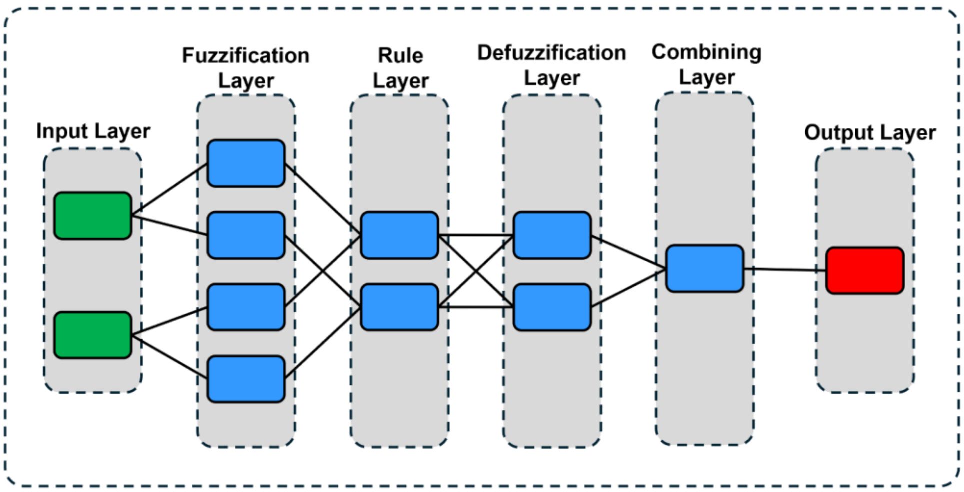

Figure 5.5: Schematic architecture of ANFIS method

5.3 Databank and Datasets

As shown in Fig. 5.1, the construction of the databank for the development of AI models involved three main parts: Part 1, which is the first phase of the experimental program (36 data points); Part 2, consisting of data collected from previous studies (454 data points); and Part 3, which is the second phase of the experimental program (24 data points). The summary information on the databank is provided in Table 5.2. According to this table, 514 unique data points were used to develop the six AI models. It is important to note that each data point used for model training and testing was derived from multiple replicate measurements or tests, as discussed below.

Table 5.2 Summary information on databank

Source		Data from test on cubic specimens	Data from test on cylindrical specimens	Total
P1: First phase of experimental program	Making cubes and cylinders	8	8	16
	Company A	0	8	8
	Company B	0	12	12
P2: Collected data		394	60	454
P3: Second phase of experimental program		0	24	24
Total		402	112	514

The first phase of the experimental program involved extracting data from concrete cubic and cylindrical specimens produced in the laboratory (16 data), as well as from concrete cylinders obtained from two local ready-mix companies (companies A and B) (20 data), which have been published in a separate study (Alavi et al., 2024b). An additional 454 data points were collected from 13 studies available in reported literature (Ali Poorarbabi, 2020; Alwash et al., 2015; Chandak & Kumavat, 2020; Cianfrone & Facaoaru, 1979; Domingo & Hirose, 2009; Jain et al., 2013; Logothetis, 1978; Masi et al., 2016; Na et al., 2009; Nikhil et al., 2015; Nobile, 2015; Poorarbabi et al., 2020; Rashid & Waqas, 2017).

Upon consolidating all the data from the first and second parts (totalling 490 data points), weaknesses in the dataset were identified. Firstly, a significant portion of the data exhibits a strength of 35 MPa or less. Secondly, most of the data were extracted from cubic specimens. To illustrate these issues, two three-dimensional graphs are presented in Fig. 5.6 containing all data points from parts one and two (the first phase of the experimental program and collected data). In this figure, the z-axis represents the concrete strength (f_c'), and the other two axes represent UPV and RN values (f_c' vs. UPV vs. RN). Accordingly, out of a total of 490 data points, 67.95% (333 data points) correspond to a strength of less than 35 MPa, 27.55% (135 data points) correspond to a strength ranging from 35 MPa to 60 MPa, and 4.48% (22 data points) correspond to a strength ranging from 60 MPa to 77 MPa. This demonstrates a gap in the data representing strengths above 35 MPa, which is not uncommon in structural concrete in construction. Fig. 5.6(A) clearly illustrates this fact, showing the density of the data representing strengths below 35 MPa at the bottom of the graph. Additionally, as observed in Fig. 5.6(B), out of the 490 data points, 82.04% (402 data points) are derived from cubic concrete specimens, while only 17.95% (88 data points) are derived from cylindrical specimens. To address these issues in the databank, additional cylinders were cast and tested to fill in sparser regions of the databank before proceeding to develop the AI models.

In Part (3) of the database development, twelve new mix designs were designed to make concrete cylinders within the strength range of 35 MPa to 60 MPa. Table 5.3 provides information regarding the mix designs. Accordingly, twelve concrete batches were made (Fig. 5.7), and for each mix six cylinders (100*200 mm) were cast (Fig. 5.7(C)), for a total of 72 specimens. Three cylinders were tested in compression at the age of 28 days and three other cylinders at the age of 90 days for each concrete mix.

NDT and DT were performed on all seventy-two concrete cylinders to extract data. Fig. 5.8 shows the test procedure for extracting data. First, the accurate length of the cylinders (l) was measured with calipers (Fig. 5.8(A)), and then UPV tests were conducted on the cylinders using 3D stands (Fig. 5.8(B)). In the next step, RN tests (the average of 10 readings) were done under a small compression load of 4 MPa as shown in Fig. 5.8(C). In the last step, the compressive test was performed on the cylinders (Fig. 5.8(D)). One unique data point was extracted from the average values obtained from the tests on each group of three cylinders. In this way, 24 unique data points were extracted from a total of 72 concrete cylinders. It is worth mentioning that this precise test procedure was also followed for the first phase of the experimental program. This method of testing has been chosen to extract high-quality data according to previous results (Alavi et al., 2024b).

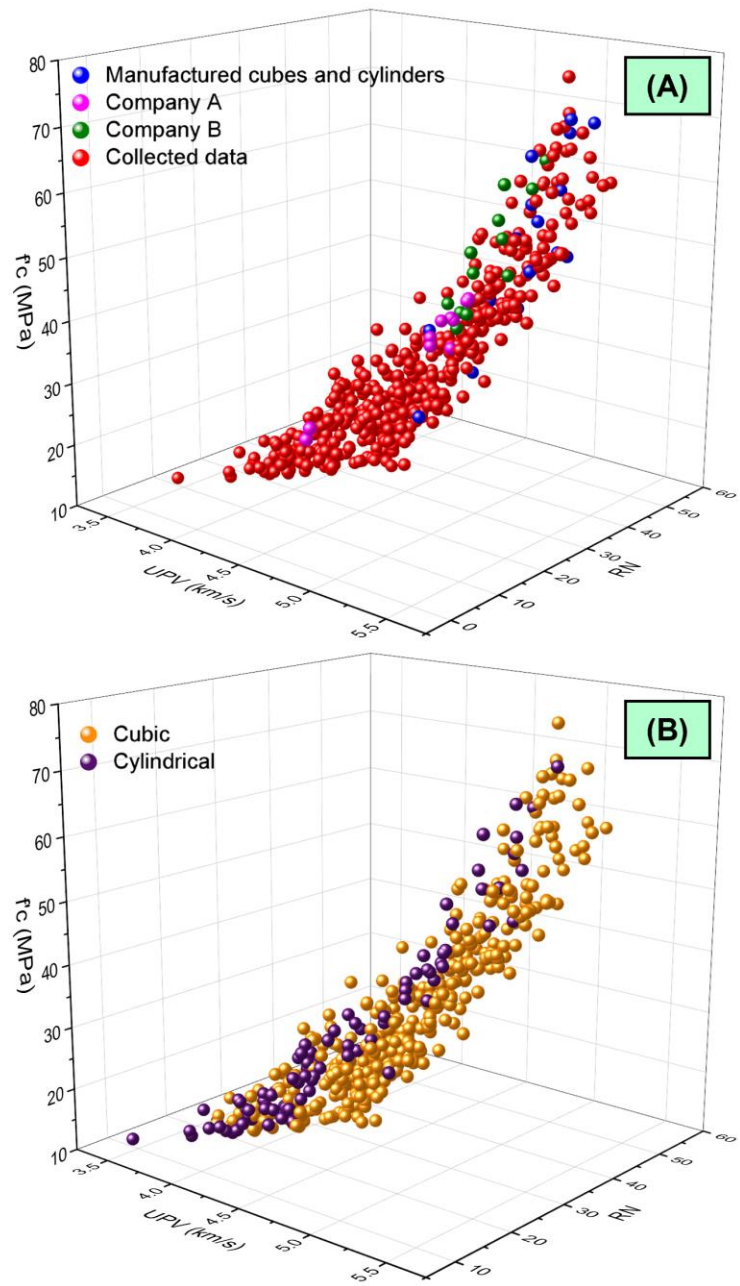

Figure 5.6: Scatter graphs representing 490 data points from the first phase of the experimental program and collected data, based on (A) the source and (B) the type of geometry

Table 5.3 Mix design information for the second phase of the experimental program

Mix ID	Cement (kg/m$^{3)}$	Slag (kg/m$^{3)}$	Coarse aggregate (kg/m$^{3)}$	Fine aggregate (kg/m$^{3)}$	Water (L/m$^{3)}$	Air entrainment (%)	W/C
MD-S1	528	-	848	822	185	-	0.35
MD-S2	576	-	848	770	190	-	0.33
MD-S3	550	-	848	726	165	7%	0.3
MD-S4	470	117	850	731	200	-	0.34
MD-S5	593	-	848	755	190	-	0.32
MD-S6	597	-	848	766	185	-	0.31
MD-S7	586	-	848	735	187	5%	0.32
MD-S8	462	116	848	773	185	-	0.32
MD-S9	528	132	848	703	224	-	0.34
MD-S10	462	198	848	698	224	-	0.34
MD-S11	481	259	848	589	244	-	0.33
MD-S12	461	308	848	562	254	-	0.33

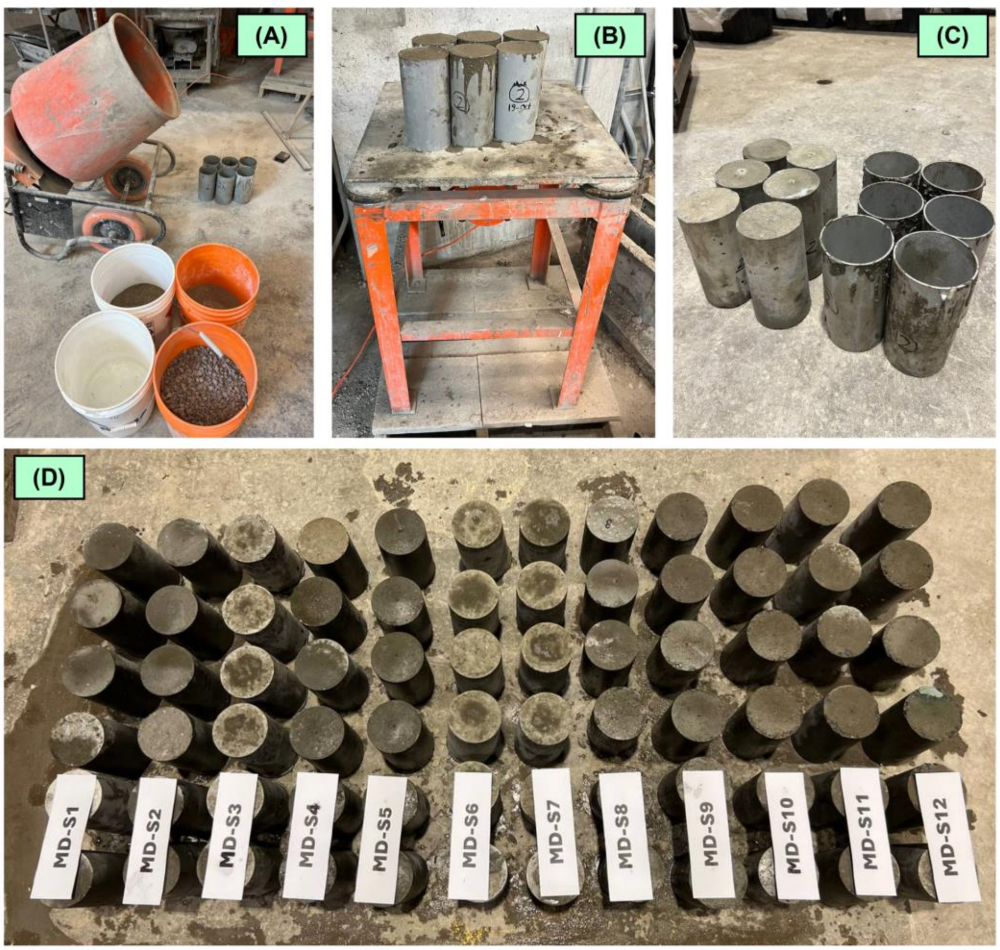

Figure 5.7: Making cylinders for the second phase of the experimental program; (A) Mixing the materials, (B) Vibration, (C) Opening the molds, and (D) All seventy-two cylinders

Finally, these twenty-four unique data from the second phase of the experimental program were added to the other 490 data from the first phase of the experiment, as well as collected data. As shown in Fig. 5.9 and Fig. 5.10, the data from the second phase of the experimental program successfully reinforced the databank in the range of 35 to 60 MPa. As a result, the total of all data reached 514 data (as mentioned in Table 5.2). Fig. 5.10 presents the distribution of data while statistical information of all 514 data is summarized in Table 5.4.

As depicted in Fig. 5.1, in the development of AI models, instead of randomly selecting data for training and testing datasets (a common practice in developing ML models), data splitting was conducted according to the data source. This approach is discussed in more detail in a previous study and is intended to eliminate biases between two datasets used for training and testing models and also to use the maximum amount of data for training (Alavi et al., 2024b; Alavi et al., 2022). This approach gives the advantage that the data used for testing the AI model will never be seen by the model during its training process. Consequently, the evaluation of the model based on the testing data is realistic and more reliable and a lower number of data is needed for testing.

Based on this, the data obtained from the second phase of the experimental program (24 data points), the collected data (454 data points), and the data obtained from company A's specimens (8 data points), totaling 486 data points, are selected as the 'Training Dataset'. Additionally, the data obtained from the manufactured cubes and cylinders in the first phase of the experimental program (16 data points) and data extracted from company B's specimens (12 data points), totaling 28 data points, are selected as the 'Testing Dataset.' Fig. 5.11 illustrates the scatter graph of the assigned data points in each of the two datasets (training or testing) in the three-dimensional graph (f_c' vs. UPV vs. RN). Also, in Fig. 5.12, the distribution of data in each of the two datasets is shown. Based on the graphs provided in Fig. 5.11 and Fig. 5.12, it can be observed how well the testing data are scattered and not congested. Since the testing data are selected from different sources than the training data, they are considered to be suitable for the unbiased evaluation of AI models.

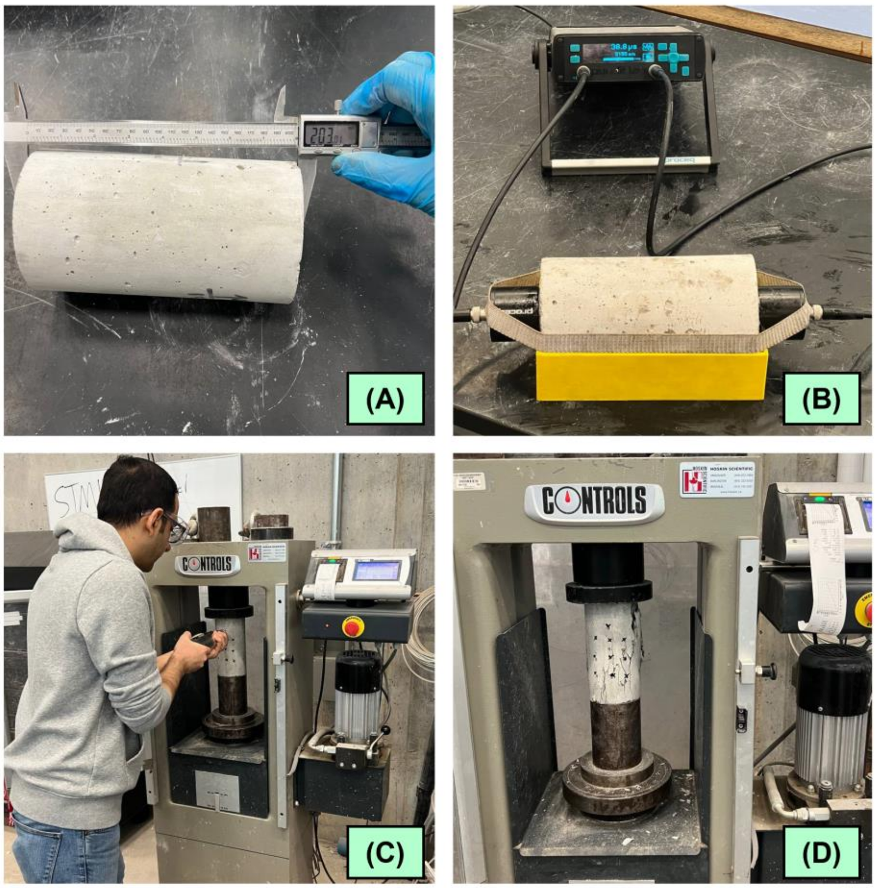

Figure 5.8: Test procedure to extract data; (A) Measurement of specimen length, (B) UPV test, (C) RN test, and (D) Compressive test

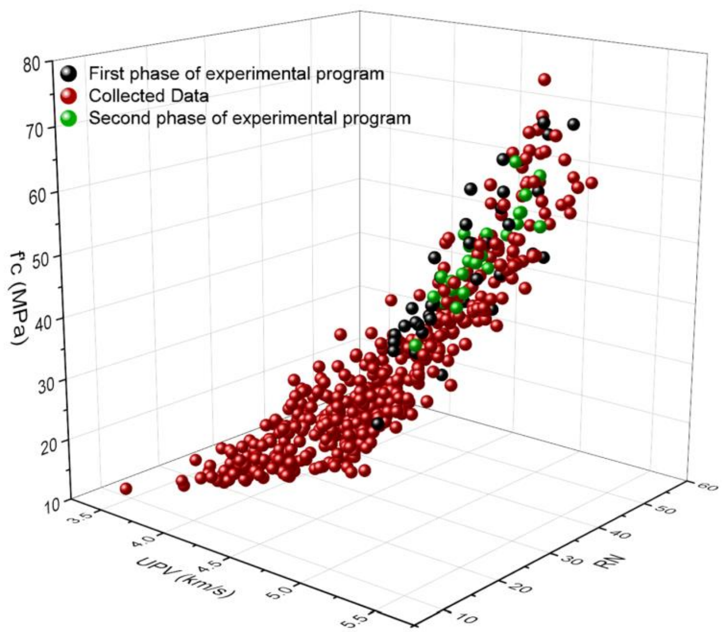

Figure 5.9: The scatter graph for all 514 data based on their source

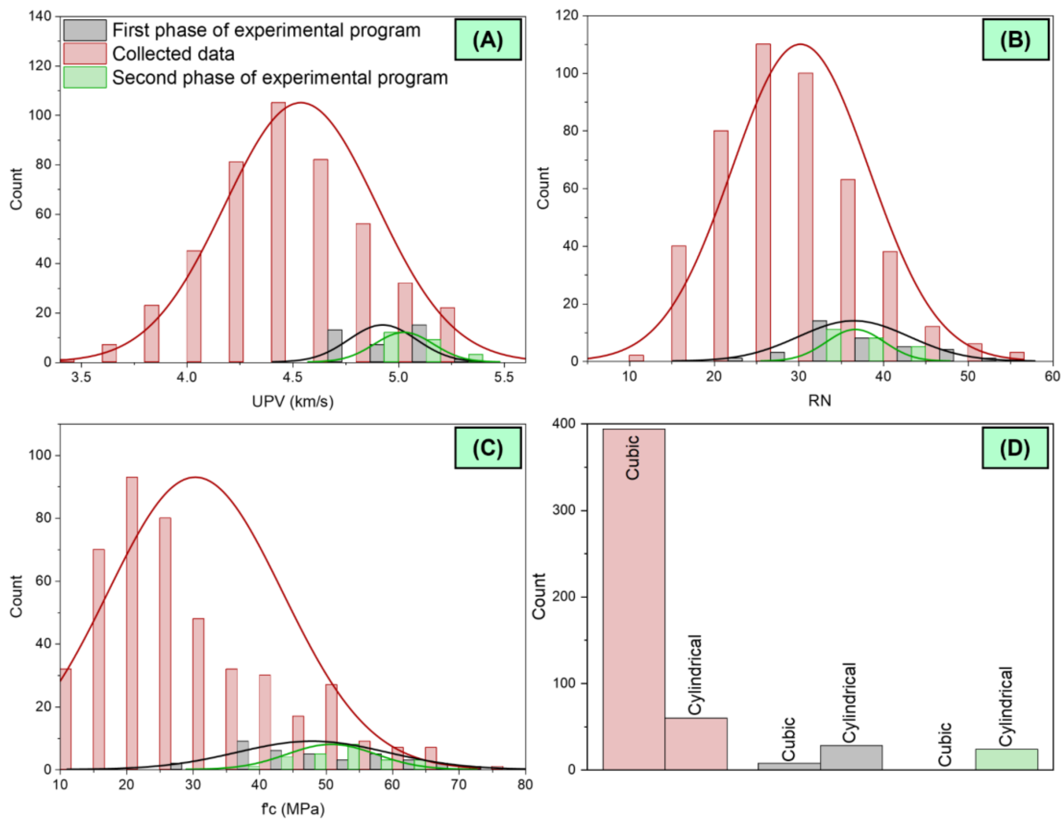

Figure 5.10: Data distribution for each source based on (A) UPV, (B) RN, (C) compressive strength, and (D) type of specimen

Table 5.4 Statistical information on databank

Parameter	Unit	Min	Max	Range	Mean	Standard Deviation
UPV	km/s	3.443	5.400	1.957	4.589	0.37
RN	-	10.33	55.50	45.17	30.96	8.11
f_c'	MPa	11.1	76.3	65.2	32.6	14.2

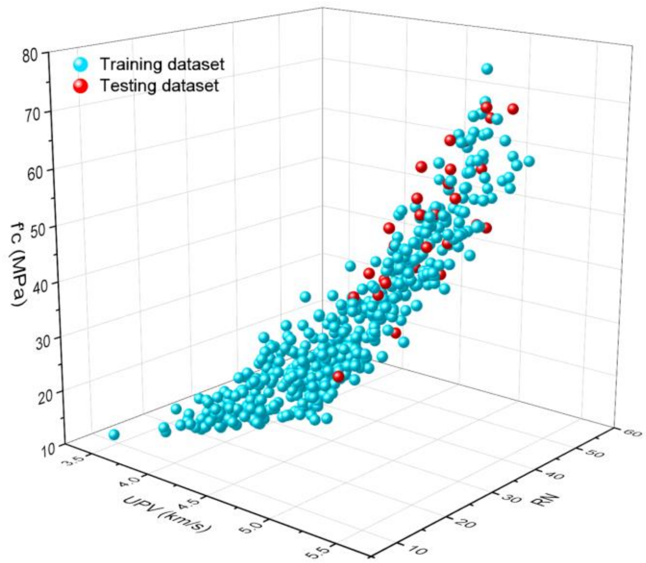

Figure 5.11: The scatter graph for all 514 data points based on the training and testing datasets

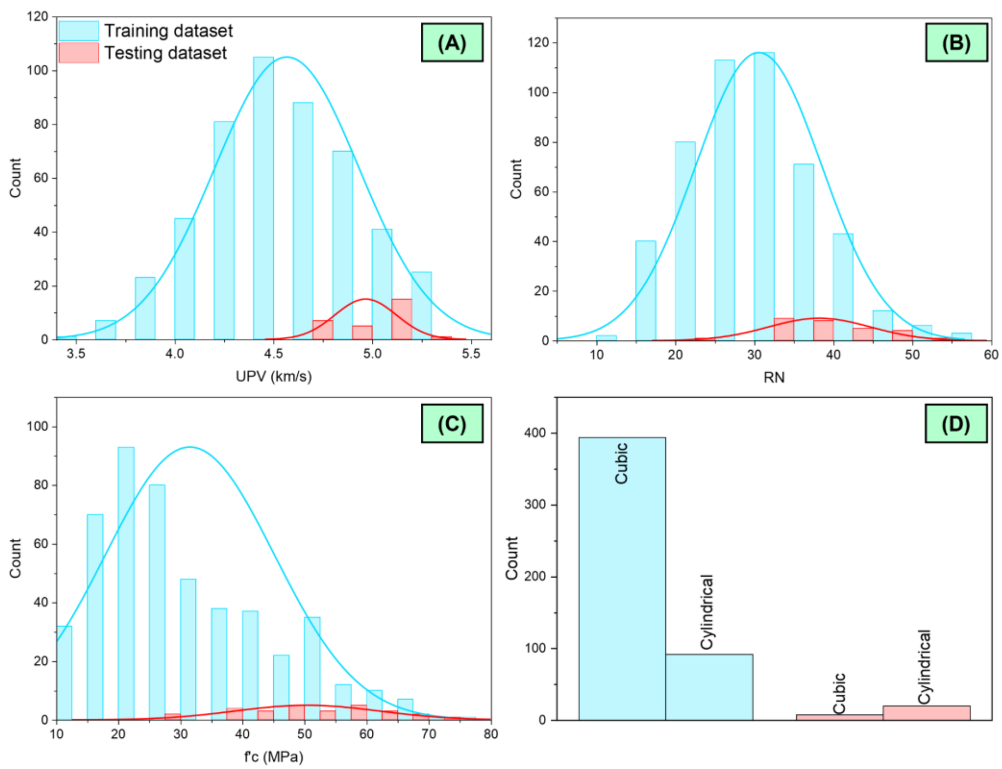

Figure 5.12: Data distribution for training and testing datasets based on (A) UPV, (B) RN, (C) compressive strength, and (D) type of specimen

5.4 Model Development and Analysis

5.4.1 AI models

As shown in Fig. 5.13, two approaches (Approach A and Approach B) were utilized with ML and DL methods, which include ANN, DNN, and ANFIS, to develop six AI models. The first three models, ANN-2i (Fig. 5.13(A)), DNN-2i (Fig. 5.13(B)), and ANFIS-2i (Fig. 5.13(C)) were developed using only two input parameters: UPV and RN to predict concrete CS (f_c'). Subsequently, models ANN-3i (Fig. 5.13(D)), DNN-3i (Fig. 5.13(E)), and ANFIS-3i (Fig. 5.13(F)) were developed. These models considered the geometry of specimens (cubic or cylindrical) as a third input parameter, in addition to UPV and RN, to predict concrete CS (f_c'). Table 5.5 summarizes the parameters used for each of the six AI models developed in this study. The training and testing datasets shown in Fig. 5.11 were used for all six models. In the development of all models, the UPV, RN, and CS values were normalized from 0.1 to 0.9 to avoid and reduce possible scaling effects during the training process. This scaling technique is an important step before developing ML models, which helps to increase both the speed and accuracy of the training process (Fakharian et al., 2023; Naderpour et al., 2018). The equation used for normalization is given by Eq. 1. In this equation, $x_{normalized}$ represents the normalized value, while x represents the unnormalized value, and x_{min} and x_{max} represent the minimum and maximum values for each parameter (UPV, RN, and f_c'), as given in Table 5.4.

$$x_{normalized} = \left[(0.8) \times \left(\frac{x - x_{min}}{x_{max} - x_{min}}\right)\right] + (0.1) \qquad \text{(Eq.1)}$$

According to Fig. 5.13, in models ANN-3i, DNN-3i, and ANFIS-3i, there is an additional input parameter which is the "type of geometry." In these three models, a binary value (zero or one) is defined for this input parameter. Specifically, the value of zero (0) is considered as "cubic specimen," and the value of one is considered as "cylindrical specimen."

Finally, all six AI models were trained by 486 data from the training set and validated by 28 data from the testing dataset. For the evaluation and comparing the results of these models, six parameters of MAPE (Mean Absolute Percentage Error), RMSE (Root Mean Square Error), MAE (Mean Absolute Error), R (correlation coefficient), R^2 (coefficient of determination), and PI (Performance Index) were selected in this study. The equations for these parameters are presented in Eq.2 to Eq.7, respectively, where $f'_{c,Pred}$ represents predicted value and $f'_{c,Exp}$ represents experimental values of the concrete CS. Also, $\overline{f'_{c,Pred}}$ and $\overline{f'_{c,Exp}}$ represent the mean values for the predicted and experimental values, respectively.

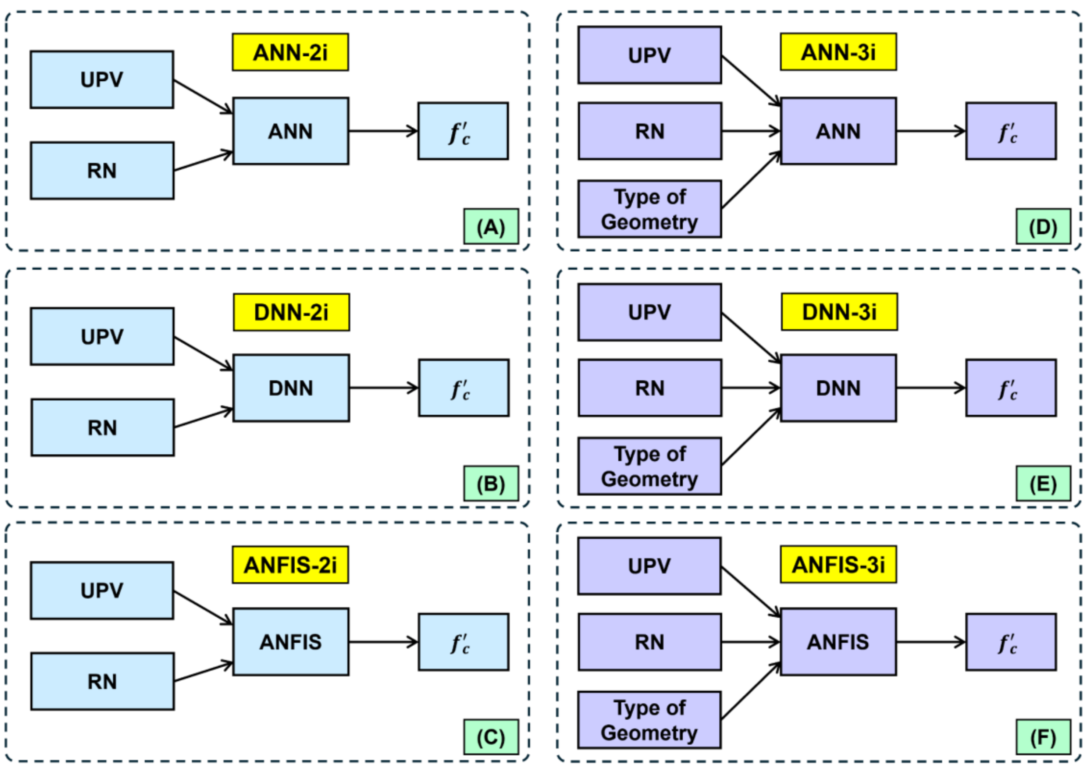

Figure 5.13: The input and output parameters for six AI models; (A) ANN-2i, (B) DNN-2i, (C) ANFIS-2i, (D) ANN-3i, (E) DNN-3i, and (F) ANFIS-3i

Table 5.5 Details of the model parameters

Model	Number of inputs	Detail
ANFIS-2i	2	Number of membership functions for each input: 2 Type of membership functions: Triangular MF Number of rules: 4
ANFIS-3i	3	Number of membership functions for each input: 3 Type of membership functions: Triangular MF Number of rules: 8
ANN2i	2	Type: Feed Forward Network Number of hidden layers: 1 Number of Neurons for hidden layer: 20
ANN3i	3	Type: Feed Forward Network Number of hidden layers: 1 Number of neurons for hidden layer: 50
DNN2i	2	Type: Feed Forward Network Number of hidden layers: 2 Number of neurons for the first hidden layer: 10 Number of neurons for the second hidden layer: 10
DNN3i	3	Type: Feed Forward Network Number of hidden layers: 2 Number of neurons for the first hidden layer: 10 Number of neurons for the second hidden layer: 10

5.4.2 Performance Metrics

Six statistical parameters (Eq.2 to Eq.7) were used to accurately evaluate and compare the performance of each AI model for predicting concrete CS. In detail, the first statistical parameter which is "MAPE" measures the average absolute percentage difference between the predicted and actual value (from the experimental measurements) of CS; the MAPE is the simplest and most common parameter used to evaluate the accuracy of prediction models (Eq.2). The second parameter of "RMSE" calculates the square root of the average squared differences between predicted and actual values; the RMSE gives information on how far predictions fall from actual true values, with lower RMSE indicating better performance (Eq.3). The third parameter of "MAE" computes the average absolute difference between predicted and actual values; the MAE gives the average size of the errors (regardless of the sign) in prediction models with lower MAE indicating better performance (Eq.4). The fourth parameter of "R" measures the strength and direction of the linear relationship between predicted and actual value, and ranges from negative one (-1) to positive one (+1). If R is equal to positive one it means a perfect positive correlation in the performance of the model, while negative one shows a perfect negative correlation (Eq.5) (Schober et al., 2018) The fifth parameter of "R^2" tells how well a model prediction correlates with measured values; the R^2 value is a number from zero to one (0-1), where a value of one indicates a perfect prediction model (Eq.6) (Chen et al., 2023; Quinino et al., 2013; Schober et al., 2018). The last parameter which is “PI” is used to evaluate the overall model performance by calculating the division of RMSE by (1 + R), where R is the correlation coefficient; a lower PI value indicates better performance (Eq.7) (Chen et al., 2023; Naser & Alavi, 2023).

$$MAPE = \frac{1}{n}\sum_{i=1}^{n}\left(\frac{\left|f'_{c,Pred}-f'_{c,Exp}\right|}{f'_{c,Exp}}\right)\times 100 \qquad \text{(Eq.2)}$$

$$RMSE = \sqrt{\frac{1}{n}\sum_{i=1}^{n}\left(f'_{c,Predi}-f'_{c,Exp}\right)^2} \qquad \text{(Eq.3)}$$

$$MAE = \frac{1}{n}\sum_{i=1}^{n}\left|f'_{c,Pred}-f'_{c,Exp}\right| \qquad \text{(Eq.4)}$$

$$R = \frac{\sum_{i=1}^{n}(f'_{c,Exp}-\overline{f'_{c,Exp}})\,(f'_{c,Pred}-\overline{f'_{c,Pred}})}{\sqrt{\sum_{i=1}^{n}(f'_{c,Exp}-\overline{f'_{c,Exp}})^2\,\sum_{i=1}^{n}(f'_{c,Pred}-\overline{f'_{c,Pred}})^2}} \qquad \text{(Eq.5)}$$

$$R^2 = 1-\frac{\sum_{i=1}^{n}(f'_{c,Pred}-f'_{c,Exp})^2}{\sum_{i=1}^{n}(f'_{c,Exp}-\overline{f'_{c,Exp}})^2} \qquad \text{(Eq.6)}$$

$$PI = \frac{(RMSE)}{(1+R)} \qquad \text{(Eq.7)}$$

In summary, MAPE, RMSE, and MAE values target the errors, R and R^2 values evaluate the correlation between predicted and actual values, whereas PI provides a general assessment of the overall performance of the model. Accordingly, Table 5.6 presents performance metrics for the different models (ANFIS, ANN, and DNN) across various datasets (Training, Testing, and All) measured by these six statistical parameters.

Table 5.6 Comparison of the performance of the AI models

Model	Dataset	MAPE (%)	RMSE (MPa)	MAE (MPa)	R	R^2	PI
ANFIS-2i	Training	12.94	4.67	3.74	0.939	0.882	2.4
	Testing	14.81	8.68	7.49	0.758	0.423	4.9
	All	13.04	4.97	3.94	0.936	0.876	2.6
ANFIS-3i	Training	11.11	4.25	3.24	0.950	0.902	2.2
	Testing	11.37	6.55	5.53	0.833	0.672	3.6
	All	11.13	4.40	3.36	0.950	0.903	2.3
ANN-2i	Training	12.23	4.43	3.48	0.946	0.894	2.3
	Testing	14.36	8.39	7.25	0.758	0.462	4.8
	All	12.34	4.73	3.68	0.943	0.888	2.4
ANN-3i	Training	10.85	3.95	3.05	0.957	0.915	2.0
	Testing	14.27	7.90	6.59	0.734	0.522	4.6
	All	11.03	4.26	3.24	0.954	0.909	2.2
DNN-2i	Training	11.24	4.12	3.20	0.953	0.908	2.1
	Testing	15.62	9.19	7.82	0.718	0.353	5.4
	All	11.47	4.54	3.45	0.947	0.897	2.3
DNN-3i	Training	10.06	3.88	2.90	0.958	0.918	2.0
	Testing	12.37	7.19	6.04	0.791	0.604	4.0
	All	10.19	4.13	3.07	0.957	0.914	2.1

5.4.3 Performance analysis of AI models

In Fig. 5.14, three-axis spider charts based on each statistical parameter are given where each axis represents the type of dataset (training, testing, and all data). According to Table 5.6 and Fig. 5.14, across all three types of models (ANFIS, ANN, and DNN), version 3i with three inputs consistently outperformed the corresponding two-input version across various evaluation metrics and datasets. This indicates that the improvements made from adding the third input parameter accounting for specimen geometry were beneficial for all three types of models. In other words, regardless of the type of algorithm (ANFIS, ANN, or DNN), considering the third input meaningfully increases the accuracy of the models. In all cases, the MAPE, RMSE, and

MAE values were decreased which indicates a reduction in the degree of error, and R and R^2 values increased (better correlation). The Performance Index (PI) shows that the overall performance of the models also improved, decreasing from 2.6 to 2.3 for the ANFIS algorithm (considering all data), from 2.4 to 2.2 for the ANN algorithm, and from 2.3 to 2.1 for the DNN algorithm. Table 5.7 ranks the performance of the models based on each statistical parameter for all data. All of the three-input models ranked higher than the three two-input models.

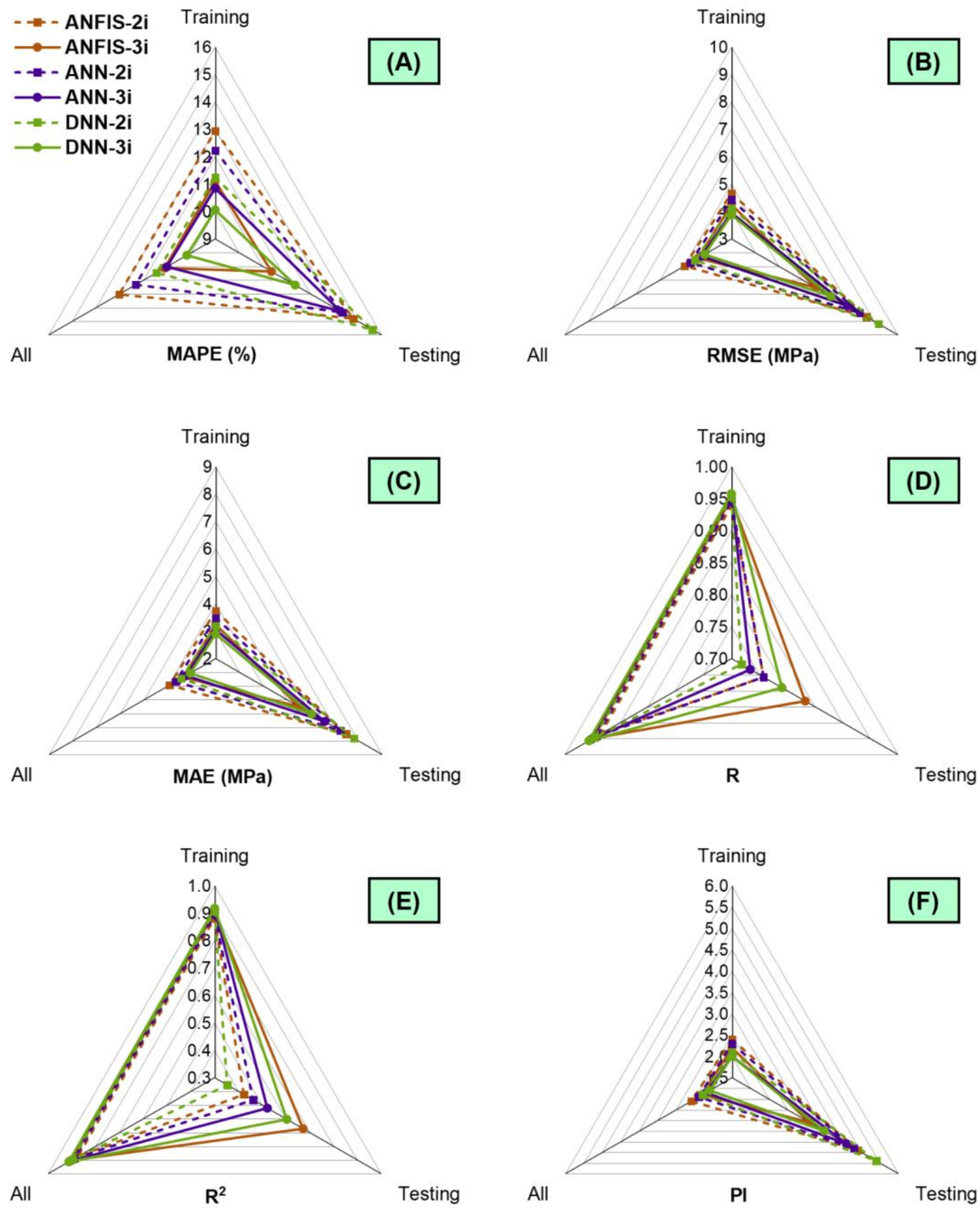

Figure 5.14: Three-axis spider chart for parameters of (A) MAPE, (B) RMSE, (C) MAE, (D) R, (E) R-squared, and (F) PI

The transition from the two-input versions (2i) to the three-input versions (3i) across ANFIS, ANN, and DNN algorithms shows a significant improvment in learning capabilities, particularly evident in the training datasets for all AI models. In detail, ANFIS-3i shows a significant improvement over ANFIS-2i, showcasing lower errors with a decrease in MAPE from 12.94% to 11.11%, RMSE from 4.67 to 4.25, and MAE from 3.74 MPa to 3.24 MPa, alongside an increase in correlation metrics such as R from 0.939 to 0.950 and R^2 from 0.882 to 0.902. This shows a refined ability to capture patterns from input parameters to predict the CS of concrete based on SonReb data. Similarly, ANN-3i demonstrates higher performance in comparison to ANN-2i, with reduced errors and improved correlations. The decrease in MAPE from 12.23% to 10.85%, RMSE from 4.43 to 3.95 MPa, and MAE from 3.48 MPa to 3.05 MPa, coupled with the increase in R from 0.946 to 0.957 and R^2 from 0.894 to 0.915, signifies improved accuracy in concrete strength predictions and indicative of better learning capabilities. Additionally, DNN-3i showcases improvement over DNN-2i, with decreased errors and enhanced correlations with a reduction in MAPE from 11.24% to 10.06%, RMSE from 4.12 to 3.88 MPa, and MAE from 3.20 MPa to 2.90 MPa, alongside the increase in R from 0.953 to 0.958 and R^2 from 0.908 to 0.918.

Table 5.7 Performance ranking based on each statistical parameter for all data

Rank*	MAPE	RMSE	RMSE	MAE	R	R^2	PI
1	DNN-3i	DNN-3i	DNN-3i	DNN-3i	DNN-3i	DNN-3i	DNN-3i
2	ANN-3i	ANN-3i	ANN-3i	ANN-3i	ANN-3i	ANN-3i	ANN-3i
3	ANFIS-3i	ANFIS-3i	ANFIS-3i	ANFIS-3i	ANFIS-3i	ANFIS-3i	ANFIS-3i
4	DNN-2i	DNN-2i	DNN-2i	DNN-2i	DNN-2i	DNN-2i	DNN-2i
5	ANN-2i	ANN-2i	ANN-2i	ANN-2i	ANN-2i	ANN-2i	ANN-2i
6	ANFIS-2i	ANFIS-2i	ANFIS-2i	ANFIS-2i	ANFIS-2i	ANFIS-2i	ANFIS-2i
*Rank one to six means best performance (high accuracy) to worst performance (lowest accuracy).							

Fig. 5.15 shows the scatter graphs for all AI models based on four datasets which are (1) training dataset for cylindrical specimens, (2) training dataset for cubic specimens, (3) testing dataset for cylindrical specimens and (4) testing dataset for cubic specimens. In these graphs, the improvement of learning abilities are evident, especially for the training datasets for cylindrical specimens that are plotted with green color dots in the graphs. It can be seen how in the three-

input version of AI models (Fig 5.15(B), Fig 5.15(D), and Fig 5.15(F)), these points are close to the X=Y line which shows the ideal performance, in comparison to the two-inputs version of the models (Fig 5.15(A), Fig 5.15(C), and Fig 5.15(E)). It is also noteworthy that the prediction accuracy is not greatly affected by concrete strength as the scatter in the results remains fairly consistent at all strength levels.

Fig. 5.16 presents a head-to-head comparison between the experimental value and predicted value of strength based on the 28 testing data for all AI models. It can be clearly seen that adding a third input improved the accuracy of the prediction for the unseen data in the testing dataset, especially for the cylindrical type. This improvement is expected, since only 92 of the total 486 training data (18%) were obtained from cylindrical specimens.

Finding the best model among all six proposed models should be done based on a careful investigation of the information presented in Table 5.6 and the graphs provided in Fig. 5.14 to Fig. 5.18.

Upon initial examination of the metrics provided in Tables 5.6 and 5.7, it appears that the best prediction model is DNN-3i, which demonstrates superior metrics with a 10.19% MAPE, 4.13 MPa RMSE, 3.07 MPa MAE, 0.957 R, 0.914 R^2, and a performance index (PI) of 2.1. However, this initial impression is not necessarily accurate since the best model could also be considered the one that can predict the strength of concrete more accurately for unseen data, enabling its use in future applications. Given that the testing dataset in this study is completely separated from the training data and was not seen during the training process, it is important to evaluate the results based on statistical parameters from the testing dataset. In the other words, the decrease in performance from training to testing datasets highlights the importance of evaluating models on unseen data to assess their true predictive abilities. Consequently, Table

5.8 is provided for this purpose, ranking the models' performance based on the testing dataset only.

According to Table 5.6 as well as Fig. 5.14, ANFIS-3i demonstrates the lowest MAPE and RMSE values in testing datasets. Compared to the training data, ANFIS-3i exhibits relatively high values for MAE and PI in the testing dataset, indicating variability in its predictions. Nevertheless, as seen in Table 5.8, when compared to other methods, ANFIS-3i was found to be the most robust model across the testing dataset. Fig. 5.17 presents the violin plots of error distribution for AI models for each subset of the database, which show the superiority of the ANFIS-3i model in terms of having a lower range of error compared to other models.

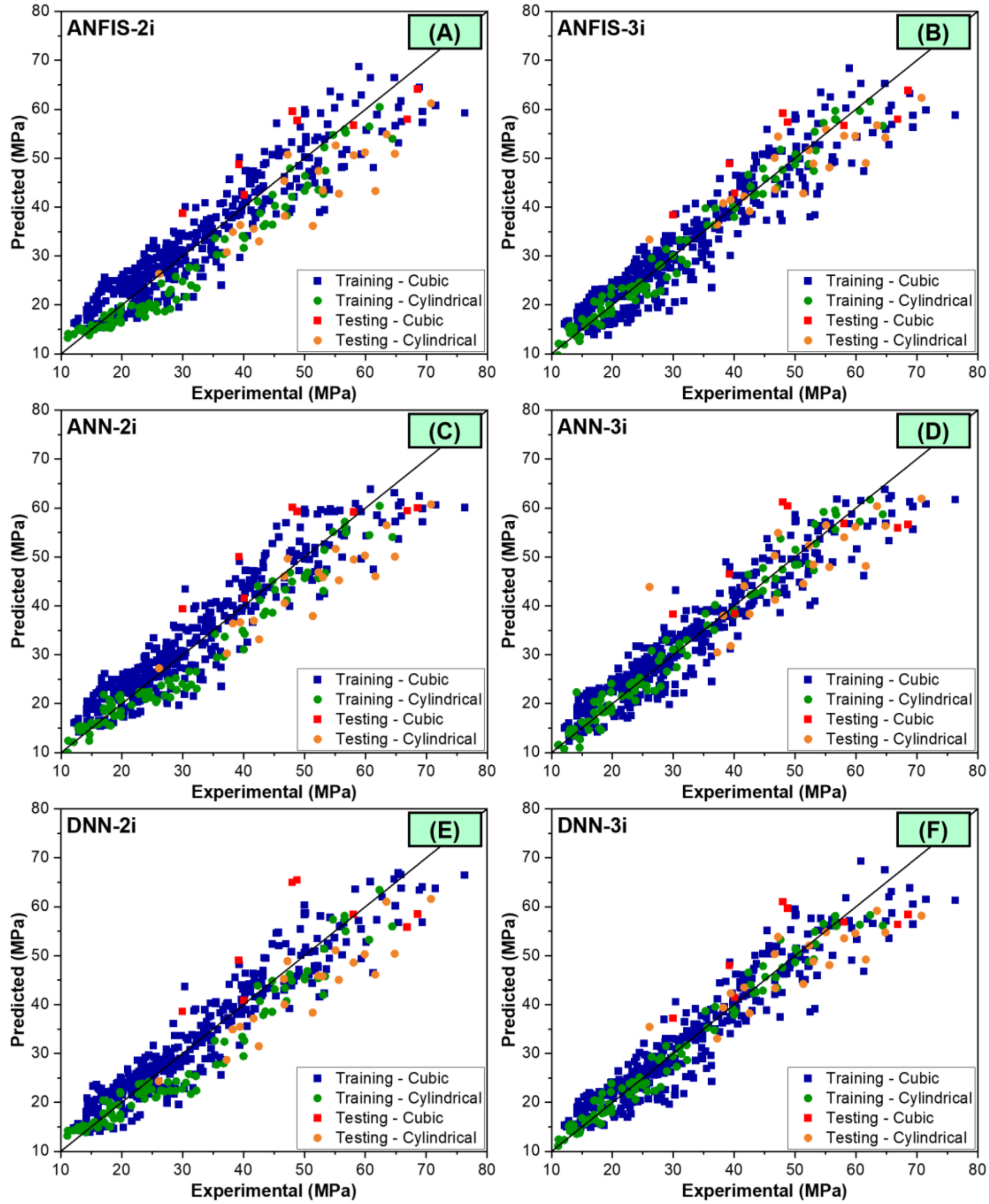

Figure 5.15: The experimental value vs predicted value of compressive strength for the model (A) ANFIS-2i, (B) ANFIS-3i, (C) ANN-2i, (D) ANN-3i, (E) DNN-2i, and (F) DNN-3i

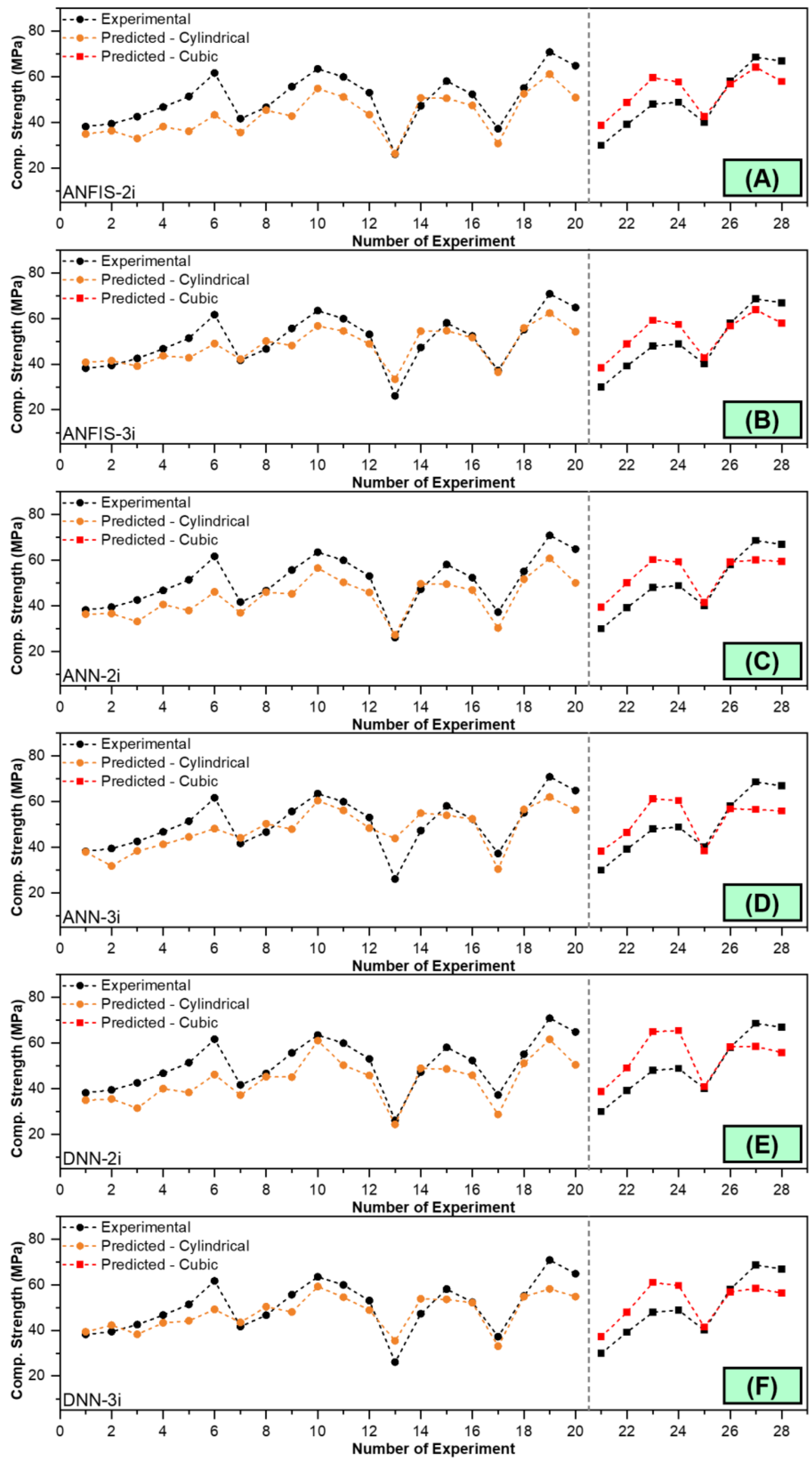

Figure 5.16: Head-to-head comparison between the experimental value and predicted value of strength based on the testing data for; (A) ANFIS-2i, (B) ANFIS-3i, (C) ANN-2i, (D) ANN-3i, (E) DNN-2i, and (F) DNN-3i

Table 5.8 Performance ranking based on each statistical parameter for testing dataset

Rank*	MAPE	RMSE	MAE	R	R^2	PI
1	ANFIS-3i	ANFIS-3i	ANFIS-3i	ANFIS-3i	ANFIS-3i	ANFIS-3i
2	DNN-3i	DNN-3i	DNN-3i	DNN-3i	DNN-3i	DNN-3i
3	ANN-3i	ANN-3i	ANN-3i	ANN-2i	ANN-3i	ANN-3i
4	ANN-2i	ANN-2i	ANN-2i	ANFIS-2i	ANN-2i	ANN-2i
5	ANFIS-2i	ANFIS-2i	ANFIS-2i	ANN-3i	ANFIS-2i	ANFIS-2i
6	DNN-2i	DNN-2i	DNN-2i	DNN-2i	DNN-2i	DNN-2i
*Rank one to six means best performance (high accuracy) to worst performance (lowest accuracy).						

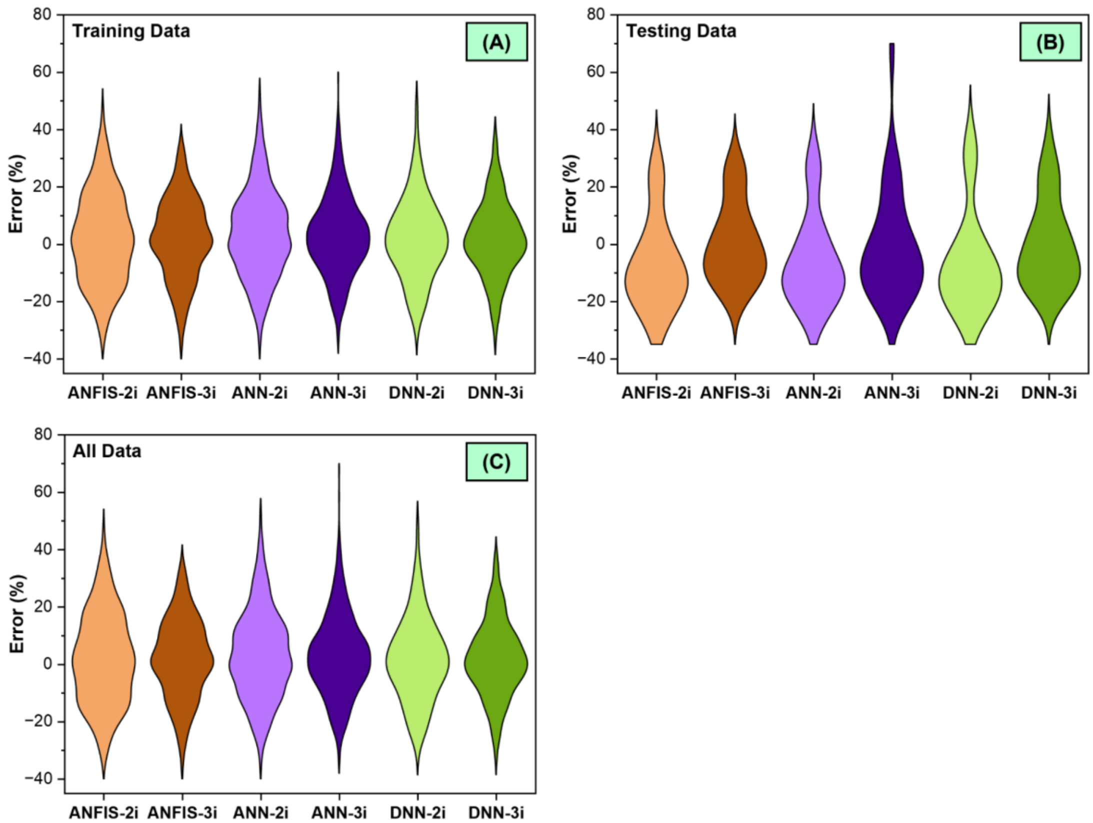

Figure 5.17: Violin plots of error distribution for AI models based on (A) Training data, (B) Testing data, and (C) All data

It is worth noting that when considering the testing data only, the ANN-3i model produced a lower R value than the ANN-2i model. Comparing Fig. 5.15 (C) and (D), it is evident that the scatter of the results (i.e., average error) is lower for ANN-3i than ANN-2i. Nevertheless, there are a couple of outliers, particularly for the cylindrical testing dataset (orange points). Given the relatively small number of test data points, this reduces the R value even though the average error is lower. This can also be observed in Fig. 5.17, where the maximum error for ANN-3i is notably higher than ANN-2i. This further supports the selection of ANFIS-3i as the most accurate and robust model for the testing dataset.

A Taylor diagram is given in Fig. 5.18 based on training (Fig. 5.18(A)), testing (Fig. 5.18(B)), and all data (Fig. 5.18(C)). A Taylor diagram is a tool used to visualize the performance of the prediction models based on the statistical parameters of standard deviation and correlation coefficient (Taylor, 2001). The best model is one that is closest to the reference point (red point) which represents the experimental data (which is the measured value of CS) corresponding to a high correlation coefficient and a spatial variability (i.e., standard deviation) that is similar to the reference. In Fig. 5.18(A), which shows the performance of all models based on the training data only, all models show a similar range of correlation coefficients indicating good performance. However, it could be said that ANFIS-3i and DNN-3i have slightly better performance since they are closer to the reference point. Fig. 5.18 (B), which shows the performance based on the testing data, shows significant differences in comparison to the training data. DNN-3i and ANFIS-3i have the best performance with the highest correlation coefficients, while other models show lower correlation which confirm the results of Table 5.8. Finally, in Fig. 5.18 (C), which represents all data, ANFIS-3i again shows stronger performance than the other models. This suggests that ANFIS-3i performs consistently well across all datasets. In conclusion, ANFIS-3i seems to be the most robust and reliable model in comparison to the other five models, which aligns with the previous analyses.

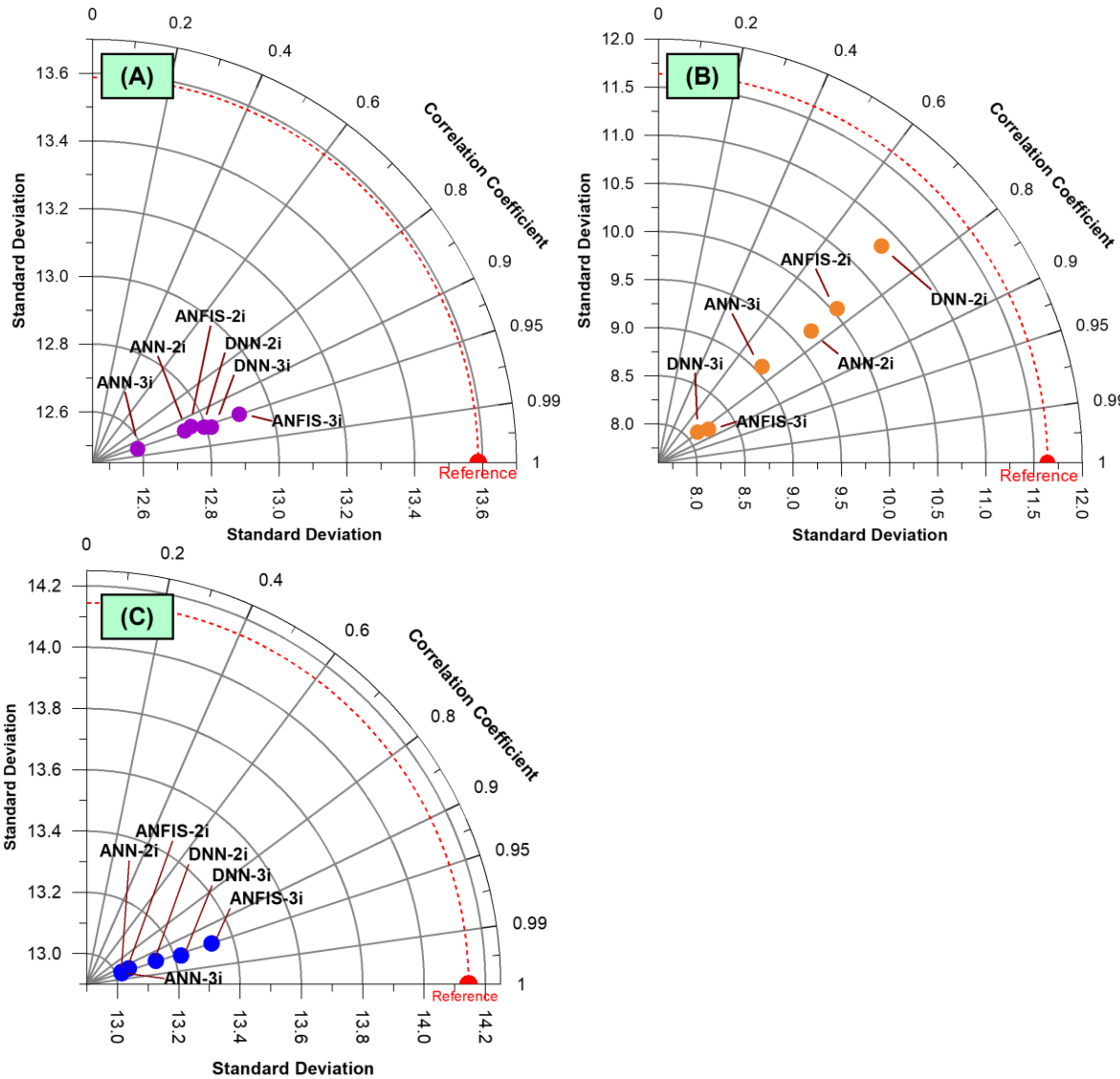

Figure 5.18: Taylor diagram for overall performance of all AI models based on (A) training data, (B) testing data, and (C) all data

5.5 Conclusions

This study investigates a novel methodology aimed at improving the accuracy of AI-based models for predicting concrete CS using the SonReb method's results. Both ML and DL techniques were used to create six AI models (based on ANN, ANFIS, and DNN algorithms). Three of the models used just two numerical inputs (UPV and RN), while the other three models incorporated three inputs; UPV, RN, and one binary input for the type of geometry. Based on the analysis of the models' outcomes, the following conclusions can be made:

(1) Adding the third binary input parameter, which is the 'type of geometry', substantially enhances both the learning capacity and prediction accuracy of the AI models compared to the conventional approach, which solely relies on UPV and RN results for concrete CS prediction.

(2) Among AI algorithms that were used in this study to develop a three-input version, the lowest error based on the training data sets belongs to DNN algorithms which is based on the deep learning technique (10.06% MAPE, 3.88 MPa RMSE, 2.9 MPa MAE, 0.958 R, and 0.918 R^2) due to complexity of its training process.

(3) The best model performance based on the testing data, which was previously unseen by the training algorithm, was obtained from the ANFIS model with three inputs, which is based on machine learning and fuzzy logic. The performance metrics show 11.13% MAPE, 4.4 MPa RMSE, 3.36 MPa MAE, with a correlation coefficient (R) of 0.95, an R-squared value of 0.903, and a performance index of 2.3.

Despite the progress presented in this study, some limitations remain to be addressed in the development of a general AI model for field use. For instance, in this study, 80% of the database corresponded to cubic specimens and 20% to cylindrical specimens; hence, adding more cylindrical data would potentially improve model outcomes. Furthermore, this study did not consider data from cores extracted from existing structures which may be affected by environmental conditions and other factors that could introduce additional uncertainty to the results. Alternative AI algorithms may also present certain advantages over those utilized in this study and are worth exploring. Finally, there is a need to quantify the reliability of applying AI and ML to the SONREB method, and it is recommended to conduct a comprehensive study on this topic.

In summary, this study confirms the potential of AI to improve the non-destructive evaluation of concrete structures while establishing a path forward towards the development of future models as part of a process of continuous improvement.

5.6 References

Aïtcin, P.-C. (2000). Cements of yesterday and today: concrete of tomorrow. Cement and Concrete Research, 30(9), 1349–1359.

Alavi, S. A., & Noël, M. (2022). Challenges for the Development of Artificial Intelligence Models to Predict the Compressive Strength of Concrete Using Non-destructive Tests: A Review. Canadian Society of Civil Engineering Annual Conference, 839–857.

Alavi, S. A., Noël, M., Layssi, H., & Moradi, F. (2024a). Can Artificial Intelligence Improve Nondestructive Evaluation of Concrete Strength? Concrete International, 46(5), 51–56.

Alavi, S. A., Noel, M., Moradi, F., & Layssi, H. (2024b). Development of a machine learning model for on-site evaluation of concrete compressive strength by SonReb. Journal of Building Engineering, 82, 108328.

Alavi, S.A., Hasak, A., Noel, M., Moradi, F., Layssi, H. (2022). Non-Destructive Evaluation of Concrete Compressive Strength Using Neuro-Fuzzy Modelling Approach. The International Symposium on Nondestructive Testing in Civil Engineering. https://www.ndt.net/search/docs.php3?id=27244

Ali Poorarbabi. (2020). Assessment of concrete compressive strength and electrical resistivity using NDT techniques and artificial neural networks. The University of Sistan & Baluchestan.

Ali-Benyahia, K., Kenai, S., Ghrici, M., Sbartaï, Z.-M., & Elachachi, S.-M. (2023). Analysis of the accuracy of in-situ concrete characteristic compressive strength assessment in real structures using destructive and non-destructive testing methods. Construction and Building Materials, 366, 130161.

Alwash, M., Breysse, D., & Sbartaï, Z. M. (2015). Non-destructive strength evaluation of concrete: Analysis of some key factors using synthetic simulations. Construction and Building Materials, 99, 235–245. https://doi.org/10.1016/J.CONBUILDMAT.2015.09.023

Amin, F., Javed, M. F., Ahmad, I., Asad, O., Khan, N., Khan, A. B., Ali, S., Abdullaev, S., Awwad, F. A., & Ismail, E. A. A. (2024). Utilization of discarded face masks in combination with recycled concrete aggregate and silica fume for sustainable civil construction projects. Scientific Reports, 14(1), 449.

Amini, K., Jalalpour, M., & Delatte, N. (2016). Advancing concrete strength prediction using non-destructive testing: Development and verification of a generalizable model. Construction and Building Materials, 102, 762–768.

Arora, H. C., Bhushan, B., Kumar, A., Kumar, P., Hadzima-Nyarko, M., Radu, D., Cazacu, C. E., & Kapoor, N. R. (2024). Ensemble learning based compressive strength prediction of concrete structures through real-time non-destructive testing. Scientific Reports, 14(1), 1824.

Asteris, P. G., & Mokos, V. G. (2020). Concrete compressive strength using artificial neural networks. Neural Computing and Applications, 32(15), 11807–11826.

Asteris, P. G., Skentou, A. D., Bardhan, A., Samui, P., & Lourenço, P. B. (2021). Soft computing techniques for the prediction of concrete compressive strength using Non-Destructive tests. Construction and Building Materials, 303, 124450.

ASTM C-597-16: Standard Test Method for Pulse Velocity Through Concrete (2023). https://doi.org/10.1520/C0597-16

Bolborea, B., Dan, S., Baeră, C., Gruin, A., Enache, F., & Perianu, I. A. (2022). Study Regarding the Evaluation of Prediction Models for Determining the Concrete Compressive Strength Using Non-Destructive Testing (NDT) Data: Validation Stage. Solid State Phenomena, 332, 173–181.

Bonagura, M. (2012). Nondestructive evaluation of concrete compression strength by means of Artificial Neural Network (ANN).

Breysse, D. (2012). Nondestructive evaluation of concrete strength: An historical review and a new perspective by combining NDT methods. Construction and Building Materials, 33, 139–163.

Chandak, N. R., & Kumavat, H. R. (2020). SonReb Method for Evaluation of Compressive Strength of Concrete. InIOP Conference Series: Materials Science and Engineering, 810(1), 12071.

Chen, L., Fakharian, P., Eidgahee, D. R., Haji, M., Arab, A. M. A., & Nouri, Y. (2023). Axial compressive strength predictive models for recycled aggregate concrete filled circular steel tube columns using ANN, GEP, and MLR. Journal of Building Engineering, 77, 107439.

Cianfrone, F., & Facaoaru, I. (1979). Study on the introduction into Italy on the combined non-destructive method, for the determination ofin situ concrete strength. Matériaux et Construction 1979 12:5, 12(5), 413–424. https://doi.org/10.1007/BF02478819

Domingo, R., & Hirose, S. (2009). Correlation between concrete strength and combined nondestructive tests for concrete using high-early strength cement. The Sixth Regional Symposium on Infrastructure Development, 12–13.

El-Mir, A., El-Zahab, S., Sbartaï, Z. M., Homsi, F., Saliba, J., & El-Hassan, H. (2023). Machine learning prediction of concrete compressive strength using rebound hammer test. Journal of Building Engineering, 64, 105538.

EN 13791:2019: Assessment of in-situ compressive strength in structures and precast concrete components. (2019). CEN-CENELEC Management Centre.

Facaoaru, I. (1961). Contribution à i'étude de la relation entre la résistance du béton à la compression et de la vitesse de propagation longitudinale des ultrasons. Rilem, 22, 125–154.

Fakharian, P., Eidgahee, D. R., Akbari, M., Jahangir, H., & Taeb, A. A. (2023). Compressive strength prediction of hollow concrete masonry blocks using artificial intelligence algorithms. Structures, 47, 1790–1802.

Forty, A. (2013). Concrete and culture: a material history. Reaktion Books.

Frappa, G., Miceli, M., & Pauletta, M. (2022). Destructive and non-destructive tests on columns and cube specimens made with the same concrete mix. Construction and Building Materials, 349, 128807.

Hannachi, S., & Guetteche, M. N. (2014). Review of the ultrasonic pulse velocity evaluating concrete compressive strength on site. Proceedings of Scientific Cooperation International Workshops on Engineering Branches, Istanbul, Turkey, 8–9.

Hu, S., Zuo, Y., Wang, L., & Liu, P. (2016). A review about building hidden layer methods of deep learning. Journal of Advances in Information Technology, 7(1).

Jain, A., Kathuria, A., Kumar, A., Verma, Y., & Murari, K. (2013). Combined use of non-destructive tests for assessment of strength of concrete in structure. Procedia Engineering, 54, 241–251.

Jang, J.-S. R. (1993). ANFIS: adaptive-network-based fuzzy inference system. IEEE Transactions on Systems, Man, and Cybernetics, 23(3), 665–685. https://doi.org/10.1109/21.256541

Janiesch, C., Zschech, P., & Heinrich, K. (2021). Machine learning and deep learning. Electronic Markets, 31(3), 685–695.

Kumar, P., & Kumar, A. (2015). Prediction of compressive strength using genetic programming involving NDT results. NATIONAL INSTITUTE OF TECHNOLOGY ROURKELA.

Li, D., Tang, Z., Kang, Q., Zhang, X., & Li, Y. (2023). Machine learning-based method for predicting compressive strength of concrete. Processes, 11(2), 390.

Logothetis, L. (1978). Combination of three non destructive methods for the determination of the strength of concrete. National Technical University of Athens.

Masi, A., Chiauzzi, L., & Manfredi, V. (2016). Criteria for identifying concrete homogeneous areas for the estimation of in-situ strength in RC buildings. Construction and Building Materials, 121, 576–587. https://doi.org/10.1016/J.CONBUILDMAT.2016.06.017

May, R., Dandy, G., & Maier, H. (2011). Review of input variable selection methods for artificial neural networks. Artificial Neural Networks-Methodological Advances and Biomedical Applications, 10(1), 19–45.

Miano, A., Ebrahimian, H., Jalayer, F., & Prota, A. (2023). Reliability Estimation of the Compressive Concrete Strength Based on Non-Destructive Tests. Sustainability, 15(19), 14644.

Moein, M. M., Saradar, A., Rahmati, K., Mousavinejad, S. H. G., Bristow, J., Aramali, V., & Karakouzian, M. (2023). Predictive models for concrete properties using machine learning and deep learning approaches: A review. Journal of Building Engineering, 63, 105444.

Na, U. J., Park, T. W., Feng, M. Q., & Chung, L. (2009). Neuro-fuzzy application for concrete strength prediction using combined non-destructive tests. Magazine of Concrete Research, 61(4), 245–256.

Naderpour, H., & Alavi, S. A. (2017). A proposed model to estimate shear contribution of FRP in strengthened RC beams in terms of Adaptive Neuro-Fuzzy Inference System. Composite Structures, 170, 215–227. https://doi.org/10.1016/J.COMPSTRUCT.2017.03.028

Naderpour, H., Rafiean, A. H., & Fakharian, P. (2018). Compressive strength prediction of environmentally friendly concrete using artificial neural networks. Journal of Building Engineering, 16, 213–219.

Naik, T. R., Malhotra, V. M., & Popovics, J. S. (2003). The ultrasonic pulse velocity method. In Handbook on Nondestructive Testing of Concrete, Second Edition (pp. 1–8). CRC Press.

Naser, M. Z., & Alavi, A. H. (2023). Error metrics and performance fitness indicators for artificial intelligence and machine learning in engineering and sciences. Architecture, Structures and Construction, 3(4), 499–517.

Ngo, T. Q. L., Wang, Y.-R., & Chiang, D.-L. (2021). Applying Artificial Intelligence to Improve On-Site Non-Destructive Concrete Compressive Strength Tests. Crystals, 11(10), 1157.

Nikhil, M. V, Minal, B. R., Deep, C. S., Vijay, G. D., Vishal, T. S., & Shweta, P. (2015). The Use of Combined Non Destructive Testing in the Concrete Strength Assessment from Laboratory Specimens and Existing Buildings. Int. J. Curr. Eng. Scientific Res., 2(5), 55–59.

Nobile, L. (2015). Prediction of concrete compressive strength by combined non-destructive methods. Meccanica, 50(2), 411–417.

Poorarbabi, A., Ghasemi, M., & Moghaddam, M. A. (2020). Concrete Compressive Strength Prediction Using Neural Networks Based on Non-destructive Tests and a Self-calibrated Response Surface Methodology. Journal of Nondestructive Evaluation, 39(4), 1–11.

Poorarbabi, A., Ghasemi, M. R., & Azhdari Moghaddam, M. (2021). Conversion factors between non-destructive tests of cubic and cylindrical concrete specimens. AUT Journal of Civil Engineering, 5(1), 1.

Quinino, R. C., Reis, E. A., & Bessegato, L. F. (2013). Using the coefficient of determination R2 to test the significance of multiple linear regression. Teaching Statistics, 35(2), 84–88.

Rashid, K., & Waqas, R. (2017). Compressive strength evaluation by non-destructive techniques: An automated approach in construction industry. Journal of Building Engineering, 12, 147–154.

RILEM. (1993). Draft recommendation for in situ concrete strength determination by combined non-destructive methods. In Mater. Struct (Vol. 26). Springer.

Sai, G. J., & Singh, V. P. (2019). Prediction of compressive strength using support vector regression. MENDEL, 25(1), 51–56.

Schober, P., Boer, C., & Schwarte, L. A. (2018). Correlation coefficients: appropriate use and interpretation. Anesthesia & Analgesia, 126(5), 1763–1768.

Shariati, M., Ramli-Sulong, N. H., Arabnejad, M. M., Shafigh, P., & Sinaei, H. (2011). Assessing the strength of reinforced concrete structures through Ultrasonic Pulse Velocity and Schmidt Rebound Hammer tests. Scientific Research and Essays, 6(1), 213–220.

Shih, Y.-F., Wang, Y.-R., Lin, K.-L., & Chen, C.-W. (2015). Improving non-destructive concrete strength tests using support vector machines. Materials, 8(10), 7169–7178.

Shishegaran, A., Varaee, H., Rabczuk, T., & Shishegaran, G. (2021). High correlated variables creator machine: Prediction of the compressive strength of concrete. Computers & Structures, 247, 106479.

Tapeh, A. T. G., & Naser, M. Z. (2022). Artificial Intelligence, Machine Learning, and Deep Learning in Structural Engineering: A Scientometrics Review of Trends and Best Practices. Archives of Computational Methods in Engineering, 1–45.

Taylor, K. E. (2001). Summarizing multiple aspects of model performance in a single diagram. Journal of Geophysical Research: Atmospheres, 106(D7), 7183–7192.

Thai, H.-T. (2022). Machine learning for structural engineering: A state-of-the-art review. Structures, 38, 448–491.

Wang, Y. R., Ngo, L. T. Q., Shih, Y. F., Lu, Y. L., & Chen, Y. M. (2018). Adapting ANNs in SONREB Test to Estimate Concrete Compressive Strength. Key Engineering Materials, 792, 166–169.

Xu, T., & Li, J. (2018). Assessing the spatial variability of the concrete by the rebound hammer test and compression test of drilled cores. Construction and Building Materials, 188, 820–832.

Chapter 6 – Uncertainty and Prediction Intervals of Machine Learning Models for Concrete Strength Prediction[1]

6.1 Introduction

In the evaluation of concrete infrastructure, the most important mechanical parameter is the compressive strength (CS) of the concrete (Masi et al., 2016; Quagliarini et al., 2016), whether in structures under construction or those already built. For structures under construction, the CS of the concrete is measured on cylindrical or cubic samples taken from fresh concrete during pouring. However, for reinforced concrete (RC) structures that were built many years ago, other means of determining concrete CS are required. Structures being considered for structural health monitoring, rehabilitation or repair, or detailed condition assessments first require engineers to find ways to assess the CS of the concrete. Usually, the most prominent option for engineers is drilling and extracting cores followed by compressive tests on the cores, which are known as a "core test" or "destructive test (DT)".

In recent years, due to issues associated with core tests, such as safety considerations, high costs, limitations of access, and repeatability, engineers and researchers have sought alternative approaches (Alavi et al., 2024b). One method that has attracted engineers' attention is non-destructive testing (NDT) of concrete (Kot et al., 2021; Prassianakis & Giokas, 2003; Schabowicz, 2019). In this method, tests are conducted using devices that do not damage the concrete, and the results are usually used to indirectly estimate the CS of the concrete (Pucinotti, 2015). Two such tests are the Rebound Number (RN) test, conducted with a Schmidt hammer,

[1] This chapter has been submitted for review and possible publication in an international journal.

and the Ultrasonic Pulse Velocity (UPV) test, conducted with a UPV device. The combined use of these two NDT methods is known as the "SONREB method” (RILEM, 1993).

Over the past two decades, alongside advancements in artificial intelligence (AI) and its most important method of machine learning (ML), researchers have also been drawn to providing ML-based engineering solutions in the construction and civil engineering industry. One such topic is predicting the CS of concrete based on the results of the SONREB method. By investigating the reviewed papers on predicting concrete strength using ML/AI methods, it becomes clear that among all the studied scenarios (e.g., predicting concrete strength based on mix design, age, type of cement, etc.), relatively few studies have exclusively used data obtained from SONREB testing (Liao et al., 2024; Tapeh & Naser, 2022; Thai, 2022; C. Wang et al., 2023), despite the fact that in many cases detailed mix design information is unavailable. The use of multiple parameters in a prediction model is understandable when trying to achieve the highest possible accuracy; however, it is worth considering that 1) such an approach makes complex models impractical for many real applications due to the lack of available data, and 2) engineers are accustomed to a certain degree of uncertainty when it comes to concrete CS (since even cylinder test results are characterized by considerable scatter) and in many cases a good approximation may be sufficient provided that the uncertainty can be quantified. Given the simplicity and accessibility of the SONREB method, it is therefore interesting to consider the limits of its predictive ability when paired with advanced tools such as ML.

Fig. 6.1 presents a timeline graph summarizing previous studies that have either partially or fully focused on ML algorithms to improve the results of a combination of UPV and RN tests (Alavi et al., 2024a; Alavi et al., 2024b; Almasaeid et al., 2022; Almasaeid et al., 2022; Arora et al., 2024; Asteris et al., 2021; Asteris & Mokos, 2020; Bonagura, 2012; Bonagura & Nobile, 2021; Demir, 2015; Du et al., 2021; Erdal et al., 2018; Kumar & Kumar, 2015; Na et al., 2009; Ngo et al., 2021; Nobile & Bonagura, 2016; Poorarbabi et al., 2020; Ramadevi et al., 2024; Sai & Singh, 2019; Shih et al., 2015; Shishegaran et al., 2021; Thapa et al., 2021; Wang et al., 2018; Alavi & Noel, 2025). It is important to note that the studies mentioned in this timeline have been conducted with various objectives. Na et al. conducted the first study that utilized a neuro-fuzzy system to improve result accuracy (Na et al., 2009). Bonagura, Nobile & Bonagura, Bonagura & Nobile, Wang et al., and Asteris & Mokos applied ANNs to estimate CS (Asteris & Mokos, 2020; Bonagura, 2012; Bonagura & Nobile, 2021; Nobile & Bonagura, 2016; Wang et al., 2018). Demir applied ANNs for hybrid fiber-added concrete to predict CS, while Almasaeid et al. applied ANNs to the CS of geopolymer concrete (Almasaeid et al., 2022; Demir, 2015). Additionally, Almasaeid et al. used ANNs for the assessment of high-temperature damaged concrete (Almasaeid et al., 2022). Kumar & Kumar used genetic programming, while Shih et al. and Sai & Singh employed Support Vector Machines (SVM) to enhance result accuracy (Kumar & Kumar, 2015; Sai & Singh, 2019; Shih et al., 2015). Poorarbabi et al. combined ANNs with response surface methodology for better predictions of CS (Poorarbabi et al., 2020). Du et al. integrated GA-BP neural networks for high-performance self-compacting concrete, while Thapa et al. developed models for concrete with recycled brick aggregates (Du et al., 2021; Thapa et al., 2021). Ngo et al., Shishegaran et al., Arora et al., Ramadevi et al., Erdal et al., and Asteris et al. discussed AI and soft computing advancements (Arora et al., 2024; Asteris et al., 2021; Erdal et al., 2018; Ngo et al., 2021; Ramadevi et al., 2024; Shishegaran et al., 2021). Park et al. used ML to extract new equations to convert the results of UPV and RN to CS (Park et al., 2024). Alavi et al. developed the first graphical user interface (GUI) app based on ML for on-site CS evaluations and then investigated its performance on case studies

(Alavi et al., 2024a; Alavi et al., 2024b). Additionally, Alavi and Noel applied ML and Deep Learning (DL) to propose a model that could work for both cylindrical and cubic strength standards (Alavi & Noel, 2025).

Regardless of the main objective of each of these studies, they all demonstrate the power of ML-based methods compared to traditional regression-based approaches. Fig. 6.1 clearly shows how the effort to find and use a new ML-based model that could predict concrete CS using the results of the SONREB method has significantly accelerated in the past four years. Despite these studies, a practical, universally applicable model has not been presented yet.

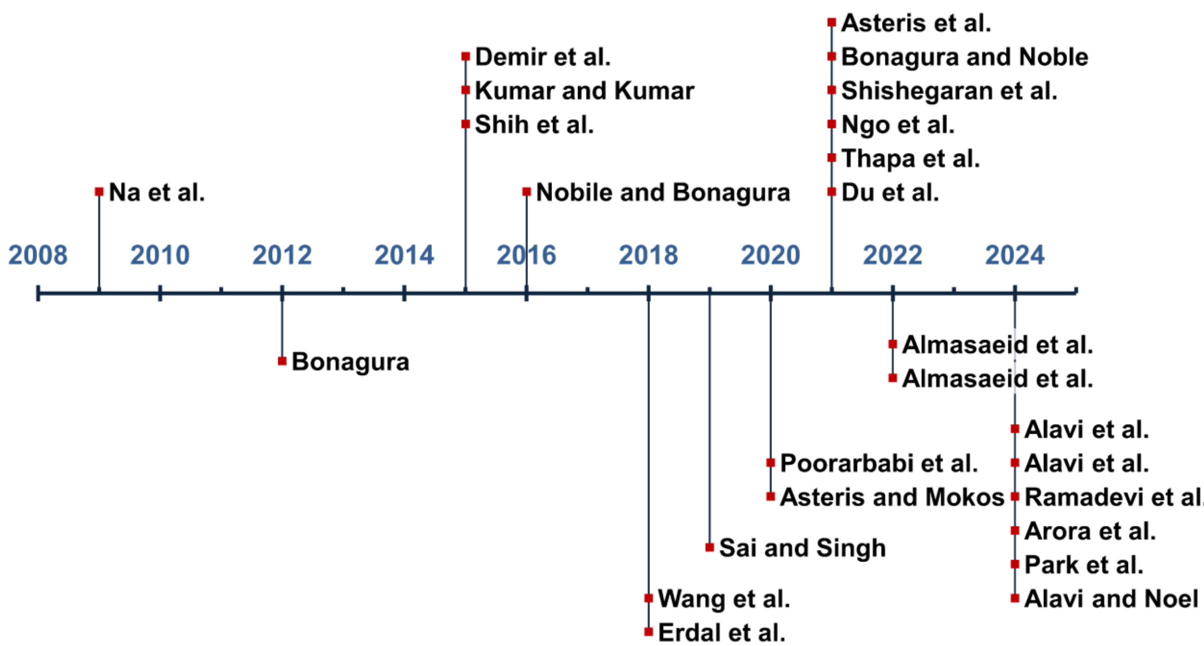

Figure 6.1: Timeline graph of previous studies on application of ML methods to the combined results of UPV and RN

The results of all the studies mentioned in Fig. 6.1, regardless of their main research topics, collectively provide a better understanding of how to develop and apply ML-based approaches for concrete CS predictions. However, before such an approach can be confidently applied in practice, it is essential that tools be developed to evaluate model performance and quantify the uncertainty that is inherent in any prediction method.

Therefore, the main objective of this study is to investigate, for the first time, the uncertainty in concrete strength prediction through a comprehensive analysis of new ML-based approaches in evaluating the CS of concrete without applying a calibration procedure (which requires core tests). This study is also the first to propose an ML-based model that considers the differences between cubic, cylindrical, and core specimens and their effects on the CS, and presents a discussion on remaining challenges. To this end, a roadmap for future model development is also presented with the aim of approaching towards a universal tool for non-destructive concrete CS prediction.

Accordingly, as shown in Fig. 6.2, two new ML-based models were developed based on large database which includes 620 collected data points. Both ML models were thoroughly examined, and the superior model was selected for further analysis and comparison to mathematical equations representing the conventional approach.

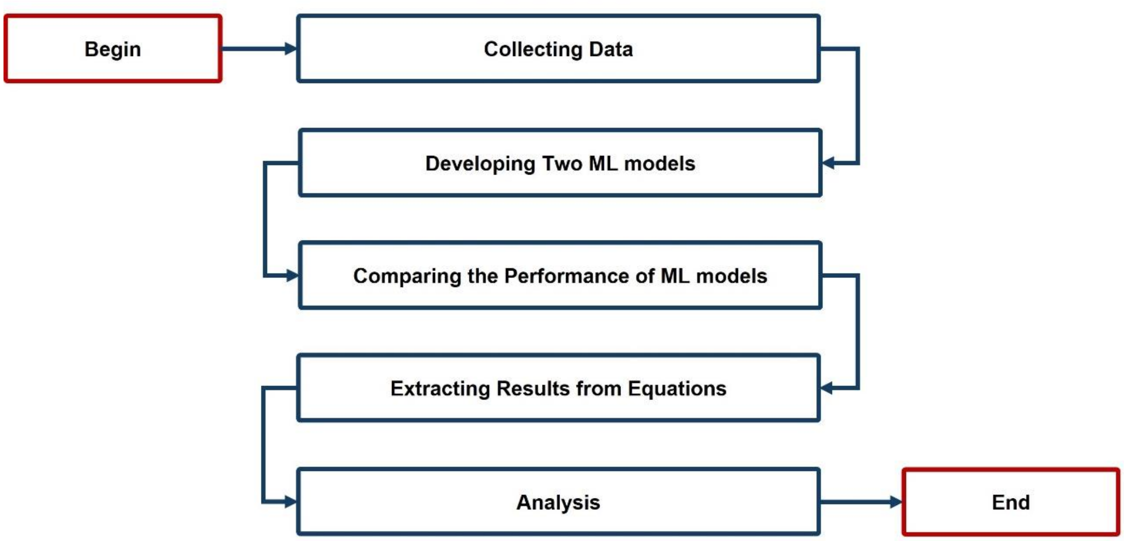

Figure 6.2: Flowchart of current study

6.2 SONREB

The SONREB method combines two NDT techniques, UPV and RN, used for CS evaluation in existing RC structures to provide more reliable estimates than either method on their own (Breysse, 2012; Uva et al., 2018). Fig. 6.3 shows how to perform the SONREB method to evaluate the CS of the concrete. The UPV device measures the transmission time (t) of an ultrasonic pulse that passes through the concrete between the transmitter and receiver. By dividing the distance between transmitter and receiver (l) by the transmission time (t) the pulse velocity (V) will be obtained. The RN test is performed at the same location using the rebound hammer (also known as the Schmidt hammer), a simple mechanical tool that releases a spring-loaded mass that strikes the target surface of the concrete with a defined force (based on the type and manufacturer). ASTM C805 requires ten readings at each location and the average is considered the final RN.

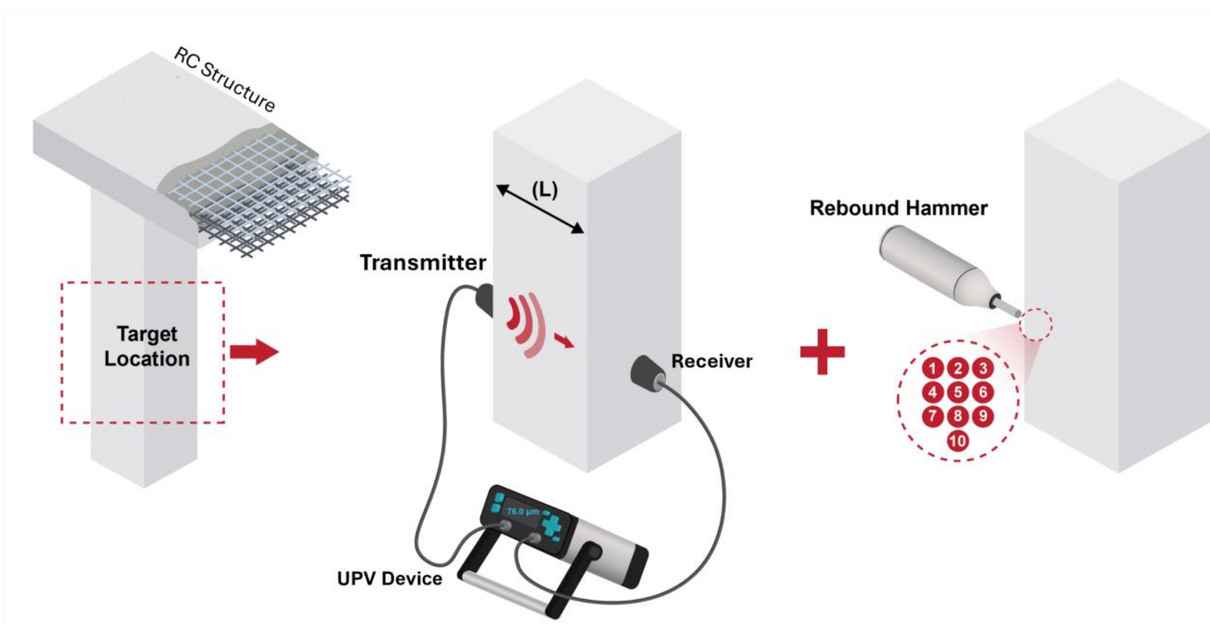

Figure 6.3: Schematic of SONREB method for CS evaluation on RC column

Based on the SONREB method, many models or equations have been proposed to predict the CS of concrete (Alavi et al., 2024b; Bolborea et al., 2022; Breysse, 2012). As shown in Fig. 6.4, these models can be divided into two general categories. The conventional approach is to use regression analysis to develop empirical equations, while more recently ML-based models have been proposed (Alavi et al., 2024b).

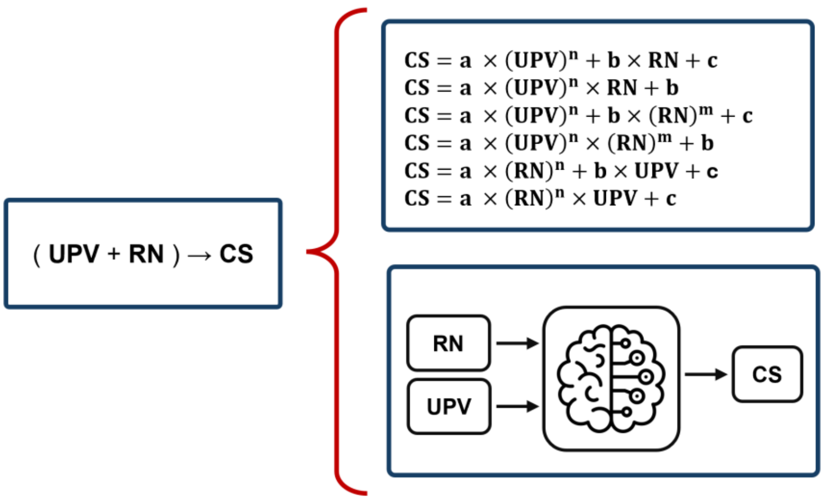

Figure 6.4: Conventional regression models vs ML-based models for SONREB method

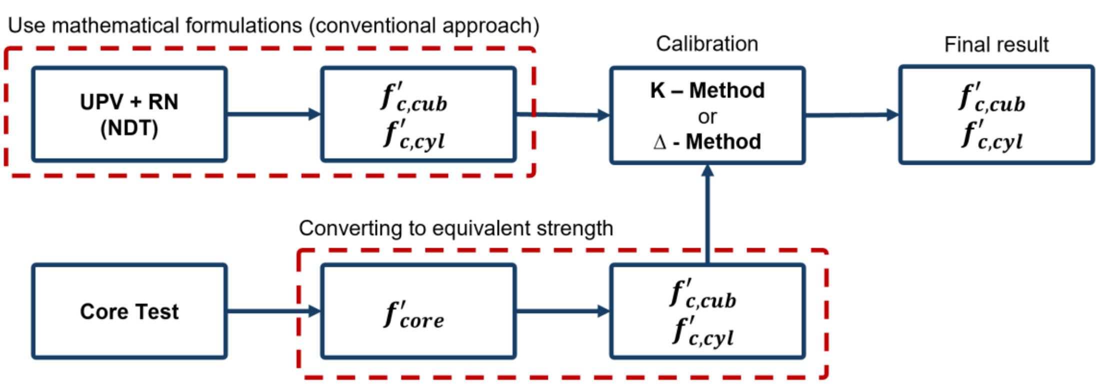

Figure 6.5: Procedure of applying conventional approach for CS evaluation

The main difference between conventional regression analysis and ML-based models lies in the calibration process. The former relies on closed-form mathematical relationships with a specified form that are "fitted" with experimental data. As shown in Fig. 6.5, current code provisions (Alavi et al., 2024a; Alavi et al., 2024b), allow engineers to use results from these mathematical relationships following a calibration process using core data from a particular structure. Two general methods are used for calibration, which are the shifting-factor method (D-Method) and the multiplying-factor method (K-method) to adjust model outputs with site-specific data (Angiulli et al., 2024; Kouddane et al., 2022; Maierhofer et al., 2010). The calibrated model can then be used to evaluate concrete CS based on NDT results at other points of the structure. While the number of cores required may be potentially reduced through the use of this NDT-based approach, the aforementioned challenges associated with core extraction remain. It should also be noted that due to safety concerns and other issues related to coring, the required core size has decreased in codes and guidelines in recent years (diameter less than 100 mm) (Alavi et al., 2024a). Therefore, it is necessary to convert the CS obtained from tests on cores into equivalent cylinder or cube CS with standard sizes, depending on the applicable standard (Khoury et al., 2014). Numerous mathematical relationships have been proposed to convert SONREB to CS in recent decades (Breysse, 2012; Cristofaro et al., 2020). In Table 6.1, eight well-known mathematical formulations are listed; Eq. 6.1 to Eq. 6.4 are based on the cylinder standard ($f'_{c,cyl}$) and Eq. 6.5 to Eq. 6.8 are based on the cubic standard ($f'_{c,cub}$).

Table 6.1: Selected formulations for converting SONREB to CS

ID	Formulation	Unit	Ref.
Eq. 6.1	$f'_{c,cyl} = -24.1 + 1.24 \times (RN) + 0.058 \times (UPV^4)$	MPa, Km/s	(Meynink & Samarin, 1979)
Eq. 6.2	$f'_{c,cyl} = -12 + 0.76 \times (RN) + 0.1 \times (UPV^4)$	MPa, Km/s	(Samarin & Dhir, 1984)
Eq. 6.3	$f'_{c,cyl} = -39.57 + 1.532 \times (RN) + 5.0614 \times (UPV)$	MPa, Km/s	(Ramyar & Kol, 1996)
Eq. 6.4	$f'_{c,cyl} = 5.9 + 2.712 \times 10^{-15} \times (RN) \times (UPV^4)$	MPa, m/s	(Beconcini & Formichi, 2003)
Eq. 6.5	$f'_{c,cub} = 0.0286 \times (RN^{1.246}) \times (UPV^{1.85})$	MPa, Km/s	(Gasparik, 1992)
Eq. 6.6	$f'_{c,cub} = 0.0158 \times (RN^{1.1171}) \times (UPV^{0.4254})$	MPa, m/s	(Kheder, 1999)
Eq. 6.7	$f'_{c,cub} = 2.6199 \times 10^{-8} \times (RN^{0.5341}) \times (UPV^{2.2878})$	MPa, m/s	(Faella et al., 2011)
Eq. 6.8	$f'_{c,cub} = 0.26511 \times (RN) + 0.01385 \times (UPV) - 34.51583$	MPa, m/s	(Faella et al., 2011)
RN: rebound number, UPV: pulse velocity, $f'_{c,cyl}$: cylindrical strength, and $f'_{c,cub}$: cubic strength.			

The main goal of new ML-based approaches is to harness the power of computer models to minimize the need for calibration as much as possible. This approach is based on the premise that more complex ML models may be developed to potentially address the challenges faced with the conventional mathematical approach. However, as previously noted, available studies in this area are still limited and the reliability of this approach requires further investigation.

6.3 New ML-Based Approach

It can be said that machine learning (ML) is one of the most important subfields of artificial intelligence (AI). This method is used when humans cannot establish a relationship between inputs and outputs using a mathematical formula, or the problem might be so complex that this process would be time-consuming and costly. By using ML algorithms and raw data, computers can learn, find the relationships, and then provide a model that can be used for new inputs (this method is generally known as supervised machine learning, Fig. 6.6).

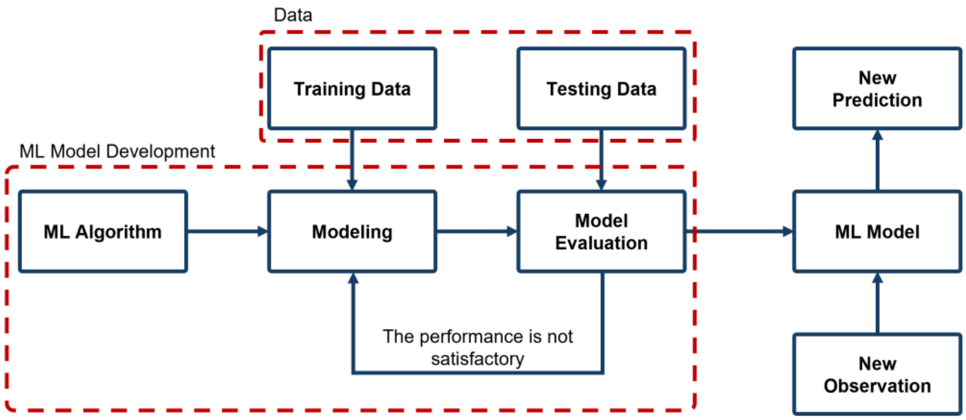

Figure 6.6: Flowchart for supervised machine learning model

As illustrated in Fig. 6.1, numerous studies in recent years have focused on applying ML to the SONREB method, targeting various objectives. These studies frequently report statistical measures such as mean absolute percentage error (MAPE), correlation (R), and other performance indicators, which provide a useful overview of model accuracy. However, these metrics alone do not fully address the practical concerns of engineers, who must evaluate the risks associated with deploying these models in real-world scenarios without prior calibration. Specifically, there is a need to understand the probability that actual strength in specific parts of a structure may significantly deviate from the predicted values, along with the potential range of errors. These considerations are crucial for assessing the reliability of ML models in this context.

Recognizing this gap, the present study not only develops a comprehensive ML model based on a large dataset but also quantifies its prediction intervals to quantify the likelihood of significant discrepancies between predicted and actual strengths, providing a more detailed assessment of the risks associated with using ML-based approaches.

6.3.1 Data

The first step in developing any ML model based on the supervised method is creating a database. In this specific case, developing a model that can predict concrete CS is challenging, as sufficient and reliable data are limited (Alavi & Noël, 2022). However, through extensive review of past studies, a total of 620 data points were collected. Table 6.2 presents the specifications of the collected data. Also, in Table 6.3, the ranges of the RN, UPV, and CS variables are provided. It is worth mentioning that experimental data obtained by the authors in previous studies are included in the database; those experimental tests were conducted on concrete obtained from multiple sources as briefly noted in the 'Detail' section of Table 6.2. More information on those tests are reported elsewhere (Alavi et al., 2024b; Alavi & Noel, 2025).

Table 6.2: Dataset information

Dataset	ID	Ref.	Number	Geometry of specimens	Detail
Training	No. 1	(Logothetis, 1978)	209	Cubic	-
	No. 2	(Poorarbabi et al., 2020)	56*	Cubic	-
	No. 3	(Rashid & Waqas, 2017)	26	Cubic	-
	No. 4	(Na et al., 2009)	20	Cubic	-
	No. 5	(Domingo & Hirose, 2009)	12	Cubic	-
	No. 6	(Cianfrone & Facaoaru, 1979)	39	Cubic	-
	No. 7	(Jain et al., 2013)	32	Cubic	-
	No. 8	(Alavi et al., 2024b)	8	Cylindrical	Company A ready-mix
	No. 9	(Ali Poorarbabi, 2020)	60*	Cylindrical	-
	No. 10	(Alavi & Noel, 2025)	24*	Cylindrical	Lab-prepared specimens
	No. 11	(Nobile & Bonagura, 2016)	16	Core	-
	No. 12	(Cristofaro et al., 2020)	69	Core	-
	No. 13	(Alavi et al., 2024b)	12*	Core	RC slab
Testing	No. 14	(Alavi & Noel, 2025)	12*	Cylindrical	Company B ready-mix
	No. 15	(Alavi et al., 2024b)	8*	Cylindrical	Lab-prepared specimens
	No. 16	(Alavi et al., 2024b)	8*	Cubic	Lab-prepared specimens
	No. 17	(Al-Neshawy & Ahmed, 2021)	9	Core	-

* Each data point was extracted from the average results of three similar specimens.

Table 6.3: Range of UPV, RN, and CS for each source of dataset

ID	Ref.	UPV (km/s)		RN		CS (MPa)	
		Min	Max	Min	Max	Min	Max
No. 1	(Logothetis, 1978)	3.850	5.220	20.00	42.00	12.16	52.17
No. 2	(Poorarbabi et al., 2020)	3.740	4.813	18.00	35.67	12.91	37.64
No. 3	(Rashid & Waqas, 2017)	4.200	4.950	31.00	39.00	20.99	51.27
No. 4	(Na et al., 2009)	4.130	4.800	20.70	55.50	20.40	56.90
No. 5	(Domingo & Hirose, 2009)	3.821	4.772	19.00	45.00	12.82	48.70
No. 6	(Cianfrone & Facaoaru, 1979)	4.820	5.390	25.00	46.00	27.96	76.32
No. 7	(Jain et al., 2013)	4.360	5.220	26.33	53.48	22.87	59.33
No. 8	(Alavi et al., 2024b)	4.682	4.884	29.30	31.70	35.28	43.58
No. 9	(Ali Poorarbabi, 2020)	3.443	4.573	10.33	29.00	11.08	32.27
No. 10	(Alavi & Noel, 2025)	4.815	5.400	30.23	42.90	36.87	64.42
No. 11	(Nobile & Bonagura, 2016)	2.450	4.095	31.90	47.33	10.00	56.60
No. 12	(Cristofaro et al., 2020)	2.766	4.135	24.10	52.80	11.12	44.49
No. 13	(Alavi et al., 2024b)	4.200	4.598	39.80	42.00	26.60	37.94
No. 14	(Alavi & Noel, 2024)	4.707	5.067	30.20	43.80	38.21	63.48
No. 15	(Alavi et al., 2024b)	4.629	5.239	24.07	42.40	26.10	70.78
No. 16	(Alavi et al., 2024b)	4.739	5.166	36.23	50.90	29.97	68.60
No. 17	(Al-Neshawy & Ahmed, 2021)	4.739	5.166	36.23	50.90	29.97	68.60

As shown in Table 6.2, seventeen different datasets were compiled to develop the ML model. The first thirteen datasets are considered as the training data, and the last four datasets (fourteen to seventeen) are used for testing. This approach for selecting training and testing data from distinct datasets is utilized according to the outcome of Alavi et al.'s study (Alavi et al., 2024b), which showed that using distinct data sources instead of randomly splitting the data into training and testing sets (i.e., 70% for training and 30% for testing), provides two advantages. First, it reduces the bias between the testing and training data, and second, it increases the number of training data points. Fig. 6.7 illustrates the distribution of data according to their geometry (core, cubic, and cylindrical).

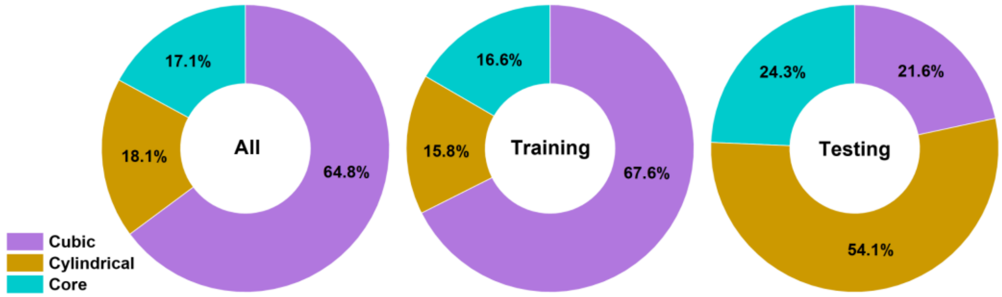

Figure 6.7: Distribution of dataset based on the geometric type

Fig. 6.8 shows the distribution of data according to three variables: UPV, RN, and CS. The upper graph plots UPV (Km/s) against CS (MPa), with blue points representing the training data and red points representing the testing data. The histograms show the frequency distribution of UPV and RN for both datasets, highlighting how the values are spread. The lower graph plots RN against CS (MPa), again with blue points for training data and red points for testing data. These visualizations are crucial for understanding the differences between the training and testing datasets, ensuring that the training data is adequate for training the model and that the testing data will be effective for evaluation. The training data shown in the two graphs are scattered over a wide range of 10 to 76 MPa, while the testing data ranges between 26 and 65 MPa. Additionally, the testing data is a good representation of the concrete typically used for structural purposes. Table 6.4 also provides more statistical information on the training and testing datasets.

Table 6.4: Statistical features of NDT and DT variables

Variable	Unit	Training			Testing		
		Min	Max	Mean	Min	Max	Mean
UPV	Km/s	2.450	5.400	4.369	2.500	5.239	4.539
RN	-	10.33	55.50	30.05	24.07	50.90	38.96
CS	MPa	10.00	76.32	32.41	26.10	70.78	49.67

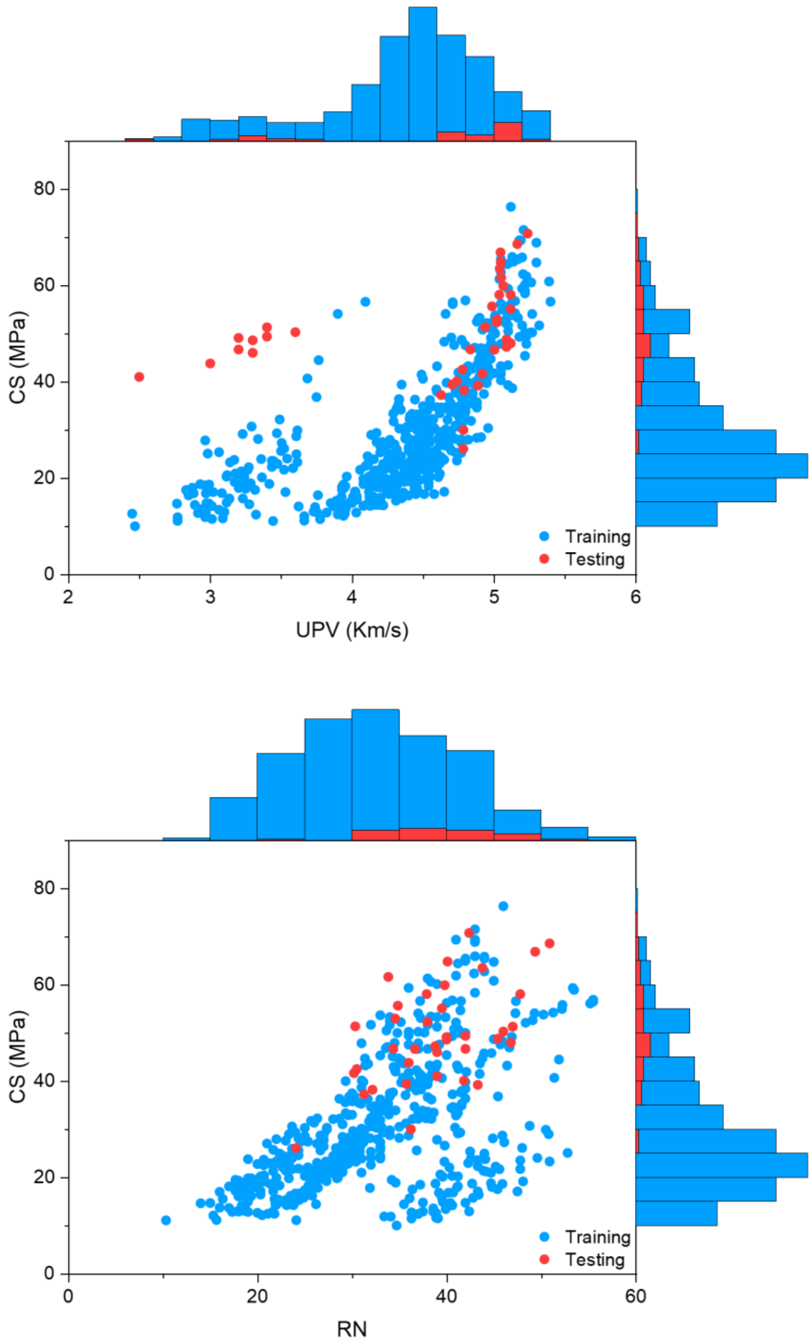

Figure 6.8: Data distribution; (Top) UPV vs. CS and (Bottom) RN vs. CS

6.3.2 ML Model Development

In the process of developing a ML-based model, one of the most important aspects is choosing the appropriate algorithm or method. In this study, the Adaptive Neuro-Fuzzy Inference System

(ANFIS) method was used following a comparison with other ML model types that is discussed elsewhere (Alavi & Noel, 2025; Shishegaran et al., 2021). It should be noted that ANFIS is a single-output method making it well-suited for this study's purpose.

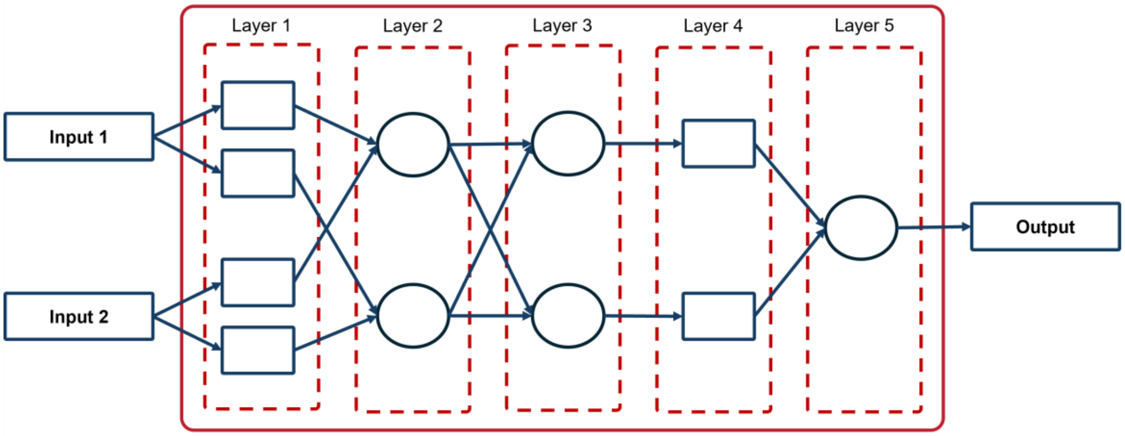

Figure 6.9: Example of ANFIS model and its layers

As shown in Fig. 6.9, models based on the ANFIS method have a structure that includes five different layers (Jang, 1993), which is technically based on the feedforward neural network (NN) that merges fuzzy logic (FL) with neural networks (Naderpour & Alavi, 2015, 2017). Layer 1, the fuzzification layer, converts crisp input values into fuzzy membership values using membership functions. In this study, triangular membership functions were utilized. Layer 2, the fuzzy rule base layer, processes these values through fuzzy if-then rules to determine rule firing strengths. Layer 3, the inference engine layer, applies fuzzy logic operations to compute output fuzzy sets. Layer 4, the defuzzification layer, transforms these fuzzy sets into crisp output values. Finally, Layer 5, the output layer, produces the final ANFIS output, which in this case is a CS value (MPa). Each layer's processing allows the model to learn and adapt, optimizing fuzzy rules and membership functions during training for accurate predictions of CS.

In this study, two ML models were developed using ANFIS and a dataset of 620 data points in MATLAB. Model No. 1 includes only two continuous numerical inputs, UPV and RN, to predict CS (Fig. 6.10). In Model No. 2, besides the two numerical inputs UPV and RN, two binary inputs were added to account for the differences between cylindrical, core, and cubic data (Fig. 6.10).

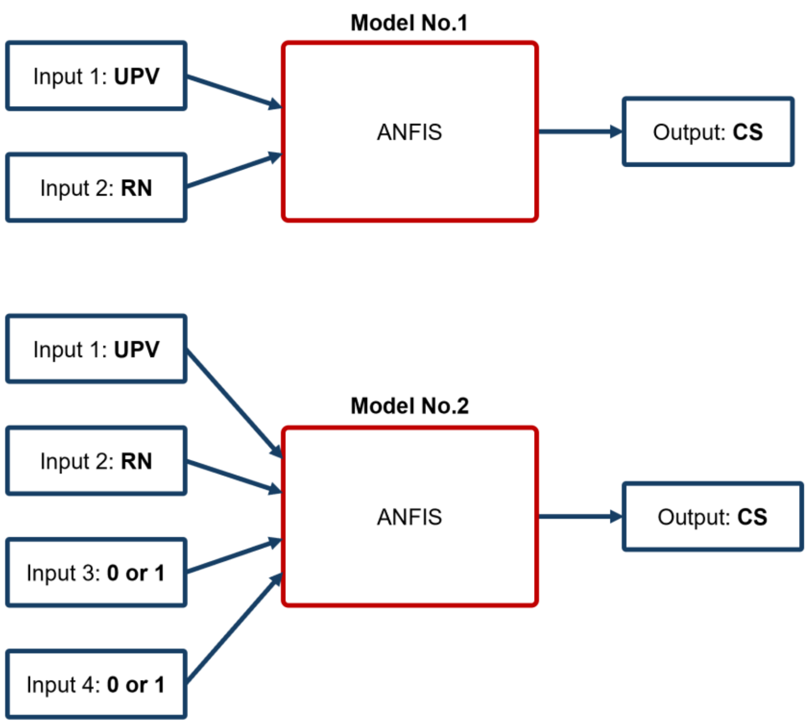

Figure 6.10: Inputs of model No.1 and model No.2

For the first and second inputs of both models (UPV and RN) and the output value (CS), which are continuous numerical variables, normalized values between 0.1 and 0.9 were used. Based on the minimum and maximum values of UPV, RN, and CS in Table 6.4, the actual data values were normalized to values between 0.1 and 0.9 according to the equations provided in Table 6.5. The normalization process is used to increase the speed and accuracy of the training process.

Table 6.5: Normalization equations for continuous numerical variables

Variable	Unit	Equation
UPV	(Km/s)	$UPV_{norm} = \left[(0.9 - 0.1) \times (\frac{UPV-2.45}{2.95})\right] + 0.1$ (Eq. 6.9)
RN	--	$RN_{norm} = \left[(0.9 - 0.1) \times (\frac{RN-10.33}{45.17})\right] + 0.1$ (Eq. 6.10)
CS	(MPa)	$CS_{norm} = \left[(0.9 - 0.1) \times (\frac{CS-10}{66.32})\right] + 0.1$ (Eq. 6.11)

In Model No. 2, as shown in Fig. 6.10, the third and fourth input variables are binary inputs used to define the geometry type of specimens for the model. This approach was first employed in a previous study by Alavi and Noel, in which a new method was introduced to define the difference between cylindrical and cubic geometry for the AI model (Alavi & Noel, 2025). In this study, an attempt was made for the first time to develop a more powerful and comprehensive model by utilizing data obtained from core sampling alongside data from cylindrical and cubic specimens prepared in a laboratory. As shown in Table 6.6, these differences were defined for the model: if both binary inputs are zero (0), the data corresponds to cubic specimens; if the third input is one (1) and the fourth input is zero (0), the data corresponds to core sampling; and if both inputs are one (1), the data corresponds to cylindrical specimens. Accordingly, as shown in Table 6.6, CS output for each of these three situations will be based on the different standard ($f'_{c,cub}$, f'_{core}, and $f'_{c,cyl}$).

Table 6.6: Definition of geometry type based on binary inputs for Model No.2

Situation	Input No. 3	Input No. 4	Definition	CS Output
1	0	0	cubic	$f'_{c,cub}$
2	1	0	core	f'_{core}
3	1	1	cylindrical	$f'_{c,cyl}$

6.3.3 ML Model Results

After running the ANFIS algorithm in MATLAB based on the model configuration shown in Fig. 6.9, the results were compared according to the type of dataset using three performance metrics: Mean Absolute Percentage Error (MAPE) (Eq. 6.12), Root Mean Squared Error (RMSE) (Eq. 6.13), and correlation coefficient (R) (Eq. 6.14). These metrics were selected to evaluate error, accuracy, and the correlation between the actual value of CS from experimental tests and the predicted value of CS obtained from the ML models. Indicators of good performance are a low MAPE value, low RMSE, and a number close to one (1) for R. In the following equations, CS_{Pred} , CS_{Exp} , $\overline{CS_{Pred}}$, and $\overline{CS_{Exp}}$ represent the predicted value, experimental value, mean predicted value, and mean experimental value of CS, respectively. The results are presented in Tables 6.7, 6.8, and 6.9, based on the type of geometry. Table 6.7 shows the results for cylindrical geometry, Table 6.8 for cubic geometry, and Table 6.9 for core geometry.

$$MAPE = \frac{1}{n}\sum_{i=1}^{n}\left(\frac{|CS_{Pred}-CS_{Exp}|}{CS_{Exp}}\right) \times 100 \quad \text{(Eq. 6.12)}$$

$$RMSE = \sqrt{\frac{1}{n}\sum_{i=1}^{n}(CS_{Pred}-CS_{Exp})^2} \quad \text{(Eq. 6.13)}$$

$$R = \frac{\sum_{i=1}^{n}(CS_{Exp}-\overline{CS_{Exp}})(CS_{Pred}-\overline{CS_{Pred}})}{\sqrt{\sum_{i=1}^{n}(CS_{Exp}-\overline{CS_{Exp}})^2(CS_{Pred}-\overline{CS_{Pred}})^2}} \quad \text{(Eq. 6.14)}$$

Table 6.7: Comparing the performance of Model No.1 and No.2 for cylindrical geometry

Parameter	Model No.1			Model No.2		
	Training	Testing	All	Training	Testing	All
MAPE (%)	12.33	15.24	12.85	7.01	9.63	7.48
RMSE (MPa)	4.59	9.18	5.69	2.47	5.90	3.35
R	0.982	0.878	0.977	0.985	0.897	0.979

Table 6.8: Comparing the performance of Model No.1 and No.2 for cubic geometry

Parameter	Model No.1			Model No.2		
	Training	Testing	All	Training	Testing	All
MAPE (%)	13.19	13.55	13.2	11.57	14.62	11.63
RMSE (MPa)	4.77	7.06	4.83	4.41	7.32	4.49
R	0.936	0.894	0.937	0.944	0.88	0.944

Table 6.9: Comparing the performance of Model No.1 and No.2 for core geometry

Parameter	Model No.1			Model No.2		
	Training	Testing	All	Training	Testing	All
MAPE (%)	17.44	56.12	20.72	15.06	58.31	18.73
RMSE (MPa)	5.52	26.51	9.36	4.74	27.50	9.21
R	0.797	0.881	0.576	0.852	0.902	0.602

According to Table 6.7, Model No. 2 significantly improves the performance of the ML model for cylindrical samples. Model No. 2 outperforms Model No. 1 across all metrics, with lower MAPE values (7.01% for training, 9.63% for testing, and 7.48% overall datasets) compared to Model No.1 (12.33%, 15.24%, and 12.85%, respectively), indicating higher prediction accuracy. It also shows better performance in RMSE (2.47 MPa for training, 5.9 MPa for testing, and 3.35 MPa overall) compared to Model No. 1 (4.59 MPa, 9.18 MPa, and 5.69 MPa, respectively), reflecting smaller deviations from actual values. Additionally, Model No. 2 achieves a slightly higher correlation coefficient (R) of 0.985 in training, 0.897 in testing, and 0.979 overall, compared to Model No.1's R values of 0.982, 0.878, and 0.977. Thus, the inclusion of binary inputs to account for geometry effects in Model No. 2 results in improved accuracy, reduced error, and a stronger correlation across both training and testing datasets.

According to Table 6.8, Model No. 2 also shows superior performance for cubic specimens when considering the training data, with a lower MAPE (11.57% vs. 13.19%) and RMSE (4.41

MPa vs. 4.77 MPa) compared to Model No. 6.1. This indicates that Model No. 2, incorporating binary inputs for geometry effects, is more accurate and precise in training scenarios. Although its testing MAPE of 14.62% and RMSE of 7.32 MPa are slightly higher than Model No. 1's MAPE of 13.55% and RMSE of 7.06 MPa, the overall correlation coefficient (0.944) surpasses Model No. 1's (0.937). Despite a slight decrease in testing dataset's performance, Model No. 2's inclusion of geometry effects provides notable advantages in capturing the complexities of the training data and gives better overall performance.

Both models performed comparatively worse for the core dataset. As summarized in Table 6.9, Model No. 2 shows a slight improvement in training accuracy (15.06% vs. 17.44%) but a modest decrease in testing accuracy (58.31% vs. 56.12%) in terms of MAPE value. In terms of RMSE, Model No. 2 performs better in training (4.74 MPa vs. 5.52 MPa) but has a higher error in testing (27.5 MPa vs. 26.51 MPa). The correlation coefficient (R) indicates that Model No. 2 has a higher correlation in both training (0.852 vs. 0.797) and testing (0.902 vs. 0.881), with a marginal improvement in the overall R value (0.602 vs. 0.576). However, there is a significant decrease in the overall R value for Model No. 2 with core geometry (0.602) compared to cylindrical (0.979) and cubic (0.944) geometries. This clearly shows a significant incompatibility between the training and testing data for core samples.

To further explore this discrepancy, Fig. 6.11 presents the distribution of each dataset according to the geometry of the specimens in three-dimensional axes (UPV vs. RN vs. CS). By comparing Fig. 6.11(B), Fig. 6.11(C), and Fig. 6.11(D), it can be seen that there is a discernable trend for cylindrical and cubic datasets (Fig. 6.11(B) and Fig. 6.11(C)) where an increase in UPV or RN generally corresponds to an increase in CS. However, it is evident in Fig. 6.11(D) that there is dispersion and irregularity in the dataset from core specimens. Notably, the data from source

No. 17, which was the only source with core samples included in the test dataset, lies well outside the data cloud containing all other data points which explains the low accuracy of both models for this subset.

One important consideration related to the core data is that while the UPV and RN tests were conducted on the structure before coring, the CS value was obtained from the core after extraction. In contrast, for cylindrical and cubic specimens, all UPV, RN, and CS values were directly obtained from tests performed on the small-scale samples. Furthermore, a detailed investigation of the core data sources mentioned in Table 6.2 suggests that the size of the core was not constant among the various studies. Other factors including potential deterioration, presence of reinforcement, imprecise field measurements, moisture gradients, etc., can also affect in-situ test results. This highlights the challenge of developing a universal model for field applications and is further discussed in Section 6.6.

It can be concluded that the inclusion of additional binary inputs in Model No. 2 generally led to improved performance, although it is acknowledged that the incompatibility between the core's training data and testing data negatively affected its overall performance.

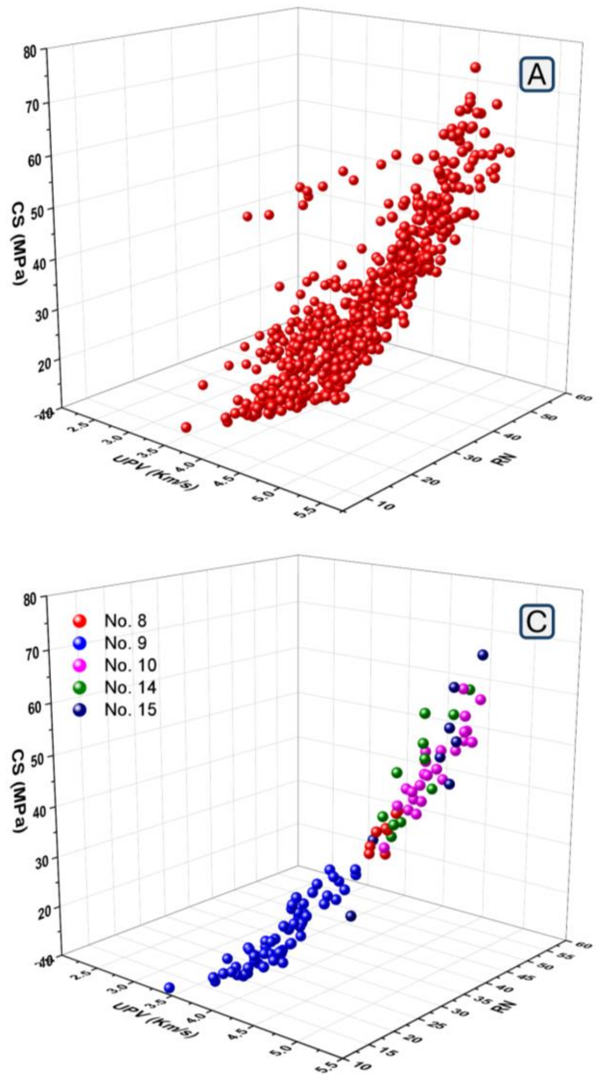

Figure 6.11: Data distribution for (A): all 620 data points, (B) all 402 cubic data points, (C) all 112 cylindrical data points, and (D) all 106 core data points

6.4 ML Model vs. Conventional Approach; Comprehensive Analysis

Model No. 2 is the first ML-based model capable of considering the geometry of three specimen types: cylindrical, cubic, and cores (issues with core data are further discussed in Section 6.6). However, as indicated in Table 6.1, the proposed mathematical equations are limited to either cylindrical or cubic CS ($f'_{c,cyl}$ and $f'_{c,cub}$). Therefore, this section assesses model performance using two datasets: 402 cubic data points and 112 cylindrical data points. According to Table

6.1, the performance of Eq. 6.1 to Eq. 6.4 are compared to Model No. 2 using the 112 cylindrical data points, while Eq. 6.5 to Eq. 6.8 are compared to Model No. 2 using the 402 cubic data points.

Tables 6.10 and 6.11 summarize the performance of the equations and Model No. 2 on three metrics: MAPE, RMSE, and R. Table 6.10 presents data based on cylindrical measurements, comparing Eq. 6.1 to Eq. 6.4 with Model No. 2. Conversely, Table 6.11 presents data based on cubic measurements, comparing Eq. 6.5 to Eq. 6.8 with Model No. 2.

Table 6.10: Comparing the performance of Eq. 6.1 to Eq. 6.4 and Model No.2 based on cylindrical data

Parameter	Eq. 6.1	Eq. 6.2	Eq. 6.3	Eq. 6.4	Model No.2
MAPE (%)	16.13	62.00	33.56	23.25	7.48
RMSE (MPa)	5.86	21.36	8.69	12.23	3.35
R	0.977	0.975	0.977	0.976	0.979

Table 6.11: Comparing the performance of Eq. 6.5 to Eq. 6.8 and Model No.2 based on cubic data

Parameter	Eq. 6.5	Eq. 6.6	Eq. 6.7	Eq. 6.8	Model No.2
MAPE (%)	22.88	15.85	35.84	35.36	11.63
RMSE (MPa)	8.23	8.53	10.05	9.91	4.49
R	0.924	0.894	0.927	0.903	0.944

According to Table 6.10, Model No. 2 outperforms all equations for cylindrical specimens with a notably lower MAPE of 7.48%. Eq. 6.1 has the next best performance with a MAPE of 16.13%, while Eq. 6.2 has the highest error rate at 62.0%. Model No. 2 also shows superior performance with the lowest RMSE of 3.35 MPa. Eq. 6.1 follows with an RMSE of 5.86 MPa, while Eq. 6.2 has the highest RMSE at 21.36 MPa. Regarding the correlation coefficient (R), which reflects the relationship between predicted and actual values, Model No. 2 has the highest R value at 0.979, slightly better than the equations, indicating a marginally stronger correlation. Overall, Model No. 2 demonstrates the most accurate and consistent performance across all metrics compared to the equations without performing calibration. Similarly, Model No. 2 performed better than the proposed equations for cubic data. It has the lowest MAPE of 11.63%, indicating the closest agreement between predicted and actual values. This is further confirmed by an RMSE of 4.49 MPa and an R-value of 0.944.

Fig. 6.12 and Fig. 6.13 present X-Y scatter plots comparing predicted (PRED) and experimental (EXP) CS values for each equation against the results of Model No. 2. Fig. 6.12 displays the data for the cylindrical dataset (Eq. 6.1 to Eq. 6.4), while Fig. 6.13 shows the data for the cubic dataset. Each scatter plot includes a diagonal line representing perfect agreement between predicted and experimental values, as well as lines indicating ±20% deviation from perfect agreement. Overall, a comparison of Fig. 6.12 and Fig. 6.13 reveals that Model No. 2 consistently outperforms all equations in terms of predictive capability.

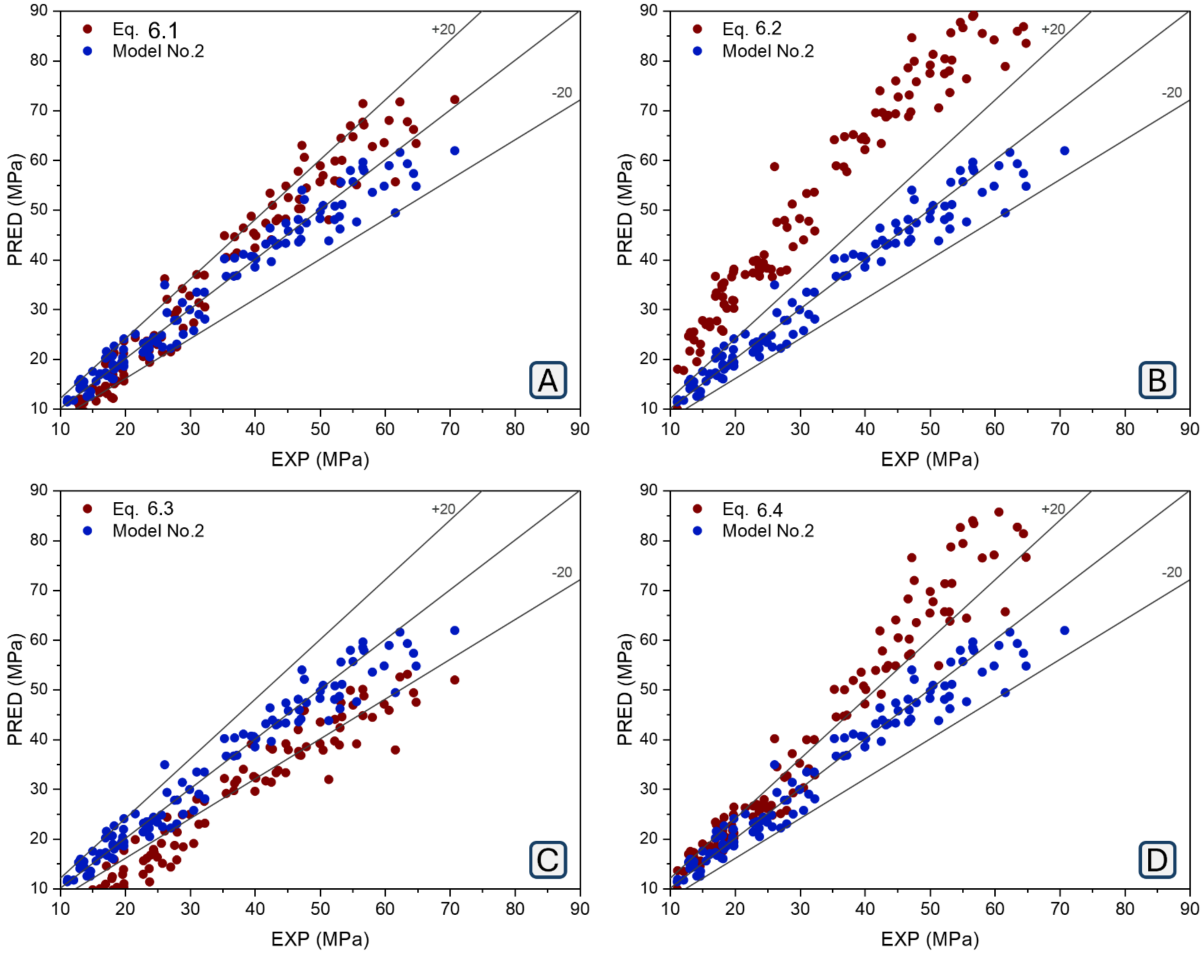

Figure 6.12: Comparison of proposed ML model results vs. (A) Eq. 6.1, (B) Eq. 6.2, (C) Eq. 6.3, and (D) Eq. 6.4

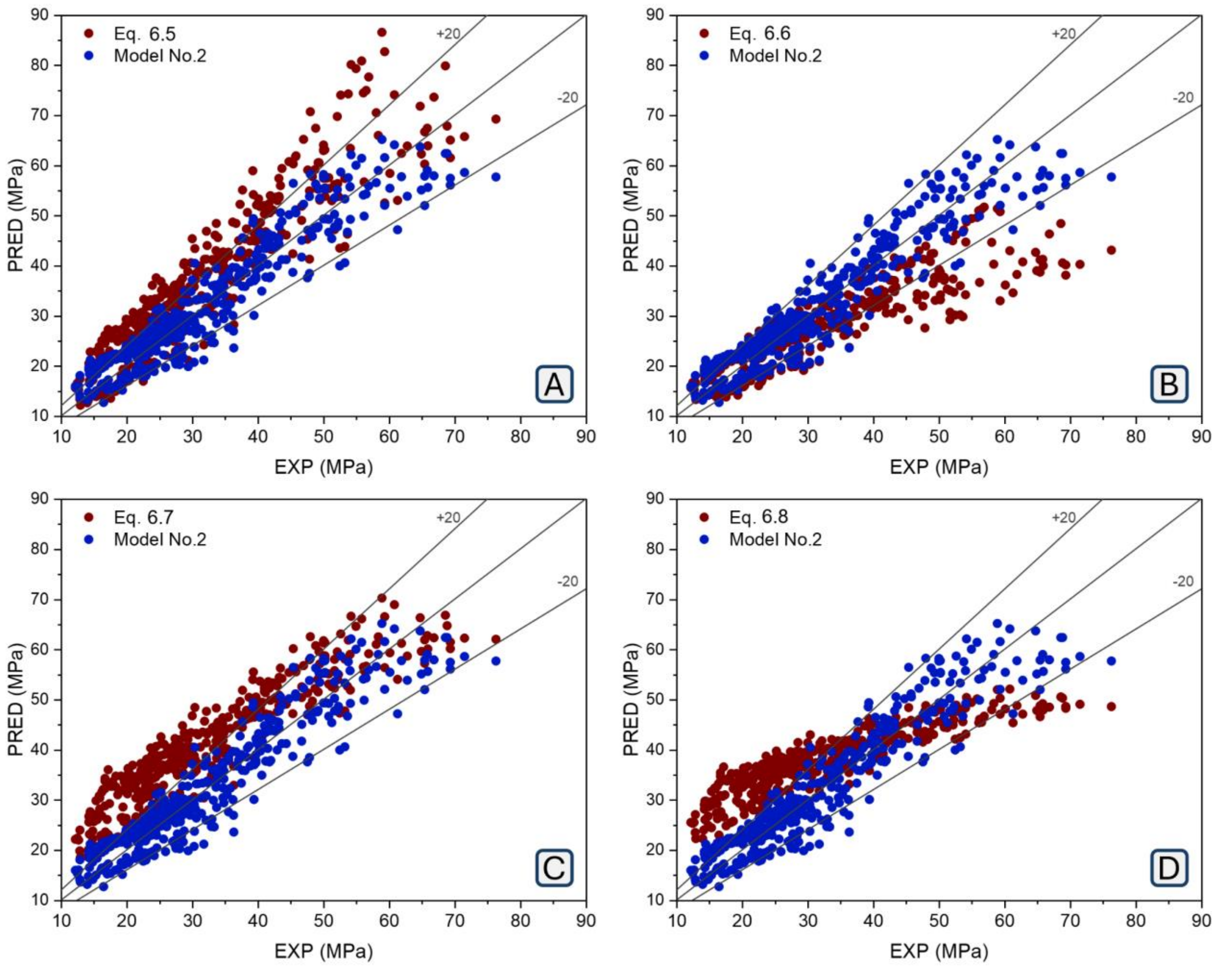

Figure 6.13: Comparison of proposed ML model results vs. (A) Eq. 6.5, (B) Eq. 6.6, (C) Eq. 6.7, and (D) Eq. 6.8

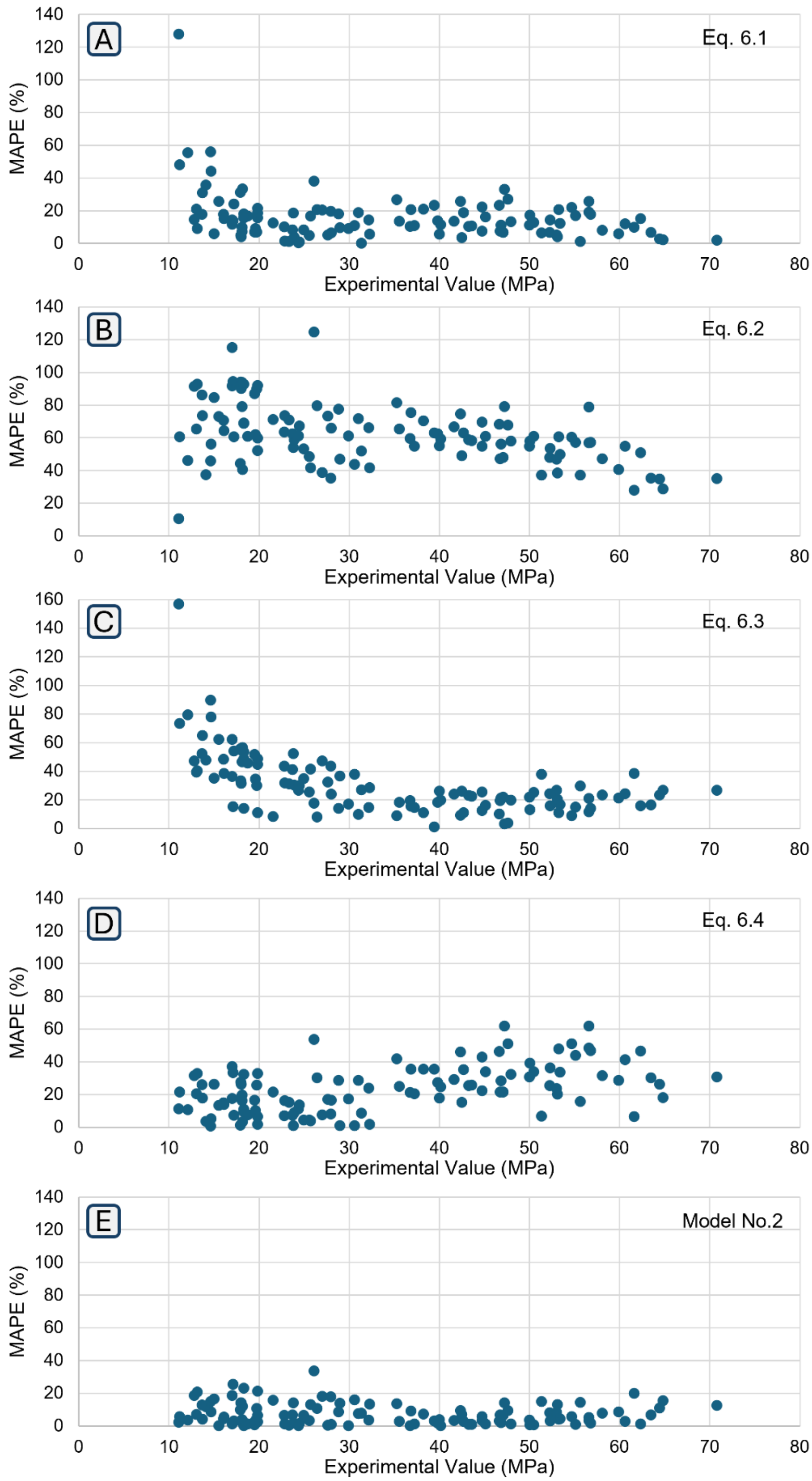

Figure 6.14: Prediction Error vs. experimental value for (A) Eq. 6.1, (B) Eq. 6.2, (C) Eq. 6.3, (D) Eq. 6.4, and (E) Model No.2

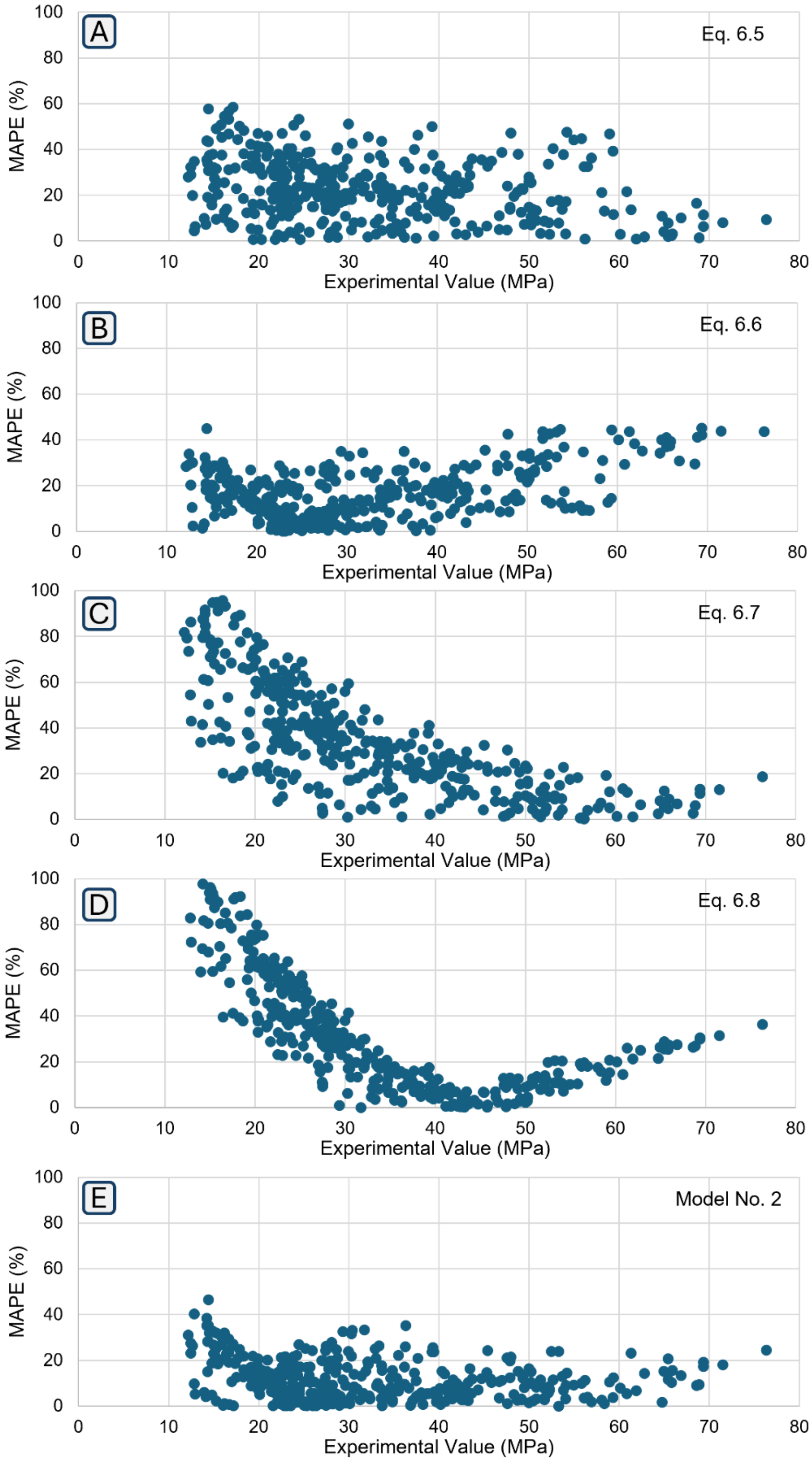

Figure 6.15: Prediction Error vs. experimental value for (A) Eq. 6.5, (B) Eq. 6.6, (C) Eq. 6.7, (D) Eq. 6.8, and (E) Model No.2

Fig. 6.14 and Fig. 6.15 present the distribution of Mean Absolute Percentage Error (MAPE) for various predictive models across experimental concrete strength values. According to Fig. 6.14 which is based on the cylindrical dataset, Eq. 6.1 shows moderate performance, with MAPE values generally below 40% for strengths above 20 MPa, though there are significant outliers for lower values, indicating reduced reliability in this range. Eq. 6.2 exhibits higher errors overall, with a clear trend of decreasing MAPE as experimental values increase; however, errors are widely scattered, particularly for strengths below 20 MPa, suggesting poor generalization for lower ranges. Eq. 6.3 demonstrates slightly improved stability, with errors more tightly distributed between 20 and 50 MPa, though MAPE increases for values exceeding 50 MPa, and outliers remain in the lower strength region. Eq. 6.4 offers better consistency compared to the previous equations, with MAPE largely staying below 40% across the range and reduced error scatter for lower strengths, suggesting improved reliability at both ends of the spectrum. Finally, Model No. 2 significantly outperforms all other models, maintaining MAPE below 20% for most experimental values above 20 MPa and exhibiting minimal scatter, indicating superior predictive accuracy and robustness across the full range. Overall, Model No. 2 is the most accurate and reliable, while Eq. 6.4 shows the best performance among the regression equations. According to Fig. 6.15 which is based on the cubic dataset, Eq. 6.5 shows high error scatter across all ranges, with MAPE frequently exceeding 40% for strengths below 30 MPa and gradually stabilizing for higher values, indicating limited accuracy for lower strengths. Eq. 6.6 performs slightly better, with reduced error scatter in the mid-range (20–50 MPa), though significant errors remain for low (<20 MPa) and high (>60 MPa) strength values. Eq. 6.7 shows a distinct trend of decreasing MAPE as strength increases, with considerable errors at lower values but a marked improvement for strengths above 30 MPa. Eq. 6.8 further improves accuracy, with MAPE generally below 40% for strengths between 20 and 50 MPa, though there is a noticeable rise in error for strengths below 20 MPa and above 60 MPa. Model No. 2 again outperforms all equations, maintaining consistently low errors across the full experimental range, with most MAPE values below 20% and minimal scatter, reflecting excellent predictive capability and generalization. Overall, Model No. 2 is the most reliable and accurate, while Eq. 6.8 shows the best performance among the equations, especially in the mid-strength range.

Fig. 6.16 and Fig. 6.17 depict the actual distribution histogram and also normal distribution curve of $CS_{experimental}/CS_{prediction}$ values across different equations and Model No. 2 based on the cylindrical dataset (Fig. 6.16) and cubic dataset (Fig. 6.17). Also, all the normal distribution curves are merged in Fig. 6.18 and Fig. 6.19. The normal distribution curve is a symmetric bell-shaped curve illustrating how data is spread around the average, using two statistical parameters of mean and standard deviation (SD). According to the Fig. 6.18 which is for cylindrical data, the vertical dashed-line at X-axes indicates the ideal ratio (value of one) where predictions perfectly match the experimental values. Also, the table in the upper right corner summarizes the mean and standard deviation (SD) of the ratios for each of four equations and ML model. Model No. 2 has the closest mean to 1 (1.0082) with a low SD (0.0984), providing the most accurate and consistent predictions. Eq. 6.1 and Eq. 6.4 also have means close to 1 but with higher SDs, while Eq. 6.2 has the lowest mean (0.6270) and Eq. 6.3 the highest mean (1.6228), indicating significant under- and over-prediction, respectively. The wider curves for Eq. 6.1, Eq. 6.3, and Eq. 6.4 compared to Model No. 2 indicate higher variability in their predictions (as also shown in Fig. 6.16). This is reflected in their SDs, where Eq. 6.3 and Eq. 6.4 have larger SDs (0.9770 and 1.1067, respectively), leading to wider curves that show a broader spread in the ratio of experimental to predicted strength. Although Eq. 6.2

has a relatively low SD (0.0806), its predictions are less accurate due to the lower mean value (0.6270). In contrast, Model No. 2 predictions are more consistent and closer to the experimental values.

According to Fig. 6.19, Model No. 2 also shows the best performance for cubic samples with a mean of 0.9999 and a low SD of 0.1483, indicating the closest agreement with experimental values and low variability. Eq. 6.5 also performs reasonably well, with a mean of 0.8637 and a low SD of 0.1497 in comparison to Eq. 6.5, Eq. 6.6, and Eq. 6.7. Model No. 2 gives the most accurate and consistent predictions, while Eq. 6.6 performs the worst in terms of accuracy and consistency.

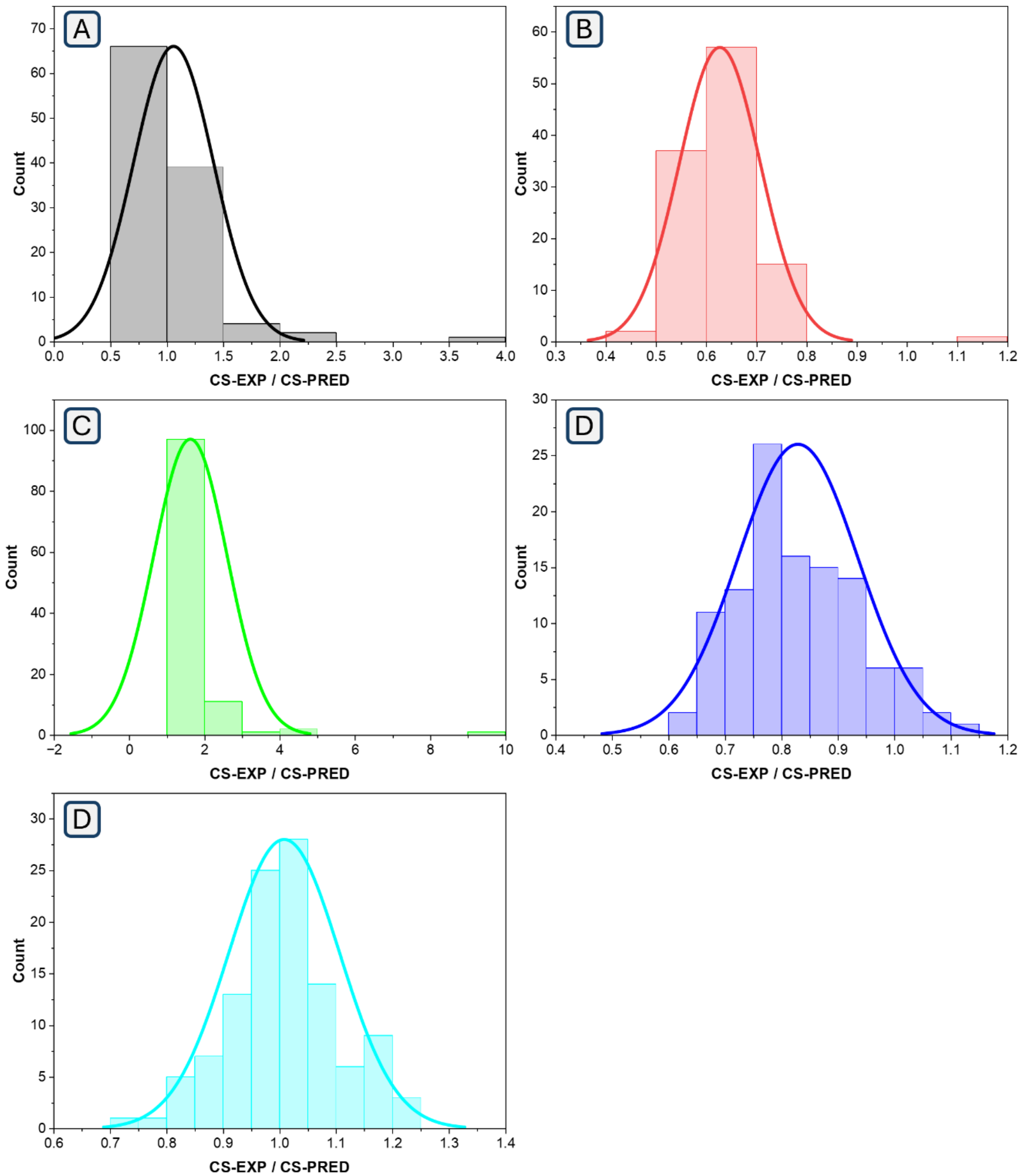

Figure 6.16: Comparison of the actual histogram of $\boldsymbol{CS_{experimental}/CS_{prediction}}$ values with the normal distribution curve for (A) Eq. 6.1, (B) Eq. 6.2, (C) Eq. 6.3, (D) Eq. 6.4, and (E) Model No. 2 for cylindrical data

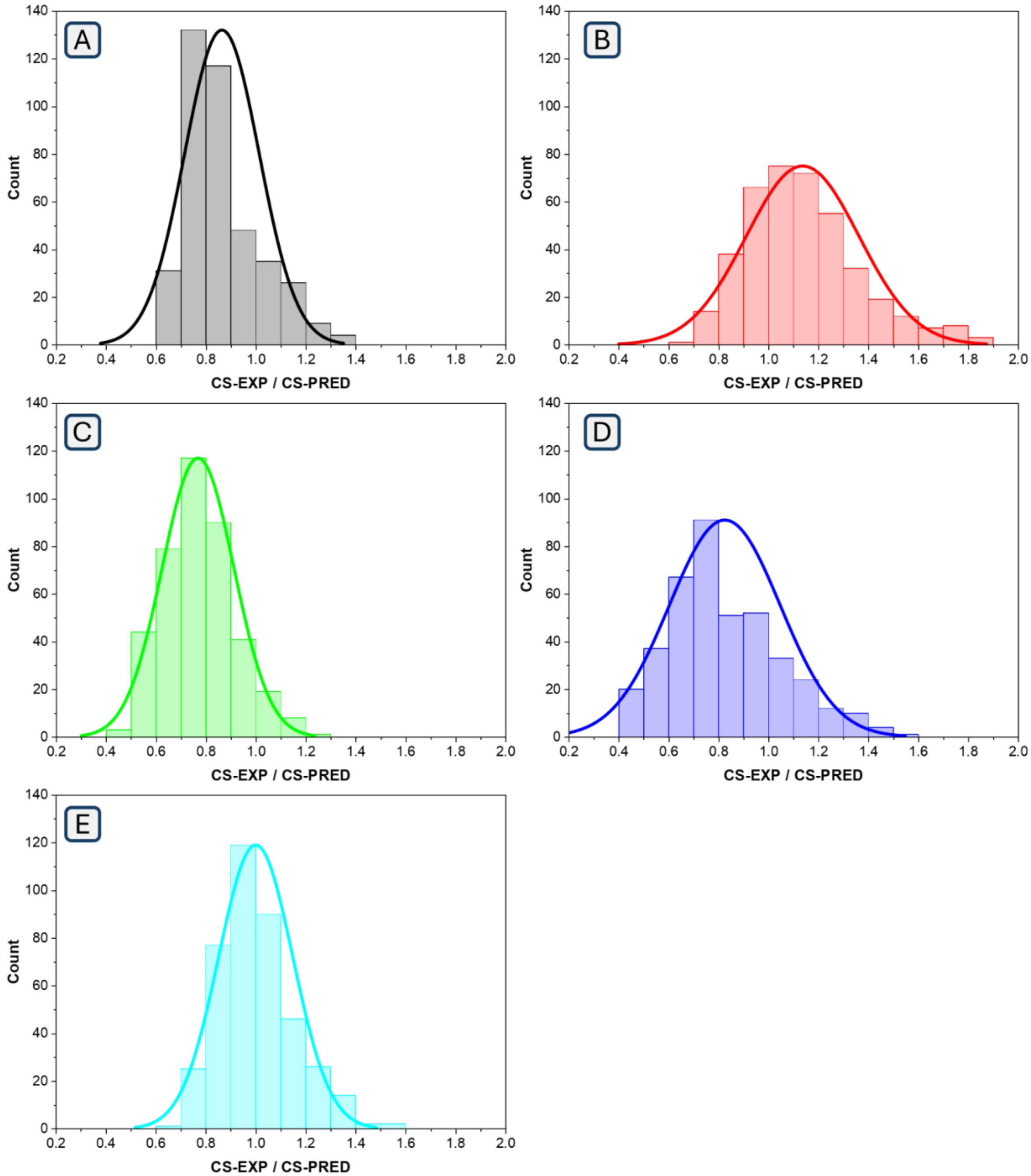

Figure 6.17: Comparison of the actual histogram of $CS_{experimental}/CS_{prediction}$ values with the normal distribution curve for (A) Eq. 6.5, (B) Eq. 6.6, (C) Eq. 6.7, (D) Eq. 6.8, and (E) Model No. 2 for cubic data

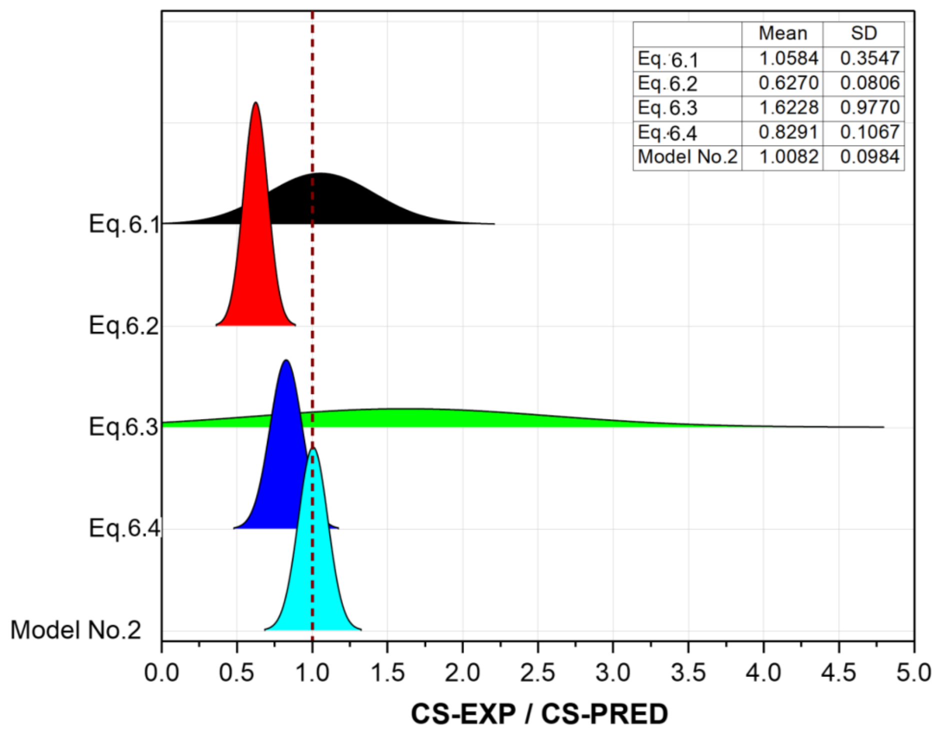

Figure 6.18: Normal distribution of $\boldsymbol{CS_{experimental}/CS_{prediction}}$ for cylindrical data

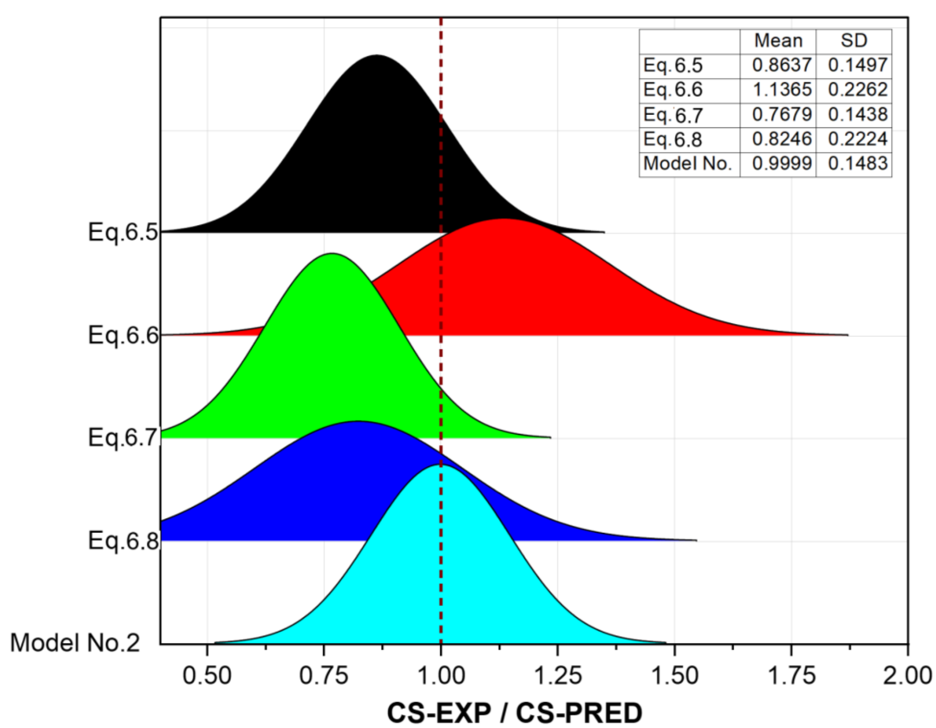

Figure 6.19: Normal distribution of $\boldsymbol{CS_{experimental}/CS_{prediction}}$ for cubic data

Moreover, Tables 6.12 and 6.13 provide detailed information about the error distribution of each model across various ranges, while Fig. 6.20 and Fig. 6.21 depict the error distribution. Table 6.12 and Fig. 6.20 are based on the cylindrical dataset, while Table 6.13 and Fig. 6.21 are based on the cubic dataset.

According to Table 6.12 and Fig. 6.20, it is clear that Model No. 2 exhibits superior performance, with a significantly higher count of errors within the 10% range and minimal counts in other categories. Additionally, the minimum error of 0.1% and maximum error of 33.6% in CS prediction for cylindrical data confirm this. In contrast, Eq. 6.2 shows a concerningly high number of errors exceeding 40%.

For the cubic dataset, as shown in Table 6.13 and Fig. 6.21, Model No. 2 exhibits the best performance in the below 10 percent error (<10%) range with 206 predictions but also has a moderate maximum error of 46.6%. Overall, Model No. 2 demonstrates the most robust performance for lower error ranges, while Eq. 6.6 shows the lowest maximum error among all models.

Table 6.12: Error distribution (count), min and max error based on cylindrical data

Model	Absolute Error Range					Min Error (%)	Max Error (%)
	<10 %	(10-20] %	(20-30] %	(30-40] %	40% <		
Eq. 6.1	40	44	17	6	5	0.19	128.28
Eq. 6.2	0	1	2	9	100	10.53	124.78
Eq. 6.3	9	29	27	17	30	1.03	156.97
Eq. 6.4	25	23	28	21	15	0.74	61.98
Model No. 2	78	29	4	1	0	0.10	33.58

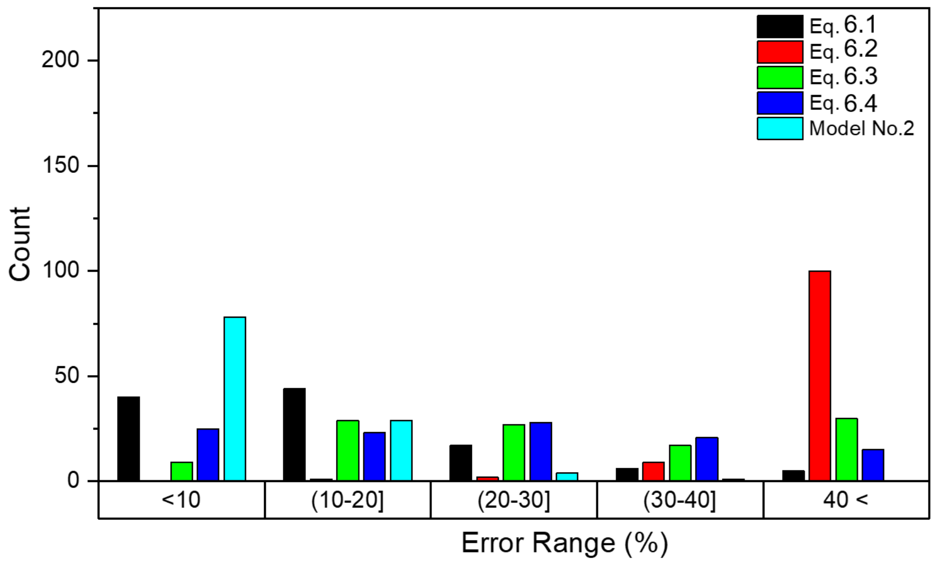

Figure 6.20: Error distribution based on cylindrical data

Table 6.13: Error distribution (count), min and max error based on cubic data

Model	Absolute Error Range					Min Error (%)	Max Error (%)
	<10 %	(10-20] %	(20-30] %	(30-40] %	40% <		
Eq. 6.5	79	100	98	81	44	0.68	58.72
Eq. 6.6	145	129	84	28	16	0.08	45.09
Eq. 6.7	58	57	69	71	147	0.23	109.76
Eq. 6.8	87	68	49	58	140	0.02	112.94
Model No.2	206	122	58	14	2	0.06	46.57

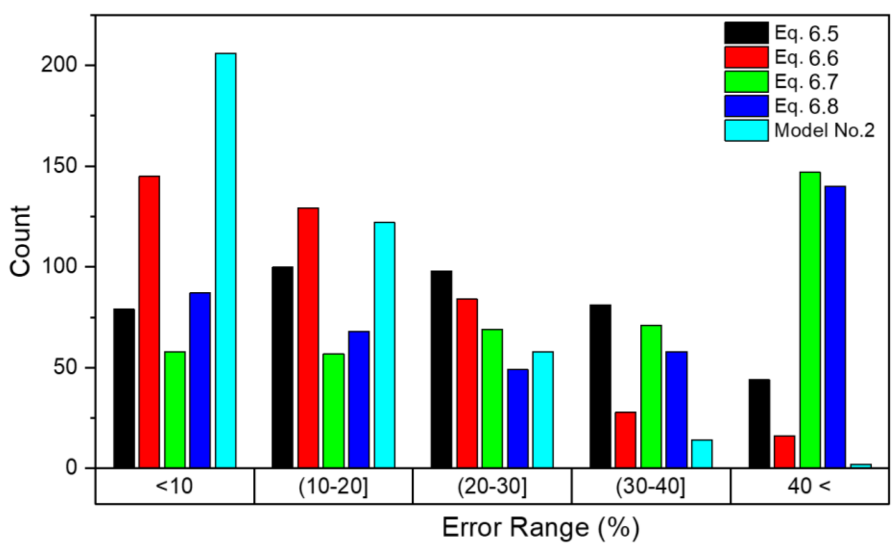

Figure 6.21: Error distribution based on cubic data

Tables 6.14 and 6.15 show the average MAPE for different models across various ranges of CS measured in MPa. Table 6.14, which is based on the cylindrical dataset, reveals that Model No.2 exhibits the lowest MAPE across most CS ranges, making it the most accurate and reliable model overall. Specifically, it achieves the best performance in the ranges (0-20 MPa), (20-35 MPa), (35-50 MPa), and (50-65 MPa), indicating its robustness across a wide spectrum of CS values. In the highest CS range (65< MPa), Eq. 6.1 outperforms the others, achieving the lowest MAPE, while Model No.2's performance, though still reasonable, is not the best in this range.

According to Table 6.15, which is based on the cubic dataset, for the lowest CS range (0-20 MPa), Model No.2 shows the best performance with a MAPE of 19.93%, significantly lower than the other equations. As the CS increases to the 20-35 MPa range, Model No.2 maintains its leading position with a MAPE of 10.10%, matching the lowest error of the other models. In the 35-50 MPa range, Model No.2 again performs best with a MAPE of 9.48%, highlighting its consistent accuracy across different CS levels. For the 50-65 MPa range, Model No.2 continues to show superior performance with an average MAPE of 8.96%, while the other equations vary more in their accuracy. However, for CS greater than 65 MPa, Model No.2's MAPE rises to 15.36%, which is still relatively low but not the best in this range, where Eq. 6.5 shows the lowest error of 7.11%.

Table 6.14: The average value of MAPE based on the range of CS for cylindrical data

CS Range (MPa)	Average MAPE (%)				
	Eq. 6.1	Eq. 6.2	Eq. 6.3	Eq. 6.4	Model No. 2
(0-20]	23.70	71.38	50.95	16.99	8.96
(20-35]	11.01	61.76	29.08	13.81	8.61
(35-50]	14.72	62.61	16.32	31.72	4.66
(50-65]	11.60	49.04	21.00	33.12	6.95
65<	1.95	34.99	26.67	30.70	12.57

Table 6.15: The average value of MAPE based on the range of CS for cubic data

CS Range (MPa)	Average MAPE (%)				
	Eq. 6.5	Eq. 6.6	Eq. 6.7	Eq. 6.8	Model No. 2
(0-20]	29.53	18.74	67.41	83.11	19.93
(20-35]	23.33	10.10	39.17	36.41	10.10
(35-50]	20.66	17.95	19.64	6.83	9.48
(50-65]	18.89	27.40	10.00	13.41	8.96
65<	7.11	39.15	9.39	28.71	15.36

Fig 6.22 provides the Prediction Intervals (PIs) defined in Eq. 6.15 for a 95% probability for various models predicting concrete strength based on the dataset type. The PI indicates the range within which future observations are expected to fall and is computed as follows:

$Prediction\ Interval = [\mu - z\sigma, \mu + z\sigma]$ (Eq. 6.15)

where μ represents the mean of the experimental-to-predicted ratio, σ is the standard deviation of the experimental-to-predicted ratio, and the z-value corresponding to the selected probability level (z=1.96 for 95% probability). Accordingly, in Fig 6.22(A), which corresponds to the cylindrical dataset, the ML model demonstrates the narrowest PI, ranging from 0.815 to 1.201, indicating higher consistency and reduced variability in predictions compared to the equations. Equation 6.3 exhibits the widest PI, spanning from -0.423 to 3.606, reflecting substantial uncertainty and reduced reliability for this dataset type and rendering it ineffective for practical use. Similarly, in Fig 6.22(B), the ML model again outperforms the equations with the narrowest PI (0.709 to 1.290), while equations (e.g., Equation 6.6 and 6.8) show relatively wider intervals, suggesting higher prediction uncertainty. Overall, the ML model consistently shows narrower PIs in both dataset types, implying better reliability and precision in predictions compared to the equations.

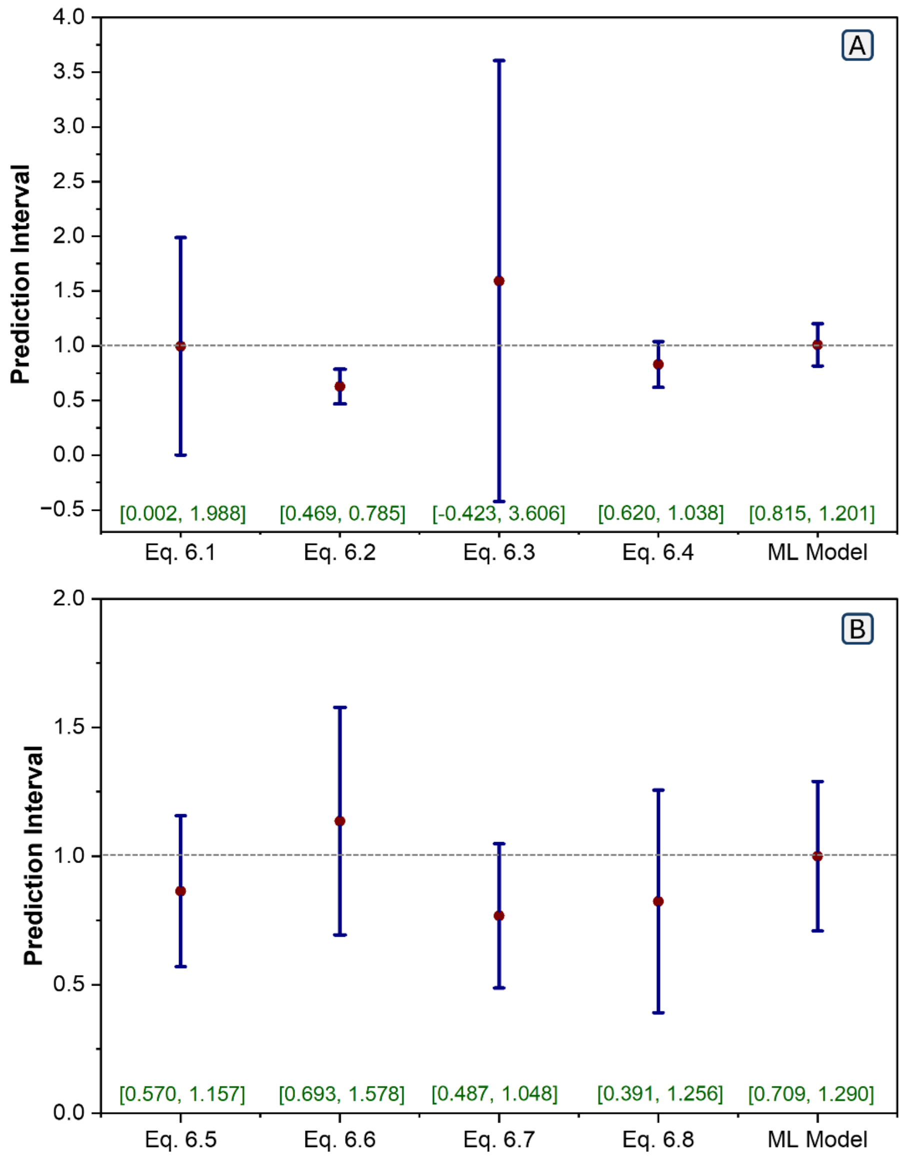

Figure 6.22: The graphs of Prediction Intervals for (A) cylindrical dataset and (B) cubic dataset

6.5 Prediction Uncertainty

The information provided in the previous section gives a comprehensive overview of the performance of the ML and regression models. However, it is important to note that this comparison may not be entirely fair because the ML model was trained on a large portion of the data (training data), which was also part of the overall dataset used for evaluation in the previous section. A more equitable comparison would involve assessing the performance of each model using only testing data from different sources that was not seen during the training phase.

Table 6.16 compares the performance of Eq. 6.1 to Eq. 6.4 and Model No.2 model across three metrics: MAPE, RMSE, and R based only on testing data for cylindrical geometry. The proposed ML model shows superior performance in all metrics, with a MAPE of 9.63%, RMSE of 5.90 MPa, and R of 0.897. Overall, the model demonstrates the best performance in terms of error metrics and correlation, indicating its effectiveness.

Table 6.16: Comparing the performance of Eq. 6.1 to 6.4 and Model No.2 based on testing data of cylindrical geometry

Parameter	Eq. 6.1	Eq. 6.2	Eq. 6.3	Eq. 6.4	Model No.2
MAPE (%)	12.73	53.52	20.35	29.60	9.63
RMSE (MPa)	6.87	25.71	12.41	15.93	5.90
R	0.880	0.881	0.828	0.877	0.897

Table 6.17 compares the performance of Eq. 6.5 to Eq. 6.8 and Model No.2 based on testing data for cubic geometry. The ML model shows superior performance across most metrics, with MAPE of 14.62% and RMSE of 7.32 MPa. Although the ML model's R value is 0.880, a good result, it is lower than some of the other equations.

Table 6.17: Comparing the performance of Eq. 6.5 to 6.8 and Model No.2 based on testing data of cubic geometry

Parameter	Eq. 6.5	Eq. 6.6	Eq. 6.7	Eq. 6.8	Model No.2
MAPE (%)	15.85	14.89	23.26	16.46	14.62
RMSE (MPa)	8.53	11.62	11.03	10.80	7.32
R	0.894	0.946	0.887	0.870	0.880

For both all data and the testing data, the ML model demonstrates superiority over conventional regression approach for predicting CS in both cubic and cylindrical standard. Previous studies indicate that there is inherent uncertainty in predicting concrete CS (Alavi et al., 2024a; Alavi et al., 2024b). Moreover, if multiple cores are taken from a similar location within a structure, the results of compressive strength tests will also vary.

Tables 6.16 and 6.17 clearly demonstrate that the ML model exhibits superior reliability and accuracy in predicting new, unseen data (testing datasets). This highlights the model's robustness in handling unfamiliar inputs. In terms of uncertainty, Fig. 6.22 presents a detailed analysis of the Prediction Intervals (PIs) for the ML model. The results show that 18 out of 20 testing data points were within the 95% PI for the cylindrical dataset, while all eight testing points from the cubic dataset were within the 95% PI. Hence, the combined prediction accuracy for the testing dataset is 93%, which validates the use of PIs to establish non-deterministic predictions for any required probability level specified by a structure owner and provides further confirmation of the model's effectiveness and consistency in making accurate predictions across different data types.

6.6 Discussion and roadmap

According to Fig. 6.11(D), which relates to core data, it was noted that the dataset with ID No.17, used as testing data in the modeling process, follows a different pattern compared to the other core data used for training. This discrepancy affected the model's performance for the core data, as shown in Table 6.9. It is possible to filter outlier data to potentially improve model performance; however, this type of filtering was avoided in this study to highlight a major challenge regarding the collection of data from the field. By investigating the sources of the datasets listed in Table 6.2, it can be seen that different procedures were utilized to extract the data in each case. Moreover, the size of the core samples differs: Dataset No. 11 did not provide the size of the cores (Nobile & Bonagura, 2016); Dataset No. 12 contains core data with a diameter of 84 mm, while the length of the samples was not provided (Cristofaro et al., 2020); Dataset No. 13 includes core data with a size of 100 mm x 200 mm (Alavi et al., 2024b); and Dataset No. 17 consists of core data with a size of 105 mm x 105 mm (Al-Neshawy & Ahmed, 2021). The low height-to-diameter ratio of the latter group may have contributed to the observed discrepancies (i.e., higher compressive strength than expected). Needless to say, these differences will affect the quality of the data, as well as the performance of the ML model. Given this fact, and in line with the primary objective of such studies—to develop a precise and reliable ML-based method to reduce, and potentially eliminate, the need for core tests in the future—it is important to note that one factor influencing data quality is the methodology used for UPV (Ultrasonic Pulse Velocity) and RN (Rebound Number) tests, where human factors can significantly affect the test results.

To improve data quality and enhance the capabilities of future ML models for field applications, it is recommended to implement consistent experimental testing procedures similar to that outlined in Fig. 6.23 and to populate a shared open-access database. This approach aims to improve data quality, model accuracy, and the overall reliability of future models. As shown in Fig. 6.23(A), the proposed approach involves the construction of RC slabs with dimensions of at least one meter by one meter and a minimum thickness of 200 mm, based on various mix designs. These slabs could be subjected to different environmental conditions to account for varying boundary conditions in the data. Each slab can be divided into four zones, with testing scheduled at different ages: Zone 1 at 14 days, Zone 2 at 28 days, Zone 3 at 90 days, and Zone 4 at 180 days after casting.

The proposed testing procedure involves conducting sequential NDT and DT, including three types of UPV tests (direct, indirect, and semi-indirect, Fig. 6.23(B)), RN tests conducted both horizontally and vertically (Fig. 6.23(C)), followed by the extraction and testing of three cores with dimensions of 100 by 200 mm (Fig. 6.23(D)). This procedure will be repeated for slabs with different specifications to create a comprehensive databank for future ML model development with up to five input parameters as illustrated in Fig. 6.24. (It should be noted that for many structural members, it may not be possible to obtain direct UPV measurements; collecting multiple measurements for the database enables the development of models for different scenarios.) Given that the concrete strength data in the database is derived from cores with dimensions of 100 by 200 mm—a standard size—the model output will be based on the strength of standard cylindrical cores, in compliance with all relevant codes.

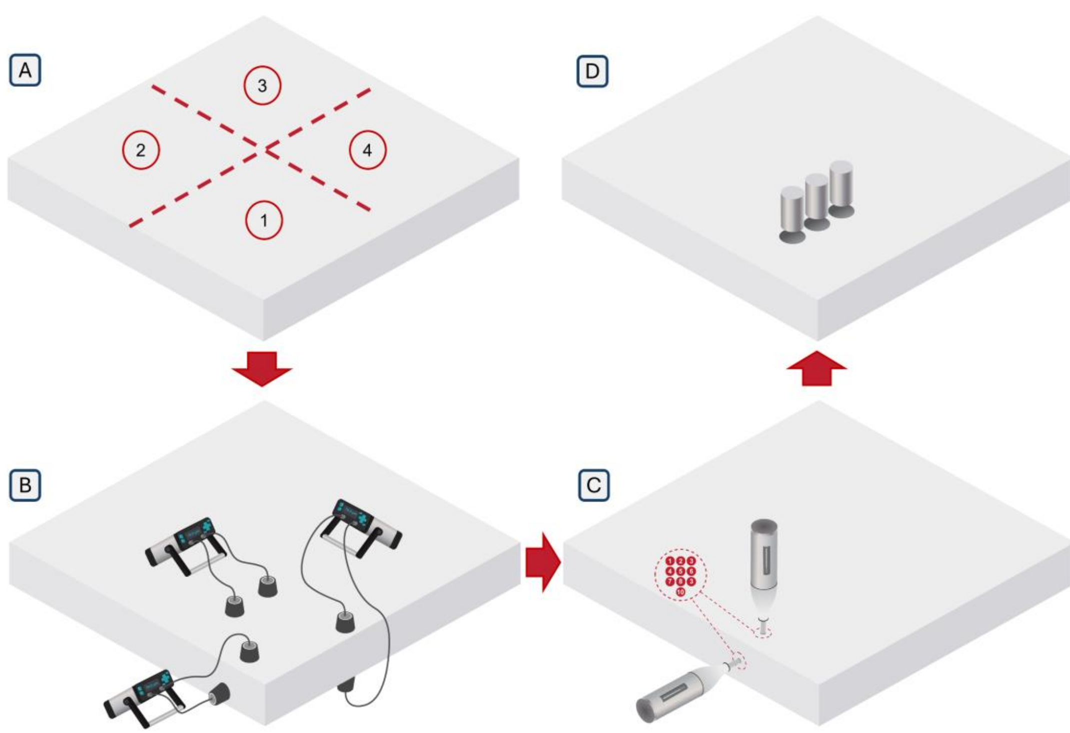

Figure 6.23: Suggested test procedure for future study

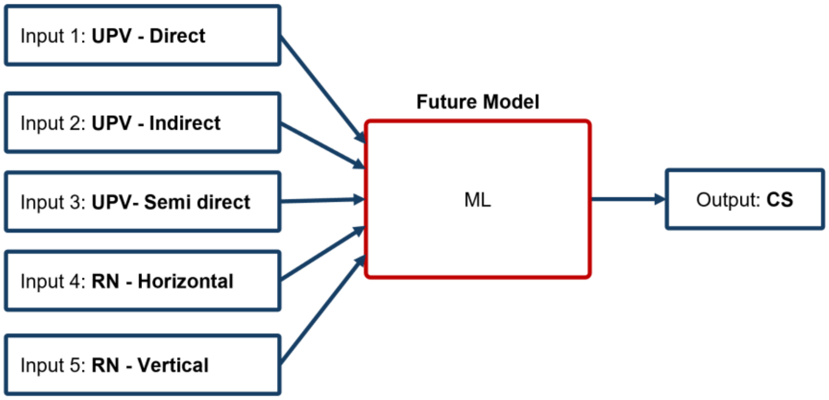

Figure 6.24: Suggested ML model architecture

6.7 Conclusion

In this study, the uncertainty and prediction intervals of a new machine learning approach for the combined non-destructive testing method of SONREB in predicting concrete strength was thoroughly evaluated. For this purpose, a new machine learning-based model was developed for the first time, capable of distinguishing between cylindrical, cubic, and core specimens. This model was developed on a comprehensive database consisting of 620 collected data points. After the model was developed, its results and reliability were compared with four well-known equations based on cylindrical standards and four well-known equations based on cubic standards. The comprehensive performance analysis in this study was conducted by directly applying the selected equations and the developed model to evaluate concrete strength, without the calibration process in using the SONREB method.

The findings of this study clearly demonstrate that the machine learning-based model is significantly more reliable and accurate than other equations in predicting concrete strength without the calibration process. It is important to note that the results of the presented machine learning model are entirely dependent on the data and the algorithms used. Therefore, it is evident that with advancements in computer processing power, improvements in algorithms, and increased data availability, we can expect to see more accurate and practical models based on artificial intelligence and machine learning in the future. This study effectively shows that the machine learning-based model can outperform traditional mathematical models. Finally, based on the results of the current study, a test procedure and ML model architecture is suggested for future study.

6.8 Reference

Alavi, S. A., & Noël, M. (2022). Challenges for the Development of Artificial Intelligence Models to Predict the Compressive Strength of Concrete Using Non-destructive Tests: A Review. Canadian Society of Civil Engineering Annual Conference, 839–857.

Alavi, S. A., & Noel, M. (2025). Effect of model architecture and input parameters to improve performance of artificial intelligence models for estimating concrete strength using SonReb. Engineering Structures, 323, 119285.

Alavi, S. A., Noël, M., Layssi, H., & Moradi, F. (2024a). Can Artificial Intelligence Improve Nondestructive Evaluation of Concrete Strength? Concrete International, 46(5), 51–56.

Alavi, S. A., Noel, M., Moradi, F., & Layssi, H. (2024b). Development of a machine learning model for on-site evaluation of concrete compressive strength by SonReb. Journal of Building Engineering, 82, 108328.

Ali Poorarbabi. (2020). Assessment of concrete compressive strength and electrical resistivity using NDT techniques and artificial neural networks. The University of Sistan & Baluchestan.

Almasaeid, H., Alkasassbeh, A., & Yasin, B. (2022). Prediction of Geopolymer Concrete Compressive Strength Utilizing Artificial Neural Network and Nondestructive Testing. Civil and Environmental Engineering.

Almasaeid, H. H., Suleiman, A., & Alawneh, R. (2022). Assessment of high-temperature damaged concrete using non-destructive tests and artificial neural network modelling. Case Studies in Construction Materials, 16, e01080.

Al-Neshawy, F., & Ahmed, H. (2021). Defining concrete compressive strength by combining the results of different NDT methods.

American Society for Testing and Materials. (n.d.). ASTM C805-08: Standard Test Method for Rebound Number of Hardened Concrete (2008th ed.).

Angiulli, G., Calcagno, S., La Foresta, F., & Versaci, M. (2024). Concrete Compressive Strength Prediction Using Combined Non-Destructive Methods: A Calibration Procedure

Using Preexisting Conversion Models Based on Gaussian Process Regression. Journal of Composites Science, 8(8), 300.

Arora, H. C., Bhushan, B., Kumar, A., Kumar, P., Hadzima-Nyarko, M., Radu, D., Cazacu, C. E., & Kapoor, N. R. (2024). Ensemble learning based compressive strength prediction of concrete structures through real-time non-destructive testing. Scientific Reports, 14(1), 1824.

Asteris, P. G., & Mokos, V. G. (2020). Concrete compressive strength using artificial neural networks. Neural Computing and Applications, 32(15), 11807–11826.

Asteris, P. G., Skentou, A. D., Bardhan, A., Samui, P., & Lourenço, P. B. (2021). Soft computing techniques for the prediction of concrete compressive strength using Non-Destructive tests. Construction and Building Materials, 303, 124450.

Beconcini, M. L., & Formichi, P. (2003). Resistenza del calcestruzzo, misure sclerometriche e di velocità di propagazione degli ultrasuoni in strutture esistenti: risultati di una campagna di indagini. 10th Congresso Nazionale Dell'AIPnD, Ravenna, Italy, 372–380.

Bolborea, B., Dan, S., Baeră, C., Gruin, A., Enache, F., & Perianu, I. A. (2022). Study Regarding the Evaluation of Prediction Models for Determining the Concrete Compressive Strength Using Non-Destructive Testing (NDT) Data: Validation Stage. Solid State Phenomena, 332, 173–181.

Bonagura, M. (2012). Nondestructive evaluation of concrete compression strength by means of Artificial Neural Network (ANN).

Bonagura, M., & Nobile, L. (2021). Artificial Neural Network (ANN) Approach for Predicting Concrete Compressive Strength by SonReb. Structural Durability & Health Monitoring, 15(2), 125.

Breysse, D. (2012). Nondestructive evaluation of concrete strength: An historical review and a new perspective by combining NDT methods. Construction and Building Materials, 33, 139–163.

Cianfrone, F., & Facaoaru, I. (1979). Study on the introduction into Italy on the combined non-destructive method, for the determination ofin situ concrete strength. Matériaux et Construction 1979 12:5, 12(5), 413–424. https://doi.org/10.1007/BF02478819

Cristofaro, M. T., Viti, S., & Tanganelli, M. (2020). New predictive models to evaluate concrete compressive strength using the SonReb method. Journal of Building Engineering, 27, 100962.

Demir, A. (2015). Prediction of hybrid fibre-added concrete strength using artificial neural networks. Computers and Concrete, 15(4), 503–514.

Domingo, R., & Hirose, S. (2009). Correlation between concrete strength and combined nondestructive tests for concrete using high-early strength cement. The Sixth Regional Symposium on Infrastructure Development, 12–13.

Du, G., Bu, L., Hou, Q., Zhou, J., & Lu, B. (2021). Prediction of the compressive strength of high-performance self-compacting concrete by an ultrasonic-rebound method based on a GA-BP neural network. Plos One, 16(5), e0250795.

Erdal, H., Erdal, M., Simsek, O., & Erdal, H. I. (2018). Prediction of concrete compressive strength using non-destructive test results. Computers and Concrete, 21(4), 407–417.

Faella, C., Guadagnuolo, M., Donadio, A., & Ferri, L. (2011). Calibrazione sperimentale del metodo SonReb per costruzioni della Provincia di Caserta degli anni'60–'80. Proceedings of 14th Anidis Conference, Bari, Italy.

Gasparik, J. (1992). Prove non distruttive nell'edilizia. Quaderno didattico AlPn. D. Brescia. Italian.

Jain, A., Kathuria, A., Kumar, A., Verma, Y., & Murari, K. (2013). Combined use of non-destructive tests for assessment of strength of concrete in structure. Procedia Engineering, 54, 241–251.

Jang, J.-S. R. (1993). ANFIS: adaptive-network-based fuzzy inference system. IEEE Transactions on Systems, Man, and Cybernetics, 23(3), 665–685. https://doi.org/10.1109/21.256541

Kheder, G. F. (1999). A two stage procedure for assessment of in situ concrete strength using combined non-destructive testing. Materials and Structures, 32(6), 410–417.

Khoury, S., Aliabdo, A. A.-H., & Ghazy, A. (2014). Reliability of core test–Critical assessment and proposed new approach. Alexandria Engineering Journal, 53(1), 169–184.

Kot, P., Muradov, M., Gkantou, M., Kamaris, G. S., Hashim, K., & Yeboah, D. (2021). Recent advancements in non-destructive testing techniques for structural health monitoring. Applied Sciences, 11(6), 2750.

Kouddane, B., Sbartaï, Z. M., Alwash, M., Ali-Benyahia, K., Elachachi, S. M., Lamdouar, N., & Kenai, S. (2022). Assessment of Concrete Strength Using the Combination of NDT—Review and Performance Analysis. Applied Sciences, 12(23), 12190.

Kumar, P., & Kumar, A. (2015). Prediction of compressive strength using genetic programming involving NDT results. NATIONAL INSTITUTE OF TECHNOLOGY ROURKELA.

Liao, W., Lu, X., Fei, Y., Gu, Y., & Huang, Y. (2024). Generative AI design for building structures. Automation in Construction, 157, 105187.

Logothetis, L. (1978). Combination of three non destructive methods for the determination of the strength of concrete. National Technical University of Athens.

Maierhofer, C., Reinhardt, H.-W., & Dobmann, G. (2010). Non-destructive evaluation of reinforced concrete structures: Non-destructive testing methods. Elsevier.

Masi, A., Chiauzzi, L., & Manfredi, V. (2016). Criteria for identifying concrete homogeneous areas for the estimation of in-situ strength in RC buildings. Construction and Building Materials, 121, 576–587.

Meynink, P., & Samarin, A. (1979). Assessment of compressive strength of concrete by cylinders, cores, and non destructive tests. Quality Control of Concrete Structures, Rilem Symposium, 1979, Stockholm, Sweden, 1.

Na, U. J., Park, T. W., Feng, M. Q., & Chung, L. (2009). Neuro-fuzzy application for concrete strength prediction using combined non-destructive tests. Magazine of Concrete Research, 61(4), 245–256.

Naderpour, H., & Alavi, S. A. (2015). Application of fuzzy logic in reinforced concrete structures. Civil-Comp Proceedings, 109.

Naderpour, H., & Alavi, S. A. (2017). A proposed model to estimate shear contribution of FRP in strengthened RC beams in terms of Adaptive Neuro-Fuzzy Inference System. Composite Structures, 170, 215–227. https://doi.org/10.1016/J.COMPSTRUCT.2017.03.028

Ngo, T. Q. L., Wang, Y.-R., & Chiang, D.-L. (2021). Applying Artificial Intelligence to Improve On-Site Non-Destructive Concrete Compressive Strength Tests. Crystals, 11(10), 1157.

Nobile, L., & Bonagura, M. (2016). Parametric Regression Model and ANN (Artificial Neural Network) Approach in Predicting Concrete Compressive Strength by SonReb Method. Int. J. Struct. Civ. Eng. Res, 5, 183–186.

Park, J. S., Park, S., Oh, B. K., Hong, T., Lee, D.-E., & Park, H. S. (2024). Estimation of Concrete Compressive Strength from Non-Destructive Tests Using a Customized Neural Network and Genetic Algorithm. Applied Soft Computing, 111941.

Poorarbabi, A., Ghasemi, M., & Moghaddam, M. A. (2020). Concrete Compressive Strength Prediction Using Neural Networks Based on Non-destructive Tests and a Self-calibrated Response Surface Methodology. Journal of Nondestructive Evaluation, 39(4), 1–11.

Prassianakis, I. N., & Giokas, P. (2003). Mechanical properties of old concrete using destructive and ultrasonic non-destructive testing methods. Magazine of Concrete Research, 55(2), 171–176.

Pucinotti, R. (2015). Reinforced concrete structure: Non destructive in situ strength assessment of concrete. Construction and Building Materials, 75, 331–341.

Quagliarini, E., Clementi, F., Maracchini, G., & Monni, F. (2016). Experimental assessment of concrete compressive strength in old existing RC buildings: A possible way to reduce the dispersion of DT results. Journal of Building Engineering, 8, 162–171.

Ramadevi, K., Banchhor, S., Kumar, P. S., Syed, R., Kiran, B. N., & Killol, A. J. (2024). Evaluation Of Compressive Strength Of Concrete Using Ndt And Artificial Intelligence Methods. Journal of Advanced Zoology, 45(2).

Ramyar, K., & Kol, P. (1996). Destructive and non-destructive test methods for estimating the strength of concrete. Cement and Concrete World, 2, 46–54.

Rashid, K., & Waqas, R. (2017). Compressive strength evaluation by non-destructive techniques: An automated approach in construction industry. Journal of Building Engineering, 12, 147–154.

RILEM. (1993). Draft recommendation for in situ concrete strength determination by combined non-destructive methods. In Mater. Struct (Vol. 26). Springer.

Sai, G. J., & Singh, V. P. (2019). Prediction of compressive strength using support vector regression. MENDEL, 25(1), 51–56.

Samarin, Alek, and Ravindra K. Dhir. "Determination of in situ concrete strength: rapidly and confidently by nondestructive testing." special publication 82 (1984): 77-94.

Schabowicz, K. (2019). Non-destructive testing of materials in civil engineering. In Materials (Vol. 12, Issue 19, p. 3237). MDPI.

Shih, Y.-F., Wang, Y.-R., Lin, K.-L., & Chen, C.-W. (2015). Improving non-destructive concrete strength tests using support vector machines. Materials, 8(10), 7169–7178.

Shishegaran, A., Varaee, H., Rabczuk, T., & Shishegaran, G. (2021). High correlated variables creator machine: Prediction of the compressive strength of concrete. Computers & Structures, 247, 106479.

Tapeh, A. T. G., & Naser, M. Z. (2022). Artificial Intelligence, Machine Learning, and Deep Learning in Structural Engineering: A Scientometrics Review of Trends and Best Practices. Archives of Computational Methods in Engineering, 1–45.

Thai, H.-T. (2022). Machine learning for structural engineering: A state-of-the-art review. Structures, 38, 448–491.

Thapa, S., Sharma, R. P., & Halder, L. (2021). Developing SonReb models to predict the compressive strength of concrete using different percentage of recycled brick aggregate. Canadian Journal of Civil Engineering, ja.

Uva, G., Porco, F., & Fiore, A. (2018). The SonReb method: critical review and practical aspects. Proceedings of Italian Concrete Days 2016, 161–171.

Wang, C., Song, L., Yuan, Z., & Fan, J. (2023). State-of-the-art AI-based computational analysis in civil engineering. Journal of Industrial Information Integration, 33, 100470.

Wang, Y. R., Ngo, L. T. Q., Shih, Y. F., Lu, Y. L., & Chen, Y. M. (2018). Adapting ANNs in SONREB Test to Estimate Concrete Compressive Strength. Key Engineering Materials, 792, 166–169.

Chapter 7 – Conclusions and Recommendations

7.1 Conclusions

This study addresses the need to enhance the reliability and accuracy of the widely used NDT method SONREB. By employing artificial intelligence (AI) techniques, the study aims to decrease or even eliminate the need for coring, which is challenging in evaluating the compressive strength of concrete in existing reinforced concrete (RC) structures and infrastructure. This is important because RC structures constitute a significant portion of all building types and structures and could have a significant impact on the industry.

A comprehensive investigation was conducted for the first time to explore the feasibility of developing an AI-based model and identify associated challenges. Based on this study's results, the following conclusions can be made:

- According to the first phase of the research (Chapter 3), the impact of training data quantity on ML model performance was observed and it was revealed that using distinct datasets for training and testing reduces bias and enhances results. The proposed ML Model in this phase (ANFIS-C model), trained with 462 data points, achieved a mean absolute percentage error (MAPE) of 11.78%, outperforming models trained with 75% and 80% of the data. It also demonstrated a MAPE of 14.95% on a testing dataset. All of the ML models outperformed regression models using linear or non-linear equations. Also, it was shown that a two-parameter ML model could estimate concrete compressive strength effectively using only UPV and RN measurements, though further improvements may require additional parameters and a more extensive database.

- In the second phase (Chapter 4), the proposed model was tested in three real-world case studies. In summary, the analysis of three distinct case studies highlights the efficacy of the proposed ML model in predicting concrete strength in the field compared to two well-known traditional equations. In the first case study involving a reinforced concrete slab, the ML model achieved the most accurate predictions with a MAPE of 9.69%. In the second case, the ML model again demonstrated superior performance, with a MAPE of 12.85%, which improved to 10.2% when outlier column measurements were excluded. In contrast, both the Breysse and Gasparik equations consistently overestimated compressive strength across all cases. However, in the third case study of an elevated foundation with significant consolidation issues, all predictive models, including the ML model, underpredicted concrete strength which highlights the role of the engineer in selecting appropriate tools and interpreting their results within the context of a particular application. While the ML model generally outperformed traditional equations, its effectiveness may vary depending on the concrete condition (quality), as the presence of defects or deterioration have not been considered.
- The third phase of the research (Chapter 5) investigated the role of model architecture. It was shown that inputting the 'type of geometry' as binary values significantly enhances the learning capacity and prediction accuracy of AI models for concrete compressive strength prediction compared to two-parameters ML models that rely solely on UPV and RN results. Among the AI algorithms evaluated, the deep neural network (DNN) demonstrated the lowest error on training data sets, achieving a mean MAPE of 10.06%, while the adaptive neuro-fuzzy inference system (ANFIS) model exhibited the best performance on unseen testing data with a MAPE of 11.13%. This phase of the study

represents a new method in the development of the SonReb model, enabling it to accommodate both cubic and cylindrical standards by integrating specimen type as an input parameter.

- In the final phase (Chapter 6), the uncertainty and prediction intervals of this new ML-based approach was analyzed. The prediction intervals were validated with the testing data subset in which 93% of the testing data points for the combined cylindrical and cubic dataset were within the 95% prediction interval and thus in close agreement with the expected results, confirming its effectiveness and consistency across different data types. This supports the use of a probabilistic approach to decision-making based on specified probability levels required by structure owners which can significantly reduce the need for cores in sound (undamaged) concrete.

In conclusion, while improvements to the model's architecture or algorithm could enhance performance, they are not the sole solution. This study demonstrates that the new approach has a good potential to be a reliable and accurate method to evaluate concrete strength without the need for core testing and calibration, compared to conventional methods. However, ML models are entirely dependent on the quality of the data on which they are trained. Chapter 6 of the thesis suggests a testing procedure that, if followed by engineers and researchers in the future, could lead to the development of a practical and reliable model, potentially improving structural health and safety.

7.2 Recommendations

Based on this study, several recommendations are proposed for future studies to improve the quality of the database and also improve the reliability and performance of future AI-based models:

1. **Methodology**: Establish standard protocols for data collection across different projects and studies based on NDT and DT on existing RC structural members such as slabs, beams, and columns rather than lab-prepared cubic and cylindrical samples. This includes standardizing the procedures for both UPV and RN tests to minimize variability introduced by human factors and using consistent core sizes for the compressive strength data. Consistency in NDT methods will likely lead to more reliable datasets.

2. **Experimental Tests**: Implement the proposed testing procedures involving the construction of a large number of RC slabs and, when possible, collecting data from real existing structures. By varying environmental conditions, ages, mix designs, and reinforcement ratio, a more comprehensive dataset can be created. This will allow the AI model to trained from a wide range of scenarios.

3. **Database**: Create a shared, open-access database that includes data from various studies, including detailed descriptions of the testing conditions, methodologies, and results. A clear and transparent database can facilitate collaborative research, allowing for more dataset utilization and comparative studies. According to the suggested methodology in Chapter 6, an example of such a dataset is presented in Appendix B.3 based on the NDT and DT results from the RC slab that was tested in this study as a template for future works.

4. **Advanced AI model**: Developing an AI model that can incorporate variations in UPV (direct vs. semi-direct vs. indirect) and RN tests (horizontal vs. vertical) can enhance predictive capabilities. Investigating different AI algorithms and architectures that can handle multiple inputs effectively will also be valuable.

5. **Continuous Validation**: Create a mechanism for continuous validation of the results from field applications and case studies of the AI-based model to help identify areas for improvement and guide future research directions.

6. **Multidisciplinary Collaboration**: Engage with experts from various fields such as software engineers and data scientists to explore innovative approaches and new solutions to develop more robust and capable AI models in the future.

By addressing these recommendations, future studies can significantly enhance data quality, improve model accuracy, and contribute to developing a reliable ML-based method for assessing concrete strength in existing RC structures.

Appendix A: MATLAB Scripts

A.1 ANFIS-C Model and GUI (Chapter 3):

```
Name='anfisc'
Type='sugeno'
Version=2.0
NumInputs=2
NumOutputs=1
NumRules=4
AndMethod='prod'
OrMethod='probor'
ImpMethod='prod'
AggMethod='sum'
DefuzzMethod='wtaver'

[Input1]
Name='input1'
Range=[0.1 0.9]
NumMFs=2
MF1='in1mf1':'trimf',[-0.702378073350073 0.285611942060067 0.859537211620787]
MF2='in1mf2':'trimf',[-0.0102117238892339 1.1075937478726 1.7]

[Input2]
Name='input2'
Range=[0.1 0.9]
NumMFs=2
MF1='in2mf1':'trimf',[-0.699858475342662 0.353955333787154 1.16164865440493]
MF2='in2mf2':'trimf',[-0.0986938830009724 0.709557238260412 1.62106127271513]

[Output1]
Name='output'
Range=[0.1 0.9]
NumMFs=4
MF1='out1mf1':'constant',[0.0280782357690555]
MF2='out1mf2':'constant',[0.251538576525874]
MF3='out1mf3':'constant',[-0.0710344344847799]
MF4='out1mf4':'constant',[1.24046900234234]

[Rules]
1 1, 1 (1) : 1
1 2, 2 (1) : 1
2 1, 3 (1) : 1
2 2, 4 (1) : 1

>>
```

- GUI app:

```
classdef AISonReb < matlab.apps.AppBase

  % Properties that correspond to app components
  properties (Access = public)
    UIFigure                   matlab.ui.Figure
```

```
    LastupdateJan23ModelMbaseLabel  matlab.ui.control.Label
    Gauge                           matlab.ui.control.Gauge
    SAAlaviMNoelLabel               matlab.ui.control.Label
    ReboundNumberRNPanel            matlab.ui.container.Panel
    ValidfororiginalschmidthammerLabel  matlab.ui.control.Label
    Range10455Label                 matlab.ui.control.Label
    RNEditField                     matlab.ui.control.NumericEditField
    UltraPulseVelocityUPVPanel      matlab.ui.container.Panel
    Range344539kmsLabel             matlab.ui.control.Label
    KmsEditField                    matlab.ui.control.NumericEditField
    KmsEditFieldLabel               matlab.ui.control.Label
    MPaEditField                    matlab.ui.control.NumericEditField
    MPaEditFieldLabel               matlab.ui.control.Label
    PowerbyAItechnologyLabel        matlab.ui.control.Label
    AISonRebLabel                   matlab.ui.control.Label
    EvaluatetheCompressiveStrengthButton  matlab.ui.control.Button
end


methods (Access = private)


end


% Callbacks that handle component events
methods (Access = private)

    % Button pushed function: EvaluatetheCompressiveStrengthButton
    function EvaluatetheCompressiveStrengthButtonPushed(app, event)
        FIS=readfis('anfisc.fis');
        i1=app.KmsEditField.Value;
        upv=((0.8*(i1-3.44333333333333)/(5.39-3.44333333333333))+0.1);
        i2=app.RNEditField.Value;
        R=(0.8*(i2-10.3333333333333)/(55.5-10.3333333333333))+0.1;
        inputs=[upv R];
        output=evalfis(FIS,inputs);
        output2=((((output-0.1)/0.8)*(76.32-11.07797521))+11.07797521);
        app.MPaEditField.Value=(output2);
        app.Gauge.Value=output2;
    end
end

% Component initialization
methods (Access = private)

    % Create UIFigure and components
    function createComponents(app)

        % Create UIFigure and hide until all components are created
        app.UIFigure = uifigure('Visible', 'off');
        app.UIFigure.Position = [100 100 592 421];
        app.UIFigure.Name = 'MATLAB App';

        % Create EvaluatetheCompressiveStrengthButton
```

```
        app.EvaluatetheCompressiveStrengthButton = uibutton(app.UIFigure, 'push');
        app.EvaluatetheCompressiveStrengthButton.ButtonPushedFcn = createCallbackFcn(app,
@EvaluatetheCompressiveStrengthButtonPushed, true);
        app.EvaluatetheCompressiveStrengthButton.BackgroundColor = [0.651 0.651 0.651];
        app.EvaluatetheCompressiveStrengthButton.FontSize = 14;
        app.EvaluatetheCompressiveStrengthButton.FontWeight = 'bold';
        app.EvaluatetheCompressiveStrengthButton.Position = [316 265 258 45];
        app.EvaluatetheCompressiveStrengthButton.Text = 'Evaluate the Compressive Strength ';

        % Create AISonRebLabel
        app.AISonRebLabel = uilabel(app.UIFigure);
        app.AISonRebLabel.FontSize = 20;
        app.AISonRebLabel.FontWeight = 'bold';
        app.AISonRebLabel.FontAngle = 'italic';
        app.AISonRebLabel.Position = [31 368 255 45];
        app.AISonRebLabel.Text = 'AI-SonReb';

        % Create PowerbyAItechnologyLabel
        app.PowerbyAItechnologyLabel = uilabel(app.UIFigure);
        app.PowerbyAItechnologyLabel.Position = [63 214 270 22];
        app.PowerbyAItechnologyLabel.Text = 'Power by AI technology';

        % Create MPaEditFieldLabel
        app.MPaEditFieldLabel = uilabel(app.UIFigure);
        app.MPaEditFieldLabel.BackgroundColor = [0.651 0.651 0.651];
        app.MPaEditFieldLabel.HorizontalAlignment = 'center';
        app.MPaEditFieldLabel.FontSize = 14;
        app.MPaEditFieldLabel.FontWeight = 'bold';
        app.MPaEditFieldLabel.Position = [477 57 47 22];
        app.MPaEditFieldLabel.Text = ' (MPa)';

        % Create MPaEditField
        app.MPaEditField = uieditfield(app.UIFigure, 'numeric');
        app.MPaEditField.FontSize = 14;
        app.MPaEditField.FontWeight = 'bold';
        app.MPaEditField.BackgroundColor = [0.651 0.651 0.651];
        app.MPaEditField.Position = [378 57 89 22];

        % Create UltraPulseVelocityUPVPanel
app.UltraPulseVelocityUPVPanel = uipanel(app.UIFigure);
app.UltraPulseVelocityUPVPanel.TitlePosition = 'centertop';
app.UltraPulseVelocityUPVPanel.Title = 'Ultra Pulse Velocity (UPV)';
app.UltraPulseVelocityUPVPanel.FontWeight = 'bold';
app.UltraPulseVelocityUPVPanel.Position = [30 203 260 120];

% Create KmsEditFieldLabel
app.KmsEditFieldLabel = uilabel(app.UltraPulseVelocityUPVPanel);
app.KmsEditFieldLabel.HorizontalAlignment = 'right';
app.KmsEditFieldLabel.Position = [114 62 30 22];
app.KmsEditFieldLabel.Text = 'Km/s';

% Create KmsEditField
app.KmsEditField = uieditfield(app.UltraPulseVelocityUPVPanel, 'numeric');
app.KmsEditField.Position = [27 62 75 22];
```

```
% Create Range344539kmsLabel
app.Range344539kmsLabel = uilabel(app.UltraPulseVelocityUPVPanel);
app.Range344539kmsLabel.Position = [27 23 147 22];
app.Range344539kmsLabel.Text = 'Range: 3.44 ~ 5.39 km/s';

% Create ReboundNumberRNPanel
app.ReboundNumberRNPanel = uipanel(app.UIFigure);
app.ReboundNumberRNPanel.TitlePosition = 'centertop';
app.ReboundNumberRNPanel.Title = 'Rebound Number (RN)';
app.ReboundNumberRNPanel.FontWeight = 'bold';
app.ReboundNumberRNPanel.Position = [30 74 260 120];

% Create RNEditField
app.RNEditField = uieditfield(app.ReboundNumberRNPanel, 'numeric');
app.RNEditField.Position = [20 63 75 22];

% Create Range10455Label
app.Range10455Label = uilabel(app.ReboundNumberRNPanel);
app.Range10455Label.Position = [20 23 147 22];
app.Range10455Label.Text = 'Range: 10.4 ~ 55';

% Create ValidfororiginalschmidthammerLabel
app.ValidfororiginalschmidthammerLabel = uilabel(app.ReboundNumberRNPanel);
app.ValidfororiginalschmidthammerLabel.Position = [21 3 217 22];
app.ValidfororiginalschmidthammerLabel.Text = 'Valid for original schmidt hammer.';

% Create SAAlaviMNoelLabel
app.SAAlaviMNoelLabel = uilabel(app.UIFigure);
app.SAAlaviMNoelLabel.Position = [31 356 270 22];
app.SAAlaviMNoelLabel.Text = 'S.A. Alavi & M. Noel';

% Create Gauge
app.Gauge = uigauge(app.UIFigure, 'circular');
app.Gauge.Limits = [10 76];
app.Gauge.Position = [369 92 164 164];

% Create LastupdateJan23ModelMbaseLabel
app.LastupdateJan23ModelMbaseLabel = uilabel(app.UIFigure);
app.LastupdateJan23ModelMbaseLabel.FontSize = 10;
app.LastupdateJan23ModelMbaseLabel.Position = [31 15 270 22];
app.LastupdateJan23ModelMbaseLabel.Text = 'Last update: Jan23, Model:Mbase';

% Show the figure after all components are created
app.UIFigure.Visible = 'on';
end
end

% App creation and deletion
methods (Access = public)

% Construct app
function app = AISonReb

% Create UIFigure and components
createComponents(app)
```

```
% Register the app with App Designer
registerApp(app, app.UIFigure)

if nargout == 0
clear app
end
end

% Code that executes before app deletion
function delete(app)

% Delete UIFigure when app is deleted
delete(app.UIFigure)
end
end
end
```

A.2 ANFIS-3i (Chapter 5):

```
fis = sugfis('Name', 'anfis31');

fis.AndMethod = 'prod';
fis.OrMethod = 'probor';
fis.ImpMethod = 'prod';
fis.AggMethod = 'sum';
fis.DefuzzMethod = 'wtaver';


fis = addInput(fis, [0.097264957 0.89998354], 'Name', 'input1');
fis = addMF(fis, 'input1', 'trimf', [-0.705371756588067 0.221596597348441 0.857345917921773], 'Name',
'in1mf1');
fis = addMF(fis, 'input1', 'trimf', [0.0205065759647367 0.996625034579459 1.702702123], 'Name', 'in1mf2');

fis = addInput(fis, [0.099881901 0.9], 'Name', 'input2');
fis = addMF(fis, 'input2', 'trimf', [-0.700236198 0.0651238937532767 1.04662390978928], 'Name', 'in2mf1');
fis = addMF(fis, 'input2', 'trimf', [0.165945162158267 0.696164059525361 1.6871865893497], 'Name',
'in2mf2');

fis = addInput(fis, [0 1], 'Name', 'input3');
fis = addMF(fis, 'input3', 'trimf', [0 0 0], 'Name', 'in3mf1'); % Membership function for 0
fis = addMF(fis, 'input3', 'trimf', [0 1 1], 'Name', 'in3mf2'); % Membership function for 1

fis = addOutput(fis, [0.099975171 0.9], 'Name', 'output');
fis = addMF(fis, 'output', 'constant', 0.181664661416603, 'Name', 'out1mf1');
fis = addMF(fis, 'output', 'constant', 0.0620875832054839, 'Name', 'out1mf2');
fis = addMF(fis, 'output', 'constant', 0.0550895633024227, 'Name', 'out1mf3');
fis = addMF(fis, 'output', 'constant', 0.198021322893656, 'Name', 'out1mf4');
fis = addMF(fis, 'output', 'constant', 0.081520860212591, 'Name', 'out1mf5');
```

```
fis = addMF(fis, 'output', 'constant', 0.0480015264855563, 'Name', 'out1mf6');
fis = addMF(fis, 'output', 'constant', 0.119227666402278, 'Name', 'out1mf7');
fis = addMF(fis, 'output', 'constant', 0.0868796219481703, 'Name', 'out1mf8');

ruleList = [1 1 1 1 1;
          2 1 1 1 1;
          1 2 1 1 1;
          2 2 1 1 1;
          1 1 2 1 1;
          2 1 2 1 1;
          1 2 2 1 1;
          2 2 2 1 1];
fis = addRule(fis, ruleList);
```

A.3 Model No.2 (Chapter 6)

```
fis = sugfis('Name', 'modelno2', 'AndMethod', 'prod', 'OrMethod', 'probor', ...
          'ImpMethod', 'prod', 'AggMethod', 'sum', 'DefuzzMethod', 'wtaver');
[Input1]
fis = addInput(fis, [0.1027 0.8999], 'Name', 'input1');
fis = addMF(fis, 'input1', 'trimf', [-0.2959 0.1189 0.5345]);
fis = addMF(fis, 'input1', 'trimf', [0.0888 0.6287 0.8756]);
fis = addMF(fis, 'input1', 'trimf', [0.3952 0.9625 1.2986]);

[Input2]
fis = addInput(fis, [0.1006 0.9], 'Name', 'input2');
fis = addMF(fis, 'input2', 'trimf', [-0.2991 0.1228 0.5194]);
fis = addMF(fis, 'input2', 'trimf', [0.0773 0.4784 0.9324]);
fis = addMF(fis, 'input2', 'trimf', [0.5670 0.8374 1.2998]);

[Input3]
fis = addInput(fis, [0 1], 'Name', 'input3');
fis = addMF(fis, 'input3', 'trimf', [-1 0 1]);

[Input4]

fis = addInput(fis, [0 1], 'Name', 'input4');
fis = addMF(fis, 'input4', 'trimf', [-1 0 1]);

fis = addOutput(fis, [0 1], 'Name', 'output1');
```

Appendix B: Data

B.1 Database for Chapter 3 (all data)

Table B.1: Database used in Chapter 3

No.	UPV	RN	f_c'	Dataset	From	Ref.
1	4.610	26.4	20.20	TR	DC	Logothetis, 1978
2	4.440	28.5	19.91	TR	DC	Logothetis, 1978
3	4.550	27.0	20.30	TR	DC	Logothetis, 1978
4	4.580	26.6	22.16	TR	DC	Logothetis, 1978
5	4.620	27.0	20.89	TR	DC	Logothetis, 1978
6	4.510	26.8	21.67	TR	DC	Logothetis, 1978
7	4.320	26.0	18.63	TR	DC	Logothetis, 1978
8	4.350	25.5	20.10	TR	DC	Logothetis, 1978
9	4.350	27.0	20.40	TR	DC	Logothetis, 1978
10	4.370	26.0	19.22	TR	DC	Logothetis, 1978
11	4.370	26.1	21.57	TR	DC	Logothetis, 1978
12	4.320	27.3	19.22	TR	DC	Logothetis, 1978
13	4.180	22.8	15.00	TR	DC	Logothetis, 1978
14	4.250	25.0	17.36	TR	DC	Logothetis, 1978
15	4.190	23.0	15.30	TR	DC	Logothetis, 1978
16	4.200	24.5	15.89	TR	DC	Logothetis, 1978
17	4.130	23.8	14.22	TR	DC	Logothetis, 1978
18	4.260	24.0	16.67	TR	DC	Logothetis, 1978
19	4.760	32.2	32.36	TR	DC	Logothetis, 1978
20	4.760	32.0	30.60	TR	DC	Logothetis, 1978
21	4.880	30.0	35.79	TR	DC	Logothetis, 1978
22	4.780	31.8	31.58	TR	DC	Logothetis, 1978
23	4.730	32.5	30.89	TR	DC	Logothetis, 1978
24	4.770	32.0	32.36	TR	DC	Logothetis, 1978
25	4.880	32.8	34.62	TR	DC	Logothetis, 1978
26	4.800	33.6	34.62	TR	DC	Logothetis, 1978
27	4.880	33.0	35.50	TR	DC	Logothetis, 1978
28	4.850	33.8	35.50	TR	DC	Logothetis, 1978
29	4.800	33.5	34.32	TR	DC	Logothetis, 1978
30	4.850	34.0	37.46	TR	DC	Logothetis, 1978
31	4.610	30.0	28.14	TR	DC	Logothetis, 1978
32	4.650	30.5	27.07	TR	DC	Logothetis, 1978
33	4.660	31.0	30.11	TR	DC	Logothetis, 1978
34	4.660	30.8	28.14	TR	DC	Logothetis, 1978
35	4.640	29.0	28.44	TR	DC	Logothetis, 1978
36	4.640	31.0	28.44	TR	DC	Logothetis, 1978
37	4.550	30.5	27.46	TR	DC	Logothetis, 1978
38	4.650	30.0	28.64	TR	DC	Logothetis, 1978
39	4.620	31.9	28.14	TR	DC	Logothetis, 1978
40	4.620	30.8	28.93	TR	DC	Logothetis, 1978
41	4.650	31.3	29.62	TR	DC	Logothetis, 1978
42	4.620	30.8	29.52	TR	DC	Logothetis, 1978
43	4.550	30.1	29.62	TR	DC	Logothetis, 1978
44	4.550	30.7	35.50	TR	DC	Logothetis, 1978

45	4.550	32.4	34.81	TR	DC	Logothetis, 1978
46	4.550	33.0	36.19	TR	DC	Logothetis, 1978
47	4.520	32.6	30.30	TR	DC	Logothetis, 1978
48	4.550	33.8	35.30	TR	DC	Logothetis, 1978
49	4.600	28.0	22.16	TR	DC	Logothetis, 1978
50	4.520	28.0	22.26	TR	DC	Logothetis, 1978
51	4.550	30.0	23.63	TR	DC	Logothetis, 1978
52	4.500	28.0	22.26	TR	DC	Logothetis, 1978
53	4.510	28.9	22.36	TR	DC	Logothetis, 1978
54	4.510	27.5	22.16	TR	DC	Logothetis, 1978
55	4.620	31.0	27.85	TR	DC	Logothetis, 1978
56	4.670	31.2	27.26	TR	DC	Logothetis, 1978
57	4.600	30.2	25.10	TR	DC	Logothetis, 1978
58	4.620	30.0	28.44	TR	DC	Logothetis, 1978
59	4.650	30.8	26.77	TR	DC	Logothetis, 1978
60	4.540	31.0	29.03	TR	DC	Logothetis, 1978
61	4.740	28.6	23.63	TR	DC	Logothetis, 1978
62	4.700	30.7	25.69	TR	DC	Logothetis, 1978
63	4.480	28.6	23.05	TR	DC	Logothetis, 1978
64	4.510	28.5	25.20	TR	DC	Logothetis, 1978
65	4.550	29.4	24.03	TR	DC	Logothetis, 1978
66	4.540	29.2	25.50	TR	DC	Logothetis, 1978
67	4.690	30.0	28.44	TR	DC	Logothetis, 1978
68	4.730	30.0	25.30	TR	DC	Logothetis, 1978
69	4.770	30.0	28.05	TR	DC	Logothetis, 1978
70	4.730	29.4	28.14	TR	DC	Logothetis, 1978
71	4.690	30.6	27.85	TR	DC	Logothetis, 1978
72	4.770	30.3	27.36	TR	DC	Logothetis, 1978
73	4.650	25.1	17.16	TR	DC	Logothetis, 1978
74	4.480	26.0	19.61	TR	DC	Logothetis, 1978
75	4.510	25.4	16.67	TR	DC	Logothetis, 1978
76	4.580	24.4	16.67	TR	DC	Logothetis, 1978
77	4.540	26.0	18.34	TR	DC	Logothetis, 1978
78	4.540	26.0	19.12	TR	DC	Logothetis, 1978
79	4.480	28.6	22.16	TR	DC	Logothetis, 1978
80	4.520	28.0	23.14	TR	DC	Logothetis, 1978
81	4.450	28.3	22.95	TR	DC	Logothetis, 1978
82	4.480	26.3	23.05	TR	DC	Logothetis, 1978
83	4.480	29.1	22.36	TR	DC	Logothetis, 1978
84	4.550	27.4	22.36	TR	DC	Logothetis, 1978
85	4.450	26.6	19.61	TR	DC	Logothetis, 1978
86	4.450	24.6	16.67	TR	DC	Logothetis, 1978
87	4.440	25.5	17.65	TR	DC	Logothetis, 1978
88	4.440	25.4	18.34	TR	DC	Logothetis, 1978
89	4.460	26.4	17.85	TR	DC	Logothetis, 1978
90	4.530	25.4	20.10	TR	DC	Logothetis, 1978
91	4.630	29.7	24.32	TR	DC	Logothetis, 1978
92	4.580	29.3	24.52	TR	DC	Logothetis, 1978
93	4.770	30.8	25.20	TR	DC	Logothetis, 1978
94	4.660	29.7	26.87	TR	DC	Logothetis, 1978
95	4.620	29.0	26.87	TR	DC	Logothetis, 1978

96	4.690	30.0	26.18	TR	DC	Logothetis, 1978
97	4.170	23.0	14.51	TR	DC	Logothetis, 1978
98	4.150	23.5	16.18	TR	DC	Logothetis, 1978
99	4.190	23.5	14.42	TR	DC	Logothetis, 1978
100	4.080	23.1	14.22	TR	DC	Logothetis, 1978
101	4.120	24.0	14.91	TR	DC	Logothetis, 1978
102	4.170	22.0	15.20	TR	DC	Logothetis, 1978
103	4.030	21.6	12.85	TR	DC	Logothetis, 1978
104	3.940	20.5	12.16	TR	DC	Logothetis, 1978
105	3.900	21.8	12.45	TR	DC	Logothetis, 1978
106	3.930	21.1	12.45	TR	DC	Logothetis, 1978
107	3.950	20.0	12.65	TR	DC	Logothetis, 1978
108	3.950	22.0	14.32	TR	DC	Logothetis, 1978
109	4.350	24.9	15.79	TR	DC	Logothetis, 1978
110	4.360	25.8	16.18	TR	DC	Logothetis, 1978
111	4.350	24.3	15.89	TR	DC	Logothetis, 1978
112	4.310	24.4	15.30	TR	DC	Logothetis, 1978
113	4.400	25.6	16.38	TR	DC	Logothetis, 1978
114	4.200	22.2	15.40	TR	DC	Logothetis, 1978
115	4.170	22.0	14.42	TR	DC	Logothetis, 1978
116	4.220	21.9	14.32	TR	DC	Logothetis, 1978
117	4.200	22.1	15.10	TR	DC	Logothetis, 1978
118	4.170	21.8	15.49	TR	DC	Logothetis, 1978
119	4.140	21.9	15.00	TR	DC	Logothetis, 1978
120	4.350	27.2	20.10	TR	DC	Logothetis, 1978
121	4.350	28.4	19.81	TR	DC	Logothetis, 1978
122	4.450	27.9	20.89	TR	DC	Logothetis, 1978
123	4.480	28.6	22.85	TR	DC	Logothetis, 1978
124	4.450	29.2	22.56	TR	DC	Logothetis, 1978
125	4.410	29.0	21.08	TR	DC	Logothetis, 1978
126	4.620	28.7	23.05	TR	DC	Logothetis, 1978
127	4.550	28.0	24.22	TR	DC	Logothetis, 1978
128	4.580	29.8	23.54	TR	DC	Logothetis, 1978
129	4.620	28.4	24.52	TR	DC	Logothetis, 1978
130	4.650	29.0	23.83	TR	DC	Logothetis, 1978
131	4.550	29.4	23.73	TR	DC	Logothetis, 1978
132	4.380	28.1	21.38	TR	DC	Logothetis, 1978
133	4.450	28.2	20.99	TR	DC	Logothetis, 1978
134	4.400	28.6	21.67	TR	DC	Logothetis, 1978
135	4.450	28.0	24.42	TR	DC	Logothetis, 1978
136	4.100	26.2	14.42	TR	DC	Logothetis, 1978
137	3.850	22.9	14.81	TR	DC	Logothetis, 1978
138	5.050	38.2	43.25	TR	DC	Logothetis, 1978
139	5.050	37.2	40.31	TR	DC	Logothetis, 1978
140	5.100	39.0	43.44	TR	DC	Logothetis, 1978
141	5.100	38.0	39.32	TR	DC	Logothetis, 1978
142	5.050	36.8	42.27	TR	DC	Logothetis, 1978
143	5.050	37.1	41.58	TR	DC	Logothetis, 1978
144	4.800	36.0	47.56	TR	DC	Logothetis, 1978
145	4.880	34.4	42.95	TR	DC	Logothetis, 1978
146	4.930	35.4	40.70	TR	DC	Logothetis, 1978

147	4.810	34.6	41.97	TR	DC	Logothetis, 1978
148	4.920	35.2	44.33	TR	DC	Logothetis, 1978
149	4.920	35.5	43.64	TR	DC	Logothetis, 1978
150	5.220	41.5	50.21	TR	DC	Logothetis, 1978
151	5.220	41.5	50.01	TR	DC	Logothetis, 1978
152	5.180	40.6	49.33	TR	DC	Logothetis, 1978
153	5.220	42.0	50.01	TR	DC	Logothetis, 1978
154	5.220	40.0	45.40	TR	DC	Logothetis, 1978
155	5.220	41.4	50.01	TR	DC	Logothetis, 1978
156	5.000	41.0	50.41	TR	DC	Logothetis, 1978
157	4.950	41.0	52.17	TR	DC	Logothetis, 1978
158	4.920	40.8	50.80	TR	DC	Logothetis, 1978
159	5.000	41.0	50.01	TR	DC	Logothetis, 1978
160	4.980	40.0	49.13	TR	DC	Logothetis, 1978
161	4.990	41.2	50.80	TR	DC	Logothetis, 1978
162	4.960	38.9	42.95	TR	DC	Logothetis, 1978
163	4.960	37.3	40.99	TR	DC	Logothetis, 1978
164	4.960	38.5	41.68	TR	DC	Logothetis, 1978
165	4.960	38.3	40.99	TR	DC	Logothetis, 1978
166	4.960	37.3	41.19	TR	DC	Logothetis, 1978
167	5.000	37.0	41.78	TR	DC	Logothetis, 1978
168	4.920	36.2	39.91	TR	DC	Logothetis, 1978
169	4.950	36.2	39.72	TR	DC	Logothetis, 1978
170	4.800	37.3	38.25	TR	DC	Logothetis, 1978
171	4.800	38.1	40.40	TR	DC	Logothetis, 1978
172	4.780	37.2	39.72	TR	DC	Logothetis, 1978
173	4.850	35.2	39.72	TR	DC	Logothetis, 1978
174	4.770	36.1	38.83	TR	DC	Logothetis, 1978
175	4.770	37.3	41.19	TR	DC	Logothetis, 1978
176	4.770	37.1	39.72	TR	DC	Logothetis, 1978
177	4.730	36.8	38.05	TR	DC	Logothetis, 1978
178	4.770	37.1	39.42	TR	DC	Logothetis, 1978
179	4.880	36.1	40.21	TR	DC	Logothetis, 1978
180	4.840	33.0	31.87	TR	DC	Logothetis, 1978
181	4.750	33.9	33.05	TR	DC	Logothetis, 1978
182	4.720	33.8	33.93	TR	DC	Logothetis, 1978
183	4.750	34.6	33.93	TR	DC	Logothetis, 1978
184	4.720	33.3	34.81	TR	DC	Logothetis, 1978
185	4.750	33.8	34.81	TR	DC	Logothetis, 1978
186	4.520	30.0	26.38	TR	DC	Logothetis, 1978
187	4.420	30.0	25.01	TR	DC	Logothetis, 1978
188	4.450	30.9	26.97	TR	DC	Logothetis, 1978
189	4.450	30.4	26.28	TR	DC	Logothetis, 1978
190	4.450	30.9	26.58	TR	DC	Logothetis, 1978
191	4.450	30.5	25.99	TR	DC	Logothetis, 1978
192	4.520	28.3	26.09	TR	DC	Logothetis, 1978
193	4.480	30.0	26.58	TR	DC	Logothetis, 1978
194	4.450	30.0	27.46	TR	DC	Logothetis, 1978
195	4.450	29.9	27.46	TR	DC	Logothetis, 1978
196	4.450	30.9	27.46	TR	DC	Logothetis, 1978
197	4.450	31.0	27.46	TR	DC	Logothetis, 1978

198	4.260	28.0	22.85	TR	DC	Logothetis, 1978
199	4.280	28.3	23.14	TR	DC	Logothetis, 1978
200	4.280	27.0	22.36	TR	DC	Logothetis, 1978
201	4.320	28.7	23.54	TR	DC	Logothetis, 1978
202	4.320	28.2	23.34	TR	DC	Logothetis, 1978
203	4.110	29.0	24.52	TR	DC	Logothetis, 1978
204	4.290	27.0	22.46	TR	DC	Logothetis, 1978
205	4.260	28.5	22.16	TR	DC	Logothetis, 1978
206	4.200	28.2	21.38	TR	DC	Logothetis, 1978
207	4.290	29.6	22.85	TR	DC	Logothetis, 1978
208	4.290	28.0	23.54	TR	DC	Logothetis, 1978
209	4.290	28.0	23.73	TR	DC	Logothetis, 1978
210*	4.033	18.3	16.20	TR	DC	Poorarbabi et al., 2020
211*	4.250	20.7	19.13	TR	DC	Poorarbabi et al., 2020
212*	4.123	19.0	16.74	TR	DC	Poorarbabi et al., 2020
213*	4.397	20.7	19.41	TR	DC	Poorarbabi et al., 2020
214*	3.760	20.3	16.45	TR	DC	Poorarbabi et al., 2020
215*	4.180	22.0	19.92	TR	DC	Poorarbabi et al., 2020
216*	4.383	22.7	22.13	TR	DC	Poorarbabi et al., 2020
217*	3.753	18.0	12.91	TR	DC	Poorarbabi et al., 2020
218*	4.123	18.0	16.05	TR	DC	Poorarbabi et al., 2020
219*	4.363	18.0	17.00	TR	DC	Poorarbabi et al., 2020
220*	3.740	18.7	13.96	TR	DC	Poorarbabi et al., 2020
221*	4.227	20.0	19.56	TR	DC	Poorarbabi et al., 2020
222*	3.870	18.3	14.14	TR	DC	Poorarbabi et al., 2020
223*	4.393	18.0	19.32	TR	DC	Poorarbabi et al., 2020
224*	3.940	21.3	18.65	TR	DC	Poorarbabi et al., 2020
225*	4.097	20.7	22.50	TR	DC	Poorarbabi et al., 2020
226*	4.477	24.3	24.60	TR	DC	Poorarbabi et al., 2020
227*	3.890	19.0	15.30	TR	DC	Poorarbabi et al., 2020
228*	4.147	20.3	20.21	TR	DC	Poorarbabi et al., 2020
229*	4.390	23.3	22.77	TR	DC	Poorarbabi et al., 2020
230*	3.930	18.3	17.54	TR	DC	Poorarbabi et al., 2020
231*	4.120	20.7	20.34	TR	DC	Poorarbabi et al., 2020
232*	4.410	23.3	23.46	TR	DC	Poorarbabi et al., 2020
233*	4.020	20.3	17.19	TR	DC	Poorarbabi et al., 2020
234*	4.157	21.7	21.30	TR	DC	Poorarbabi et al., 2020
235*	4.527	25.3	22.10	TR	DC	Poorarbabi et al., 2020
236*	3.953	19.7	18.28	TR	DC	Poorarbabi et al., 2020
237*	4.220	21.3	22.94	TR	DC	Poorarbabi et al., 2020
238*	4.430	23.7	23.98	TR	DC	Poorarbabi et al., 2020
239*	4.230	24.3	21.83	TR	DC	Poorarbabi et al., 2020
240*	4.407	26.7	25.60	TR	DC	Poorarbabi et al., 2020
241*	4.620	25.0	28.61	TR	DC	Poorarbabi et al., 2020
242*	4.113	22.0	23.03	TR	DC	Poorarbabi et al., 2020
243*	4.250	26.7	27.19	TR	DC	Poorarbabi et al., 2020
244*	4.510	27.0	27.73	TR	DC	Poorarbabi et al., 2020
245*	4.220	22.7	22.54	TR	DC	Poorarbabi et al., 2020
246*	4.407	24.3	28.06	TR	DC	Poorarbabi et al., 2020
247*	4.530	27.3	30.30	TR	DC	Poorarbabi et al., 2020
248*	4.207	25.3	27.43	TR	DC	Poorarbabi et al., 2020

249*	4.293	25.7	31.74	TR	DC	Poorarbabi et al., 2020
250*	4.627	32.0	34.66	TR	DC	Poorarbabi et al., 2020
251*	4.157	23.0	21.41	TR	DC	Poorarbabi et al., 2020
252*	4.317	23.7	25.91	TR	DC	Poorarbabi et al., 2020
253*	4.673	28.0	32.09	TR	DC	Poorarbabi et al., 2020
254*	4.057	23.7	21.69	TR	DC	Poorarbabi et al., 2020
255*	4.213	24.7	27.48	TR	DC	Poorarbabi et al., 2020
256*	4.637	26.7	28.73	TR	DC	Poorarbabi et al., 2020
257*	4.173	25.3	27.48	TR	DC	Poorarbabi et al., 2020
258*	4.423	29.3	33.34	TR	DC	Poorarbabi et al., 2020
259*	4.723	33.7	33.73	TR	DC	Poorarbabi et al., 2020
260*	4.173	24.0	29.35	TR	DC	Poorarbabi et al., 2020
261*	4.333	28.7	36.33	TR	DC	Poorarbabi et al., 2020
262*	4.740	34.3	37.64	TR	DC	Poorarbabi et al., 2020
263*	4.333	25.0	30.27	TR	DC	Poorarbabi et al., 2020
264*	4.443	31.7	36.29	TR	DC	Poorarbabi et al., 2020
265*	4.813	35.7	37.06	TR	DC	Poorarbabi et al., 2020
266	4.300	31.0	20.99	TR	DC	Rashid & Waqas, 2017
267	4.400	32.0	22.61	TR	DC	Rashid & Waqas, 2017
268	4.500	33.0	23.90	TR	DC	Rashid & Waqas, 2017
269	4.600	33.0	24.47	TR	DC	Rashid & Waqas, 2017
270	4.500	33.0	27.30	TR	DC	Rashid & Waqas, 2017
271	4.700	34.0	28.76	TR	DC	Rashid & Waqas, 2017
272	4.500	36.0	28.69	TR	DC	Rashid & Waqas, 2017
273	4.800	37.0	32.16	TR	DC	Rashid & Waqas, 2017
274	4.300	32.0	24.07	TR	DC	Rashid & Waqas, 2017
275	4.200	32.0	25.33	TR	DC	Rashid & Waqas, 2017
276	4.400	33.0	25.79	TR	DC	Rashid & Waqas, 2017
277	4.400	33.0	26.37	TR	DC	Rashid & Waqas, 2017
278	4.700	34.0	29.81	TR	DC	Rashid & Waqas, 2017
279	4.400	35.0	30.50	TR	DC	Rashid & Waqas, 2017
280	4.800	38.0	33.66	TR	DC	Rashid & Waqas, 2017
281	4.800	38.0	36.67	TR	DC	Rashid & Waqas, 2017
282	4.900	39.0	41.14	TR	DC	Rashid & Waqas, 2017
283	4.390	31.0	28.18	TR	DC	Rashid & Waqas, 2017
284	4.450	32.0	31.39	TR	DC	Rashid & Waqas, 2017
285	4.720	33.0	33.67	TR	DC	Rashid & Waqas, 2017
286	4.660	33.0	34.70	TR	DC	Rashid & Waqas, 2017
287	4.770	34.0	36.83	TR	DC	Rashid & Waqas, 2017
288	4.780	36.0	39.45	TR	DC	Rashid & Waqas, 2017
289	4.800	36.0	41.76	TR	DC	Rashid & Waqas, 2017
290	4.920	37.0	46.68	TR	DC	Rashid & Waqas, 2017
291	4.950	39.0	51.27	TR	DC	Rashid & Waqas, 2017
292	4.660	49.3	54.10	TR	DC	Na et al., 2009
293	4.710	55.2	56.10	TR	DC	Na et al., 2009
294	4.710	55.5	56.50	TR	DC	Na et al., 2009
295	4.800	55.5	56.90	TR	DC	Na et al., 2009
296	4.500	39.5	40.60	TR	DC	Na et al., 2009
297	4.720	45.7	47.60	TR	DC	Na et al., 2009
298	4.650	45.9	48.30	TR	DC	Na et al., 2009
299	4.700	46.9	49.20	TR	DC	Na et al., 2009

300	4.350	37.9	39.40	TR	DC	Na et al., 2009
301	4.490	43.5	41.50	TR	DC	Na et al., 2009
302	4.750	42.1	41.90	TR	DC	Na et al., 2009
303	4.600	46.4	43.20	TR	DC	Na et al., 2009
304	4.410	29.6	32.90	TR	DC	Na et al., 2009
305	4.500	30.0	33.00	TR	DC	Na et al., 2009
306	4.500	32.4	33.70	TR	DC	Na et al., 2009
307	4.600	36.6	34.70	TR	DC	Na et al., 2009
308	4.130	20.7	20.40	TR	DC	Na et al., 2009
309	4.250	23.1	23.30	TR	DC	Na et al., 2009
310	4.300	22.6	24.20	TR	DC	Na et al., 2009
311	4.300	26.3	27.00	TR	DC	Na et al., 2009
312	3.821	19.0	12.80	TR	DC	Domingo & Hirose, 2009
313	4.000	22.0	14.80	TR	DC	Domingo & Hirose, 2009
314	4.200	29.0	21.80	TR	DC	Domingo & Hirose, 2009
315	3.963	25.0	20.30	TR	DC	Domingo & Hirose, 2009
316	4.154	31.0	23.90	TR	DC	Domingo & Hirose, 2009
317	4.375	35.0	28.20	TR	DC	Domingo & Hirose, 2009
318	4.385	32.0	30.60	TR	DC	Domingo & Hirose, 2009
319	4.500	38.0	33.60	TR	DC	Domingo & Hirose, 2009
320	4.667	42.0	39.80	TR	DC	Domingo & Hirose, 2009
321	4.458	37.0	33.20	TR	DC	Domingo & Hirose, 2009
322	4.596	42.0	38.40	TR	DC	Domingo & Hirose, 2009
323	4.773	45.0	48.70	TR	DC	Domingo & Hirose, 2009
324	4.820	25.0	27.96	TR	DC	Cianfrone & Facaoaru, 1979
325	5.130	31.0	38.65	TR	DC	Cianfrone & Facaoaru, 1979
326	5.230	37.0	47.87	TR	DC	Cianfrone & Facaoaru, 1979
327	5.050	40.0	56.21	TR	DC	Cianfrone & Facaoaru, 1979
328	4.880	34.0	52.48	TR	DC	Cianfrone & Facaoaru, 1979
329	5.130	43.0	65.92	TR	DC	Cianfrone & Facaoaru, 1979
330	5.190	41.0	69.36	TR	DC	Cianfrone & Facaoaru, 1979
331	5.050	42.0	65.43	TR	DC	Cianfrone & Facaoaru, 1979
332	4.910	33.0	45.32	TR	DC	Cianfrone & Facaoaru, 1979
333	5.210	43.0	71.51	TR	DC	Cianfrone & Facaoaru, 1979
334	5.180	43.0	69.36	TR	DC	Cianfrone & Facaoaru, 1979
335	5.120	46.0	76.32	TR	DC	Cianfrone & Facaoaru, 1979
336	5.140	42.0	64.94	TR	DC	Cianfrone & Facaoaru, 1979
337	5.080	38.0	52.29	TR	DC	Cianfrone & Facaoaru, 1979
338	5.230	41.0	61.90	TR	DC	Cianfrone & Facaoaru, 1979
339	5.300	43.0	68.87	TR	DC	Cianfrone & Facaoaru, 1979
340	5.170	44.0	65.43	TR	DC	Cianfrone & Facaoaru, 1979
341	4.880	25.0	28.35	TR	DC	Cianfrone & Facaoaru, 1979
342	5.050	44.0	62.78	TR	DC	Cianfrone & Facaoaru, 1979
343	5.200	44.0	65.83	TR	DC	Cianfrone & Facaoaru, 1979
344	5.300	45.0	64.75	TR	DC	Cianfrone & Facaoaru, 1979
345	5.220	43.0	58.37	TR	DC	Cianfrone & Facaoaru, 1979
346	5.390	45.0	60.82	TR	DC	Cianfrone & Facaoaru, 1979
347	4.900	34.0	53.27	TR	DC	Cianfrone & Facaoaru, 1979
348	5.040	38.0	61.31	TR	DC	Cianfrone & Facaoaru, 1979
349	5.050	31.0	47.87	TR	DC	Cianfrone & Facaoaru, 1979
350	5.100	34.0	51.70	TR	DC	Cianfrone & Facaoaru, 1979

351	5.320	32.0	51.70	TR	DC	Cianfrone & Facaoaru, 1979
352	4.930	30.0	37.47	TR	DC	Cianfrone & Facaoaru, 1979
353	5.270	36.0	50.23	TR	DC	Cianfrone & Facaoaru, 1979
354	5.230	36.0	49.44	TR	DC	Cianfrone & Facaoaru, 1979
355	5.200	38.0	51.70	TR	DC	Cianfrone & Facaoaru, 1979
356	5.260	37.0	50.23	TR	DC	Cianfrone & Facaoaru, 1979
357	4.980	38.0	46.70	TR	DC	Cianfrone & Facaoaru, 1979
358	5.150	33.0	53.66	TR	DC	Cianfrone & Facaoaru, 1979
359	5.220	39.0	60.14	TR	DC	Cianfrone & Facaoaru, 1979
360	5.270	37.0	54.05	TR	DC	Cianfrone & Facaoaru, 1979
361	5.170	39.0	53.27	TR	DC	Cianfrone & Facaoaru, 1979
362	5.200	36.0	59.35	TR	DC	Cianfrone & Facaoaru, 1979
363	4.360	26.3	22.87	TR	DC	Jain et al., 2013
364	4.500	32.7	27.92	TR	DC	Jain et al., 2013
365	4.510	27.2	23.30	TR	DC	Jain et al., 2013
366	4.910	29.9	28.50	TR	DC	Jain et al., 2013
367	4.510	35.7	31.23	TR	DC	Jain et al., 2013
368	4.690	37.5	33.89	TR	DC	Jain et al., 2013
369	4.530	36.4	32.12	TR	DC	Jain et al., 2013
370	4.780	40.6	37.28	TR	DC	Jain et al., 2013
371	4.790	41.3	42.53	TR	DC	Jain et al., 2013
372	4.930	43.8	44.75	TR	DC	Jain et al., 2013
373	4.820	41.1	43.23	TR	DC	Jain et al., 2013
374	4.960	44.0	45.74	TR	DC	Jain et al., 2013
375	4.970	48.4	52.12	TR	DC	Jain et al., 2013
376	5.060	52.2	54.96	TR	DC	Jain et al., 2013
377	5.010	50.3	53.80	TR	DC	Jain et al., 2013
378	5.100	53.4	59.33	TR	DC	Jain et al., 2013
379	4.510	30.4	23.25	TR	DC	Jain et al., 2013
380	4.660	33.3	29.32	TR	DC	Jain et al., 2013
381	4.590	30.8	25.69	TR	DC	Jain et al., 2013
382	4.960	33.1	30.38	TR	DC	Jain et al., 2013
383	4.570	37.9	32.26	TR	DC	Jain et al., 2013
384	4.780	38.4	36.15	TR	DC	Jain et al., 2013
385	4.620	38.7	33.48	TR	DC	Jain et al., 2013
386	4.850	41.5	37.65	TR	DC	Jain et al., 2013
387	4.800	41.3	42.77	TR	DC	Jain et al., 2013
388	4.910	44.7	45.81	TR	DC	Jain et al., 2013
389	4.890	43.5	43.67	TR	DC	Jain et al., 2013
390	4.910	46.7	46.97	TR	DC	Jain et al., 2013
391	5.080	49.1	52.65	TR	DC	Jain et al., 2013
392	5.110	52.3	55.82	TR	DC	Jain et al., 2013
393	5.150	51.3	54.22	TR	DC	Jain et al., 2013
394	5.220	53.5	58.93	TR	DC	Jain et al., 2013
395*	3.730	18.7	13.02	TR	DC	Ali Poorarbabi, 2020
396*	3.930	18.0	18.15	TR	DC	Ali Poorarbabi, 2020
397*	4.227	19.7	17.94	TR	DC	Ali Poorarbabi, 2020
398*	3.443	10.3	11.07	TR	DC	Ali Poorarbabi, 2020
399*	3.917	15.0	14.69	TR	DC	Ali Poorarbabi, 2020
400*	4.307	18.7	16.99	TR	DC	Ali Poorarbabi, 2020
401*	3.623	18.7	14.11	TR	DC	Ali Poorarbabi, 2020

402*	3.943	18.0	17.90	TR	DC	Ali Poorarbabi, 2020
403*	4.327	17.7	19.48	TR	DC	Ali Poorarbabi, 2020
404*	3.663	15.7	11.16	TR	DC	Ali Poorarbabi, 2020
405*	3.920	16.0	13.70	TR	DC	Ali Poorarbabi, 2020
406*	4.243	16.0	16.99	TR	DC	Ali Poorarbabi, 2020
407*	3.663	15.3	12.07	TR	DC	Ali Poorarbabi, 2020
408*	3.880	14.0	14.61	TR	DC	Ali Poorarbabi, 2020
409*	4.147	17.7	18.32	TR	DC	Ali Poorarbabi, 2020
410*	3.910	17.3	12.82	TR	DC	Ali Poorarbabi, 2020
411*	4.033	16.3	15.53	TR	DC	Ali Poorarbabi, 2020
412*	4.300	17.0	18.11	TR	DC	Ali Poorarbabi, 2020
413*	4.007	18.0	16.07	TR	DC	Ali Poorarbabi, 2020
414*	4.127	19.3	19.81	TR	DC	Ali Poorarbabi, 2020
415*	4.300	19.0	23.77	TR	DC	Ali Poorarbabi, 2020
416*	3.920	18.0	13.11	TR	DC	Ali Poorarbabi, 2020
417*	4.023	17.7	17.19	TR	DC	Ali Poorarbabi, 2020
418*	4.287	20.7	19.73	TR	DC	Ali Poorarbabi, 2020
419*	3.927	19.3	16.11	TR	DC	Ali Poorarbabi, 2020
420*	4.080	19.0	19.82	TR	DC	Ali Poorarbabi, 2020
421*	4.253	22.7	23.90	TR	DC	Ali Poorarbabi, 2020
422*	3.957	17.0	13.65	TR	DC	Ali Poorarbabi, 2020
423*	4.127	18.3	18.32	TR	DC	Ali Poorarbabi, 2020
424*	4.330	21.7	22.82	TR	DC	Ali Poorarbabi, 2020
425*	3.987	19.0	14.99	TR	DC	Ali Poorarbabi, 2020
426*	4.180	18.3	18.11	TR	DC	Ali Poorarbabi, 2020
427*	4.297	20.0	22.77	TR	DC	Ali Poorarbabi, 2020
428*	4.120	21.7	17.11	TR	DC	Ali Poorarbabi, 2020
429*	4.240	23.3	19.82	TR	DC	Ali Poorarbabi, 2020
430*	4.347	22.7	24.48	TR	DC	Ali Poorarbabi, 2020
431*	4.080	19.0	18.73	TR	DC	Ali Poorarbabi, 2020
432*	4.213	24.3	25.59	TR	DC	Ali Poorarbabi, 2020
433*	4.380	23.3	28.94	TR	DC	Ali Poorarbabi, 2020
434*	4.200	20.0	18.03	TR	DC	Ali Poorarbabi, 2020
435*	4.320	20.7	23.69	TR	DC	Ali Poorarbabi, 2020
436*	4.537	23.0	27.60	TR	DC	Ali Poorarbabi, 2020
437*	4.160	25.0	21.57	TR	DC	Ali Poorarbabi, 2020
438*	4.230	21.7	25.73	TR	DC	Ali Poorarbabi, 2020
439*	4.457	27.3	29.94	TR	DC	Ali Poorarbabi, 2020
440*	4.173	22.3	18.32	TR	DC	Ali Poorarbabi, 2020
441*	4.280	23.3	24.36	TR	DC	Ali Poorarbabi, 2020
442*	4.443	27.0	26.44	TR	DC	Ali Poorarbabi, 2020
443*	4.093	20.7	19.61	TR	DC	Ali Poorarbabi, 2020
444*	4.270	22.3	24.94	TR	DC	Ali Poorarbabi, 2020
445*	4.457	25.0	28.01	TR	DC	Ali Poorarbabi, 2020
446*	4.330	22.0	23.31	TR	DC	Ali Poorarbabi, 2020
447*	4.470	26.0	31.35	TR	DC	Ali Poorarbabi, 2020
448*	4.543	27.0	28.81	TR	DC	Ali Poorarbabi, 2020
449*	4.280	21.0	27.02	TR	DC	Ali Poorarbabi, 2020
450*	4.407	26.3	32.273	TR	DC	Ali Poorarbabi, 2020
451*	4.573	28.7	32.18	TR	DC	Ali Poorarbabi, 2020
452*	4.267	22.0	27.94	TR	DC	Ali Poorarbabi, 2020

453*	4.413	23.7	30.56	TR	DC	Ali Poorarbabi, 2020
454*	4.560	29.0	31.02	TR	DC	Ali Poorarbabi, 2020
455*	4.770	29.3	39.99	TR	CW	-
456*	4.796	31.2	39.80	TR	CW	-
457*	4.788	31.0	35.28	TR	CW	-
458*	4.785	31.0	40.14	TR	CW	-
459*	4.695	29.3	35.58	TR	CW	-
460*	4.682	29.7	36.75	TR	CW	-
461*	4.884	31.7	43.58	TR	CW	-
462*	4.881	31.4	43.24	TR	CW	-
463*	5.023	34.6	52.99	TS	CW	-
464*	4.800	32.2	38.21	TS	CW	-
465*	4.779	30.5	42.51	TS	CW	-
466*	4.937	30.3	51.35	TS	CW	-
467*	4.784	24.1	26.09	TS	CW	-
468*	5.090	38.8	47.23	TS	CW	-
469*	5.119	37.9	58.07	TS	CW	-
470*	5.020	38.0	52.30	TS	CW	-
471*	4.629	31.3	37.22	TS	CW	-
472*	5.117	39.5	55.09	TS	CW	-
473*	5.239	42.4	70.77	TS	CW	-
474*	5.049	40.1	64.82	TS	CW	-
475*	4.785	36.2	29.97	TS	CW	-
476*	4.888	43.3	39.23	TS	CW	-
477*	5.119	46.8	47.99	TS	CW	-
478*	5.089	45.4	48.81	TS	CW	-
479*	4.739	41.8	40.10	TS	CW	-
480*	5.038	47.8	58.06	TS	CW	-
481*	5.166	50.9	68.60	TS	CW	-
482*	5.047	49.4	66.86	TS	CW	-

- The data marked with (*) have been extracted from the average of three concrete specimens.
- TR = Training data, TS = Testing data, DC = Data collection, CW = Current work
- The units for UPV and f_c' are km/s and MPa respectively.

References:

Ali Poorarbabi. (2020). Assessment of concrete compressive strength and electrical resistivity using NDT techniques and artificial neural networks. The University of Sistan & Baluchestan.

Cianfrone, F., & Facaoaru, I. (1979). Study on the introduction into Italy on the combined non-destructive method, for the determination ofin situ concrete strength. Matériaux et Construction 1979 12:5, 12(5), 413–424. https://doi.org/10.1007/BF02478819

Domingo, R., & Hirose, S. (2009). Correlation between concrete strength and combined nondestructive tests for concrete using high-early strength cement. The Sixth Regional Symposium on Infrastructure Development, 12–13.

Jain, A., Kathuria, A., Kumar, A., Verma, Y., & Murari, K. (2013). Combined use of non-destructive tests for assessment of strength of concrete in structure. Procedia Engineering, 54, 241–251.

Logothetis, L. (1978). Combination of three non destructive methods for the determination of the strength of concrete. National Technical University of Athens.

Na, U. J., Park, T. W., Feng, M. Q., & Chung, L. (2009). Neuro-fuzzy application for concrete strength prediction using combined non-destructive tests. Magazine of Concrete Research, 61(4), 245–256.

Poorarbabi, A., Ghasemi, M., & Moghaddam, M. A. (2020). Concrete Compressive Strength Prediction Using Neural Networks Based on Non-destructive Tests and a Self-calibrated Response Surface Methodology. Journal of Nondestructive Evaluation, 39(4), 1–11.

Rashid, K., & Waqas, R. (2017). Compressive strength evaluation by non-destructive techniques: An automated approach in construction industry. Journal of Building Engineering, 12, 147–154.

B.2 Experimental Data

Table B.2: First phase of experimental program (making cubes and cylinders)

Mix	Age (day)	UPV (Km/s)	RN	CS (MPa)	Geometry
M1	28	4.784	24.07	26.10	Cylindrical
M2	28	5.090	38.80	47.23	Cylindrical
M5	28	5.119	37.90	58.08	Cylindrical
M6	28	5.020	37.96	52.30	Cylindrical
M1	90	4.629	31.27	37.22	Cylindrical
M2	90	5.117	39.50	55.10	Cylindrical
M5	90	5.239	42.40	70.78	Cylindrical
M6	90	5.049	40.10	64.83	Cylindrical
M1	28	4.785	36.23	29.97	Cubic
M2	28	4.888	43.30	39.23	Cubic
M5	28	5.119	46.80	48.00	Cubic
M6	28	5.089	45.43	48.81	Cubic
M1	90	4.739	41.84	40.10	Cubic
M2	90	5.038	47.80	58.06	Cubic
M5	90	5.166	50.90	68.60	Cubic
M6	90	5.047	49.37	66.86	Cubic
- Each data extracted from the average of three concrete specimens.					

Table B.3: First phase of experimental program (Company A and Company B)

Dataset	UPV (Km/s)	RN	CS (MPa)	Type
Company A-1	4.770	29.33	40.00	Cylindrical
Company A-2	4.796	31.20	39.80	Cylindrical
Company A-3	4.788	30.97	35.28	Cylindrical
Company A-4	4.785	31.03	40.14	Cylindrical
Company A-5	4.695	29.30	35.58	Cylindrical
Company A-6	4.682	29.70	36.75	Cylindrical
Company A-7	4.884	31.70	43.58	Cylindrical
Company A-8	4.881	31.40	43.25	Cylindrical
Company B-1	4.790	32.17	38.21	Cylindrical
Company B-2	4.707	35.75	39.43	Cylindrical
Company B-3	4.779	30.50	42.51	Cylindrical
Company B-4	4.834	34.37	46.73	Cylindrical
Company B-5	4.937	30.33	51.36	Cylindrical
Company B-6	5.051	33.83	61.62	Cylindrical
Company B-7	4.919	30.20	41.64	Cylindrical
Company B-8	5.004	36.65	46.65	Cylindrical
Company B-9	4.987	34.85	55.65	Cylindrical
Company B-10	5.042	43.80	63.48	Cylindrical

Company B-11	5.067	39.80	59.90	Cylindrical
Company B-12	5.023	34.57	52.99	Cylindrical
- Each data extracted from the average of three concrete specimens.				

Table B.4: Second phase of experimental program

Mix ID	Age (day)	UPV (Km/s)	RN	CS (MPa)	Geometry
S1	28	5.101	33.63	50.49	Cylindrical
S1	90	5.400	37.20	56.62	Cylindrical
S2	28	4.896	31.37	44.72	Cylindrical
S2	90	5.009	38.33	53.40	Cylindrical
S3	28	4.943	34.53	42.33	Cylindrical
S3	90	4.991	39.23	47.60	Cylindrical
S4	28	5.264	38.33	60.63	Cylindrical
S4	90	5.206	42.90	62.33	Cylindrical
S5	28	5.131	41.53	56.59	Cylindrical
S5	90	5.097	41.20	64.42	Cylindrical
S6	28	4.941	33.57	46.82	Cylindrical
S6	90	5.093	39.90	53.24	Cylindrical
S7	28	4.815	30.23	36.87	Cylindrical
S7	90	4.848	34.60	42.69	Cylindrical
S8	28	4.920	34.29	45.12	Cylindrical
S8	90	5.002	35.17	52.26	Cylindrical
S9	28	4.977	34.90	44.74	Cylindrical
S9	90	4.999	37.67	50.06	Cylindrical
S10	28	4.865	33.73	47.07	Cylindrical
S10	90	4.891	37.27	53.08	Cylindrical
S11	28	4.980	34.50	47.92	Cylindrical
S11	90	5.150	40.60	56.76	Cylindrical
S12	28	5.010	34.80	50.02	Cylindrical
S12	90	5.110	41.47	54.69	Cylindrical
- Each data extracted from the average of three concrete specimens.					

B.3 Proposed Data Based on the Suggested Test Plan

Table B.5: NDT and DT test plan on the slab

Location	Detail
Depth 200 mm with reinforcement	At each circle, 1 direct UPV, 1 indirect UPV (200 mm spacing between transducers), 1 set of rebound hammer, 1 concrete core
Depth 300 mm with reinforcement	At each circle, 1 direct UPV, 1 indirect UPV (300 mm spacing between transducers), 1 set of rebound hammer, 1 concrete core
Depth 200 mm without reinforcement	At each circle, 1 direct UPV, 1 indirect UPV (200 mm spacing between transducers), 1 set of rebound hammer, 1 concrete core
Depth 300 mm without reinforcement	At each circle, 1 direct UPV, 1 indirect UPV (300 mm spacing between transducers), 1 set of rebound hammer, 1 concrete core
	1 set of rebound hammer at each triangle. Do the test at both side with and without reinforcement.

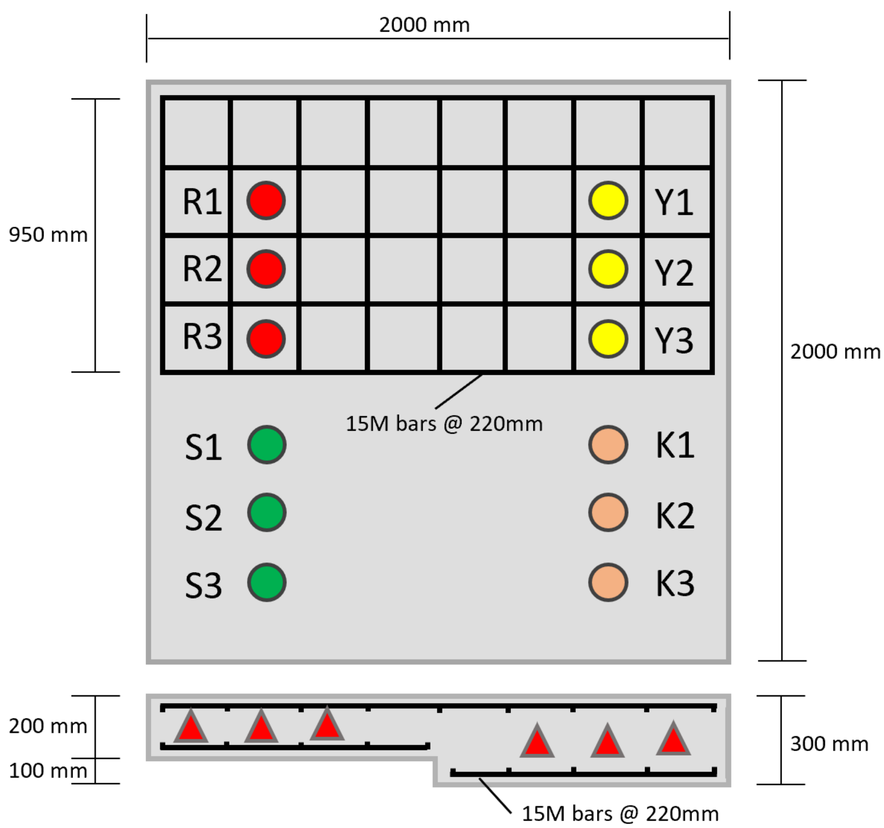

Figure B.1: NDT and DT testing points on the slab

Table B.2: Direct UPV, indirect UPV, downward RN, and core tests results

Point	UPV (μs)		RN (Vertical-downward)	Core Test (MPa) (100*200 mm core)
	UPV Direct	UPV Indirect	RN	
R1	47.0	49.0	38.6	34.93
R2	47.4	49.5	38.2	33.4
R3	47.7	49.8	39	36.39
Y1	68.3	76.3	37.5	34.44
Y2	66.4	79.2	37.8	34.19
Y3	68.2	76.8	38.6	35.27
S1	46.6	50.3	37.7	34.63
S2	46.7	51.5	37.9	30.36
S3	45.7	49.4	38	32.86
K1	66.7	78.1	37.8	34.02
K2	68.0	82.6	38.6	37.94
K3	68.7	81.0	36.8	26.6

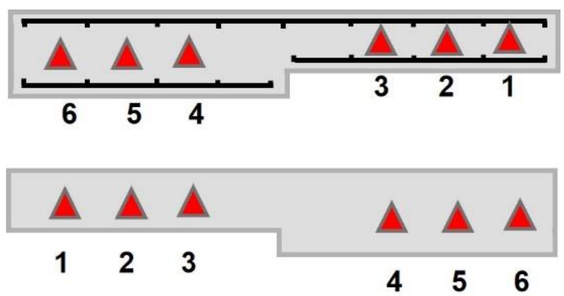

Figure B.2: Horizontal-RN testing points

Table B.7: Horizontal-RN tests results

Point	RN
With reinforcement	
1	36.8
2	38.2
3	36.6
4	37.2
5	37.3
6	38.4
Without reinforcement	
1	37
2	37.8
3	38
4	37.6
5	36
6	37.8

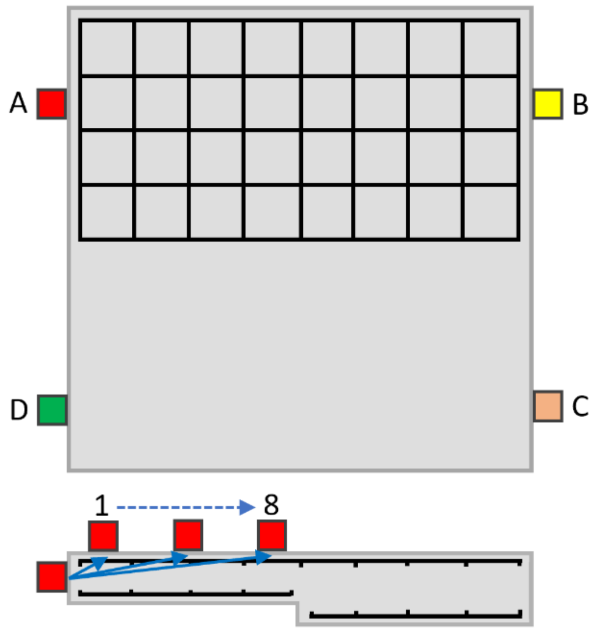

Figure B.3: Semi-direct UPV testing points

Table B.8: Semi-direct UPV tests results

POINT/STEP	1 (10cm)	2 (20cm)	3 (30cm)	4 (40cm)	5 (50cm)	6 (60cm)	7 (70cm)	8 (80cm)
A (*20cm)	35 (µs)	53.5 (µs)	73.5 (µs)	93.5 (µs)	114.7 (µs)	136.0 (µs)	159.8 (µs)	189 (µs)
B (*29.5cm)	43.2 (µs)	59.3 (µs)	79.6 (µs)	102 (µs)	123.7 (µs)	`147.7 (µs)	170.7 (µs)	190.8 (µs)
C (*29.2cm)	41.7 (µs)	58.6 (µs)	77.8 (µs)	103.6 (µs)	123.1 (µs)	146.5 (µs)	168.5 (µs)	190 (µs)
D (*19cm)	30 (µs)	51 (µs)	75.5 (µs)	98 (µs)	121.5 (µs)	142.6 (µs)	170.0 (µs)	195 (µs)
* The actual thickness of the section where the transducer was placed at the mid-elevation.								